The roles of papain-like protease-related proteins in viral replication and host immunity

by

Pengcheng Shang

B.S., Shandong Agricultural University, 2010
M.S., China Agricultural University, 2013

AN ABSTRACT OF A DISSERTATION

submitted in partial fulfillment of the requirements for the degree

DOCTOR OF PHILOSOPHY

Department of Diagnostic Medicine and Pathobiology
College of Veterinary Medicine

KANSAS STATE UNIVERSITY
Manhattan, Kansas

2018

Abstract

Viral papain-like proteases (PLPs)-related proteins have been shown to be actively involved in host innate immunity manipulation and virus replication. In this dissertation, the research were focused on the elucidation of biological roles of nidoviral PLPs-related proteins in innate immunity suppression and viral RNA transcription regulation.

Porcine Respiratory and Reproductive Syndrome Virus (PRRSV) is the most prominent swine diseases worldwide. Understanding PRRSV pathogenesis and development efficient vaccines are highly required in swine industry. PRRSV nsp2-related proteins including nsp2 and two ribosomal frameshifting products-nsp2TF and nsp2N share the same N-terminal PLP2 domain. In chapter 2, nsp2TF and nsp2N were demonstrated to be critical for host innate immunity suppression at least through the PLP2 domain-mediated deubiquitination and deISGylation effects. The infection of nsp2TF/nsp2N knockout mutants significantly upregulated antiviral innate immune responses *in vitro*. Furthermore, manipulating the expression of nsp2TF/nsp2N could enhance innate and adaptive immunity in pigs, providing potential basis for modified live vaccine development.

In addition to the PLP2 domain of PRRSV nsp2-related proteins, the biological roles and biochemical nature of the poorly investigated long mysterious PLP2 downstream region was also characterized in Chapter 3. This long unknown region is also shared by nsp2-related proteins. At first, the hyper-phosphorylation nature of nsp2-related proteins was demonstrated. Physical features of this uncharacterized region was then delineated, including two intrinsically disordered hypervariable regions spaced by a structured inter-species conserved domain. One critical phosphorylated residues in the conserved domain were later proved to be of great importance in recombinant virus rescue and subgenomic RNAs accumulation. Collectively, our investigations

underline the pleiotropic effects exerted by nsp2-related proteins in virus life cycle and potential contributions with pathogenesis.

In Chapter 4, potential functions of PLP encoded by other nidovirus was also investigated. We discovered a unique cross-order recombination event, in which the chimeric picornavirus-enterovirus G expresses the PLP gene, homologous to torovirus (ToV) PLPs. Like other nidoviral PLPs, the recombinant ToV-PLP was proved to be a highly active deubiquinase/deISGylase and potent innate immune antagonist. After PLP knockout, viral fitness is significantly decreased and the suppression on host ubiquitination/ISGylation is largely reduced. Furthermore, host antiviral innate immune responses have been greatly upregulated post PLP knockout mutant infection. Our study underscores potential contributions of PLP domain in viral pathogenicity, and further provides an ideal example for how recombination shapes virus evolution.

In summary, studies in this dissertation highlight the critical roles of nidoviral PLPs-related proteins in host immunity manipulation and virus replication, and more importantly, potential links with viral pathogenicity and application in vaccine development.

The roles of papain-like protease-related proteins in viral replication and host immunity

by

Pengcheng Shang

B.S., Shandong Agricultural University, 2010
M.S., China Agricultural University, 2013

A DISSERTATION

submitted in partial fulfillment of the requirements for the degree

DOCTOR OF PHILOSOPHY

Department of Diagnostic Medicine and Pathobiology
College of Veterinary Medicine

KANSAS STATE UNIVERSITY
Manhattan, Kansas

2018

Approved by:

Major Professor
Dr. Ying Fang

Copyright

Abstract

Viral papain-like proteases (PLPs)-related proteins have been shown to be actively involved in host innate immunity manipulation and virus replication. In this dissertation, the research were focused on the elucidation of biological roles of nidoviral PLPs-related proteins in innate immunity suppression and viral RNA transcription regulation.

Porcine Respiratory and Reproductive Syndrome Virus (PRRSV) is the most prominent swine diseases worldwide. Understanding PRRSV pathogenesis and development efficient vaccines are highly required in swine industry. PRRSV nsp2-related proteins including nsp2 and two ribosomal frameshifting products-nsp2TF and nsp2N share the same N-terminal PLP2 domain. In chapter 2, nsp2TF and nsp2N were demonstrated to be critical for host innate immunity suppression at least through the PLP2 domain-mediated deubiquitination and deISGylation effects. The infection of nsp2TF/nsp2N knockout mutants significantly upregulated antiviral innate immune responses *in vitro*. Furthermore, manipulating the expression of nsp2TF/nsp2N could enhance innate and adaptive immunity in pigs, providing potential basis for modified live vaccine development.

In addition to the PLP2 domain of PRRSV nsp2-related proteins, the biological roles and biochemical nature of the poorly investigated long mysterious PLP2 downstream region was also characterized in Chapter 3. This long unknown region is also shared by nsp2-related proteins. At first, the hyper-phosphorylation nature of nsp2-related proteins was demonstrated. Physical features of this uncharacterized region was then delineated, including two intrinsically disordered hypervariable regions spaced by a structured inter-species conserved domain. One critical phosphorylated residues in the conserved domain were later proved to be of great importance in recombinant virus rescue and subgenomic RNAs accumulation. Collectively, our investigations

underline the pleiotropic effects exerted by nsp2-related proteins in virus life cycle and potential contributions with pathogenesis.

In Chapter 4, potential functions of PLP encoded by other nidovirus was also investigated. We discovered a unique cross-order recombination event, in which the chimeric picornavirus-enterovirus G expresses the PLP gene, homologous to torovirus (ToV) PLPs. Like other nidoviral PLPs, the recombinant ToV-PLP was proved to be a highly active deubiquinase/deISGylase and potent innate immune antagonist. After PLP knockout, viral fitness is significantly decreased and the suppression on host ubiquitination/ISGylation is largely reduced. Furthermore, host antiviral innate immune responses have been greatly upregulated post PLP knockout mutant infection. Our study underscores potential contributions of PLP domain in viral pathogenicity, and further provides an ideal example for how recombination shapes virus evolution.

In summary, studies in this dissertation highlight the critical roles of nidoviral PLPs-related proteins in host immunity manipulation and virus replication, and more importantly, potential links with viral pathogenicity and application in vaccine development.

Table of Contents

List of Figures

List of Tables

Acknowledgements

At first, I would like to express the most genuine appreciation to my major advisor-Dr. Ying Fang for all the guidance and support both academically and personally. I feel deeply indebted to Dr. Fang. She offered me the training opportunity in this top-end swine pathobiology laboratory. In the past five years, I have acquired unprecedented academic freedom, technical instructions, and more importantly, spiritual encouragements, without which any achievements would not be even possible. The five-year high-intensity training at all possible aspects in Dr. Fang's laboratory have become the milestone of my career life. I could never give enough credits for everything she has ever gave and taught to me. She has already set a role model about how to be a qualified and ambitious scientist and a better person. She has been always very supportive on my career goals. Well trained and equipped in this laboratory, I'm confident that I'm ready to step out and move up to the next level.

Besides my major advisor, I am also grateful to all of great advices and helps during my Ph.D study and job-hunting from dear committee members-Dr. Jodi McGill, Dr. Bob Rowland, Dr. Saurav Misra, and Dr. Zhilong Yang. In particular, I would like to thank Dr. Misra for all his persistent instructions. He is a passionate scientist, a patient instructor, and a helpful collaborator. I always feel being encouraged and inspired by the adventurous spirit and insightfulness in science he conveyed.

I would like to also express gratitude to all my lab mates with whom I have been enjoying work with. Really appreciate all the continuous supports and advices from Yanhua Li, Rui Guo, Fangfeng Yuan, Xingyu Yan, Russel Ransburgh, and Sailesh Menon. In addition, I would like to specially thank Dr. T. G. Nagaraja, Dr. M. M. Chengappa, Dr. Derek A. Mosier,

and other faculties and staffs in College of Veterinary Medicine for all the helps in course of my Ph.D degree.

Nobody are more important to me than family members, especially my parents and brother. Nothing and nobody could ever replace their unconditional love and endless supports, which have been with me all the time in the pursuit of Ph.D degree oversea.

Chapter 1 - Literature review

1.1. Introduction of PRRS and PRRSV

The order *Nidovirale* is classified into four known families: *Coronaviridae* and *Arterivirdae,* infecting vertebrates (mostly mammals), *Roniviridae* and *Mesoniviridae* infecting invertebrates (1-4). The family *Coronaviridae* is further divided into two subfamilies- *Coronavirinae* and *Torovirinae* (1, 4). The order *Nidovirales* contains a large group of viruses including several important human and animal pathogens with significant social and economic impacts (1, 4). For example, zoonotic coronaviruses (CoVs)- such as severe acute respiratory syndrome (SARS) CoV and Middle East respiratory syndrome CoV (MERS) caused episodes of severe respiratory infection in humans (1, 4). For the past three decades, porcine arterivirus- Porcine Reproductive and Respiratory Syndrome Virus (PRRSV) has been one of the most prominent pathogens threatening the swine industry (5-8).

Porcine reproductive and respiratory syndrome virus (PRRSV) is the etiological agent of Porcine Reproductive and Respiratory Syndrome (PRRS) (5-8). It is characterized by respiratory diseases in growing pigs and reproductive failure in sows (5-8) . PRRS was first recognized in the United States in the late 1980s, then in Europe in the early 1990s (8-12). Since then, PRRSV has rapidly developed into the leading pathogen with occasional outbreaks. It has caused nearly $650 million in annual economic loss for the swine industry in United States alone (8, 13).

As the member of the family *Arteriviridae* and the order *Nidovirales*, PRRSV contains an enveloped positive-sense (+) single-stranded (ss) non-segmented RNA genome of approximatly 15 kilo nucleotide in length, which includes 11 known open reading frames (ORFs) (14-16). Replicases-associated nonstructural proteins (nsps)- are encoded by ORF1a, ORF1b, and ORF1a'-TF (17) which occupy 5' proximal three-quarters of the genome (14-16). Downstream

ORF2a, ORF2b, ORF3, ORF4, ORF5, ORF5a, ORF6, and ORF7 encode viral structural proteins GP2a, E, GP3, GP4, GP5, GP5a, M, and N, respectively (14-16) (Fig. 1.1).

In the past nearly three decades, PRRSV was partitioned into two genotypes: genotype I (European, EU, genotype) and genotype II (North American, NA, genotype) (5-7, 18). In spite of similar clinical signs and concurrent emergences, the two genotypes display great divergence both genetically and antigenically sharing only about 56% identity at the genomic level (19, 20). The two PRRSV genotypes have been re-classified as two species: PRRSV-1 and PRRSV-2 (21).

Epidemiological investigation reveals a worldwide distribution of both species. PRRSV-1 is mainly endemic in Europe and PRRSV-2 predominantly circulates in North America and Asia (5, 6, 8). Since its discovery, PRRSV-2 has been frequently associated with severe outbreaks in swine populations on two continents, including the MN184-like virus outbreak in United States at 2001 (22), the catastrophic outbreak of highly pathogenic PRRSVs (HP-PRRSVs) in China at 2006 (23, 24), and the pathogenic NADC30-like strains emergence in China during 2013-2014 (25-32). Since 2014, occurrence of pathogenic PRRSV-2 infections have been frequently reported across swine farms in the United States. The epidemic variants were characterized as 1-7-4 pattern using the restriction fragment length polymorphism (RFLP) analysis on the highly variable ORF5 region (33, 34).

Pigs, including wild boars (*Sus scrofa*) and domestic pigs (*Sus scrofa domesticus*), are the natural hosts of PRRSV infection (8, 35). Swine are susceptible to several infection routes including intranasal, oral, intrauterine, vaginal, and vertical (transplacental) (8). Diseases caused by PRRSV infection are primarily the consequence of acute viremia and transplacental transmission (8). Clinical manifestations of PRRSV infection vary greatly among swine herds

and strains, ranging from asymptomatic to devastating outcomes (8, 36). Common clinical signs include high fever, anorexia, breathing difficulties, discoloring on skins of ear (blue ear) and vulva, lymphadenopathy, lung lesions, and abortion (8, 36).

PRRSV primarily infects subsets of monocyte-macrophage lineage which display two receptors- main receptor CD163 (cysteine-rich scavenger receptor) and accessory receptor CD169 (sialoadhesin, siglec-1) (8, 37). In addition to proteins including heparan sulfate, vimentin, CD151, DC-SIGN (dendritic cell-specific intercellular adhesion melecule-3-grabbing non-integrin; CD209), and siglec-10 were also identified as accessory receptors (37, 38). In PRRSV virions, minor glycoproteins-GP2/GP3/GP4 forms heterotrimer or GP2/GP4 heterodimer (36), interact with main receptor-CD163 (37, 39). Heterodimers of GP5/M linked by disulfide bonds were found to interact with accessory receptors (37, 40). Pulmonary alveolar macrophages (PAMs), pulmonary intravascular macrophages (PIMs), and macrophages in lymphoid tissues are the predominant cell subsets susceptible to PRRSV infection (8, 36). Therefore, viral RNAs and antigens are mainly observed in the lungs and lymph nodes/tonsils (8). In contrast, lymphoid organs serve as the primary sites for virus accumulation in stillborn and live-born pigs infected congenitally (8). Generally speaking, the highest viremia are achieved at 7 to 14 days post infection (DPI) in the lungs and lymph nodes (8, 15). After that, viremia quickly drop and become undetectable after four weeks for most infected pigs (8, 15). Following the acute infection stage, PRRSV develops into persistent infection in lymphoid tissues including the tonsils and lymph nodes (8, 15, 36).

PRRSV infection causes aberrant immunological phenotypes, characterized by poor and delayed responses in both innate and adaptive immunity (15, 16, 41-43). PRRSV has been demonstrated to employ diverse strategies to suppress host anti-viral innate immunity responses

(16). So far, seven nsps (nsp1α, nsp1β, nsp2, nsp2TF, nsp2N, nsp4, nsp11) and one structural protein (N protein) have been identified to function as interferon (IFN) antagonists, with acting mechanisms well reviewed in previous publications (16, 42). Our studies in this dissertation demonstrated the important roles of nsp2-related proteins, especially newly identified-nsp2TF and nsp2N, in innate immunity modulation. In PRRSV infected pigs, specific humoral responses against nsp1α, nsp1β, nsp2-related proteins, nsp7, all GPs, M, and N proteins could be vigorously detected immediately post infection (16, 41, 43). Nsps specific antibodies in particular last at least to 202 day post infection (dpi) (16). However, the generation of neutralizing antibodies is weak and delayed, which is considered as one of the major barriers in disease control (15, 16, 41-43). Due to essential roles in the development of specific immune responses, cell-mediated immune (CMI) responses is also believed to be critical for anti-PRRSV immunity (15, 16, 41-43). However, significance of CMI responses post PRRSV infection remains largely unclear (15, 16, 41-43). PRRSV specific CMI responses were observed to be highly variable in both acutely and persistently infected animals, without clear correlation with viral clearance (16, 41, 43). Peripheral $CD4^+$ T cells undergo a transient decrease at 3 to 7 dpi, and return to normal by 7 to 14 dpi (44, 45). The abundance of $CD8^+$ T cells have been frequently observed to increase after 4 to 5 weeks post infection (41, 43). A higher percentage of $CD8^+$ or $CD4^+CD8^+$ T cells were observed in infected lungs and lymphoid tissues (41, 43). Regulatory T (Treg) cells with inhibitory effect on $CD4^+$ T cells and $CD8^+$ T cells were found to be significantly induced (46). MHC class I and II molecules on the surface of virus-infected cells were also found to be downregulated (47-50).

1.2. Nidoviral RNA transcription strategy

For viruses with polycistronic (+) ssRNA genome, the synthesis of subgenomic RNAs (sgRNAs) as messager RNA (mRNA) is a widely adopted strategy to place downstream ORFs at the ribosome-accessible 5' end for the translation of 3'-proximal genes (51, 52). However, as independent subgenomic transcripts, the synthesis of sgRNAs would be more likely to be manipulated spatially, temporally, and quantitatively (51, 52).

In the order of *Nidovirales*, sgRNAs are responsible for the expression of 3'-proximal ORFs including both structural and accessory proteins (3, 53). All nidoviral sgRNAs share the same 3' end with parental full-length genomic RNAs (gRNAs) (3, 53). Furthermore, sgRNAs of arteriviruses and coronaviruses have uniform 5' and 3' ends with parental gRNAs. The 5' end of sgRNAs-leader sequence is directly transcribed from the 5' end of gRNA (3, 53). Ligation of apparent discontinuous sequence of sgRNAs has been proved to occur during the minus-strand RNA synthesis, rather than the post-transcriptional splicing (53). The discontinuous transcription of minus-strand (-) sgRNAs is the widely accepted model for explaining nidoviral sgRNAs synthesis (51, 53) (Fig. 1.2). In this model, (-) sgRNAs are discontinuously transcribed from full-length (+) gRNAs and/or longer (+) sgRNAs, then used as templates to continuously synthesize (+) sgRNAs (3, 53, 54).

Maintenance of the constant accumulation ratio between gRNAs and sgRNAs is crucial for nidoviral fitness (53). The nidoviral discontinuous transcription process has been demonstrated to be precisely regulated by both *cis*-acting and *trans*-acting factors (3, 53-56). The first recognized regulatory *cis*-acting factor is the short conserved AU-rich element-transcription-regulating sequence (TRS), including leader-TRS (L-TRS) and body-TRS (B-TRS) (3, 53, 54). L-TRS is present immediately downstream of the leader sequence within full-length (+) gRNA;

B-TRSs are found upstream of 3'-proximal ORFs (3, 53, 54). The discontinuous transcription is controlled by the base-pairing interaction between sense (+) TRS and antisense (-) TRS. The activities of the replication and transcription complex (RTC) will be attenuated at each B-TRS site and redirected to L-TRS by disrupting the (-) B-TRS of nascent (-) strand and (+) B-TRS on template base-pairing interaction and re-establishing the interaction with L-TRS. After template-switching, RTC will continue the transcription and synthesize (-) the leader sequence. Only the RTCs without any interruption at B-TRSs could transcribe a full-length (-) gRNA (3, 53, 54). The full-length genomic RNA production cycle of (+) gRNA to (-) gRNA to (+) gRNA is traditionally designated as replication, while the discontinuous synthesis of subgenomic RNAs is referred as transcription for differentiation (3, 53). Sequence conservation of B-TRS and the thermos-stability of duplex between (-) B-TRS and (+) L-TRS have been shown to be associated with the transcription of sgRNAs (3, 53-56). In addition, a hairpin structure found at 5' proximal arteriviral genome was shown to be critical in presenting L-TRS for the (-) B-TRS and (+) L-TRS duplex formation in discontinuous transcription (57, 58). Another known *cis*-acting RNA structure in regulating nidovirus discontinuous transcription was found during investigations of prototypical coronavirus-transmissible gastroenteritis virus (TGEV), in which two exceptional intragenomic, long-distance RNA-RNA interactions were proved to enhance the transcription of the most abundant N protein-coding sgRNA (54, 56, 59-61). The presence of these two exceptionally long-distance RNA-RNA interactions is able to attenuate transcription activities of RTC, promote the physical proximity of nascent minus strand with L-TRS, and thus can facilitate template switch (54, 56).

In addition to *cis*-acting RNA structures, key regulatory roles in the discontinuous transcription of several *trans*-acting factors have also been demonstrated. Nsp1 of equine

arterivirus (EAV) was demonstrated to function as a "transcription factor" controlling the abundance of sgRNAs by an intricate subdomain interaction network (62, 63). A mutagenesis study on the EAV helicase-nsp10 also highlighted its essential involvement in discontinuous sgRNA synthesis (64-66). In the investigation of another prototypic coronavirus-mouse hepatitis virus (MHV), host kinase GSK-3-mediated N protein in the phosphorylation state was proved to selectively manipulate coronaviral sgRNAs transcription (67). Interestingly, the phosphorylated N proteins were found to be able to recruit the host factor DDX1, which may promote B-TRS read-through to increase the production of longer sgRNAs and gRNA (67).

1.3. Ubiquitination and ubiquitination regulation on antiviral innate immunity pathways

Post-translational modification by ubiquitin (Ub), referred as ubiquitination, is universally present in almost every cellular activity. It modulate protein functions, localization, and turnover (68-70). The 8.6-kD Ub maintains conservation across eukaryotic organisms (68, 69). It adopts a compact β-grasp fold with a flexible C-terminal tail, which is covalently linked to substrate proteins (68, 69). Ubiquitin modification could be in a monomer, dimer or polymeric chain form (68, 69). Ubiquitination is a sequential catalytic process including three steps termed as activation, conjugation, and ligation. It is executed by three distinct classes of enzymes (68-71) (Fig.1.3). The ATP-dependent first step-activation is carried out by the ubiquitin-activating enzyme-E1, which links the Ub C-terminus to an active cysteine group of E1 by a thioester bond; secondly, Ub will be transferred to the Ub conjugating enzyme-E2 at the catalytic cysteine site. In the final step, E3 Ub ligase will eventually transfer the Ub moiety to a lysine residue substrate protein in the form of an isopeptide bond with Ub C-terminal glycine (68-71). Ubiquitination is a reversible process, antagonized by deubiquitinses (DUBs) encoded by hosts and pathogens (68,

69, 71) (Fig.1.3). If Ub *per se* serves as substrate, it leads to the formation of polymeric chain (68, 69). Seven different lysine residues (K6, K11, K27, K29, K33, K48, and K63) of Ub provide diverse linkage types. A N-terminal M1 residue of acceptor Ub could also be utilized to form a linear linkage (68, 69). Ub chains could be homogenous if the same residue in Ub is consistently modified in the chain elongation reaction (68, 69). Interestingly, a heterologous chain could also be formed by incorporating Ub moiety with alternative linkages (68, 69). Different physiological functions are achieved through diverse ubiquitination linkages. Currently, only the roles of K48-linkage in protein proteasomal degradation and the K-63 linkage in signaling transduction have been studied in detail (68-71). In recent investigations the biological roles of M1-linked linear ubiquitination in NF-κB activation and TNF-α signaling pathway have been gradually recognized (72-75). This head-to-tail-linked linear ubiquitination is produced by a E3 ligase complex-LUBAC (linear Ub chain assembly complex). It is composed by hemeoxidized iron-responsive element binding protein 2 Ub ligase-1 (HOIL-1), HOIL-1-interacting protein (HOIP) and SHANK-associated RH domain-interacting protein (SHARPIN) (72-75). So far, the human genome only encodes two E1 enzymes, but at least 38 E2 enzymes and, surprisingly, over 600 E3 enzymes (70). Given the diverse ubiquitination process, the realization that precise functional modulation requires that the right Ub linkage type should be correctly incorporated into intended substrate at accurate positions (70). Linkage specificity is mainly ensured by E2 Ub conjugating enzymes. In contrast, substrates are tightly selected by the highly diversified E3 Ub ligases (70).

As the front line to defend microbe invasion, innate immunity provides faster and less specific responses than adaptive immunity (70, 71, 76, 77). When innate immunity is activated, pattern-recognition receptors (PRRs) of immune and non-immune cells are utilized to detect microbial infection products pathogen-associated molecular patterns (PAMPs), as well as

damage-associated molecular patterns (DAMPs) released by damaged or stressed cells (70, 71, 76, 77). The PRR comprise diverse families including RIG-I-like receptors (RLRs), Toll-like receptors (TLRs), NOD-like receptors (NLRs), and DNA sensors such as cGAS, etc (70, 71, 76, 77). Activation of PRRs triggers signaling pathways to produce type I/III interferons and inflammatory cytokines/chemokines (70, 71, 76, 77). Post-infection cytokines and chemokines lead to the establishment of anti-infection state and inflammatory responses to recruit immune cells to infection or tissue damage site (70, 71, 76, 77).

Extensive investigations reveal that the activation of innate immune pathways is tightly regulated by ubiquitination and deubiquitination (70, 71, 75-77). Intracelluar viral RNA sensors-RLRs belong to DExD/H box helicase family, including two best known members-retinoic acid-inducible gene-I (RIG-I) and melanoma differentiation-associated protein 5 (MDA5) (78, 79). RIG-I and MDA5 have varied ligands preference with the recognition on short, 5' triphosphate uncapped double-stranded RNA (dsRNA) and long dsRNA, respectively (78, 79). RIG-I and MDA5 both harbor two tandem caspase activation and recruitment domains (CARDs) at N-terminal (78, 79). After ligand-binding, RIG-I and MDA5 will undergo oligomerization and interact with MASV on mitochondria or peroxisomes via CARD-CARD interaction (78, 79). Activation of MAVS initiates signaling cascades which converge with downstream components of other innate immunity pathways such as TLR and cGAS-sting pathway (76, 78-80). It has been well investigated that the activation of RIG-I is regulated by ubiquitination (70, 76, 79) (Fig. 1.4A). Upon RNA ligand binding, multiple sites of N-terminal CARDs domain of RIG-I will undergo activation-essential K63-linked poly-ubiquitination mediated by tripartite motif (TRIM) protein family member-TRIM25 E3 ligase (70, 76, 81). The K63-linked ubiquitination at c-terminal domain induced by another E3 ligase-Riplet (Ring Finger Protein 135, RNF135) is

also proven to be critical for RIG-I activation (70, 76, 82). Additionally, E3 ligases TRIM4 and MEX3C have also been shown to mediate the K63-linked polyubiquitination of RIG-I (76, 83, 84). However, the roles of K63-linked ubiquitination in MDA5 activation by chains remain largely uncharacterized (76, 83, 84). Consistently, as a potential negative regulation mechanism, the activation-related ubiquitination state of RIG-I could be reversed by host DUBs including Cylindromatosis (CYLD), ubiquitin-specific protease 21 (USP21), and USP4 (85-87). In addition to being modified by K63-linked polyubiquitin chain, RIG-I was reported to be degraded in a proteasome-dependent manner, which is mediated by E3 ligase RNF125 induced by K48-linked ubiquitination (88). Like RIG-I, the turnover of MDA5 was also found to be negatively regulated by TRIM13 and RNF125-mediated K48-linked ubiquitination (88, 89).

MAVS protein occupies the central position in RLR cascade (70, 76, 78, 79). Mitochondria and peroxisomes serve as platforms for immune signaling complex formation upon MAVS aggregation stimulated by the translocation of activated RIG-I and MDA5 (70, 76, 78, 79) (Fig. 1.4A). Upon virus infection, MAVS could be negatively regulated by K48-linked ubiquitination for proteasome-dependent degradation (70, 76). Known E3 ligases include TRIM25, mitochondria-located membrane-associated RING finger protein 5 (MARCH5), RNF5, RNF125, atrophin-1–interacting protein 4 (AIP4), and SMAD ubiquitination regulatory factor 1/2 (Smurf 1/2) (88, 90-94). Recently, TRIM31 was found to interact with MAVS and catalyze K63-linked ubiquitination at K10, K311, and K461 residue of MAVS, which promote MAVS aggregation and signaling transduction (95). However, the E3 ligase of known K63-linked ubiquitination of K500 of MAVS is still unclear (76, 96). For sustainable and adjustable innate immune responses TRIM25, the critical E3 ligase for RIG-I activation, is also reversibly

regulated by K48-linked ubiquitination and deubiquitination mediated by LUBAC and USP15, respectively (97, 98).

The TLR family comprise a group of type I transmembrane proteins, which respond to diverse PAMPs derived from viruses, bacteria, fungi, and parasites (76, 80, 99). Currently, ten human homologous genes (TLR1-10) have been discovered (76, 80, 99). For detecting virus invasion, TLR7/8 and TLR3 are activated by ssRNA and dsRNA respectively. TLR9 reacts with unmethylated CpG dinucleotides DNA ligand (76, 80, 99). In addition TLR2 and TLR4 could sense structural proteins of measles virus and respiratory syncytial virus, respectively (80, 99). As type I transmembrane proteins, TLRs share a consensus structural pattern including a ligand-binding ectodomain composed by leucine-rich repeats (LLR), a transmembrane segment, and a cytoplasmic Toll/IL-1R (TIR) domain (76, 80, 99). Upon stimulation, TIR domains dimerize and serve as a scaffold to recruit downstream adaptors myeloid differentiation primary response protein 88 (MyD88) or TIR domain containing adaptor protein inducing IFNβ (TRIF), which also harbor homologous TIR domains for the interaction with TLRs (76, 80, 99). Adaptors engagement could respectively initiate the assembly of two high-order protein complexes-the "Myddosome" mediated by MyD88 and "Triffosome" mediated by TRIF (76, 80, 99) (Fig. 1.4B). MyD88 recruits the IL-1R-associated serine/threonine kinases (IRAKs) to transduce TLRs activation signal to tumor necrosis factor receptor-associated factor 6 (TRAF6), then to activate inhibitor of nuclear factor κ-B (IκB), kinase α/β/γ (IKK α/β/γ), and TGFβ-activated kinase 1 (TAK1), which eventually induces the nuclear translocation of NF-κB and pro-inflammatory gene transcription (76, 80, 99) (Fig. 1.5). In contrast, TRIF transduce signals downstream through TRAF3 to IKKε and TANK-binding kinase-1(TBK1), which activate and stimulate the nuclear translocation of IFN-regulatory factors 3/7 (IRF3/7) for the induction of type I interferon

genes transcription (76, 80, 99) (Fig. 1.5). Among all the TLRs, only TLR3 will transduce signaling through MyD88-dependent pathway; TLR4 could activate both MyD88- and TRIF-dependent pathways (76, 80, 99).

Consistent with the RLRs pathway, the biological fate of critical molecules in TLRs pathway are also carefully controlled by ubiquitination (70, 71, 76, 80, 99) (Fig. 1.4B). The turnover of signaling transducers are modulated by K48-linked ubiquitination. E3 ligase RNF216 (Triad3A) was identified to mediate the K-48 linked ubiquitination of TLR3, 4, 5, and 9 (100). Key adaptor TRIF was found to be targeted for K48-linked ubiquitination by E3 ligase WW domain-containing protein 2 (WWP2) (101). The K48-linked polymeric chains on MyD88 is conjugated by another E3 ligases-Smurf1/2 and neuregulin receptor degradation protein 1 (Nrdp1) (102, 103). Nrdp1 was also found to mediate the K63-linked polyubiquitination of TBK1 for the activation of IRFs (103). Therefore, Nrdp1 with dual roles is believed to coordinate the balance of two TLRs downstream pathways by dampening the pro-inflammatory responses and enhancing interferon responses (103). Despite the negative modulatory effects of K48-linked ubiquitination, K63-linked ubiquitination could play positive roles in signaling transduction (70, 76). IRAK1 can be modified by Pellino E3 ligase family members or E3 ligase TRAF6 (104). In the TRIF-dependent pathway branch, RIP1 was also found to be conjugated with K63-linked polyubiquitin chain by Pellino 1 (105).

PRRs ligand-binding signals are conducted through central adaptors MAVS and TRIF/MyD88 and converge at common downstream molecules-TRAF3 and TRAF6, which eventually result in the nuclear translocation of transcription factors-IRF3/7, NF-κB, and AP-1 (76, 78, 80, 99) (Fig. 1.5). E3 ligases-TRAF6 and TRAF3 can induce auto-ubiquitination, providing scaffold platforms for downstream molecules assembly. The K63-linked auto-

ubiquitination of TRAF6 leads to the sequential recruitment of the TAK1/TAB2/TAB3 complex and then the IKKα/β/γ complex to activate IκBα by phosphorylation (76, 78, 80, 99). TRAF6 is also modified by K48-linked ubiquitination and degradation by E3 ligase TRIM38 to prevent excessive NF-κB responses (70, 71, 76). Several cellular DUBs including A20, CYLD, and the OTU deubiquitinase 2 (OTUB2) are able to counteract the K63-ubiquitination of TRAF6 (106-110). K48-linked ubiquitination mediated proteasome-dependent degradation has been identified to be essential for NF-κB activation (70, 71, 76, 80, 99). IKKβ phosphorylates and activates NF-κB inhibitor-IκBα, which further recruits E3 ligase $SCF^{\beta TrCP}$ for K48-linked ubiquitination (111, 112). The proteasome-dependent degradation of IκBα release the suppression on NF-κB (70, 76, 80, 99).

The auto-catalyzed K63-linked polymeric chain of TRAF3 also recruits IKKγ (NEMO), which further binds a complex composed by TANK and TBK1/IKKε (70, 71, 76). Kinase complex TBK1/IKKε then phosphorylate type I interferon transcription factors-IRF3 and IRF7 (70, 71, 76). K48-linked ubiquitination-mediated by E3 ligase of RNF216 (Triad3A) was also reported to specifically module the turnover of TRAF3 in order to avoid excessive antiviral genes expression (113). Similar to the TRAF6, K63-linked auto-ubiquitination of TRAF3 is also removed by several host DUBs, such as deubiquitinating enzyme A (DUBA), OTUB1, ubiquitin carboxyl-terminal hydrolase L1 (UCHL1), and OTUD7B (OTU domain-containing protein 7B) (109, 114-116). Downstream TBK1 was also found to be ubiquitinated in K63-linked manner by E3 ligases including Mind bomb 1/2 (MIB 1/2), Nrdp1, and TRAF3 (76, 103, 117). The K63-linked ubiquitination on TBK1 is essential for kinase activity (70, 76). Conversely, its K63-linked ubiquitination can be antagonized by DUBs such as USP2b, CYLD, and A20 (85, 118, 119). Furthermore, TBK1 was also found to be destabilized by E3 ligases DTX4 and TRAF-

interacting protein (TRIP) (120, 121). As a negative feedback mechanism, IRF3 and IRF7 are also targeted by K48-linked ubiquitination mediated proteasome-dependent degradation. HOIL-1 (RBCC protein interacting with PKC1, RBCK1), TRIM21, and RAUL (RTA-Associated Ubiquitin Ligase) serve as E3 ligases of IRF3 (122-124). TRIM21 and RAUL were identified as E3 ligase for the K48-linked ubiquitination of IRF7 (124, 125). As a critical kinase utilized for both NF-κB and IRF3/7 activation, the activities of NEMO are under the tight regulation of ubiquitination (70, 71, 76). NEMO has been found to be ubiquitinated in diverse forms including K27-linkage, K29-linkage, and M1-linkage, which are mediated by E3 ligases-TRIM23, TRAF7, and LUBAC, respectively (126-128). In contrast to the enhancement role of TRIM23-mediated ubiquitination in antiviral responses, K29-linked and M1-linked ubiquitination on NEMO serve as negative regulation mechanism (127, 128). Interestingly, K29-linked ubiquitination seems to mediate the lysosomal degradation of NEMO (127). Studies reveal that linear ubiquitination mediated by LUBAC have opposite roles on the involvement of NEMO in both IRF3/7-dependent and NF-κB-dependent pathways (72, 74, 75, 128). On the one hand, it promotes the interaction with TRAF3 and disrupts the association of MAVS-TRAF3 complex, and therefore specifically inhibits the IRF3-dependent pathway (128, 129). In contrast, the linear ubiquitination also facilitate the activation of NF-κB-dependent pathway possibly by stabilizing the interaction between TAK1/TABs with IKK complexes (128). In addition to the direct Ub conjugation, NEMO also has the ability to bind K63-linked or mixed linked diUb, and M1-linked Ub chain, which are essential for NF-κB activation (130-132).

1.4. Roles of ubiquitin-like molecule-ISG15 in antiviral innate immunity

When facing pathogen invasion, the expression of type I/III interferons will elicit hundreds of downstream interferon-stimulated genes (ISGs) as a counteraction in which an

ubiquitin-like molecule-ISG15 is abundantly and rapidly induced (133-136) (Fig. 1.6). ISG15 contains two ubiquitin-like domains, with ~30% amino acid (aa) identity to ubiquitin, spaced by a short hinge region (133-136). ISG15 is firstly expressed as a 17 kDa precursor form, and then rapidly processed into mature 15 kDa protein via protease cleavage on the c-terminal LRLRGG motif, which is identical to the c-terminal tail of Ub (133-136). ISG15 is covalently conjugated on target substrates with the LRLRGG motif through an ubiquitination-like three-step catalytic cascade-ISGylation (133-136) (Fig. 1.6). ISGylation utilizes UBE1L as E1 activating enzyme, UbcH8 (human) or UBCM8 (mice) as E2 conjugating enzyme, and HERC5 (human) HERC6 (mouse) as main E3 ligase (133-136). HERC5 was identified to be physically associated with polyribosomes, indicating the model that ISGylation may occur in a co-translational manner on newly synthesized proteins (134-136). Similar to ubiquitination, ISG15 modification can also be reversed by deconjugating enzyme-USP18, a process referred as deISGylation (133-136).

ISG15 was initially identified from type I interferon-treated cells (134-136). Moreover, ISG15, conjugation enzymes, and USP18 are all induced by interferon treatment or viral infections (133-136). Therefore, ISG15 is believed to be a *bona fide* antiviral protein, limiting viral replication in a conjugation-dependent manner (133-136). *In vitro* studies showed viral infection can be inhibited in cell with ISG15 overexpression or knockdown (134, 136, 137). There has been more evidence from *in vivo* studies based on knockout mice. ISG15 or UBE1L knockout mice were found to be more susceptible to influenza A virus (IAV), IBV, Sindbis virus, and coxsackievirus B3 virus (CVB3) infection (133-137). Mice knocked in by USP18 with disrupted deISGylation activity have a phenotype with enhanced ISGylation and resistance to IBV and vaccinia virus infection, suggesting the conjugation-dependent antiviral roles of ISG15 (134, 137). Further investigations revealed that ISGylation has direct inhibitory effects on

multiple steps in virus replication (134). Whether ISGylation substrates belong to viruses or hosts is still under active investigation (133-136). In virus-infected cells, viral proteins are the dominant newly produced proteins, which may constitute substrates for ISGylation (134). So far, proteins of both RNA and DNA viruses have been identified to be modified by ISG15 (134-136). For example, the first identified viral substrate was NS1 protein of IAV, which has diverse roles in virus replication and innate immunity suppression (134-136). NS1 is able to inhibit the induction of type I interferons and the activation of protein kinase R (PKR), selectively boost viral mRNA translation, and interfere with host mRNA processing (134, 138, 139). ISGylation modification on NS1 inhibits the nuclear translocation by disrupting interaction with importin-α. Furthermore, ISGylation disrupts the interactions of NS-1 proteins with several binding partners including Protein kinase R (PKR), U6 small nuclear RNA (snRNA), and dsRNA, therefore interferes the immune evasion functions of NS-1 proteins (133-136). Another study on the IBV nucleoprotein (NP) showed that modified NP proteins function as dominant-negative inhibitor for oligomerization, which is required for the formation of viral ribonucleoprotein (vRNP) and RNA synthesis (134, 136). Studies about extracellular unconjugated form of ISG15 proposed that it may act as an immunomodulatory cytokine or chemokine to promote NK cell proliferation, dendritic cell maturation, and neutrophil recruitment (133, 134). Binding with the specific receptor-lymphocyte function-associated antigen 1 (LFA1) leads to the release of IFNγ and IL-10 in IL-12-primed cells (133, 134). Exact impacts of extracellular unconjugated form in viral infection remains unclarified (133, 134).

Solid evidences highlighting the significance of ISGylation in antiviral responses stem from increasing research to identify viral proteins targeting ISGylation pathway (133, 134). Interestingly, the counterpart of IAV NS1 protein-NS1 protein of IBV was the first identified

viral factor to antagonize ISGylation pathway (133, 134). NS1 of IBV is able to directly bind human and primate ISG15 (not murine ISG15) and disrupt its interaction with the E1 activating enzyme-UBE1L (133, 134). In addition, NS1 sequesters ISGylated NP to prevent the miscorporation of modified NPs into vRNPs, thereby avoiding interference on viral RNA synthesis (134). The most famous viral factor antagonizing ISGylation process is deconjugating enzymes encoded by nidoviruses, nairoviruses, and picornaviruses (134, 140, 141) which will be summarized later.

1.5. The deubiquitination and deISGylation functions of nidoviral papain-like proteases-related proteins

As stated previously, ubiquitination has broad regulatory impacts on host antiviral innate immune pathways. Ubiquitination is a reversible process, in which conjugated ubiquitin(s) could be removed from substrates by DUBs. This mechanism has been widely exploited by viruses, which encode viral DUBs to disrupt host ubiquitination-dependent innate immune pathways, and thereby, to promote virus replication (140, 141). Virus-encoded DUBs have been identified and characterized from both RNA viruses (nidoviruses, picornaviruses, nairoviruses and tymoviruses) and DNA viruses (adenoviruses and herpesviruses) (134, 140, 141) (Fig. 1.7). Here I will only focus on the papain-like proteases (PLPs) encoded by members of *Nidovirales*, which have been widely recognized as DUBs and deISGylases with innate immune modulatory functions (140, 141).

Among all the PLPs in *Coronaviridae*, the PL^{pro} encoded by nsp3 of severe acute respiratory syndrome (SARS) CoV (SARS-CoV) and Middle East respiratory syndrome (MERS) CoV (MERS-CoV) are the ones most investigated (142). The first known function of SARS-CoV PL^{pro} is for the proteolytic cleavage of nsp1-nsp2-nsp3-nsp4 junctions in polyproteins (143).

PL^{pro} was found to recognize a consensus motif-LXGG which is homologous to the Ub c-terminus RLRGG motif (144, 145). Furthermore, structural modeling analysis pinpointed the structural similarity between SARS-CoV PLpro and host DUB herpesvirus-associated USP (HAUSP), indicating that the viral enzyme may also adopt a papain-like fold (146). Collectively, it led to the hypothesis that SARS-CoV PL^{pro} may act as both DUB and deISGylase (146). Later, the DUB activities targeting K48-/K63-linked polyUb and deISGylation activities were confirmed by *in vitro* characterizations (147, 148). It has been demonstrated that PL^{pro} is able to directly disrupt IRF3 activation and suppress the transcription activity driven by NF-κB-responsive promoter and dsRNA sensors (RIG-I/MDA5/TLR3)-mediated IFN-β promoter (149, 150). The crystal structure of SARS-CoV PL^{pro} is consistent with the initial modeling result which adopts a right hand like structure including thumb, palm, and finger subdomains (151-153). Moreover, the biochemical nature and structural basis of the interaction between SARS-CoV PL^{pro} and substrates have been elucidated by unveiling the binding interface with Ub and human/murine ISG15s (153-156). Consistent with SARS-CoV PL^{pro}, MERS-CoV PL^{pro} has a similar role in viral replicase polyprotein proteolytic processing (157, 158). MERS-CoV PL^{pro} was found to possess global deconjugation effects toward ubiquitination and ISGylation from cellular substrates in cell culture (157-160). *In vitro* de-conjugation assay showed that MERS-CoV PL^{pro} displays cleavage activities toward mono Ub, K48-, and K63-linked polyUb, K6-/K11-/K29-/K33-linked diUb, and ISG15 (157, 159, 161-163). Furthermore, its innate immune suppression effects were confirmed in IFN-β promoter-based dual luciferase assay (157-160). Similar to SARS-CoV PL^{pro}, MERS-CoV PL^{pro} also has a right hand like conformation including thumb/palm/finger subdomains (159, 164). Mutation on one residue (V1691R) at the interface could selectively only interrupt the interaction between with Ub to abolish DUB activities,

without disrupting the basic polyprotein cleavage (159). Expectedly, DUB-deficient PL^{pro} was unable to suppress the transcription of IFN-β promoter (159). Successfully decoupling two distinct functions of PL^{pro} helps decipher the roles of DUBs and deISGylation in pathogenesis in virus infection context and provides basis for potential genetically modified live vaccine (MLV) development (159). In additional to the two representative proteases of SARS-CoV and MERS-CoV, PLPs encoded by other coronaviruses including the PLP2 of human coronavirus (HCoV) NL63, PLP2 of mouse hepatitis virus (MHV), PLP2 of porcine epidemic diarrhea virus (PEDV), PLP1 of transmissible gastroenteritis coronavirus (TGEV), and PL^{pro} of infectious bronchitis virus (IBV) have been characterized (140, 141). Consistently, three functional roles of these coronaviral PLPs including the primary involvement in polyprotein proteolytic processing, DUB/deISGylation, and innate immunity suppression have been described (140, 141). Functions of torovirus PLP (ToV-PLP) have been recently characterized by our research team due to a rare cross-order recombination event (165). An enterovirus G (EVG) was identified to contain a torovirus (*Torovirinae, Coronaviridae*) PLP gene insertion between the 2C and 3A junction, flanked by two potential $3C^{pro}$ cleavage sites (165). Structural modeling revealed that the protein encoded by the foreign gene may adopt a minimal PLP core domain, leading to the hypothesis that this protein may also possess DUB/deISGylation activities (165). Ectopic expression confirmed the strong global deconjugation effect on host substrate ubiquitination and ISGylation of ToV-PLP in cell culture. Furthermore, *in vitro* characterization assays reveal robust cleavage preference towards K48/K63-linked polyubiquitin chains and ISG15 precursor, and modest activity on M1-linked linear polyubiquitin chain (165). As expected, ectopically expressed ToV-PLP showed strong innate immunity suppression effect which is further confirmed by virus infection study mediated by ToV-PLP knockout recombinant virus (165). Moreover, PLP

knockout largely abolished the DUB/deISGylation effect of wild-type virus in infected cells and greatly decreased viral fitness (165). Our study provides a novel example about how recombination drives virus evolution by acquiring an innate immunity antagonist through the cross-order recombination, and further underscores the importance of viral DUB/deISGylase in virus life cycle (165).

The PLP2 domain of arterivirus nsp2-related proteins have also been identified as a potent DUB/deISGylase (140, 141). Similar to the coronaviral PLPs, the first recognized function of arteriviral PLP2 domain is the proteolytic cleavage on nsp2-nsp3 junction in polyprotein processing (166, 167). The PLP2 encoded by prototypical arterivirus-equine arterivirus (EAV) belongs to a novel ovarian tumor protease (OTU)-like superfamily of cysteine proteases (168-170). Ectopically expressed EAV PLP2 resulted in global decrease of both Ub and ISG15 conjugates in cell culture (171, 172). The *in vitro* cleavage activities towards K48/K63-linked polyubiquitin chains confirmed that EAV PLP2 acts as *bona fide* DUB (171). Moreover, EAV PLP2 also possess inhibitory effects on the transcription of NF-κB and IFN-β promoter (171, 172). The ubiquitination of RIG-I was found to be suppressed by ectopically expressed EAV PLP2 (171). The crystal structure of EAV PLP2 bound with Ub revealed a remarkably compact OTU fold, including an unprecedented C4 zinc finger (169, 170). The polyprotein processing function and DUB activities of EAV PLP2 could be decoupled by selectively disrupting the Ub-binding interface (169). Mutant PLP2 showed attenuated inhibition effects on IFN-β promoter activation (169). Moreover, DUB-negative mutant virus infection significantly upregulated host innate immune responses, which supports the direct association of viral DUB with host antiviral innate immunity (169).

The PRRSV PLP2 domain is shared by three nsp2-related proteins-nsp2 and two newly identified isoforms-nsp2TN and nsp2N, which are generated by nsp1β-transactivated programmed ribosomal frameshifting mechanism discovered by our team (17, 173-175). In studies performed by our team and other groups, the ectopically expressed PRRSV-1 PLP2 could lead to a significant decrease of Ub and ISG15 conjugates in cultured cells (171, 172, 176, 177). We found that PRRSV-1 PLP2 domain could interfere the K48-linked polyubiquitination mediated proteasomal degradation of IκBα in order to suppress NF-κB activation and translocation (177). Interestingly, RIG-I ubiquitination could be greatly inhibited by ectopically expressed PRRSV-1 PLP2, but not PRRSV-2 PLP2 (171). We demonstrated that the PRRSV-1 PLP2 domain acts as a *bona fide* DUB against K48-linked polyubiquitin chain in the *in vitro* deconjugation assay (177). The cleavage preference of PRRSV-2 PLP2 domain on diUb was later described (178). Results revealed that PLP2 domains of highly pathogenic PRRSV (HP-PRRSV) and low pathogenic PRRSV (LP-PRRSV) are all able to cleave seven types of linked diUb but not a linear one; HP-PRRSV PLP2 is more active towards K63-linked diUb than LP-PRRSV PLP2 (178). However, whether PRRSV PLP2 domain is a genuine deISGylase is still controversial since purified prokaryotically expressed HP-/LP-PRRRSV PLP-2 failed to display detectable cleavage activities towards diverse ISG15 substrates (178). Given that the PLP2 domain is harbored by three nsp2-related proteins, the biological roles of PLP2 domain in the diverse context of full-length proteins need to be described in detail. Our recent study characterized the DUB and deISGylation activities of PRRSV-2 nsp2-related proteins, which revealed significant inhibitory effects on Ub and ISG15 conjugates in cell culture (179). This raised the question about how exactly PRRSV PLP2 antagonizes host ISGylation reaction. In the ectopic expression system, PLP2 domain alone and nsp2N seem to have higher inhibitory effects

on host ubiquitination and ISGylation than nsp2 and nsp2TF (179). In the dual luciferase assay driven by IFN-β promoter, PRRSV nsp2-related proteins and PLP2 domain exhibited strong suppression on the reporter gene transcription. Moreover, the antagonism effect on of nsp2 and PLP2 could be largely abrogated by inactivation of catalytic sites. In contrast, catalytic mutants of nsp2TF and nsp2N still showed robust suppression on reporter gene expression, suggesting that regions downstream of PLP2 in nsp2TF/nsp2N also have to contain innate immunity inhibition activities through unknown mechanism(s) (179). To assess whether the innate immune suppression effect exhibited by overexpressed nsp2TF/nsp2N reflect the actual circumstances of virus infection context, nsp2TF/nsp2N knockout mutants were generated which have attenuated growth phenotype both *in vitro* and *in vivo* (179). Immune gene expression profiling both in infected permissive cell line and primary macrophages showed that nsp2TF/nsp2N knockout mutant infections could greatly upregulate host innate immune responses more than wild-type virus (179). In the *in vivo* characterization, knockout mutant infections could consistently upregulate host innate immune responses as indicated by earlier serum IFN-α production and enhanced NK-mediated cytotoxicity. T cell-mediated adaptive immunity was also augmented in nsp2TF/nsp2N knockout mutants infected pigs. The results in the in vivo characterization underline the important immunity modulation effects of frameshifting products-nsp2TF/nsp2N (179).

1.6. Phosphorylation and nidoviral phospho-proteome

Phosphorylation is the most universal and best-studied post-translational modification (PTM) form (180-184). Protein phosphorylation is catalyzed by protein kinases through transferring the ATP γ-phosphate to serine, threonine, or tyrosine residues of target proteins (180-184). Phosphate on substrate proteins could then be removed by phosphatases (PPs) (180-

184). Phosphorylation has profound biological impacts on substrate proteins by inducing allosteric conformational change or altering protein-protein interactions (180-184).

Phosphorylation is known to be intimately involved in the modulation of every cellular processes (180-184). As intercellular pathogens which replicate exclusively in live cells, viruses are able to manipulate host signaling pathway regulated by phosphorylation and have acquired the capacities to utilize host phosphorylation machinery to modify viral proteins (185, 186). Phosphorylation events on viral proteins regulate virus replication and control host immune responses (185, 186). Understanding the roles of phosphorylation in the virus life cycle sheds light on the development of therapeutic measures and genetically modified live vaccines (MLVs). So far, investigation of the nidoviral phospho-proteome research has been limited to coronaviral and arteriviral nucleocapsid (N) proteins (187-189). Primary function of coronaviral N proteins is to package viral genomic RNA into ribonucleoprotein complexes (188). N proteins of representative coronaviral species including; MHV, IBV, TGEV, and SARS-CoV, are shown to be phosphorylated (187, 188, 190-198). The phosphorylation state of IBV N protein regulates the binding affinity with viral leader sequence suggesting potential roles of phosphorylated N in discontinuous transcription regulation (193, 196). Mutations on IBV N proteins phospho-sites caused reduced recombinant virus rescue (193). Phosphorylation of MHV N protein mediated by host GSK3 kinase may affect conformational transitions and regulate the interaction with DDX1 helicase in order to adjust the sgRNAs discontinuous transcription (67). Phosphorylation broadly modulates biological activities of SARS-CoV N protein including host cell translation inhibition, self-oligomerization, and translocation to stress granules (190, 192, 194, 197, 199, 200). Shuttling of SARS-CoV N protein between nucleus and cytoplasm is regulated by host 14-3-3 proteins whose interaction with partners is also phosphorylation-dependent (192). Like the

abovementioned coronaviral N proteins, N protein of EAV and PRRSV is also phosphorylated (16, 201-203). However, the specific functional significance of N protein phosphorylation in the arteriviral life cycle is poorly understood (16, 201, 202). Phosphorylation of nidoviral proteins other than the N proteins have not been investigated systematically and remain largely uncharacterized.

1.7. Intrinsically structural disorder and viral disordered proteins

From the traditional point of view, the realization of protein functions heavily rely on a well-folded three-dimensional structure (204-207). Unstructured regions within proteins were traditionally viewed as passive linker of structured domains (204-207). However, two decades' efforts bring the unstructured polypeptide segments within proteins out of the shadows and highlight their important biological significance under physiological conditions (204-207). Polypeptide segments with less likelihood to form a defined 3D structure are named as intrinsically disordered regions (IDRs); proteins with entirely disordered sequence are referred to as intrinsically disordered proteins (IDPs) (204-207). IDRs and IDPs are highly prevalent in eukaryotic functional proteome (204-207). It has been estimated that about 44% of human proteins contain IDRs over 30 aa length (204-207). The typical sequence signature of IDRs/IDPs is the biased amino acid composition-low presence of bulky hydrophobic residues and high proportion of polar and charged residues, causing less hydrophobic effects to form stable hydrophobic core (204-207). Hence, IDRs/IDPs generally are unable to fold independently under native unbound conditions and usually undergo disorder-to-order transition after binding with partners (204-207). IDRs/IDPs exist as dynamic ensembles of transient and heterogeneous conformations with rapid interconversion (204-207). Therefore, IDRs/IDPs carry out functions in a variety of cellular processes through a different manner compared with classical structured

globular proteins (204-207). According to investigation on IDRs in proteins with known functions, the functionality of IDRs/IDPs could be further categorized into six different classes, including entropic chains, display sites, assemblers, chaperones, effectors, and scavengers (204-207). Entropic chains typically include flexible linkers or spacers with disordered structure, which allow relative independent movement of domains (204-207). Loose conformational constraints of IDRs/IDPs encourage the exposure of PTM motifs and facilitate easy access of proteins which introduce and read the PTMs (204-207). Transient binding of IDRs in chaperones with misfolded substrates may both induce the reversible local folding of IDRs and the unfolding-to-refolding conversion of substrate in an ATP-independent manner (204-207). Intrinsic disorder is a common structural feature for hub proteins in the protein-protein interaction (PPI) network (204-207). Open and versatile structures facilitate IDRs/IDPs to act as assemblers or scaffolds for high-order complexes formation by offering large binding interface with less steric hindrance (204-207). It has been know that IDRs are highly prevalent in both RNA and protein chaperones even though the molecular mechanism of disordered chaperones remain largely unclear (204-207). Structural flexibility possibly provides certain advantages for disordered chaperones in rapid searching and broad matching with binding partners (204-207). In addition, IDRs/IDPs could also act as effectors to modulate the activities of binding partners, or scavengers to store and neutralize small ligands (204-207).

Theoretically, IDRs/IDPs could have faster evolutionary rates than structured domains/proteins due to less purifying selection pressure in structure maintenance (204-208). However, IDRs/IDPs also exhibit diverse evolutionary characteristics (204-208). A yeast comparative genomics study revealed that IDRs could be classified into three biologically distinct phenomena: flexible disorder with conserved disorder propensity *per se* but fast

changing aa sequences, constrained disorder with both conserved disorder propensity and aa sequence, and non-conserved disorder (206, 209). Gene ontology enrichment analysis revealed a clear functional dichotomy between flexible and constrained disorder (206, 209). Flexible disordered regions display the classical disorder characteristics and are more involved in regulation-related activities such as cell cycle and signaling transduction (206, 209). Flexible disordered residues are commonly found to localize on exposed loops, which may facilitate the presentation of linear motifs for signaling partners (206, 209). In contrast, constrained disordered residues are enriched in proteins involved in biogenesis including ribosome translation, lipid metabolism, and protein folding. (206, 209).

Structurally disordered proteins are more commonly found in viral proteomes, especially for RNA viruses (206, 210). Extremely compact genomes of RNA viruses intrinsically require the multi-functionality of viral proteins, which could be endowed by flexible disordered structure (206, 210). In addition, the disorder propensity could be more resistant to deleterious mutations introduced by the transcription error of low-fidelity RNA polymerase (206, 210). Structural disorder is widely present in viral structural, nonstructural, and accessory proteins. Here, I will present examples of two well-studied disordered nonstructural proteins encoded by RNA viruses, which inspire our current and future investigations.

Hepatitis C virus (HCV) NS5A is a 447−466 aa protein with known IDRs (211-213). NS5A has an ER membrane-association amphipathic helix at N-terminal followed by three structurally distinct ectodomains-domain 1/2/3 (D1/2/3) (211-213). Three domains are separated by two low-complexity sequences, (LCS) I and II (211-213). NS5A-D1/D2 was shown to play important roles in RNA replication and NS5A-D3 is associated with particle assembly (211-213). The highly conserved NS5A-D1 has a stable structure with a novel zinc-binding motif and

a disulfide bond (211-213). NS5A-D1 adopts a homodimer with claw-shaped conformation which is proposed to be viral RNA binding (211-213). In contrast, the variable NS5A-D2/D3 are demonstrated to be highly disordered (211-213). The conformational flexibility of disordered NS5A-D2/D3 is believed to serve as a potential structural basis as hub protein for PPI network development (211-213). NS5A-D2 interacts with RNA-dependent RNA polymerase (RdRp)-NS5B and host innate immune receptor-PKR (211-213). NS5A-D2 is able to inhibit PKR activation and subsequent eIF2α phosphorylation (211-213). NS5A-D2 is able to tolerate large deletion without detectable inhibitory effects on replication and assembly (211-213). Both NS5A-D2 and NS5A-D3 are both found to mediate with the critical interaction with host factor-cyclophilin A (CypA), forming a membrane-associated complex with NS5A and NS5B for RNA transcription and replication (211-214). LCS-2 is a proline-rich region including two class II PxxP motifs (PP2.1 and PP2.2) and class I motif (PP1.2) (211-213). The highly conserved PP2.2 motif is able to interact with a group SH3 domain-harboring Src kinases including Fyn, Lyn, Lck, Hck,, and the SH3 domains of the adaptor proteins Grb2 and Bin1 (211-213). NS5A is expressed as a phosphoprotein with a hyper-phosphorylation and hypo-phosphorylation form (211-213). Host kinase casein kinase Iα (CK Iα) mediates the hyperphosphorylation of LCSI, which is key to the localization of NS5A to lipid droplets (LD)-associated low-density membranes (REF). The phosphorylation of NS5A-D3 mediated by CK II is required for HCV core protein interaction and for particle assembly.

Convincing evidence for the correlation between structurally disordered hypervariable region and virus evolution and/or pathogenesis comes from the nonstructural protein 3 (nsP3) of alphaviruses (215-217). Alphavirus nsP3 protein is critical for formation of viral replication complexes (vRCs) and regulation of minus-strand and subgenomic RNA synthesis (215-217). At

the c-terminal of nsP3 there is a ~200 residue-long hypervariable domain (HVD) that is partially resistant to deletions and insertions (215-217). Like HVRs of PRRSV nsp2-related proteins, the HVD of alphaviruses is largely intrinsically structurally disordered (215-217). Furthermore, it is also hyper-phosphorylated and enriched with functional motifs including an SH3 domain-binding PXPXPR motif that interacts with amphiphysins, and a Src homology 2 (SH2) domain-binding YXXM motif that interfaces with the PI3K-Akt-mTOR pathway (215, 217). Moreover, HVD repeat motifs mediate direct binding to critical host stress granule (SG) proteins including G3BP1/2 and/or FXR family proteins (215-217). The direct effect of these interactions is the disassembly of SGs (215-217). Apart from SGs inhibition, G3BPs and/or FXR proteins are recruited as important factors in vRCs assembly (215-217). The replication of Old World alphaviruses including Chikungunya virus (CHIKV), Semliki Forest virus (SFV), and Sindbis virus (SINV) heavily depends on the interaction with G3BPs (215-217). In contrast, the New World alphavirus, Venezuelan equine encephalitis virus (VEEV), uses FXR family proteins for efficient replication (215-217). Recent studies on Eastern equine encephalitis virus (EEEV) revealed a dual interaction of G3BPs and FXRs with nsP3 caused by co-existing binding motifs in the nsP3 HVD, and demonstrated functional redundancy of these interactions for EEEV replication (215, 216). The functional redundancy in the disordered nsP3 HVD may confer significant evolutionary advantages with regard to host-factor usage. This would allow the virus to replicate broadly and efficiently in a variety of cells, and possibly contribute to the exceptionally high virulence of EEEV (215, 216). Accumulation studies suggest that alphavirus nsP3 HVDs serve as selective hub of proteins for particular species in order to achieve the best fitness (or subsequently higher virulence) in different replication environments (215, 216, 218).

1.8. Purpose of this research

Viral papain-like proteases (PLPs)-related proteins have been demonstrated to be important viral factors actively involved in virus life cycle including replication and immune evasion. Therefore, the overall goal of this dissertation is to elucidate the critical regulatory roles of swine nidoviral PLPs-related proteins involved in viral replication and host innate immune responses. Three chapters are included in this dissertation. Chapter 2 is to determine the key functions of PRRSV nsp2-related proteins in modulation of host immune responses, and to examine the potential strategy of modified live vaccine development using recombinant PRRSV with impaired expression of frameshifting products ; Chapter 3 is to identify and characterize the hyper-phosphorylation state of PRRSV nsp2-related proteins; In Chapter 4, a natural recombinant enterovirus was characterized, which expresses an exogenous torovirus PLP through a cross-order recombination event; potential contributions of PLP recombination in the fitness of enterovirus was investigated.

1.9. Reference

1. De Groot R, Cowley J, Enjuanes L, Faaberg K, Perlman S, Rottier P, Snijder E, Ziebuhr J, Gorbalenya A. 2012. Order nidovirales. Virus Taxonomy: Ninth Report of the International Committee on Taxonomy of Viruses:785-795.
2. Lauber C, Goeman JJ, del Carmen Parquet M, Nga PT, Snijder EJ, Morita K, Gorbalenya AE. 2013. The footprint of genome architecture in the largest genome expansion in RNA viruses. PLoS pathogens 9:e1003500.
3. Posthuma CC, te Velthuis AJ, Snijder EJ. 2017. Nidovirus RNA polymerases: complex enzymes handling exceptional RNA genomes. Virus research 234:58-73.
4. Fehr AR, Perlman S. 2015. Coronaviruses: an overview of their replication and pathogenesis, p 1-23, Coronaviruses. Springer.
5. Shi M, Lam TT-Y, Hon C-C, Hui RK-H, Faaberg KS, Wennblom T, Murtaugh MP, Stadejek T, Leung FC-C. 2010. Molecular epidemiology of PRRSV: a phylogenetic perspective. Virus research 154:7-17.
6. Shi M, Lam TT-Y, Hon C-C, Murtaugh MP, Davies PR, Hui RK-H, Li J, Wong LT-W, Yip C-W, Jiang J-W. 2010. Phylogeny-based evolutionary, demographical, and geographical dissection of North American type 2 porcine reproductive and respiratory syndrome viruses. Journal of virology 84:8700-8711.
7. Murtaugh MP, Stadejek T, Abrahante JE, Lam TT, Leung FC-C. 2010. The ever-expanding diversity of porcine reproductive and respiratory syndrome virus. Virus research 154:18-30.
8. Stevenson G, Torremorell M. 2012. Porcine reproductive and respiratory syndrome virus (porcine arterivirus). Diseases of Swine, 10th ed; Zimmerman, JJ, Karriker, LA, Ramirez, A, Schwartz, KJ, Stevenson, GW, Eds:461-486.
9. Hill H. Overview and history of mystery swine disease (swine infertility/respiratory syndrome), p 29-30. *In* (ed),
10. Wensvoort G, Terpstra C, Pol J, Ter Laak E, Bloemraad M, De Kluyver E, Kragten C, Van Buiten Ld, Den Besten A, Wagenaar F. 1991. Mystery swine disease in The Netherlands: the isolation of Lelystad virus. Veterinary Quarterly 13:121-130.

11. Hopper S, White M, Twiddy N. 1992. An outbreak of blue-eared pig disease (porcine reproductive and respiratory syndrome) in four pig herds in Great Britain. The Veterinary Record 131:140-144.
12. Plana J, Vayreda M, Vilarrasa J, Bastons M, Rosell R, Martinez M, San Gabriel A, Pujols J, Badiola JL, Ramos JA. 1992. Porcine epidemic abortion and respiratory syndrome (mystery swine disease). Isolation in Spain of the causative agent and experimental reproduction of the disease. Veterinary microbiology 33:203-211.
13. Holtkamp DJ, Kliebenstein JB, Neumann EJ, Zimmerman JJ, Rotto HF, Yoder TK, Wang C, Yeske PE, Mowrer CL, Haley CA. 2013. Assessment of the economic impact of porcine reproductive and respiratory syndrome virus on United States pork producers. Journal of Swine Health and Production 21:72-84.
14. Ying Fang, Snijder EJ. 2010. The PRRSV replicase: Exploring the multifunctionality of an intriguing set of nonstructural proteins. Virus Research 154 61-76.
15. Lunney JK, Fang Y, Ladinig A, Chen N, Li Y, Rowland B, Renukaradhya GJ. 2016. Porcine reproductive and respiratory syndrome virus (PRRSV): pathogenesis and interaction with the immune system. Annual review of animal biosciences 4:129-154.
16. Snijder EJ, Kikkert M, Fang Y. 2013. Arterivirus molecular biology and pathogenesis. Journal of General Virology 94:2141-2163.
17. Fang Y, Treffers EE, Li Y, Tas A, Sun Z, Van Der Meer Y, De Ru AH, Van Veelen PA, Atkins JF, Snijder EJ. 2012. Efficient− 2 frameshifting by mammalian ribosomes to synthesize an additional arterivirus protein. proceedings of the National Academy of Sciences:201211145.
18. Brar MS, Shi M, Murtaugh MP, Leung FC-C. 2015. Evolutionary diversification of type 2 porcine reproductive and respiratory syndrome virus. Journal of General Virology 96:1570-1580.
19. Murtaugh M, Elam M, Kakach L. 1995. Comparison of the structural protein coding sequences of the VR-2332 and Lelystad virus strains of the PRRS virus. Archives of virology 140:1451-1460.
20. Nelsen CJ, Murtaugh MP, Faaberg KS. 1999. Porcine reproductive and respiratory syndrome virus comparison: divergent evolution on two continents. Journal of virology 73:270-280.

21. Kuhn JH, Lauck M, Bailey AL, Shchetinin AM, Vishnevskaya TV, Bào Y, Ng TFF, LeBreton M, Schneider BS, Gillis A. 2016. Reorganization and expansion of the nidoviral family Arteriviridae. Archives of virology 161:755-768.
22. Han J, Wang Y, Faaberg KS. 2006. Complete genome analysis of RFLP 184 isolates of porcine reproductive and respiratory syndrome virus. Virus research 122:175-182.
23. Tian K, Yu X, Zhao T, Feng Y, Cao Z, Wang C, Hu Y, Chen X, Hu D, Tian X. 2007. Emergence of fatal PRRSV variants: unparalleled outbreaks of atypical PRRS in China and molecular dissection of the unique hallmark. PloS one 2:e526.
24. Zhou L, Zhang J, Zeng J, Yin S, Li Y, Zheng L, Guo X, Ge X, Yang H. 2009. The 30-amino-acid deletion in the Nsp2 of highly pathogenic porcine reproductive and respiratory syndrome virus emerging in China is not related to its virulence. Journal of virology 83:5156-5167.
25. Li C, Zhuang J, Wang J, Han L, Sun Z, Xiao Y, Ji G, Li Y, Tan F, Li X. 2016. Outbreak Investigation of NADC30-Like PRRSV in South-East China. Transboundary and emerging diseases 63:474-479.
26. Li X, Bao H, Wang Y, Tian K. 2016. Widespread of NADC30-like PRRSV in China: Another Pandora's box for Chinese pig industry as the outbreak of highly pathogenic PRRSV in 2006? Infection, genetics and evolution: journal of molecular epidemiology and evolutionary genetics in infectious diseases 49:12.
27. Li X, Wu J, Tan F, Li Y, Ji G, Zhuang J, Zhai X, Tian K. 2016. Genome characterization of two NADC30-like porcine reproductive and respiratory syndrome viruses in China. SpringerPlus 5:1677.
28. Han J, Zhou L, Ge X, Guo X, Yang H. 2017. Pathogenesis and control of the Chinese highly pathogenic porcine reproductive and respiratory syndrome virus. Veterinary Microbiology.
29. Liu J-k, Zhou X, Zhai J-q, Li B, Wei C-h, Dai A-l, Yang X-y, Luo M-l. 2017. Emergence of a novel highly pathogenic porcine reproductive and respiratory syndrome virus in China. Transboundary and Emerging Diseases.
30. Wang L-j, Xie W, Chen X-x, Qiao S, Zhao M, Gu Y, Zhao B-l, Zhang G. 2017. Molecular epidemiology of porcine reproductive and respiratory syndrome virus in

Central China since 2014: The prevalence of NADC30-like PRRSVs. Microbial Pathogenesis 109:20-28.

31. Shi M, Holmes EC, Brar MS, Leung FC-C. 2013. Recombination is associated with an outbreak of novel highly pathogenic porcine reproductive and respiratory syndrome viruses in China. Journal of virology 87:10904-10907.
32. Zhao K, Ye C, Chang X-B, Jiang C-G, Wang S-J, Cai X-H, Tong G-Z, Tian Z-J, Shi M, An T-Q. 2015. Importation and recombination are responsible for the latest emergence of highly pathogenic porcine reproductive and respiratory syndrome virus in China. Journal of virology 89:10712-10716.
33. Workman AM, Smith TP, Osorio FA, Vu HL. 2016. Complete genome sequence of highly virulent porcine reproductive and respiratory syndrome virus variants that recently emerged in the United States. Genome announcements 4:e00772-16.
34. Wesley RD, Mengeling WL, Lager KM, Clouser DF, Landgraf JG, Frey ML. 1998. Differentiation of a porcine reproductive and respiratory syndrome virus vaccine strain from North American field strains by restriction fragment length polymorphism analysis of ORF 5. Journal of Veterinary Diagnostic Investigation 10:140-144.
35. Reiner G, Fresen C, Bronnert S, Willems H. 2009. Porcine reproductive and respiratory syndrome virus (PRRSV) infection in wild boars. Veterinary microbiology 136:250-258.
36. Eric J. Snijder, Marjolein Kikkert, Fang Y. 2013. Arterivirus molecular biology and pathogenesis. Journal of General Virology 94:2141–2163.
37. Zhang Q, Yoo D. 2015. PRRS virus receptors and their role for pathogenesis. Veterinary microbiology 177:229-241.
38. Xie J, Christiaens I, Yang B, Van Breedam W, Cui T, Nauwynck HJ. 2017. Molecular cloning of porcine Siglec-3, Siglec-5 and Siglec-10, and identification of Siglec-10 as an alternative receptor for porcine reproductive and respiratory syndrome virus (PRRSV). Journal of General Virology 98:2030-2042.
39. Das PB, Dinh PX, Ansari IH, De Lima M, Osorio FA, Pattnaik AK. 2010. The minor envelope glycoproteins GP2a and GP4 of porcine reproductive and respiratory syndrome virus interact with the receptor CD163. Journal of virology 84:1731-1740.
40. Van Breedam W, Van Gorp H, Zhang JQ, Crocker PR, Delputte PL, Nauwynck HJ. 2010. The M/GP5 glycoprotein complex of porcine reproductive and respiratory

syndrome virus binds the sialoadhesin receptor in a sialic acid-dependent manner. PLoS pathogens 6:e1000730.

41. Darwich L, Díaz I, Mateu E. 2010. Certainties, doubts and hypotheses in porcine reproductive and respiratory syndrome virus immunobiology. Virus research 154:123-132.

42. Ke H, Yoo D. 2017. The viral innate immune antagonism and an alternative vaccine design for PRRS virus. Veterinary microbiology.

43. Loving CL, Osorio FA, Murtaugh MP, Zuckermann FA. 2015. Innate and adaptive immunity against porcine reproductive and respiratory syndrome virus. Veterinary immunology and immunopathology 167:1-14.

44. Nielsen J, Bøtner A. 1997. Hematological and immunological parameters of 412-month old pigs infected with PRRS virus. Veterinary microbiology 55:289-294.

45. Shimizu M, Yamada S, Kawashima K, Ohashi S, Shimizu S, Ogawa T. 1996. Changes of lymphocyte subpopulations in pigs infected with porcine reproductive and respiratory syndrome (PRRS) virus. Veterinary immunology and immunopathology 50:19-27.

46. Silva-Campa E, Mata-Haro V, Mateu E, Hernández J. 2012. Porcine reproductive and respiratory syndrome virus induces CD4+ CD8+ CD25+ Foxp3+ regulatory T cells (Tregs). Virology 430:73-80.

47. Qi P, Liu K, Wei J, Li Y, Li B, Shao D, Wu Z, Shi Y, Tong G, Qiu Y. 2017. Nonstructural protein 4 of porcine reproductive and respiratory syndrome virus modulates cell surface swine leukocyte antigen class I expression by downregulating β2-microglobulin transcription. Journal of virology 91:e01755-16.

48. Du J, Ge X, Liu Y, Jiang P, Wang Z, Zhang R, Zhou L, Guo X, Han J, Yang H. 2016. Targeting swine leukocyte antigen class I molecules for proteasomal degradation by the nsp1α replicase protein of the Chinese highly pathogenic porcine reproductive and respiratory syndrome virus strain JXwn06. Journal of virology 90:682-693.

49. Cao QM, Subramaniam S, Ni Y-Y, Cao D, Meng X-J. 2016. The non-structural protein Nsp2TF of porcine reproductive and respiratory syndrome virus down-regulates the expression of Swine Leukocyte Antigen class I. Virology 491:115-124.

50. Flores-Mendoza L, Silva-Campa E, Reséndiz M, Osorio FA, Hernández J. 2008. Porcine reproductive and respiratory syndrome virus infects mature porcine dendritic cells and up-regulates interleukin-10 production. Clinical and Vaccine Immunology 15:720-725.
51. Sztuba-Solińska J, Stollar V, Bujarski JJ. 2011. Subgenomic messenger RNAs: mastering regulation of (+)-strand RNA virus life cycle. Virology 412:245-255.
52. Miller WA, Koev G. 2000. Synthesis of subgenomic RNAs by positive-strand RNA viruses. Virology 273:1-8.
53. Pasternak AO, Spaan WJ, Snijder EJ. 2006. Nidovirus transcription: how to make sense…? Journal of general virology 87:1403-1421.
54. Sola I, Almazán F, Zúñiga S, Enjuanes L. 2015. Continuous and discontinuous RNA synthesis in coronaviruses. Annual review of virology 2:265-288.
55. Lehmann KC, Snijder EJ, Posthuma CC, Gorbalenya AE. 2015. What we know but do not understand about nidovirus helicases. Virus research 202:12-32.
56. Sola I, Mateos-Gomez PA, Almazan F, Zuñiga S, Enjuanes L. 2011. RNA-RNA and RNA-protein interactions in coronavirus replication and transcription. RNA biology 8:237-248.
57. van den Born E, Gultyaev AP, Snijder EJ. 2004. Secondary structure and function of the 5′-proximal region of the equine arteritis virus RNA genome. Rna 10:424-437.
58. Van Den Born E, Posthuma CC, Gultyaev AP, Snijder EJ. 2005. Discontinuous subgenomic RNA synthesis in arteriviruses is guided by an RNA hairpin structure located in the genomic leader region. Journal of virology 79:6312-6324.
59. Mateos-Gomez PA, Morales L, Zuñiga S, Enjuanes L, Sola I. 2013. Long-distance RNA-RNA interactions in the coronavirus genome form high-order structures promoting discontinuous RNA synthesis during transcription. Journal of virology 87:177-186.
60. Mateos-Gómez PA, Zuñiga S, Palacio L, Enjuanes L, Sola I. 2011. Gene N proximal and distal RNA motifs regulate coronavirus nucleocapsid mRNA transcription. Journal of virology 85:8968-8980.
61. Moreno JL, Zúñiga S, Enjuanes L, Sola I. 2008. Identification of a coronavirus transcription enhancer. Journal of virology 82:3882-3893.

62. Nedialkova DD, Gorbalenya AE, Snijder EJ. 2010. Arterivirus Nsp1 modulates the accumulation of minus-strand templates to control the relative abundance of viral mRNAs. PLoS pathogens 6:e1000772.
63. Tijms MA, van Dinten LC, Gorbalenya AE, Snijder EJ. 2001. A zinc finger-containing papain-like protease couples subgenomic mRNA synthesis to genome translation in a positive-stranded RNA virus. Proceedings of the national academy of sciences 98:1889-1894.
64. Van Dinten LC, Den Boon JA, Wassenaar AL, Spaan WJ, Snijder EJ. 1997. An infectious arterivirus cDNA clone: identification of a replicase point mutation that abolishes discontinuous mRNA transcription. Proceedings of the National Academy of Sciences 94:991-996.
65. Seybert A, Posthuma CC, van Dinten LC, Snijder EJ, Gorbalenya AE, Ziebuhr J. 2005. A complex zinc finger controls the enzymatic activities of nidovirus helicases. Journal of virology 79:696-704.
66. van Dinten LC, van Tol H, Gorbalenya AE, Snijder EJ. 2000. The predicted metal-binding region of the arterivirus helicase protein is involved in subgenomic mRNA synthesis, genome replication, and virion biogenesis. Journal of virology 74:5213-5223.
67. Wu C-H, Chen P-J, Yeh S-H. 2014. Nucleocapsid phosphorylation and RNA helicase DDX1 recruitment enables coronavirus transition from discontinuous to continuous transcription. Cell host & microbe 16:462-472.
68. Komander D. 2009. The emerging complexity of protein ubiquitination. Biochemical Society Transactions 37:937-953.
69. Komander D, Rape M. 2012. The ubiquitin code. Annual review of biochemistry 81:203-229.
70. Zinngrebe J, Montinaro A, Peltzer N, Walczak H. 2013. Ubiquitin in the immune system. EMBO reports:e201338025.
71. Heaton SM, Borg NA, Dixit VM. 2015. Ubiquitin in the activation and attenuation of innate antiviral immunity. Journal of Experimental Medicine:jem. 20151531.
72. Iwai K, Fujita H, Sasaki Y. 2014. Linear ubiquitin chains: NF-κB signalling, cell death and beyond. Nature reviews Molecular cell biology 15:503.

73. Rieser E, Cordier SM, Walczak H. 2013. Linear ubiquitination: a newly discovered regulator of cell signalling. Trends in biochemical sciences 38:94-102.
74. Rittinger K, Ikeda F. 2017. Linear ubiquitin chains: enzymes, mechanisms and biology. Open biology 7:170026.
75. Shimizu Y, Taraborrelli L, Walczak H. 2015. Linear ubiquitination in immunity. Immunological reviews 266:190-207.
76. Davis ME, Gack MU. 2015. Ubiquitination in the antiviral immune response. Virology 479-480:52-65.
77. Sun SC. 2008. Deubiquitylation and regulation of the immune response. Nat Rev Immunol 8:501-11.
78. Loo Y-M, Gale Jr M. 2011. Immune signaling by RIG-I-like receptors. Immunity 34:680-692.
79. Wu B, Hur S. 2015. How RIG-I like receptors activate MAVS. Current opinion in virology 12:91-98.
80. Kawai T, Akira S. 2007. Signaling to NF-κB by Toll-like receptors. Trends in molecular medicine 13:460-469.
81. Gack MU, Shin YC, Joo C-H, Urano T, Liang C, Sun L, Takeuchi O, Akira S, Chen Z, Inoue S. 2007. TRIM25 RING-finger E3 ubiquitin ligase is essential for RIG-I-mediated antiviral activity. Nature 446:916.
82. Oshiumi H, Matsumoto M, Hatakeyama S, Seya T. 2009. Riplet/RNF135, a RING finger protein, ubiquitinates RIG-I to promote interferon-β induction during the early phase of viral infection. Journal of Biological Chemistry 284:807-817.
83. Kuniyoshi K, Takeuchi O, Pandey S, Satoh T, Iwasaki H, Akira S, Kawai T. 2014. Pivotal role of RNA-binding E3 ubiquitin ligase MEX3C in RIG-I–mediated antiviral innate immunity. Proceedings of the National Academy of Sciences 111:5646-5651.
84. Yan J, Li Q, Mao A-P, Hu M-M, Shu H-B. 2014. TRIM4 modulates type I interferon induction and cellular antiviral response by targeting RIG-I for K63-linked ubiquitination. Journal of molecular cell biology 6:154-163.
85. Friedman CS, O'donnell MA, Legarda-Addison D, Ng A, Cárdenas WB, Yount JS, Moran TM, Basler CF, Komuro A, Horvath CM. 2008. The tumour suppressor CYLD is a negative regulator of RIG-I-mediated antiviral response. EMBO reports 9:930-936.

86. Wang L, Zhao W, Zhang M, Wang P, Zhao K, Zhao X, Yang S, Gao C. 2013. USP4 positively regulates RIG-I-mediated antiviral response through deubiquitination and stabilization of RIG-I. Journal of virology:JVI. 00031-13.
87. Fan Y, Mao R, Yu Y, Liu S, Shi Z, Cheng J, Zhang H, An L, Zhao Y, Xu X. 2014. USP21 negatively regulates antiviral response by acting as a RIG-I deubiquitinase. Journal of Experimental Medicine 211:313-328.
88. Arimoto K-i, Takahashi H, Hishiki T, Konishi H, Fujita T, Shimotohno K. 2007. Negative regulation of the RIG-I signaling by the ubiquitin ligase RNF125. Proceedings of the National Academy of Sciences 104:7500-7505.
89. Narayan K, Waggoner L, Pham ST, Hendricks GL, Waggoner SN, Conlon J, Wang JP, Fitzgerald KA, Kang J. 2014. TRIM13 is a negative regulator of MDA5-mediated type I IFN production. Journal of virology:JVI. 02593-13.
90. Zhong B, Zhang Y, Tan B, Liu T-T, Wang Y-Y, Shu H-B. 2010. The E3 ubiquitin ligase RNF5 targets virus-induced signaling adaptor for ubiquitination and degradation. The Journal of Immunology:ji_0903748.
91. Castanier C, Zemirli N, Portier A, Garcin D, Bidère N, Vazquez A, Arnoult D. 2012. MAVS ubiquitination by the E3 ligase TRIM25 and degradation by the proteasome is involved in type I interferon production after activation of the antiviral RIG-I-like receptors. BMC biology 10:44.
92. Wang Y, Tong X, Ye X. 2012. Ndfip1 Negatively Regulates RIG-I–Dependent Immune Signaling by Enhancing E3 Ligase Smurf1-Mediated MAVS Degradation. The Journal of Immunology:1201445.
93. You F, Sun H, Zhou X, Sun W, Liang S, Zhai Z, Jiang Z. 2009. PCBP2 mediates degradation of the adaptor MAVS via the HECT ubiquitin ligase AIP4. Nature immunology 10:1300.
94. Pan Y, Li R, Meng J-L, Mao H-T, Zhang Y, Zhang J. 2014. Smurf2 Negatively Modulates RIG-I–Dependent Antiviral Response by Targeting VISA/MAVS for Ubiquitination and Degradation. The Journal of Immunology:1302632.
95. Liu B, Zhang M, Chu H, Zhang H, Wu H, Song G, Wang P, Zhao K, Hou J, Wang X. 2017. The ubiquitin E3 ligase TRIM31 promotes aggregation and activation of the

signaling adaptor MAVS through Lys63-linked polyubiquitination. Nature immunology 18:214.

96. Paz S, Vilasco M, Arguello M, Sun Q, Lacoste J, Nguyen TL-A, Zhao T, Shestakova EA, Zaari S, Bibeau-Poirier A. 2009. Ubiquitin-regulated recruitment of IκB kinase ε to the MAVS interferon signaling adapter. Molecular and cellular biology 29:3401-3412.

97. Inn K-S, Gack MU, Tokunaga F, Shi M, Wong L-Y, Iwai K, Jung JU. 2011. Linear ubiquitin assembly complex negatively regulates RIG-I-and TRIM25-mediated type I interferon induction. Molecular cell 41:354-365.

98. Pauli E-K, Chan YK, Davis ME, Gableske S, Wang MK, Feister KF, Gack MU. 2014. The ubiquitin-specific protease USP15 promotes RIG-I–mediated antiviral signaling by deubiquitylating TRIM25. Sci Signal 7:ra3-ra3.

99. Gay NJ, Symmons MF, Gangloff M, Bryant CE. 2014. Assembly and localization of Toll-like receptor signalling complexes. Nature reviews Immunology 14:546-558.

100. Chuang T-H, Ulevitch RJ. 2004. Triad3A, an E3 ubiquitin-protein ligase regulating Toll-like receptors. Nature immunology 5:495.

101. Yang Y, Liao B, Wang S, Yan B, Jin Y, Shu H-B, Wang Y-Y. 2013. E3 ligase WWP2 negatively regulates TLR3-mediated innate immune response by targeting TRIF for ubiquitination and degradation. Proceedings of the National Academy of Sciences:201220271.

102. Lee YS, Park JS, Kim JH, Jung SM, Lee JY, Kim S-J, Park SH. 2011. Smad6-specific recruitment of Smurf E3 ligases mediates TGF-β1-induced degradation of MyD88 in TLR4 signalling. Nature communications 2:460.

103. Wang C, Chen T, Zhang J, Yang M, Li N, Xu X, Cao X. 2009. The E3 ubiquitin ligase Nrdp1'preferentially'promotes TLR-mediated production of type I interferon. Nature immunology 10:744.

104. Schauvliege R, Janssens S, Beyaert R. 2006. Pellino proteins are more than scaffold proteins in TLR/IL-1R signalling: A role as novel RING E3–ubiquitin-ligases. FEBS letters 580:4697-4702.

105. Chang M, Jin W, Sun S-C. 2009. Peli1 facilitates TRIF-dependent Toll-like receptor signaling and proinflammatory cytokine production. Nature immunology 10:1089.

106. Wertz IE, O'rourke KM, Zhou H, Eby M, Aravind L, Seshagiri S, Wu P, Wiesmann C, Baker R, Boone DL. 2004. De-ubiquitination and ubiquitin ligase domains of A20 downregulate NF-κB signalling. Nature 430:694.
107. Shembade N, Ma A, Harhaj EW. 2010. Inhibition of NF-κB signaling by A20 through disruption of ubiquitin enzyme complexes. Science 327:1135-1139.
108. Zhang M, Wu X, Lee AJ, Jin W, Chang M, Wright A, Imaizumi T, Sun S-C. 2008. Regulation of IκB kinase-related kinases and antiviral responses by tumor suppressor CYLD. Journal of Biological Chemistry 283:18621-18626.
109. Li S, Zheng H, Mao A-P, Zhong B, Li Y, Liu Y, Gao Y, Ran Y, Tien P, Shu H-B. 2010. Regulation of virus-triggered signaling by OTUB1-and OTUB2-mediated deubiquitination of TRAF3 and TRAF6. Journal of Biological Chemistry 285:4291-4297.
110. Boone DL, Turer EE, Lee EG, Ahmad R-C, Wheeler MT, Tsui C, Hurley P, Chien M, Chai S, Hitotsumatsu O. 2004. The ubiquitin-modifying enzyme A20 is required for termination of Toll-like receptor responses. Nature immunology 5:1052.
111. Yaron A, Hatzubai A, Davis M, Lavon I, Amit S, Manning AM, Andersen JS, Mann M, Mercurio F, Ben-Neriah Y. 1998. Identification of the receptor component of the IκBα–ubiquitin ligase. Nature 396:590.
112. Heissmeyer V, Krappmann D, Hatada EN, Scheidereit C. 2001. Shared pathways of IκB kinase-induced SCFβTrCP-mediated ubiquitination and degradation for the NF-κB precursor p105 and IκBα. Molecular and cellular biology 21:1024-1035.
113. Nakhaei P, Mesplede T, Solis M, Sun Q, Zhao T, Yang L, Chuang T-H, Ware CF, Lin R, Hiscott J. 2009. The E3 ubiquitin ligase Triad3A negatively regulates the RIG-I/MAVS signaling pathway by targeting TRAF3 for degradation. PLoS pathogens 5:e1000650.
114. Peng Y, Xu R, Zheng X. 2014. HSCARG negatively regulates the cellular antiviral RIG-I like receptor signaling pathway by inhibiting TRAF3 ubiquitination via recruiting OTUB1. PLoS pathogens 10:e1004041.
115. Kayagaki N, Phung Q, Chan S, Chaudhari R, Quan C, O'rourke KM, Eby M, Pietras E, Cheng G, Bazan JF. 2007. A deubiquitinase that regulates type I interferon production. Science 318:1628-1632.
116. Karim R, Tummers B, Meyers C, Biryukov JL, Alam S, Backendorf C, Jha V, Offringa R, van Ommen G-JB, Melief CJ. 2013. Human papillomavirus (HPV) upregulates the

cellular deubiquitinase UCHL1 to suppress the keratinocyte's innate immune response. PLoS pathogens 9:e1003384.

117. Wang L, Li S, Kong Y-Y, Dorf M. 2010. Mindbomb proteins are E3 ubiquitin ligases essential for TBK1-mediated antiviral activity (136.6). Am Assoc Immnol.

118. Zhang L, Zhao X, Zhang M, Zhao W, Gao C. 2014. Ubiquitin-specific protease 2b negatively regulates IFN-β production and antiviral activity by targeting TANK-binding kinase 1. The Journal of Immunology:1302634.

119. Parvatiyar K, Barber GN, Harhaj EW. 2010. TAX1BP1 and A20 inhibit antiviral signaling by targeting TBK1/IKKi kinases. Journal of Biological Chemistry:jbc. M110. 109819.

120. Cui J, Li Y, Zhu L, Liu D, Songyang Z, Wang HY, Wang R-F. 2012. NLRP4 negatively regulates type I interferon signaling by targeting the kinase TBK1 for degradation via the ubiquitin ligase DTX4. Nature immunology 13:387.

121. Zhang M, Wang L, Zhao X, Zhao K, Meng H, Zhao W, Gao C. 2012. TRAF-interacting protein (TRIP) negatively regulates IFN-β production and antiviral response by promoting proteasomal degradation of TANK-binding kinase 1. Journal of Experimental Medicine 209:1703-1711.

122. Higgs R, Gabhann JN, Larbi NB, Breen EP, Fitzgerald KA, Jefferies CA. 2008. The E3 ubiquitin ligase Ro52 negatively regulates IFN-β production post-pathogen recognition by polyubiquitin-mediated degradation of IRF3. The Journal of Immunology 181:1780-1786.

123. Zhang M, Tian Y, Wang R-P, Gao D, Zhang Y, Diao F-C, Chen D-Y, Zhai Z-H, Shu H-B. 2008. Negative feedback regulation of cellular antiviral signaling by RBCK1-mediated degradation of IRF3. Cell research 18:1096.

124. Yu Y, Hayward GS. 2010. The ubiquitin E3 ligase RAUL negatively regulates type i interferon through ubiquitination of the transcription factors IRF7 and IRF3. Immunity 33:863-877.

125. Young JA, Sermwittayawong D, Kim H-J, Nandu S, An N, Erdjument-Bromage H, Tempst P, Coscoy L, Winoto A. 2011. Fas-associated death domain (FADD) and the E3 ubiquitin-protein ligase TRIM21 interact to negatively regulate virus-induced interferon production. Journal of Biological Chemistry 286:6521-6531.

126. Arimoto K-i, Funami K, Saeki Y, Tanaka K, Okawa K, Takeuchi O, Akira S, Murakami Y, Shimotohno K. 2010. Polyubiquitin conjugation to NEMO by triparite motif protein 23 (TRIM23) is critical in antiviral defense. Proceedings of the National Academy of Sciences 107:15856-15861.
127. Zotti T, Uva A, Ferravante A, Vessichelli M, Scudiero I, Ceccarelli M, Vito P. 2011. TRAF7 protein promotes Lys-29-linked polyubiquitination of IκB kinase (IKKγ)/NF-κB essential modulator (NEMO) and p65/RelA protein and represses NF-κB activation. Journal of Biological Chemistry 286:22924-22933.
128. Tokunaga F, Sakata S-i, Saeki Y, Satomi Y, Kirisako T, Kamei K, Nakagawa T, Kato M, Murata S, Yamaoka S. 2009. Involvement of linear polyubiquitylation of NEMO in NF-κB activation. Nature cell biology 11:123.
129. Belgnaoui SM, Paz S, Samuel S, Goulet M-L, Sun Q, Kikkert M, Iwai K, Dikic I, Hiscott J, Lin R. 2012. Linear ubiquitination of NEMO negatively regulates the interferon antiviral response through disruption of the MAVS-TRAF3 complex. Cell host & microbe 12:211-222.
130. Ivins FJ, Montgomery MG, Smith SJ, Morris-Davies AC, Taylor IA, Rittinger K. 2009. NEMO oligomerization and its ubiquitin-binding properties. Biochemical Journal 421:243-251.
131. Lo Y-C, Lin S-C, Rospigliosi CC, Conze DB, Wu C-J, Ashwell JD, Eliezer D, Wu H. 2009. Structural basis for recognition of diubiquitins by NEMO. Molecular cell 33:602-615.
132. Rahighi S, Ikeda F, Kawasaki M, Akutsu M, Suzuki N, Kato R, Kensche T, Uejima T, Bloor S, Komander D. 2009. Specific recognition of linear ubiquitin chains by NEMO is important for NF-κB activation. Cell 136:1098-1109.
133. Jeon YJ, Yoo HM, Chung CH. 2010. ISG15 and immune diseases. Biochimica et Biophysica Acta (BBA)-Molecular Basis of Disease 1802:485-496.
134. Perng Y-C, Lenschow DJ. 2018. ISG15 in antiviral immunity and beyond. Nature Reviews Microbiology:1.
135. Skaug B, Chen ZJ. 2010. Emerging role of ISG15 in antiviral immunity. Cell 143:187-190.

136. Zhang D, Zhang D-E. 2011. Interferon-stimulated gene 15 and the protein ISGylation system. Journal of interferon & cytokine research 31:119-130.
137. Hermann M, Bogunovic D. 2017. ISG15: in sickness and in health. Trends in immunology 38:79-93.
138. Hale BG, Randall RE, Ortín J, Jackson D. 2008. The multifunctional NS1 protein of influenza A viruses. Journal of general virology 89:2359-2376.
139. Krug RM. 2015. Functions of the influenza A virus NS1 protein in antiviral defense. Current opinion in virology 12:1-6.
140. Bailey-Elkin BA, Knaap RC, Kikkert M, Mark BL. 2017. Structure and function of viral deubiquitinating enzymes. Journal of molecular biology.
141. Mielech AM, Chen Y, Mesecar AD, Baker SC. 2014. Nidovirus papain-like proteases: multifunctional enzymes with protease, deubiquitinating and deISGylating activities. Virus research 194:184-190.
142. Sutton TC, Subbarao K. 2015. Development of animal models against emerging coronaviruses: From SARS to MERS coronavirus. Virology 479:247-258.
143. Snijder EJ, Bredenbeek PJ, Dobbe JC, Thiel V, Ziebuhr J, Poon LL, Guan Y, Rozanov M, Spaan WJ, Gorbalenya AE. 2003. Unique and conserved features of genome and proteome of SARS-coronavirus, an early split-off from the coronavirus group 2 lineage. Journal of molecular biology 331:991-1004.
144. Harcourt BH, Jukneliene D, Kanjanahaluethai A, Bechill J, Severson KM, Smith CM, Rota PA, Baker SC. 2004. Identification of severe acute respiratory syndrome coronavirus replicase products and characterization of papain-like protease activity. Journal of virology 78:13600-13612.
145. Thiel V, Ivanov KA, Putics A, Hertzig T, Schelle B, Bayer S, Weißbrich B, Snijder EJ, Rabenau H, Doerr HW. 2003. Mechanisms and enzymes involved in SARS coronavirus genome expression. Journal of General Virology 84:2305-2315.
146. Sulea T, Lindner HA, Purisima EO, Ménard R. 2005. Deubiquitination, a new function of the severe acute respiratory syndrome coronavirus papain-like protease? Journal of virology 79:4550-4551.

147. Barretto N, Jukneliene D, Ratia K, Chen Z, Mesecar AD, Baker SC. 2005. The papain-like protease of severe acute respiratory syndrome coronavirus has deubiquitinating activity. Journal of virology 79:15189-15198.
148. Lindner HA, Fotouhi-Ardakani N, Lytvyn V, Lachance P, Sulea T, Ménard R. 2005. The papain-like protease from the severe acute respiratory syndrome coronavirus is a deubiquitinating enzyme. Journal of virology 79:15199-15208.
149. Devaraj SG, Wang N, Chen Z, Chen Z, Tseng M, Barretto N, Lin R, Peters CJ, Tseng C-TK, Baker SC. 2007. Regulation of IRF-3 dependent innate immunity by the papain-like protease domain of the sars coronavirus. Journal of Biological Chemistry.
150. Frieman M, Ratia K, Johnston RE, Mesecar AD, Baric RS. 2009. Severe acute respiratory syndrome coronavirus papain-like protease ubiquitin-like domain and catalytic domain regulate antagonism of IRF3 and NF-κB signaling. Journal of virology 83:6689-6705.
151. Ratia K, Saikatendu KS, Santarsiero BD, Barretto N, Baker SC, Stevens RC, Mesecar AD. 2006. Severe acute respiratory syndrome coronavirus papain-like protease: structure of a viral deubiquitinating enzyme. Proceedings of the National Academy of Sciences 103:5717-5722.
152. Hu M, Li P, Li M, Li W, Yao T, Wu J-W, Gu W, Cohen RE, Shi Y. 2002. Crystal structure of a UBP-family deubiquitinating enzyme in isolation and in complex with ubiquitin aldehyde. Cell 111:1041-1054.
153. Chou C-Y, Lai H-Y, Chen H-Y, Cheng S-C, Cheng K-W, Chou Y-W. 2014. Structural basis for catalysis and ubiquitin recognition by the severe acute respiratory syndrome coronavirus papain-like protease. Acta Crystallographica Section D: Biological Crystallography 70:572-581.
154. Daczkowski CM, Dzimianski JV, Clasman JR, Goodwin O, Mesecar AD, Pegan SD. 2017. Structural insights into the interaction of coronavirus papain-like proteases and interferon-stimulated gene product 15 from different species. Journal of molecular biology 429:1661-1683.
155. Békés M, Ekkebus R, Ovaa H, Huang TT, Lima CD. 2016. Recognition of Lys48-linked di-ubiquitin and deubiquitinating activities of the SARS coronavirus papain-like protease. Molecular cell 62:572-585.

156. Ratia K, Kilianski A, Baez-Santos YM, Baker SC, Mesecar A. 2014. Structural basis for the ubiquitin-linkage specificity and deISGylating activity of SARS-CoV papain-like protease. PLoS pathogens 10:e1004113.
157. Báez-Santos YM, Mielech AM, Deng X, Baker S, Mesecar AD. 2014. Catalytic function and substrate specificity of the PLpro domain of nsp3 from the Middle East respiratory syndrome coronavirus (MERS-CoV). Journal of virology:JVI. 01294-14.
158. Yang X, Chen X, Bian G, Tu J, Xing Y, Wang Y, Chen Z. 2014. Proteolytic processing, deubiquitinase and interferon antagonist activities of Middle East respiratory syndrome coronavirus papain-like protease. Journal of General Virology 95:614-626.
159. Bailey-Elkin BA, Knaap RC, Johnson GG, Dalebout TJ, Ninaber DK, van Kasteren PB, Bredenbeek PJ, Snijder EJ, Kikkert M, Mark BL. 2014. Crystal structure of the MERS coronavirus papain-like protease bound to ubiquitin facilitates targeted disruption of deubiquitinating activity to demonstrate its role in innate immune suppression. Journal of Biological Chemistry:jbc. M114. 609644.
160. Mielech AM, Kilianski A, Baez-Santos YM, Mesecar AD, Baker SC. 2014. MERS-CoV papain-like protease has deISGylating and deubiquitinating activities. Virology 450:64-70.
161. Békés M, Rut W, Kasperkiewicz P, Mulder MP, Ovaa H, Drag M, Lima CD, Huang TT. 2015. SARS hCoV papain-like protease is a unique Lys48 linkage-specific di-distributive deubiquitinating enzyme. Biochemical Journal:BJ20141170.
162. Lin M-H, Chuang S-J, Chen C-C, Cheng S-C, Cheng K-W, Lin C-H, Sun C-Y, Chou C-Y. 2014. Structural and functional characterization of MERS coronavirus papain-like protease. Journal of biomedical science 21:54.
163. Lei J, Hilgenfeld R. 2016. Structural and mutational analysis of the interaction between the Middle-East respiratory syndrome coronavirus (MERS-CoV) papain-like protease and human ubiquitin. Virologica Sinica 31:288-299.
164. Lei J, Mesters JR, Drosten C, Anemüller S, Ma Q, Hilgenfeld R. 2014. Crystal structure of the papain-like protease of MERS coronavirus reveals unusual, potentially druggable active-site features. Antiviral research 109:72-82.
165. Shang P, Misra S, Hause B, Fang Y. 2017. A naturally occurring recombinant enterovirus expresses a torovirus deubiquitinase. Journal of virology:JVI. 00450-17.

166. Snijder EJ, Wassenaar AL, Spaan WJ, Gorbalenya AE. 1995. The arterivirus Nsp2 protease. An unusual cysteine protease with primary structure similarities to both papain-like and chymotrypsin-like proteases. Journal of Biological Chemistry 270:16671-16676.
167. Han J, Rutherford MS, Faaberg KS. 2009. The porcine reproductive and respiratory syndrome virus nsp2 cysteine protease domain possesses both trans-and cis-cleavage activities. Journal of virology 83:9449-9463.
168. Makarova KS, Aravind L, Koonin EV. 2000. A novel superfamily of predicted cysteine proteases from eukaryotes, viruses and Chlamydia pneumoniae. Trends in biochemical sciences 25:50-52.
169. van Kasteren PB, Bailey-Elkin BA, James TW, Ninaber DK, Beugeling C, Khajehpour M, Snijder EJ, Mark BL, Kikkert M. 2013. Deubiquitinase function of arterivirus papain-like protease 2 suppresses the innate immune response in infected host cells. Proceedings of the National Academy of Sciences 110:E838-E847.
170. Bailey-Elkin BA, van Kasteren PB, Snijder EJ, Kikkert M, Mark BL. 2014. Viral OTU deubiquitinases: a structural and functional comparison. PLoS pathogens 10:e1003894.
171. van Kasteren PB, Beugeling C, Ninaber DK, Frias-Staheli N, van Boheemen S, García-Sastre A, Snijder EJ, Kikkert M. 2012. Arterivirus and nairovirus ovarian tumor domain-containing deubiquitinases target activated RIG-I to control innate immune signaling. Journal of virology 86:773-785.
172. Frias-Staheli N, Giannakopoulos NV, Kikkert M, Taylor SL, Bridgen A, Paragas J, Richt JA, Rowland RR, Schmaljohn CS, Lenschow DJ. 2007. Ovarian tumor domain-containing viral proteases evade ubiquitin-and ISG15-dependent innate immune responses. Cell host & microbe 2:404-416.
173. Li Y, Treffers EE, Napthine S, Tas A, Zhu L, Sun Z, Bell S, Mark BL, van Veelen PA, van Hemert MJ. 2014. Transactivation of programmed ribosomal frameshifting by a viral protein. Proceedings of the National Academy of Sciences 111:E2172-E2181.
174. Li Y, Shyu D-L, Shang P, Bai J, Ouyang K, Dhakal S, Hireamt J, Binjawadagi B, Renukaradhya GJ, Fang Y. 2016. Mutations in a highly conserved motif of nsp1β protein attenuate the innate immune suppression function of porcine reproductive and respiratory syndrome virus (PRRSV). Journal of virology:JVI. 03069-15.

175. Napthine S, Treffers EE, Bell S, Goodfellow I, Fang Y, Firth AE, Snijder EJ, Brierley I. 2016. A novel role for poly (C) binding proteins in programmed ribosomal frameshifting. Nucleic acids research 44:5491-5503.
176. Sun Z, Li Y, Ransburgh R, Snijder EJ, Fang Y. 2012. Nonstructural protein 2 of porcine reproductive and respiratory syndrome virus inhibits the antiviral function of interferon-stimulated gene 15. Journal of virology:JVI. 06466-11.
177. Sun Z, Chen Z, Lawson SR, Fang Y. 2010. The cysteine protease domain of porcine reproductive and respiratory syndrome virus nonstructural protein 2 possesses deubiquitinating and interferon antagonism functions. J Virol 84:7832-46.
178. Deaton MK, Spear A, Faaberg KS, Pegan SD. 2014. The vOTU domain of highly-pathogenic porcine reproductive and respiratory syndrome virus displays a differential substrate preference. Virology 454-455:247-53.
179. Li Y, Shang P, Shyu D, Carrillo C, Naraghi-Arani P, Jaing CJ, Renukaradhya G, Firth AE, Snijder E, Fang Y. 2018. Nonstructural proteins nsp2TF and nsp2N of porcine reproductive and respiratory syndrome virus (PRRSV) play important roles in suppressing host innate immune responses. Virology 517:164-176.
180. Humphrey SJ, James DE, Mann M. 2015. Protein phosphorylation: a major switch mechanism for metabolic regulation. Trends in Endocrinology & Metabolism 26:676-687.
181. Hunter T. 1995. Protein kinases and phosphatases: the yin and yang of protein phosphorylation and signaling. Cell 80:225-236.
182. Johnson LN. 2009. The regulation of protein phosphorylation. Biochemical Society Transactions 37:627-641.
183. Tarrant MK, Cole PA. 2009. The chemical biology of protein phosphorylation. Annual review of biochemistry 78:797-825.
184. Ubersax JA, Ferrell Jr JE. 2007. Mechanisms of specificity in protein phosphorylation. Nature reviews Molecular cell biology 8:530.
185. Keating JA, Striker R. 2012. Phosphorylation events during viral infections provide potential therapeutic targets. Reviews in medical virology 22:166-181.

186. Keck F, Ataey P, Amaya M, Bailey C, Narayanan A. 2015. Phosphorylation of single stranded RNA virus proteins and potential for novel therapeutic strategies. Viruses 7:5257-5273.
187. Stohlman S, Lai M. 1979. Phosphoproteins of murine hepatitis viruses. Journal of virology 32:672-675.
188. McBride R, van Zyl M, Fielding BC. 2014. The coronavirus nucleocapsid is a multifunctional protein. Viruses 6:2991-3018.
189. Dokland T. 2010. The structural biology of PRRSV. Virus research 154:86-97.
190. Wu C-H, Yeh S-H, Tsay Y-G, Shieh Y-H, Kao C-L, Chen Y-S, Wang S-H, Kuo T-J, Chen D-S, Chen P-J. 2009. Glycogen synthase kinase-3 regulates the phosphorylation of severe acute respiratory syndrome coronavirus nucleocapsid protein and viral replication. Journal of Biological Chemistry 284:5229-5239.
191. White TC, Yi Z, Hogue BG. 2007. Identification of mouse hepatitis coronavirus A59 nucleocapsid protein phosphorylation sites. Virus research 126:139-148.
192. Surjit M, Kumar R, Mishra RN, Reddy MK, Chow VT, Lal SK. 2005. The severe acute respiratory syndrome coronavirus nucleocapsid protein is phosphorylated and localizes in the cytoplasm by 14-3-3-mediated translocation. Journal of virology 79:11476-11486.
193. Spencer K-A, Dee M, Britton P, Hiscox JA. 2008. Role of phosphorylation clusters in the biology of the coronavirus infectious bronchitis virus nucleocapsid protein. Virology 370:373-381.
194. Peng TY, Lee KR, Tarn WY. 2008. Phosphorylation of the arginine/serine dipeptide-rich motif of the severe acute respiratory syndrome coronavirus nucleocapsid protein modulates its multimerization, translation inhibitory activity and cellular localization. The FEBS journal 275:4152-4163.
195. Mohandas DV, Dales S. 1991. Endosomal association of a protein phosphatase with high dephosphorylating activity against a coronavirus nucleocapsid protein. FEBS letters 282:419-424.
196. Chen H, Gill A, Dove BK, Emmett SR, Kemp CF, Ritchie MA, Dee M, Hiscox JA. 2005. Mass spectroscopic characterization of the coronavirus infectious bronchitis virus nucleoprotein and elucidation of the role of phosphorylation in RNA binding by using surface plasmon resonance. Journal of virology 79:1164-1179.

197. Chang C-K, Hsu Y-L, Chang Y-H, Chao F-A, Wu M-C, Huang Y-S, Hu C-K, Huang T-H. 2009. Multiple nucleic acid binding sites and intrinsic disorder of severe acute respiratory syndrome coronavirus nucleocapsid protein: implications for ribonucleocapsid protein packaging. Journal of virology 83:2255-2264.
198. Calvo E, Escors D, Lopez J, Gonzalez J, Alvarez A, Arza E, Enjuanes L. 2005. Phosphorylation and subcellular localization of transmissible gastroenteritis virus nucleocapsid protein in infected cells. Journal of general virology 86:2255-2267.
199. Chang C-k, Sue S-C, Yu T-h, Hsieh C-M, Tsai C-K, Chiang Y-C, Lee S-j, Hsiao H-h, Wu W-J, Chang W-L. 2006. Modular organization of SARS coronavirus nucleocapsid protein. Journal of biomedical science 13:59-72.
200. Rowland RR, Chauhan V, Fang Y, Pekosz A, Kerrigan M, Burton MD. 2005. Intracellular localization of the severe acute respiratory syndrome coronavirus nucleocapsid protein: absence of nucleolar accumulation during infection and after expression as a recombinant protein in vero cells. Journal of virology 79:11507-11512.
201. Wootton SK, Rowland RR, Yoo D. 2002. Phosphorylation of the porcine reproductive and respiratory syndrome virus nucleocapsid protein. Journal of virology 76:10569-10576.
202. Yoo D, Wootton SK, Li G, Song C, Rowland RR. 2003. Colocalization and interaction of the porcine arterivirus nucleocapsid protein with the small nucleolar RNA-associated protein fibrillarin. Journal of virology 77:12173-12183.
203. Zeegers J, Van der Zeijst B, Horzinek M. 1976. The structural proteins of equine arteritis virus. Virology 73:200-205.
204. Oldfield CJ, Dunker AK. 2014. Intrinsically disordered proteins and intrinsically disordered protein regions. Annual review of biochemistry 83:553-584.
205. Uversky VN. 2013. A decade and a half of protein intrinsic disorder: biology still waits for physics. Protein Science 22:693-724.
206. Van Der Lee R, Buljan M, Lang B, Weatheritt RJ, Daughdrill GW, Dunker AK, Fuxreiter M, Gough J, Gsponer J, Jones DT. 2014. Classification of intrinsically disordered regions and proteins. Chemical reviews 114:6589-6631.
207. Wright PE, Dyson HJ. 2015. Intrinsically disordered proteins in cellular signalling and regulation. Nature reviews Molecular cell biology 16:18.

208. Ahrens JB, Nunez-Castilla J, Siltberg-Liberles J. 2017. Evolution of intrinsic disorder in eukaryotic proteins. Cellular and Molecular Life Sciences 74:3163-3174.
209. Bellay J, Han S, Michaut M, Kim T, Costanzo M, Andrews BJ, Boone C, Bader GD, Myers CL, Kim PM. 2011. Bringing order to protein disorder through comparative genomics and genetic interactions. Genome biology 12:R14.
210. Xue B, Blocquel D, Habchi J, Uversky AV, Kurgan L, Uversky VN, Longhi S. 2014. Structural disorder in viral proteins. Chemical reviews 114:6880-6911.
211. Shanmugam S, Nichols AK, Saravanabalaji D, Welsch C, Yi M. 2018. HCV NS5A dimer interface residues regulate HCV replication by controlling its self-interaction, hyperphosphorylation, subcellular localization and interaction with cyclophilin A. PLoS pathogens 14:e1007177.
212. Badillo A, Receveur-Brechot Vr, Sarrazin Sp, Cantrelle Fo-X, Delolme Fdr, Fogeron M-L, Molle J, Montserret R, Bockmann A, Bartenschlager R. 2017. Overall structural model of NS5A protein from Hepatitis C Virus and modulation by mutations confering resistance of virus replication to cyclosporin A. Biochemistry 56:3029-3048.
213. Sólyom Z, Ma P, Schwarten M, Bosco M, Polidori A, Durand G, Willbold D, Brutscher B. 2015. The disordered region of the HCV protein NS5A: conformational dynamics, SH3 binding, and phosphorylation. Biophysical journal 109:1483-1496.
214. Verdegem D, Badillo A, Wieruszeski J-M, Landrieu I, Leroy A, Bartenschlager R, Penin F, Lippens G, Hanoulle X. 2011. Domain 3 of NS5A protein from the hepatitis C virus has intrinsic α-helical propensity and is a substrate of cyclophilin A. Journal of Biological Chemistry 286:20441-20454.
215. Götte B, Liu L, McInerney GM. 2018. The Enigmatic Alphavirus Non-Structural Protein 3 (nsP3) Revealing Its Secrets at Last. Viruses 10:105.
216. Frolov I, Akhrymuk M, Mobley JA, Frolova EI. 2017. Hypervariable domain of eastern equine encephalitis virus nsP3 redundantly utilizes multiple cellular proteins for replication complex assembly. Journal of virology 91:e00371-17.
217. Rupp JC, Sokoloski KJ, Gebhart NN, Hardy RW. 2015. Alphavirus RNA synthesis and non-structural protein functions. Journal of General Virology 96:2483-2500.
218. Chetan D. Meshram PA, Nikita Shiliaev, Nadya Urakova, James A. Mobley, Tatiana Agback, Elena I. Frolova, Ilya Frolov. 2018. Multiple Host Factors Interact with

Hypervariable Domain of Chikungunya Virus nsP3 and Determine Viral Replication in Cell-Specific Mode. Journal of virology 92.

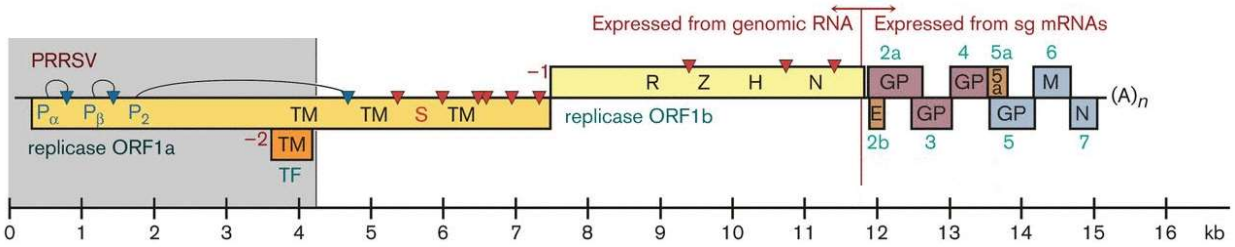

Figure 1.1. Genome architecture of porcine reproductive and respiratory syndrome virus.

5' terminal ORF1a and ORF1b encode all known 16 nonstructural proteins. Structural proteins are expressed by 3' ORFs. Figure adapted from Snijder et al., 2013.

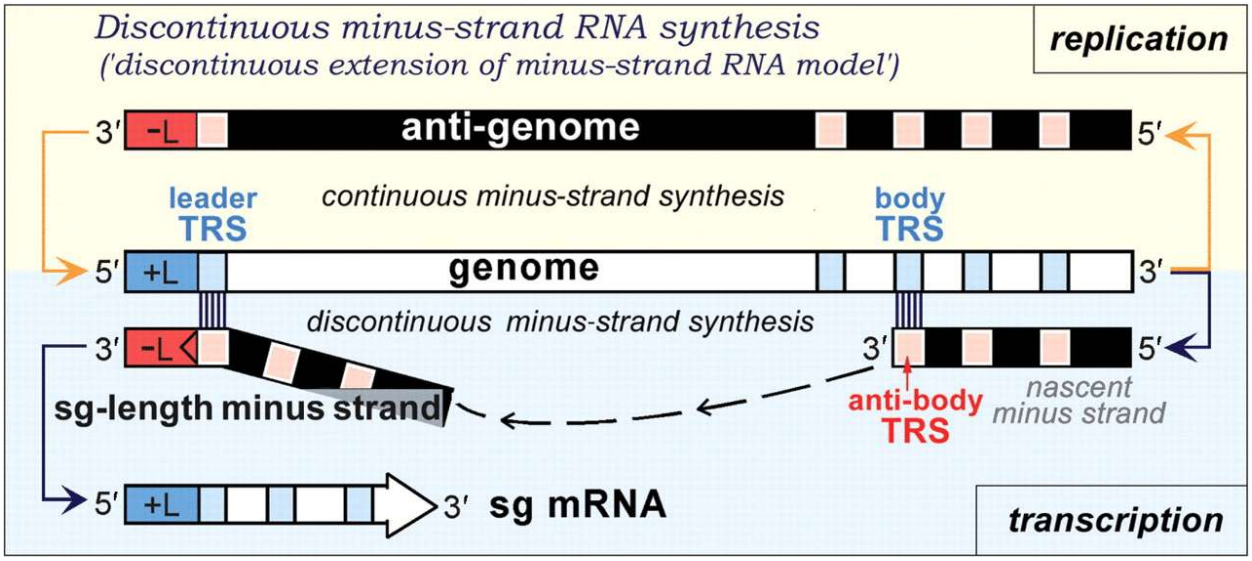

Figure 1.2. Subgenome transcription strategy of arteriviruses and coronaviruses.

Minus-strand subgenomes are synthesized discontinuously and used as templates for the continuous transcription of plus-strand subgenomes. Figure adapted from Pasternak et al., 2006.

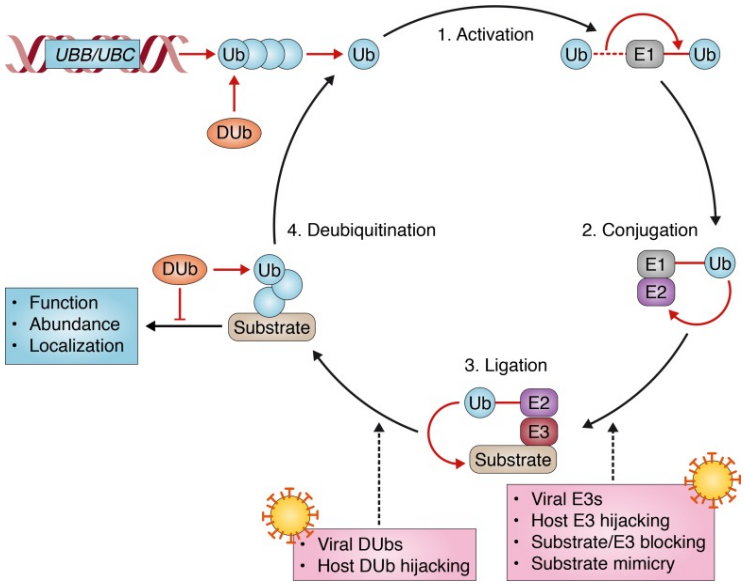

Figure 1.3. Host ubiquitination mechanism and strategies of viral manipulation.

Ubiquitin are conjugated on substrates through sequential reactions mediated by E1/E2/E3 enzymes. Ubiquitination could be reversed by DUBs. Figure adapted from Heaton et al., 2016.

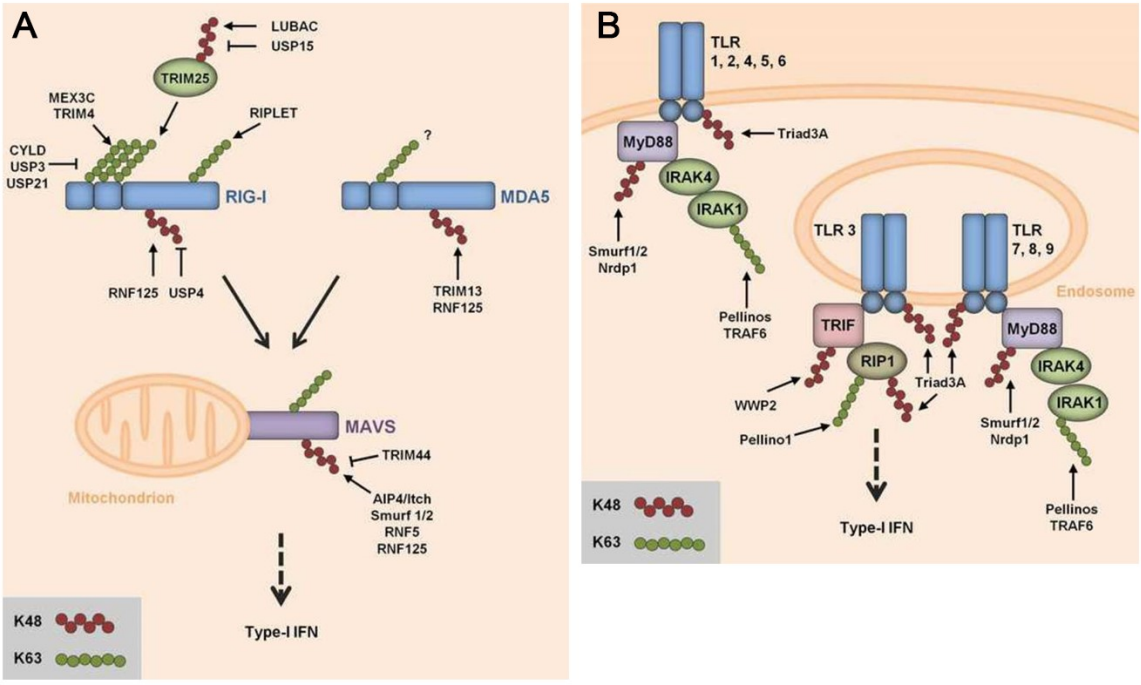

Figure 1.4. Ubiquitination-dependent regulation of RLRs and TLRs.

(A) RIG-I-like receptors pathway. (B) Toll-like receptors pathways. Figure adapted from Davis and Gack., 2015.

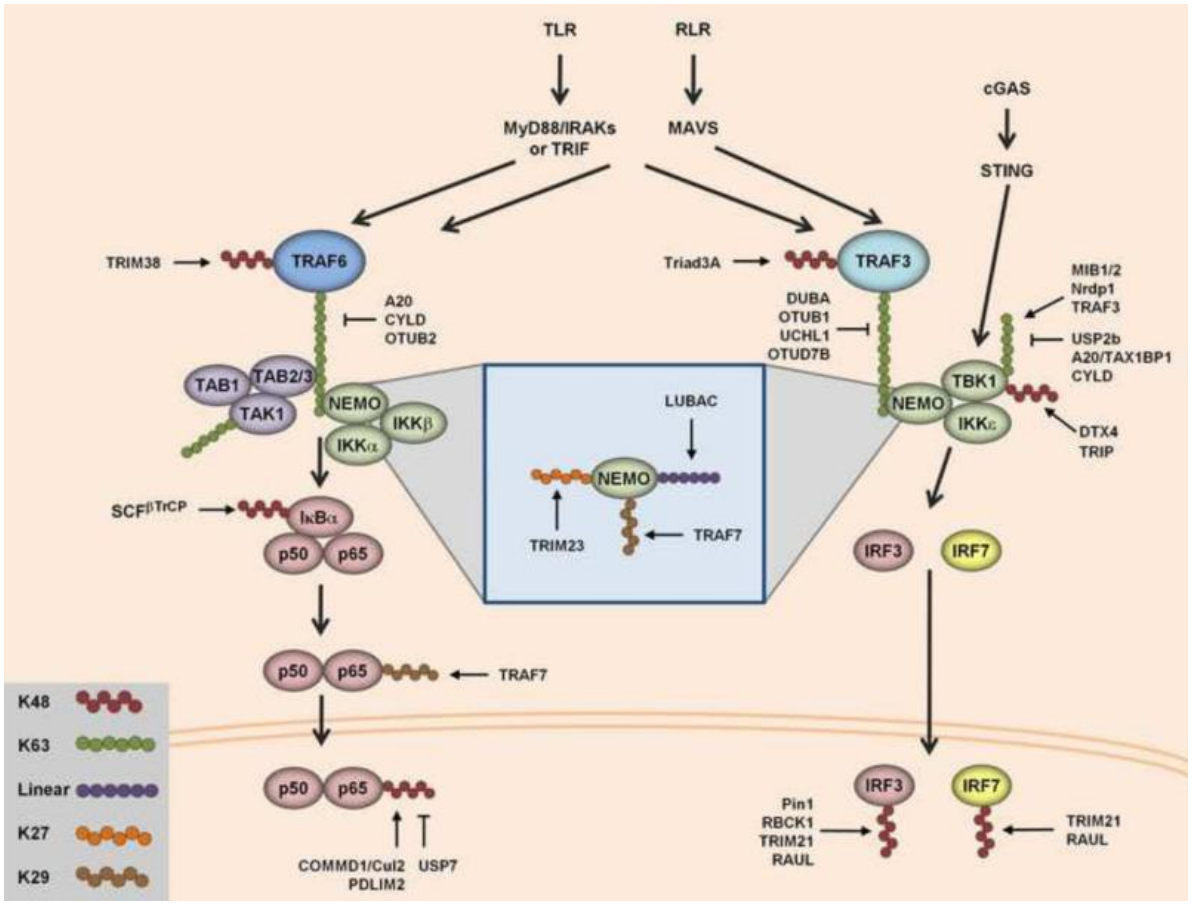

Figure 1.5. Ubiquitination regulation on converged downstream innate immune pathways.

After ligand recognition, RLRs and TLRs activation signals are transducted through key adaptors MAVS and MyD88/TRIF, respectively. Then signals of adaptor proteins will converge at TRAF6 for NF-κB activation or TRAF3 for IRF3/7 activation. Figure adapted from Davis and Gack., 2015.

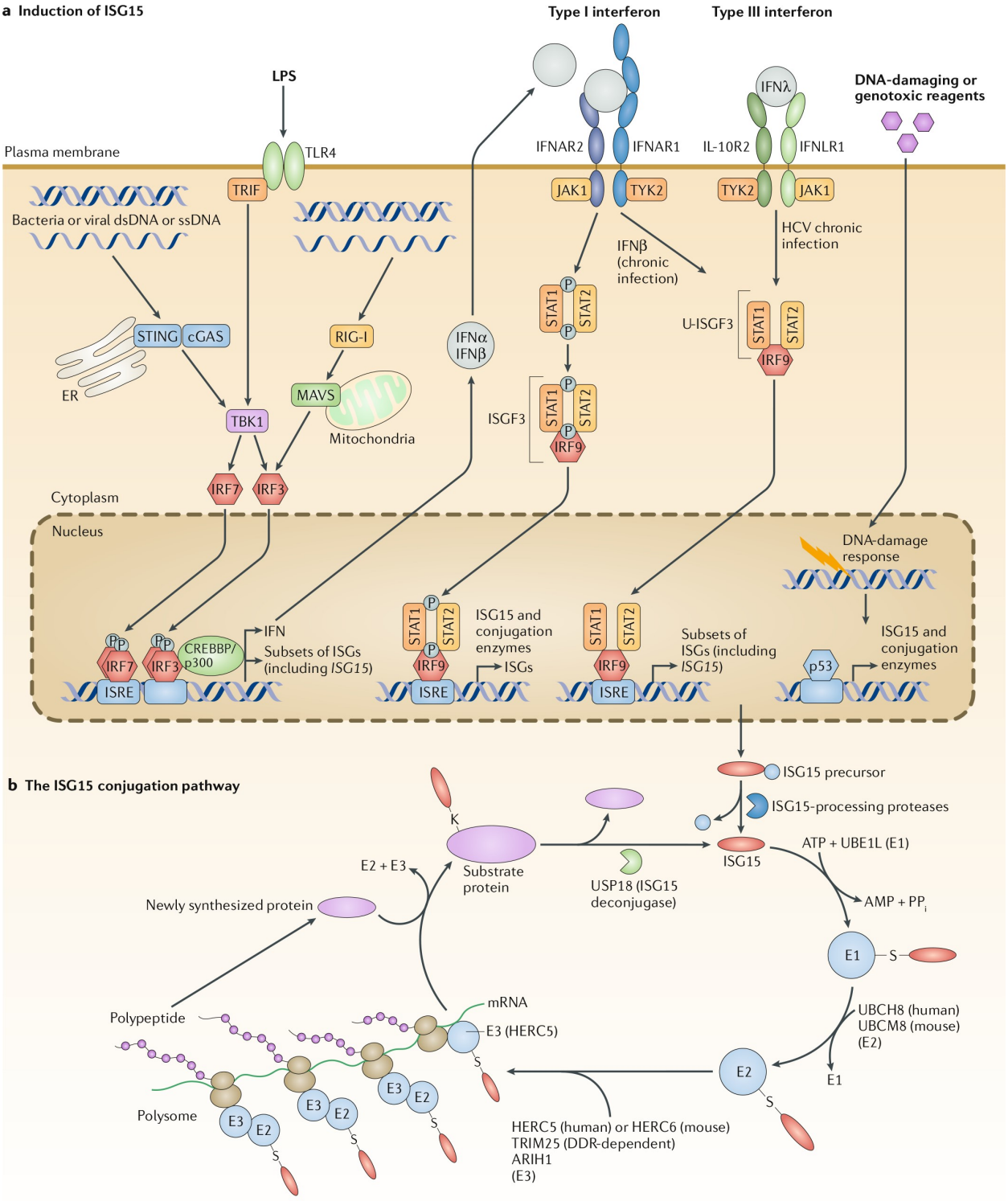

Figure 1.6. The induction of ISG15 expression and ISGylation pathway.

(A) The expression of ubiquitin-like protein ISG15 induced by PRRs activation. (B) ISG15 conjugation and deconjugation reaction. Figure adapted from Perng and Lenschow., 2018.

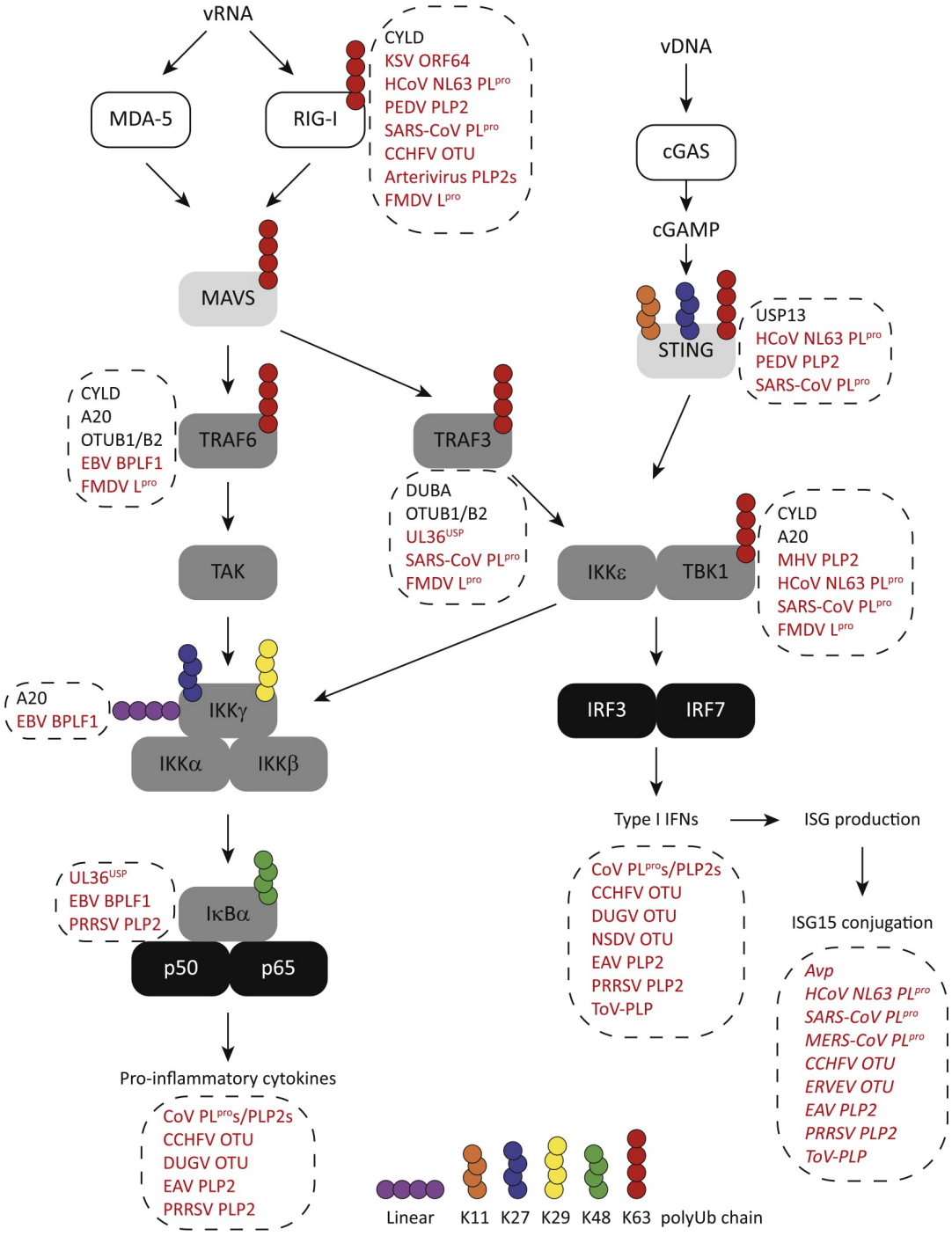

Figure 1.7. Illustration of innate immune pathways manipulated by viral DUBs.

Viral DUBs derived from both DNA and RNA viruses are able to interfere type I IFN production or NF-κB activation pathway. Figure adapted from Bailey-Elkin et al., 2017.

Chapter 2 - Nonstructural proteins nsp2TF and nsp2N of porcine reproductive and respiratory syndrome virus (PRRSV) play important roles in suppressing host innate immune responses

ABSTRACT: Recently, we identified a unique -2/-1 ribosomal frameshift mechanism in PRRSV, which yields two truncated forms of nonstructural protein (nsp) 2 variants, nsp2TF and nsp2N. Here, in vitro expression of individual PRRSV nsp2TF and nsp2N demonstrated their ability to suppress cellular innate immune responses in transfected cells. Two recombinant viruses were further analyzed, in which either nsp2TF was C-terminally truncated (vKO1) or expression of both nsp2TF and nsp2N was knocked out (vKO2). Host cellular mRNA profiling showed that a panel of cellular immune genes, in particular those involved in innate immunity, was upregulated in cells infected with vKO1 and vKO2. Compared to the wild-type virus, vKO1 and vKO2 expedited the IFN-α response and increased NK cell cytotoxicity, and subsequently enhanced T cell immune responses in infected pigs. Our data strongly implicate nsp2TF/nsp2N in arteriviral immune evasion and demonstrate that nsp2TF/nsp2N-deficient PRRSV is less capable of counteracting host innate immune responses.

2.1. Introduction

The innate immune response provides the first line of defense against intruding pathogens. It is essential for the initial control of infection and allows time for launching an adequate adaptive immune response. The type I interferon (IFN) system is a key component of the innate immune response (1, 2). Initially, pathogen-associated molecular patterns, like double-stranded RNA (dsRNA) in the case of RNA virus infection, are recognized by host cell receptors to activate protein signaling cascades, which results in the activation of transcription factors, including IRF3, NF-κB, and ATF-2/c JUN. Their coordinated activation leads to the formation of transcriptionally competent enhanceosomes in the cell nucleus, which induce the expression of type I IFNs. After being secreted from infected cells, type I IFNs bind to receptors on the surface of adjacent cells to activate the so-called JAK-STAT signaling pathway. This induces the transcription of a range of interferon-stimulated genes (ISGs), whose products function as effector molecules in the host cell response to viral infection (3, 4).

To counteract the host cell's defense mechanisms, many viruses express proteins that suppress or delay innate immune responses (1, 2, 5). Previous studies have implicated multiple proteins of porcine reproductive and respiratory syndrome virus (PRRSV) in suppressing the type I IFN response [reviewed in (6-9). PRRSV is an enveloped, positive-stranded RNA virus, which belongs to the order Nidovirales, family Arteriviridae. The family also includes equine arteritis virus (EAV), mouse lactate dehydrogenase-elevating virus (LDV), simian hemorrhagic fever virus (SHFV) [reviewed in (7)], and a number of more recently identified members, many of which are of simian origin (10, 11). Historically, PRRSV isolates have been divided into two distinct genotypes, European genotype (Type 1) and North American genotype (Type 2), which were recently promoted to the species level and named PRRSV-1 and PRRSV-2, respectively

(11). For both species, the genome is about 15 kb in length and contains at least 11 open reading frames (ORFs). The replicase gene is composed of ORF1a and ORF1b and occupies the 5'-proximal three-quarters of the viral genome. It encodes two large nonstructural polyproteins, pp1a and pp1ab, with the expression of the latter depending on -1 programmed ribosomal frameshift in the short ORF1a/ORF1b overlap region. The PRRSV pp1a and pp1ab precursors are processed into at least 14 functional nonstructural proteins (nsps) by a complex proteolytic cascade that is directed by four ORF1a-encoded protease domains: three papain-like proteases (PLP1α and PLP1β in nsp1α and nsp1β, respectively, and PLP2 in the N-terminal region of nsp2) and a chymotrypsin-like serine protease (SP) located in nsp4. PLP1α, PLP1β, and PLP2 cleave the junctions between nsp1α/1β, nsp1β/2, and nsp2/3, respectively, thus mediating the rapid release of nsp1α, nsp1β, and nsp2 from the nascent polyproteins (6). The nsp2 is the largest viral protein, and previous studies suggest that, in addition to its functions directly related to viral replication, it also serves as an innate immune antagonist (12-16). Frias-Staheli et al. (2007) first demonstrated that PRRSV-2 nsp2 exhibits general deubiquitinase (DUB) activity towards cellular ubiquitin (Ub) conjugates and showed deISGylation activity to remove the conjugates of the IFN-induced Ub homolog ISG15. The DUB activity of the PRRSV PLP2 domain was further characterized in an in vitro expression system for both PRRSV species (16, 17). The de-ISGylation activity of the PRRSV-1 PLP2 domain was observed in both in vitro expression system and infected porcine alveolar macrophages (15), although the level of de-ISGylation activity of purified PRRSV-2 PLP2 needs to be evaluated in more detail (18). The biological significance of these activities was supported by the ability of PLP2 to inhibit type I IFN activation and antagonize the antiviral effect of ISG15 (12, 15-17).

Recently, in all arteriviruses except for EAV, a new ORF was discovered that overlaps the nsp2-coding region of ORF1a in the –2/+1 reading frame (19). This ORF is translated via a unique –2 programmed ribosomal frameshift (PRF) mechanism, which produces a previously unknown transframe product (nsp2TF) consisting of approximately the N-terminal two-thirds of nsp2 and a unique C-terminal extension that is specified by the novel TF ORF (19). Remarkably, the same frameshift site was also found to direct an efficient -1 PRF, which is followed by a stop codon, thus yielding a second truncated nsp2 variant named nsp2N (19, 20). Our recent work demonstrated that efficient –2 and –1 PRF at this site in the nsp2-coding region depends on the transactivation of frameshifting by the upstream replicase subunit nsp1β, which is thought to bind together with cellular poly(C) binding proteins to the genomic region containing the –2/–1 PRF signal, possibly to form a roadblock for the translating ribosome (20, 21).

The newly identified nsp2TF and nsp2N proteins add to the functional complexity of the nsp2 region of the viral replicase, a region that has also been explored in the context of the development of genetically modified live virus (MLV) vaccines [reviewed in (6, 9)]. Importantly, nsp2, nsp2TF, and nsp2N all include the N-terminal PLP2 domain, which has been implicated in disrupting type I interferon signaling by deubiquitination and deISGylation of cellular proteins, as outlined above. In this study, we analyzed the effect of nsp2TF and nsp2N expression on host innate immune responses, both in an in vitro expression system and using recombinant viruses with impaired nsp2TF/nsp2N expression. An immune gene mRNA profiling system was employed to analyze the expression of a predefined set of 579 immune genes in cells infected with wild-type or nsp2TF/nsp2N-deficient viruses. A panel of innate immune genes was found to be upregulated in cells infected with nsp2TF/nsp2N-deficient viruses. Subsequent in vivo studies consistently showed that nsp2TF/nsp2N-deficient viruses were less capable of

interfering with the innate immune response in infected pigs. These studies provide important insights into the potential role(s) of PRRSV nsp2TF and nsp2N in the modulation of host innate immune responses.

2.2. Materials and Methods

Viruses and Cells: PRRSV-2 isolate SD95-21 (GenBank accession no. KC469618) and its nsp2TF/nsp2N-deficient mutants were used in all experiments. BHK-21 cells were used for initial transfection and recovery of recombinant viruses. MARC-145 cells were used for recombinant virus production and subsequent experiments. These cells were maintained in minimum essential medium (Invitrogen) supplemented with 10% heat-inactivated fetal bovine serum and antibiotics (100 units/mL of penicillin, 100 µg/mL of streptomycin and 0.25 µg/mL of fungizone) at 37 °C with 5% CO2. Porcine alveolar macrophages (PAMs) were obtained by lung lavage of 6-week-old PRRSV-naive piglets using a method described previously (22). The Sendai virus (SeV) Cantell strain was grown in embryonated chicken eggs, and virus titer was determined by hemagglutination assay using chicken red blood cells as described previously (23).

Plasmids: As indicated in Fig. 2.1A, a panel of plasmids expressing different regions of nsp2 was constructed by cloning corresponding viral genomic sequences into plasmid vector p3xFLAG-Myc-CMV-24 (Sigma-Aldrich, St. Louis, MO) using the restriction sites of NotI and BamHI. This panel of plasmids was designated as pFLAG-nsp2, pFLAG-nsp2TF, pFLAG-nsp2N, pFLAG-PLP2, pFLAG-nsp2$_{(599–1233)}$, pFLAG-nsp2TF$_{(599–1402)}$ and pFLAG-nsp2$_{(599–1579)}$. In the nsp2TF construct, the -2/-1 PRF region was modified to ensure expression of only nsp2TF using QuickChange™ site-directed mutagenesis kit (Agilent Technologies, Santa Clara, CA). Based on these constructs, a panel of mutant plasmids expressing nsp2-related proteins was

created using QuickChange™ site-directed mutagenesis kit (Agilent Technologies, Santa Clara, CA), in which PLP2 protease function was inactivated by introducing alanine substitutions at Cys^{433} and His^{503} (C/H>A). This panel of plasmids was designated as pFLAG-nsp2-C/H>A, pFLAG-nsp2TF-C/H>A, pFLAG-nsp2N-C/H>A, or pFLAG-PLP2-C/H>A. The full-length cDNA clones, pCMV-SD95-21 and pCMV-SD95-21-KO2, were used to recover SD95-21 WT virus and mutant vKO2 as we described previously (20). To create a full-length cDNA clone in which the TF ORF was truncated, three stop codons were introduced using QuickChange™ site-directed mutagenesis kit to generate infectious clone of pCMV-SD95-21-KO1 (Fig. 2.5A) (19). In luciferase reporter assay, two reporter plasmids, the p125-Luc and pRL-SV40 were used as described previously (14). The p125-Luc reporter plasmid was kindly provided by Takashi Fujita (Yoneyama et al., 1996) and expresses the firefly luciferase under the control of the IFN-β promoter. The pRL-SV40 plasmid that expresses a *Renilla* luciferase under the control of a simian virus 40 (SV40) promoter was purchased from Promega (Madison, WI).

Antibodies: To detect the expression of nsp2, nsp2TF, nps2N and PLP2, the α-FLAG monoclonal antibody (mAb) M2 (Sigma-Aldrich, St. Louis, MO) and mAb 140-68 specific for the PRRSV-2 PLP2 domain were used. A polyclonal antibody (pAb) specifically recognizing the unique C-terminal domain of nsp2TF was used to detect full-length nsp2TF (20). A rabbit pAb specifically recognizing the nsp2 C-terminus was used to detect full-length nsp2 (24). The mAb SDOW17 that is specific for the PRRSV nucleocapsid protein was used to detect viral infection in cell culture (25). The anti-GAPDH pAb sc-25778 (Santa Cruz Biotechnology, Dallas, TX) was used to detect the expression of housekeeping gene GAPDH.

Luciferase reporter assay: HEK-293T cells were transfected with 0.5 μg plasmid DNA of p125-luc (a luciferase reporter plasmid containing IFN-β promoter), 20 ng plasmid DNA of pRL-

SV40, and 1.0 µg plasmid DNA expressing 3xFLAG-tagged nsp2, nsp2TF, nsp2N, nsp2$_{(599–1233)}$, nsp2TF$_{(599–1402)}$, nsp2$_{(599–1579)}$, PLP2, nsp2-C/H>A, nsp2TF-C/H>A, nsp2N-C/H>A, PLP2-C/H>A, or empty vector (EV). Transfection was conducted using TransIT®-LT1 Transfection Reagent (Mirus Bio LLC, Madison, WI) following the manufacturer's instructions. At 24 h post transfection, cells were stimulated by infection with SeV at 100 HA unit per mL for 16 h. Cells were harvested and subjected to a reporter gene assay using a dual luciferase reporter system (Promega, Madison, WI) according to the manufacturer's instructions. Firefly or Renilla luciferase activity was measured in FLUOstar Omega (BMG Labtech). Relative luciferase activities were calculated by normalizing the firefly luciferase to Renilla luciferase activities. Cell lysates were further used on SDS-PAGE and Western blot analysis to evaluate protein expression. To determine the possible cytotoxicity caused by transfection and protein expression, triplicate cell cultures were subjected to test cell viability using CellTiter 96® AQueous One Solution Cell Proliferation Assay (MTS) (Promega, Madison, WI), following the manufacturer's instructions.

Radioimmunoprecipitation: MARC-145 cells were infected with PRRSV WT or nsp2TF/nsp2N-deficient mutants at a multiplicity of infection (MOI) of 0.1 for 24 h. After three washes with PBS, cells starved for 30 min in methionine- and cysteine-free medium (Thermo Fisher Scientific, Waltham, MA). Subsequently, protein synthesis in the infected cells was metabolically labeled for 2 h in methionine- and cysteine-free medium supplemented with 200 mCi [35S]methionine/cysteine mixture (Perkin-Elmer). After labelling, cells were harvested in lysis buffer [20 mM Tris/HCl (pH 7.6), 150 mM NaCl, 1% NP-40, 0.1% sodium deoxycholate, 0.1% SDS] and cell debris were removed by centrifugation. Immunoprecipitaion was performed with mAb 140-68 that recognizes PLP2 domain of nsp2, nsp2TF and nsp2N as described

previously (26). The protein complexes were dissolved in Laemmli sample buffer and heated at 96 °C for 6 min prior to loading onto Novex™ 6% Tris-Glycine Mini Gel (Thermofisher scientific, Waltham, MA). Gel was dried and exposed to autoradiography film (Sigma-Aldrich, St. Louis, MO).

Western blot analysis: To evaluate protein expression in DNA-transfected or virus-infected cells, western blot analysis was performed using the method described previously (27, 28). Briefly, cells were harvested with passive lysis buffer of Dual-Luciferase® Reporter Assay System (Promega, Madison, WI) or Pierce IP Lysis Buffer (Thermo Fisher Scientific, Waltham, MA) containing protease inhibitor cocktail (Sigma-Aldrich, St. Louis, MO). After being clarified by centrifugation at 15,000g for 15 min, cell lysates were mixed with Laemmli sample buffer (4X) and heated at 95 °C for 6 min or 37 °C for 30 min. Proteins were separated by sodium dodecyl sulfate-polyacrylamide gel electrophoresis (SDS-PAGE) and transferred onto a nitrocellulose membrane. After overnight blocking with 5% skim milk at 4 °C, the membrane was incubated with the primary antibody at an appropriate dilution at room temperature for 1 h. The membrane was washed three times with PBS containing 0.05% TWEEN 20 (PBST), and then incubated with the secondary antibody, IRDye® 800CW Goat anti-Mouse IgG (H + L) or/and IRDye® 680RD Goat anti- Rabbit IgG (H + L) (LI-COR Biosciences, Lincoln, NE) at an appropriate dilution for 1 h at room temperature. After extensively washing with PBST, the target proteins were visualized using a digital image system (Odyssey infrared imaging system; LI-COR Biosciences, Lincoln, NE).

Recovery of recombinant viruses from infectious cDNA clones: The recombinant viruses were launched by transfecting BHK-21 cells as described previously (27). Briefly, BHK-21 cells (70–80% confluency) were transfected with 2 μg of the type 2 PRRSV full-length cDNA clone

of pCMV-SD95-21 or the mutated full-length cDNA clones (pCMV-SD95-21-KO1 and pCMV-SD95-21-KO2) using FuGENE HD reagent (Promega, Madison, WI). At 48 h post transfection, cell culture supernatant was harvested and passaged onto MARC-145 cells. The viability of recombinant viruses was confirmed by indirect immunofluorescence assay using mAb SDOW17. The recombinant viruses were serially passaged on MARC-145 cells, and the passage 4 viruses were used for further analysis.

***In vitro* growth characterization of recombinant viruses in cell culture:** Growth kinetics of the recombinant and parental viruses were examined by infecting MARC-145 cells at an MOI of 0.01. Infected cells were collected at 0, 12, 24, 36, 48, 60, 72 h post-infection (hpi). Viral titers were determined by microtitration assay on MARC-145 cells and calculated as TCID50/mL according to the Reed and Muench method (29).

nCounter mRNA Profiling for detecting immune gene expression: MARC-145 cells were infected with WT PRRSV SD95-21, vKO1, or vKO2 at an MOI of 1.0. At 12 hpi, cells were harvested and subjected to total RNA extraction using SV Total RNA Isolation kit (Promega, Madison, WI) following the manufacturer's instructions. Total RNA (100 ng/sample) was used in cellular gene expression profiling. The expression levels of 579 immunological genes were evaluated by the nCounter assay with nCounter® Human Immunology v2 kit according to the manufacturer's instruction (NanoString Technologies, Seatle, WA), and 15 housekeeping genes were included for data normalization. Briefly, hybridization reactions were prepared with 5 µl diluted sample RNA according to the manufacturer's instruction. After 18 h of hybridization at 65 °C, the excess probes were removed and the hybridized probe/target complexes were immobilized in an nCounter cartridge using the nCounter Prep Station (Nanostring Technologies, Seatle, WA). Sample Cartridges were placed in a Digital Analyzer for data collection. The gene

expression data were analyzed with nSolver 2.6 according to the manufacturer's instruction (NanoString Technologies, Seatle, WA). Using gene expression in uninfected control cells as a reference, genes in virus-infected cells with a p-value lower than 0.05 and a fold change greater than 2 were defined as differentially expressed genes (DEGs).

KEGG Pathway Enrichment and Protein-Protein Interaction Network Analysis: The Database for Annotation, Visualization and Integrated Discovery (DAVID) (30, 31) was used to perform KEGG functional enrichment analysis of biological pathways that significantly enriched with DEGs from individual viral infection. A minimum count of 4 genes was used as the cut-off for determination of enriched biological pathways, and the p-values adjusted by Benjamini-Hochberg correction less than 0.05 were defined as significant enrichment. Protein-protein interaction (PPI) networks were constructed using Search Tool for the Retrieval of Interacting Genes/Proteins (STRING v10.0, http://string-db.org) (32) using DEG list from each viral infection. PPI confidence networks were generated using the confidence view option at a medium confidence of 0.400.

Quantitative RT-PCR for immune gene detection: To verify the results of nCounter gene expression profiling, the expression levels of selected genes were further evaluated by quantitative RT-PCR using the total RNA of the same sample for nCounter analysis. Briefly, cDNA was generated with 1 μg total RNA using SuperScript VILO cDNA Synthesis Kit (Life Technologies, Carlsbad, CA). According to the manufacturer's instruction, PCR reaction was formulated with 10 μl TaqMan Fast Advanced Master Mix (Applied Biosystems, Foster City, CA), 1 μl cDNA, and 1 μl of predesigned primer/probe sets (Applied Biosystems, Foster City, CA) for IFN-α, IFN-β, IRF-7, IL-28B, IFIT1, IFITM1 and TBP (TATA Box Binding Protein). Reactions were completed on CFX96 Real-Time PCR system (Bio-Rad) under the following

conditions: 2 min of 50 °C for UNG activation, 20 s of 95 °C for polymerase activation, 40 amplification cycles of 30 s of 95 °C and 30 s of 60 °C. The mRNA expression levels of IFN-α, IFN-β, IRF-7, IL-28B, IFIT1 and IFITM1 were normalized to the endogenous TBP mRNA level. To assess the ability of mutant viruses to stimulate innate immune responses in virus-infected swine macrophages, PAMs were infected with WT virus, vKO1 or vKO2 at an MOI of 1.0. At 12 hpi, cells were harvested in TRIzol LS (Life Technologies, Carlsbad, CA) and total cellular RNA was extracted according to the manufacturer's instruction. The mRNA expression levels of IFN-α, IFN-β, IRF-7, IL-28B, IFIT1, IFITM1 were quantified by quantitative RT-PCR using predesigned probe/primer sets (Applied Biosystems, Foster City, CA) and normalized to the housekeeping gene GAPDH mRNA.

Pig groups, sample collection and preparation: A total of thirty-six 4-week-old PRRSV-naive pigs were obtained from a certified PRRSV-negative herd. They were divided randomly into 4 groups (n=9) and housed separately in an animal isolation facility. After a four-day acclimation period, group 1 pigs were mock-infected with cell culture medium, while pigs from group 2–4 were inoculated with WT virus (group 2), vKO1 (group 3) or vKO2 (group 4). Pigs were immunized through both intranasal (IN) and intramuscular (IM) routes with 1 mL (1×106 TCID50) of the virus suspension in MEM to each nostril and to each side of the neck. Pigs were observed daily and serum samples were collected at 0, 1, 2, 6, 21, 28 DPI. Three pigs from each group were sequentially euthanized at 6, 21, and 28 DPI. During necropsy, whole blood was collected from each pig for preparation of peripheral blood mononuclear cells (PBMCs), and gross lung lesions were evaluated using the method described previously (33). The pig experiment was performed according to the protocol approved by the Institutional Animal Care and Use Committee (IACUC) of The Ohio State University, Ohio.

Quantification of viral load: For the detection of viral RNA and quantification of viral load, serum samples were examined using a quantitative RT-PCR method as described previously (28).

Analysis of swine cytokine response: Serum samples collected at 0, 1, 2 and 6 DPI were used to evaluate IFN-α production using ProcartaPlex Porcine IFN alpha Simplex kit (eBioscience, San Diego, CA) per manufacturer's instructions.

Pig NK cell cytotoxic assay: Pig natural killer (NK) cell-mediated cytotoxicity was determined with an immunofluorescence-based assay using a modified method described previously (34). A 7-aminoactinomycin D (7-AAD)/carboxyfluorescein succinimidyl ester (CFSE) cell-mediated cytotoxicity assay kit (Cayman Chemical, Ann Arbor, MI) was used. PBMCs were used as the source of NK cells (effectors), and K562 (human myeloblastoid cell line) cells were used as target cells.

Flow cytometry analysis: To measure the frequencies of virus-specific lymphocyte population, PBMCs isolated at 6, 21 and 28 DPI were restimulated with WT virus at an MOI of 0.1. At 72-h post stimulation, cells were subjected to flow cytometry analysis to determine the frequency of T-helper cells (CD3+CD4+CD8α-) and cytotoxic T cells (CD3+CD4-CD8αβ+) using the modified method described previously (35, 36). Briefly, PBMCs plated in a 96 well-plate were surface-labeled with swine lymphocyte specific fluorochrome- or biotin-conjugated monoclonal antibody, and then stained with fluorochrome-labeled anti-mouse isotype specific antibody or streptavidin. Antibodies used in the flow cytometry were anti-porcine CD3, CD4α and CD8α (Southernbiotech, AL) and CD8β (BD Biosciences, CA). Immunostained cells were acquired using the FACS Aria II (BD Biosciences) flow cytometer and analyzed using FlowJo (Tree Star,

Ashland, OR, USA) software. All specific cell population frequencies were presented as the percentage of CD3+ cells in PBMCs.

Statistical analysis: Statistical analysis was performed using GraphPad InStat version 5.0 (GraphPad Software). Comparisons among treatment groups were performed using one-way analysis of variance (ANOVA) followed by Tukey's post hoc test to determine the statistical significance. A p-value below 0.05 was considered to indicate a statistically significant difference between treatment groups. Due to co-housing of pigs infected with the same virus (WT or a mutant virus), co-housed pigs are not strictly speaking completely independent samples. Thus p-values in Fig. 2.8, Fig. 2.9, and Fig. 2.10 should be treated with caution.

2.3. Results

In vitro expression of PRRSV nsp2TF or nsp2N affects cellular innate immune responses

To investigate the innate immune suppression capability of nsp2TF and nsp2N, we expressed them individually in the context of a luciferase reporter assay, which is based on the expression of a firefly luciferase reporter gene under the control of an IFN-β promoter (37). IFN-β signaling was activated by infection with Sendai virus and the luciferase expression level was measured at 16 h after stimulation. PRRSV sequences (PRRSV-2, strain SD95-21) encoding full-length nsp2, nsp2TF, or nsp2N were expressed as an N-terminally FLAG-tagged fusion protein using a eukaryotic expression vector (Fig. 2.1A). The empty vector (EV) and a plasmid expressing the FLAG-tagged PLP2 domain, pFLAG-PLP2, were included as negative and positive controls, respectively. Similar transfection rate of ~80% was confirmed by immunofluorescence assay in HEK-293T cells transfected with these expression constructs (Fig. 2.2). No obvious cytotoxic effects of protein expression were observed in transfected cells as determined by cell viability assay (Fig. 2.3). Protein expression was evaluated by western blot analysis (Fig. 2.1B). Of note, many nsp2-related proteins of smaller size (less than 100 kDa)

were detected using the antibody (M2) recognizing the N-terminal FLAG-tag, yielding a similar pattern (with some exceptions) for the constructs expressing nsp2, nsp2TF, and nsp2N. This suggested that these products are C-terminally truncated expression products of distinct size.

In line with previous studies (14-16), expression of PLP2 strongly suppressed luciferase reporter gene expression from the IFN-β promoter following SeV infection. Expression of nsp2, nsp2TF, and nsp2N showed inhibitory effects on the IFN-β promoter activity, as indicated by around 60%, 80%, and 90% reduction of luciferase activity, respectively, in comparison to EV-transfected control cells (Fig. 2.1C). Next, to assess whether these inhibitory effects were directly linked to PLP2's protease/DUB activity, we engineered a panel of constructs in which the PLP2 catalytic residues Cys437 and His506 were both substituted with alanine (C/H>A). In HEK-293T cells transfected with these constructs, nsp2-related proteins were expressed (Fig. 2.1B). Most of the nsp2-related proteins of smaller size were also observed, suggesting these proteins did not result from PLP2-mediated cleavage of the expression products. Surprisingly, expression of nsp2TF-C/H>A and nsp2N-C/H>A still significantly inhibited IFN-β signaling following SeV stimulation (about 50% and 70% reduction compared to EV-transfected control cells). In contrast, in the context of the expression of full-length nsp2 or the PLP2 domain only, introduction of the PLP2-C/H>A mutation strongly impaired its ability to inhibit luciferase expression (Fig. 2.1C). Compared to the PLP2 construct, nsp2TF and nsp2N contain an additional 804 amino acids (aa 599–1402) and 635 amino acids (aa 599–1233), respectively. Our data suggested that, besides the PLP2/DUB domain, the downstream sequences of nsp2TF [nsp2TF(599–1402), see Fig. 2.1A] and nsp2N [nsp2(599–1233), see Fig. 2.1A] could also contain activities that antagonize innate immune signaling. Consistent with this hypothesis, the ectopically expressed nsp2TF(599–1402) and nsp2(599–1233) exhibited strong inhibitory effects

on IFN-β promoter activity (about 70% and 80% reduction) in comparison to that of EV control (Fig. 2.1C).

Since PLP2 was reported to also act as a deubiquitinase (13, 14, 16, 18), we further compared the effect of full-length nsp2, nsp2TF, and nsp2N on host cell protein ubiquitination. HEK-293T cells were transfected with a plasmid expressing HA-tagged ubiquitin and a plasmid expressing FLAG-tagged full-length nsp2, nsp2TF, or nsp2N. Again, the plasmid expressing the PLP2 domain and the empty vector were used as controls. As shown in Fig. 2.4A, expression of all four PLP2-containing products resulted in a decreased level of ubiquitin-conjugated proteins, but compared to full-length nsp2 and nsp2TF, nsp2N had a stronger effect and its DUB ability was comparable to that of the PLP2 domain. Subsequently, we analyzed the effect of nsp2TF and nsp2N expression on cellular protein ISGylation. In HEK-293T cells, ISG15 conjugates were generated by co-transfecting plasmids expressing ISG15 and three conjugation enzymes E1, E2, and E3. Cells were co-transfected with plasmids expressing one of the individual nsp2-related proteins. Co-expression of either nsp2TF or nsp2N resulted in a clear decrease in the level of ISGylated cellular proteins (Fig. 2.4B). To directly link the DUB and deISGylation activity to the PLP2 domain of these proteins, we repeated the assays using the respective C/H>A mutants. As shown in Fig. 2.4, compared to cells expressing the wild type nsp2-related proteins, much higher levels of ubiquitin and ISG15 conjugation were detected in cells expressing any of the corresponding C/H>A mutants. Taken together, these data revealed that individually expressed nsp2, nsp2TF, and nsp2N have the ability to interfere with cellular protein ubiquitination and ISGylation processes to variable degrees, with nsp2N showing the strongest effect. Moreover, the deconjugating activities of these nsp2-related proteins can be impaired by inactivating their PLP2 activity.

Construction and characterization in vitro properties of nsp2TF/nsp2N-deficient mutants

To determine whether the immune suppression potential of nsp2TF and nsp2N observed in in vitro expression systems reflect their actual function in PRRSV-infected cells, we employed a previously described strategy to create PRRSV-1 and PRRSV-2 mutants that are partially or completely deficient in expression of nsp2TF/nsp2N (19, 20). For the present study, PRRSV-2 mutants were analyzed, in which -2/-1 PRF-inactivating mutations were engineered in the full-length cDNA clone of PRRSV-2 strain SD95-21 (Fig. 2.5A). Mutant vSD95-21-KO1 (vKO1) retained an intact PRF signal, meaning that the relative translation of the three different ORFs should not be affected. However, whereas production of nsp2 and nsp2N was unchanged, nsp2TF was truncated due to the insertion of three stop codons in the TF ORF, resulting in the production of a C-terminally truncated form of nsp2TF (98.5 kDa, indicated by a red arrow in Fig. 2.5B). Mutant vSD95-21-KO2 (vKO2) carried a combination of mutations that disrupt the PRF slippery sequence and the downstream PRF-stimulatory CCCANCUCC motif. These mutations were previously shown to fully inactivate the PRRSV -2/-1 PRF without affecting nsp2 expression, since all mutations used were translationally silent with respect to ORF1a (19, 20). As shown in Fig. 2.5B, the expression of nsp2 appeared not to be affected in MARC-145 cells infected with either of these mutants. In comparison to the WT virus in MARC-145 cells, replication of vKO1 and vKO2 mutants was impaired, with 1- to 2-log decreased virus titers before 48 hpi. The peak titer of vKO2 was 0.5-log lower than that of WT virus, while vKO1 reached a similar peak titer as WT virus 12 h later (at 60 hpi, Fig. 2.5C).

Cellular immune gene expression is strongly upregulated in cells infected with nsp2TF/nsp2N-deficient PRRSV

To investigate whether impaired nsp2TF/nsp2N expression would alter the ability of PRRSV to interfere with cellular immune gene expression, an immune gene mRNA expression profile was determined for MARC-145 cells (a cell line of African green monkey origin) infected with WT PRRSV-2 strain SD95-21 and mutants vKO1 and vKO2. Since there is no monkey gene specific nCounter kit commercially available, we used the nCounter system that was designed for simultaneously analyzing the expression of a predefined set of 579 human immune genes (Human_Immunology_v2_Panel; NanoString Technologies, Seattle, WA). In comparison to mock-infected cells, a total of 11 differentially expressed genes (DEGs) were identified in WT virus-infected cells, while 96 and 78 DEGs were identified in cells infected with vKO1 and vKO2, respectively (Fig. 2.5A, Table 1). Among these hits, 10, 94, and 75 DEGs were upregulated in cells infected with WT virus, vKO1, and vKO2, respectively. Venn diagram analysis showed that the expression of 9 immune genes was upregulated in cells infected with all three viruses, whereas 63 DEGs were upregulated only in cells infected with either vKO1 or vKO2, and 1, 22, and 3 DEGs were specifically upregulated in cells infected with WT virus, vKO1, and vKO2, respectively (Fig. 2.6B, Table 3). In comparison to WT virus, vKO1 and vKO2 infection upregulated the expression of 84 and 65 more immune genes in host cells, respectively. To identify biological pathways associated with the identified DEGs, we performed a KEGG pathway enrichment analysis using the DAVID program (30, 31) to identify pathways that were consistently enriched in target cells (Fig. 2.6C, Table 2). The cytokine and cytokine receptor interaction and TNF signaling pathway were enriched pathways in WT virus-infected cells. By contrast, there were many additional pathways enriched in cells infected with vKO1 and vKO2, and the most strongly activated pathways identified were those involved in cytokine-cytokine receptor interaction, TNF signaling, Toll-like receptor signaling, NOD-like receptor

signaling, NF-κB signaling, RIG-I-like receptor signaling, chemokine signaling, JAK-STAT signaling, cytosolic DNA-sensing, and natural killer cell mediated cytotoxicity. Most of these strongly activated pathways are involved in the host cell's innate immune response.

To better understand the DEGs and visualize relevant activated pathways, the protein-protein interactions (PPI) networks of DEGs identified in infected cells were generated using the Search Tool for the Retrieval of Interacting Genes/Proteins (STRING), which is a database that provides a critical assessment and integration of protein–protein interactions, including direct (physical) as well as indirect (functional) associations (32). Consistent with the KEGG pathway enrichment analysis using DAVID, all enriched pathways in vKO1- and vKO2-infected cells identified above were significantly activated in PPI networks, while only cytokine-cytokine receptor interaction and TNF signaling pathways were significantly activated pathways in WT virus-infected cells. The representative enriched pathways in cells infected with WT, KO1 virus, and KO2 virus were highlighted in the protein-protein interactions networks of DEGs, respectively (Fig. 2.7).

The above data analysis showed that most of the pathways activated by vKO1 and vKO2 infection are involved in the host's innate immune response. Next, we performed quantitative RT-PCR (qRT-PCR) to independently verify the gene expression levels of six representative innate immune genes: IFN-α, IFN-β, IRF7, IL-28A, IFIH1, and IFITM1. Based on the analysis using the nCounter system, these genes had significantly higher expression levels in vKO1- and vKO2-infected cells than in WT virus-infected cells (Fig. 2.8A). Using the same RNA samples for multiplex digital mRNA profiling, the expression levels of these genes were evaluated with commercially available TaqMan Gene Expression assays (Thermofisher Scientific, Waltham, MA), and their relative expression levels were calculated. The TaqMan probes were specifically

designed for the targeted monkey genes. As shown in Fig. 2.8B, the relative gene expression levels of the six innate immune genes generally were highly consistent with the data generated using the nCounter system (Fig. 2.8A).

To further confirm the results generated using nCounter and TaqMan analysis, the ability of WT and mutant viruses to stimulate the expression of this panel of representative genes was verified in porcine alveolar macrophages (PAM), the primary target cell of PRRSV in infected animals. PAM cells were infected with the WT and mutant viruses at an MOI of 1, and harvested at 12 hpi. Swine gene specific qRT-PCR assays were used to analyze the expression levels of the selected immune genes. Consistent with the increased expression levels detected in MARC-145 cells, vKO1 and vKO2 induced significantly higher expression levels of IFN-α, IFN-β, IRF7, IL-28B, IFIH1, and IFITM1 in PAM cells (Fig. 2.8C).

Effect of nsp2TF/nsp2N deficiency on innate and cell-mediated immune responses in PRRSV-infected pigs

To assess whether the in vitro data described above could be reproduced in PRRSV-infected pigs, we investigated the impact of nsp2TF/nsp2N-deficient mutations on innate immune responses in PRRSV-infected nursery pigs. Four groups of pigs (n=9) were used, which were infected with WT virus (group 1), vKO1 (group 2), vKO2 (group 3), while the negative control group (group 4) was kept uninfected. To verify that WT and both mutant viruses replicated in vivo, serum samples collected by 6 days post infection (DPI) were used for virus isolation on MARC-145 cells. Virus was recovered from the serum samples of the pigs in groups 1–3, indicating active replication of WT and mutant viruses in pigs. The mutations introduced into the vKO1 and vKO2 genomes were found to be genetically stable throughout the study, as determined by sequencing of RT-PCR products derived from serum samples of vKO1- and

vKO2-infected pigs at 21 dpi. Viral load in serum samples collected at 1, 2, 6, 21, 28 DPI was further quantified by qRT-PCR. The results showed reduced viral loads in pigs infected with vKO1 and vKO2, which is consistent with the observations made in cell culture (Fig. 2.5C). At 1, 2 and 21 DPI, the group of pigs infected with vKO1 had significantly lower viral load (0.5–1.2 logs lower) than those pigs infected with WT virus (Fig. 2.9A, B and D). At 2, 6 and 21 DPI, viral loads in serum of vKO2-infected pigs were about 0.9–2 logs lower than those of WT virus-infected pigs (Fig. 2.9B-D).

To assess innate immune responses, IFN-α production in serum samples at 1, 2 and 6 DPI was initially evaluated with a ProcartaPlex Porcine IFN alpha Simplex kit (eBioscience, San Diego, CA). Compared with WT virus, vKO1 and vKO2 infection induced an earlier IFN-α response (Fig. 2.10A). Although similar peak concentrations of IFN-α were detected in all three groups of infected pigs, IFN-α level peaked one day earlier (at 1 DPI) in pigs infected with vKO1 and vKO2 compared to pigs infected with WT-virus. Of note, the IFN-α production in pigs correlated well with the viral loads that were measured (Fig. 2.9). In terms of IFN-α titer and viral load, the largest difference between WT virus and mutant virus infection groups was observed at 2 DPI.

The IFN-α response is critical for natural killer (NK) cell-mediated cytotoxicity. In our nCounter analysis, the genes associated with the NK cell cytotoxicity pathway were enriched in vKO1- and vKO2-infected cells (Fig. 2.6C; Table 2). Therefore, we further evaluated NK cell-mediated cytotoxicity in our experimentally infected pigs. Peripheral blood mononuclear cells (PBMCs) isolated from pigs infected with vKO1, vKO2 and WT virus were used as a source of NK cells (effectors; E) to evaluate NK cell cytotoxic activity using human myeloblastoid K562

cells as target (T) cells. At both E:T ratios used (100:1 and 50:1), increased NK cell cytotoxicity was observed in PBMCs from vKO1 and vKO2-infected pigs at 6 DPI (Fig. 2.10B).

A strong innate immune response following a viral infection is expected to enhance the cell-mediated adaptive immunity (38, 39). We further measured the frequency of different T cell subpopulations in PBMCs. Swine T cells expressing the combination of phenotypic markers CD3+CD4+CD8α- are T-helper cells, and cells with CD3+CD4-CD8αβ+ are exclusively cytotoxic T lymphocytes (CTLs) (40, 41). In the current study, PBMCs isolated at 6, 21 and 28 DPI were restimulated with WT virus and immunostained cells were analyzed by flow cytometry to identify the important T cell subsets. This analysis showed that the frequency of T-helper cells in PBMCs from vKO1-infected pigs was significantly increased by DPI 28 compared to that from mock-infected pigs (Fig. 2.11A), while the frequencies of cytotoxic T cells were significantly increased in PBMCs from both vKO1- and vKO2-infected pigs compared to that from mock-infected animals (Fig. 2.11B). These data indicate that the NK cells and the two important T cell subsets were activated, particularly in vKO1/vKO2-infected pigs, suggesting that early activation of innate immune responses following infection with nsp2TF/nsp2N-deficient mutants could enhance the innate and cell-mediated adaptive immunity, in comparison to an infection with WT virus.

2.4. Discussion

PRRSV infection is known to elicit poor innate immune responses (42-46). Previous studies identified the nsp2 PLP2/DUB domain as a major innate immune antagonist (13-16). The recently identified nsp2TF and nsp2N proteins (19, 20) share their N-terminal ~850 amino acid residues with nsp2, including the PLP2 domain, which raised the question whether all three nsp2 variants are individually able to antagonize the innate immune response in infected cells.

Potentially, they could exhibit different substrate specificities, a possibility that was highlighted by the previous observation that nsp2 and nsp2TF, which include different predicted transmembrane domains, appear to localize to different intracellular membrane structures (19), whereas the truncated nsp2N is predicted to be a cytosolic protein.

In this study, we compared the ability of full-length nsp2, nsp2TF and nsp2N to suppress the host innate immune response. These proteins were initially analyzed in an in vitro expression system and the results suggested that nsp2TF and nsp2N expression results in a much stronger inhibitory effect on type I IFN production. The deubiquitylation and deISGylation assays consistently showed that all three proteins have the ability to interfere with these processes which act on host cell (or viral) substrates, while nsp2N showed the strongest inhibitory effects. Interestingly, mutations targeting the catalytic residues of the PLP2 domain impaired the DUB and deISGylation activities of nsp2TF and nsp2N, but did not completely impair its immune suppression function, as demonstrated in the luciferase reporter assay (Fig. 2.1C). The data suggest that sequences downstream of the PLP2 domain of nsp2TF and nsp2N are also capable of suppressing innate immune functions (Fig. 2.1C). This may explain why in all assays nsp2N expression interfered most strongly with innate immune signaling. The activity of this part of nsp2N may depend on the localization, conformation or interactions of the protein, as both nsp2 and nsp2TF also contain this domain, but do not appear to counter innate immunity at the same level.

Obviously, we cannot formally exclude the possibility that the properties and/or relative activities of the three nsp2 variants may be different in virus-infected cells, which is why we proceeded to carefully compare the impact on the innate and cell-mediated immune (CMI) response of infection with WT virus and mutants vKO1 and vKO2, which lack expression of

functional nsp2TF and nsp2TF/nsp2N, respectively. The results obtained were consistent with those from the in vitro expression systems, with both mutants showing a clearly impaired ability to suppress innate immune gene expression. DEG profiles identified specific biological pathways that were consistently upregulated in vKO1- or vKO2-infected cells. Most of these pathways are involved in host innate immune responses, including RIG-I-like receptor signaling pathway, Jak-STAT signaling pathway, and NF-κB signaling pathway. These data are also consistent with previous reports that PLP2 has the ability to interfere with the ubiquitination of RIG-I and IκB, thus suppressing RIG-I-mediated innate immune signaling, including NF-κB activation and downstream effects on the Jak-STAT pathway towards ISG expression (14-16). Since the nCounter assay was originally designed for analyzing human gene expression, while our DEG profiling was conducted using PRRSV-infected MARC-145 cells (a cell line of African green monkey origin), we further confirmed the DEG profiling results using cytokine qRT-PCR to detect innate immune genes expression in PRRSV-infected MARC-145 cells as well as in PRRSV-infected swine macrophages. The results consistently showed that, compared to infection with WT virus, type I IFN (IFA 1/13, IFNB1), type III IFN (IL28B), and ISGs (IRF7, IFIH1 and IFITM1) are strongly upregulated in both MARC-145 cells and swine macrophages infected with the vKO1 and vKO2 mutants, which further implicates nsp2TF/nsp2N in innate immune suppression.

In both vKO1- and vKO2-infected cells, the nsp2 expression was not affected. The data from the in vitro expression system and virus infection condition made us speculate that nsp2TF and/or nsp2N might have evolved different mechanism(s) from nsp2 in the suppression of the host innate immune response. In PRRSV-infected cells, nsp2TF was found to be targeted to a different location from full-length nsp2 (19), *i.e.* the membranes of the exocytic pathway rather

than the replication structures formed from modified ER membranes, a process in which nsp2 is one of the key players (47, 48). It is also worth noting that, while the TF region of nsp2TF contains a predicted TM domain, nsp2N does not contain any predicted TM domain, meaning it could be a cytosolic protein possessing unique function(s). This is also supported by the observed activity in suppression of innate immune signaling exerted by the nsp2N part downstream of PLP2, which is apparently not related to DUB activity. The mechanistic aspects of the role of PRRSV nsp2TF and nsp2N in counteracting host innate immune response need to be further studied.

Besides the panel of innate immune cytokine genes showing significant upregulation in vKO1- and vKO2-infected cells, DEG profiling also identified other upregulated genes which are associated with cellular signaling pathways. Some of these are linked to pathways of the CMI response. It is worth noting here that the expression of the DEGs associated with the antigen processing and presentation pathway was also upregulated in vKO1- and vKO2-infected cells, more specifically the expression of the human leukocyte antigen (HLA-B), which is related to major histocompatibility complex (MHC) class I (Table 1). In comparison to mock-infected cells, a 13% decrease (statistically significant) of HLA-B expression was observed in WT virus-infected cells; in contrast, expression of HLA-B was 3- and 2.5-fold increased in cells infected with vKO1 and vKO2, respectively. Since the KO1 mutations result in the expression of a C-terminally truncated form of nsp2TF, without affecting nsp2 and nsp2N expression, the data suggest that nsp2TF could be involved in modulating the expression of HLA-B. The HLA complex encodes the MHC proteins, which are expressed on the cell surface for the regulation of the human immune system (49). In pigs, the corresponding gene complex is termed swine leukocyte antigen (SLA-1). The HLAs/SLAs present peptides on the cell surface, which are

derived from proteins (both native and foreign) produced inside the cell. Upon virus infection, the HLA/SLA system related to MHC class I presents viral peptides on the cell surface so that infected cells can be recognized and destroyed by CD8+ cytotoxic T cells (49, 50). Previous studies showed that PRRSV infection down-regulates the expression of SLA class I (SLA-1) in macrophages and dendritic cells (51-53). More importantly, a recent study demonstrated that SLA-1 expression was down-regulated by the expression of nsp2TF, and the C-terminal 68 amino acids of the TF domain were concluded to be critical for this activity (54). This result is consistent with our findings presented here and further implicates nsp2TF in the CMI response during PRRSV infection. This also provides an insight into the possible molecular mechanism of impaired CMI response in PRRSV infection. The involvement of nsp2TF in modulation of the CMI response is currently under investigation in our laboratory.

We further used a nursery pig model to assess the reduced ability of nsp2TF/nsp2N-deficient mutants to interfere with the innate immune response in vivo. Both mutants were found to have attenuated growth in pigs and no clinical symptoms or adverse side effects of vKO1/2 infection were observed (data not shown). Viable mutant viruses could be isolated from the serum of infected pigs by 6 days post infection, demonstrating viral replication in pigs. Genome sequencing confirmed the stability of the mutations introduced in the nsp2 region of the vKO1/2 mutants. Compared to WT virus, both mutants produced lower viral loads, with mutant vKO2 consistently being most impaired. In general, IFN-α production in pigs correlated well with viral loads. In vKO1 and vKO2 infected pigs, IFN-α reached peak titer one day earlier than that in WT virus infected pigs. The stronger IFN-α response also correlated well with NK cell-mediated cytotoxicity. In our nCounter analysis, the NK cell cytotoxicity pathway was enriched in vKO1 and vKO2 infected cells. At 6 DPI, increased NK cell cytotoxicity was observed in vKO1 and

vKO2-infected pigs. In addition, such a positive correlation is further demonstrated by the results of increased activation of Th1 CMI responses in vKO1 and vKO2-infected pigs. Collectively, these data suggest that expression of nsp2TF and nsp2N helps to delay the onset of the innate immune response following PRRSV infection in pigs, which may contribute to the weak induction of cell-mediated immunity during the later stage of viral infection.

It was expected that the mutations introduced in vKO1 might have less of an effect on the ability of the virus to suppress host innate immune responses, since they only C-terminally truncated nsp2TF without preventing frameshifting and the expression of nsp2N (and a truncated form of nsp2TF). Using our in vitro gene expression assays (Fig. 2.1C), both nsp2TF and nsp2N were found to antagonize innate immune signaling, with nsp2N expression having the strongest effect. The vKO2 mutations knock out the expression of both nsp2TF and nsp2N, which could have been expected to exert a stronger effect. However, when tested in the context of PRRSV infection, the qRT-PCR results consistently showed higher cytokine gene expression levels in vKO1-infected cells, although the difference was not statistically significant. Moreover, vKO1-infected pigs showed higher frequencies of T-helper and cytotoxic T cells than vKO2-infected pigs (Fig. 2.11). One explanation for this phenomenon could be the reduced ability of mutant vKO2 to replicate in infected cells and animals compared to vKO1. Even if vKO1 has a lower intrinsic IFN-inducing potential than vKO2, this could be compensated by a higher level of viral replication, eventually resulting in a comparable or stronger stimulation of the immune responses in infected cells or animals.

In conclusion, our results show that nsp2TF and nsp2N can modulate the host's innate immune responses against infection with PRRSV and, most likely, other arteriviruses. Recombinant viruses with impaired expression of these frameshift-derived nsp2 variants are

attenuated upon infection of animals. Since the ribosomal frameshift site in the nsp2-coding region is highly conserved among different PRRSV strains, manipulating the expression of nsp2TF and nsp2N may provide a rational basis for developing improved PRRSV vaccines in the future.

2.5. References

1. Randall RE, Goodbourn S. 2008. Interferons and viruses: an interplay between induction, signalling, antiviral responses and virus countermeasures. J Gen Virol 89:1-47.
2. Haller O, Kochs G, Weber F. 2006. The interferon response circuit: induction and suppression by pathogenic viruses. Virology 344:119-30.
3. Schoggins JW, Rice CM. 2011. Interferon-stimulated genes and their antiviral effector functions. Curr Opin Virol 1:519-25.
4. Raftery N, Stevenson NJ. 2017. Advances in anti-viral immune defence: revealing the importance of the IFN JAK/STAT pathway. Cell Mol Life Sci 74:2525-2535.
5. Versteeg GA, Garcia-Sastre A. 2010. Viral tricks to grid-lock the type I interferon system. Curr Opin Microbiol 13:508-16.
6. Fang Y, Snijder EJ. 2010. The PRRSV replicase: exploring the multifunctionality of an intriguing set of nonstructural proteins. Virus Res 154:61-76.
7. Snijder EJ, Kikkert M, Fang Y. 2013. Arterivirus molecular biology and pathogenesis. J Gen Virol 94:2141-63.
8. Ke H, Yoo D. 2017. The viral innate immune antagonism and an alternative vaccine design for PRRS virus. Vet Microbiol doi:S0378-1135(16)30632-0 [pii]
9. Lunney JK, Fang Y, Ladinig A, Chen N, Li Y, Rowland B, Renukaradhya GJ. 2016. Porcine Reproductive and Respiratory Syndrome Virus (PRRSV): Pathogenesis and Interaction with the Immune System. Annu Rev Anim Biosci 4:129-54.
10. Kuhn JH, Lauck M, Bailey AL, Shchetinin AM, Vishnevskaya TV, Bao Y, Ng TF, LeBreton M, Schneider BS, Gillis A, Tamoufe U, Diffo Jle D, Takuo JM, Kondov NO, Coffey LL, Wolfe ND, Delwart E, Clawson AN, Postnikova E, Bollinger L, Lackemeyer MG, Radoshitzky SR, Palacios G, Wada J, Shevtsova ZV, Jahrling PB, Lapin BA, Deriabin PG, Dunowska M, Alkhovsky SV, Rogers J, Friedrich TC, O'Connor DH, Goldberg TL. 2016. Reorganization and expansion of the nidoviral family Arteriviridae. Arch Virol 161:755-68.
11. Gulyaeva A, Dunowska M, Hoogendoorn E, Giles J, Samborskiy D, Gorbalenya AE. 2017. Domain Organization and Evolution of the Highly Divergent 5' Coding Region of Genomes of Arteriviruses, Including the Novel Possum Nidovirus. J Virol 91.

12. Beura LK, Sarkar SN, Kwon B, Subramaniam S, Jones C, Pattnaik AK, Osorio FA. 2010. Porcine reproductive and respiratory syndrome virus nonstructural protein 1beta modulates host innate immune response by antagonizing IRF3 activation. J Virol 84:1574-84.
13. Frias-Staheli N, Giannakopoulos NV, Kikkert M, Taylor SL, Bridgen A, Paragas J, Richt JA, Rowland RR, Schmaljohn CS, Lenschow DJ, Snijder EJ, Garcia-Sastre A, Virgin HWt. 2007. Ovarian tumor domain-containing viral proteases evade ubiquitin- and ISG15-dependent innate immune responses. Cell Host Microbe 2:404-16.
14. Sun Z, Chen Z, Lawson SR, Fang Y. 2010. The cysteine protease domain of porcine reproductive and respiratory syndrome virus nonstructural protein 2 possesses deubiquitinating and interferon antagonism functions. J Virol 84:7832-46.
15. Sun Z, Li Y, Ransburgh R, Snijder EJ, Fang Y. 2012. Nonstructural protein 2 of porcine reproductive and respiratory syndrome virus inhibits the antiviral function of interferon-stimulated gene 15. J Virol 86:3839-50.
16. van Kasteren PB, Beugeling C, Ninaber DK, Frias-Staheli N, van Boheemen S, Garcia-Sastre A, Snijder EJ, Kikkert M. 2012. Arterivirus and nairovirus ovarian tumor domain-containing Deubiquitinases target activated RIG-I to control innate immune signaling. J Virol 86:773-85.
17. Sun Z, Liu C, Tan F, Gao F, Liu P, Qin A, Yuan S. 2010. Identification of dispensable nucleotide sequence in 3' untranslated region of porcine reproductive and respiratory syndrome virus. Virus Res 154:38-47.
18. Deaton MK, Spear A, Faaberg KS, Pegan SD. 2014. The vOTU domain of highly-pathogenic porcine reproductive and respiratory syndrome virus displays a differential substrate preference. Virology 454-455:247-53.
19. Fang Y, Treffers EE, Li Y, Tas A, Sun Z, van der Meer Y, de Ru AH, van Veelen PA, Atkins JF, Snijder EJ, Firth AE. 2012. Efficient -2 frameshifting by mammalian ribosomes to synthesize an additional arterivirus protein. Proc Natl Acad Sci U S A 109:E2920-8.
20. Li Y, Treffers EE, Napthine S, Tas A, Zhu L, Sun Z, Bell S, Mark BL, van Veelen PA, van Hemert MJ, Firth AE, Brierley I, Snijder EJ, Fang Y. 2014. Transactivation of

programmed ribosomal frameshifting by a viral protein. Proc Natl Acad Sci U S A doi:201321930 [pii]

21. Napthine S, Treffers EE, Bell S, Goodfellow I, Fang Y, Firth AE, Snijder EJ, Brierley I. 2016. A novel role for poly(C) binding proteins in programmed ribosomal frameshifting. Nucleic Acids Res 44:5491-503.
22. Zeman D, Neiger R, Yaeger M, Nelson E, Benfield D, Leslie-Steen P, Thomson J, Miskimins D, Daly R, Minehart M. 1993. Laboratory investigation of PRRS virus infection in three swine herds. J Vet Diagn Invest 5:522-8.
23. Yonemitsu Y, Kaneda Y. 1999. Hemagglutinating virus of Japan liposome-mediated gene delivery to vascular cells. Methods Mol Med 30:295-306.
24. Guo R, Katz BB, Tomich JM, Gallagher T, Fang Y. 2016. Porcine Reproductive and Respiratory Syndrome Virus Utilizes Nanotubes for Intercellular Spread. J Virol 90:5163-75.
25. Nelson EA, Christopher-Hennings J, Drew T, Wensvoort G, Collins JE, Benfield DA. 1993. Differentiation of U.S. and European isolates of porcine reproductive and respiratory syndrome virus by monoclonal antibodies. J Clin Microbiol 31:3184-9.
26. Li Y, Tas A, Snijder EJ, Fang Y. 2012. Identification of porcine reproductive and respiratory syndrome virus ORF1a-encoded non-structural proteins in virus-infected cells. J Gen Virol 93:829-39.
27. Li Y, Zhu L, Lawson SR, Fang Y. 2013. Targeted mutations in a highly conserved motif of the nsp1beta protein impair the interferon antagonizing activity of porcine reproductive and respiratory syndrome virus. J Gen Virol 94:1972-83.
28. Li Y, Shyu DL, Shang P, Bai J, Ouyang K, Dhakal S, Hiremath J, Binjawadagi B, Renukaradhya GJ, Fang Y. 2016. Mutations in a Highly Conserved Motif of nsp1beta Protein Attenuate the Innate Immune Suppression Function of Porcine Reproductive and Respiratory Syndrome Virus. J Virol 90:3584-99.
29. Reed LJ, Muench H. 1938. A simple method of estimating fifty per cent endpoints. American journal of epidemiology 27:493-497.
30. Huang da W, Sherman BT, Lempicki RA. 2009. Systematic and integrative analysis of large gene lists using DAVID bioinformatics resources. Nat Protoc 4:44-57.

31. Huang da W, Sherman BT, Lempicki RA. 2009. Bioinformatics enrichment tools: paths toward the comprehensive functional analysis of large gene lists. Nucleic Acids Res 37:1-13.
32. Szklarczyk D, Franceschini A, Wyder S, Forslund K, Heller D, Huerta-Cepas J, Simonovic M, Roth A, Santos A, Tsafou KP, Kuhn M, Bork P, Jensen LJ, von Mering C. 2015. STRING v10: protein-protein interaction networks, integrated over the tree of life. Nucleic Acids Res 43:D447-52.
33. Halbur PG, Paul PS, Frey ML, Landgraf J, Eernisse K, Meng XJ, Lum MA, Andrews JJ, Rathje JA. 1995. Comparison of the pathogenicity of two US porcine reproductive and respiratory syndrome virus isolates with that of the Lelystad virus. Vet Pathol 32:648-60.
34. Lecoeur H, Fevrier M, Garcia S, Riviere Y, Gougeon ML. 2001. A novel flow cytometric assay for quantitation and multiparametric characterization of cell-mediated cytotoxicity. J Immunol Methods 253:177-87.
35. Binjawadagi B, Dwivedi V, Manickam C, Ouyang K, Torrelles JB, Renukaradhya GJ. 2014. An innovative approach to induce cross-protective immunity against porcine reproductive and respiratory syndrome virus in the lungs of pigs through adjuvanted nanotechnology-based vaccination. Int J Nanomedicine 9:1519-35.
36. Dhakal S, Hiremath J, Bondra K, Lakshmanappa YS, Shyu DL, Ouyang K, Kang KI, Binjawadagi B, Goodman J, Tabynov K, Krakowka S, Narasimhan B, Lee CW, Renukaradhya GJ. 2017. Biodegradable nanoparticle delivery of inactivated swine influenza virus vaccine provides heterologous cell-mediated immune response in pigs. J Control Release 247:194-205.
37. Yoneyama M, Suhara W, Fukuhara Y, Sato M, Ozato K, Fujita T. 1996. Autocrine amplification of type I interferon gene expression mediated by interferon stimulated gene factor 3 (ISGF3). J Biochem 120:160-9.
38. Iwasaki A, Medzhitov R. 2015. Control of adaptive immunity by the innate immune system. Nat Immunol 16:343-53.
39. Jain A, Pasare C. 2017. Innate Control of Adaptive Immunity: Beyond the Three-Signal Paradigm. J Immunol 198:3791-3800.

40. Talker SC, Kaser T, Reutner K, Sedlak C, Mair KH, Koinig H, Graage R, Viehmann M, Klingler E, Ladinig A, Ritzmann M, Saalmuller A, Gerner W. 2013. Phenotypic maturation of porcine NK- and T-cell subsets. Dev Comp Immunol 40:51-68.
41. Sinkora M, Butler JE. 2009. The ontogeny of the porcine immune system. Dev Comp Immunol 33:273-83.
42. Albina E, Piriou L, Hutet E, Cariolet R, L'Hospitalier R. 1998. Immune responses in pigs infected with porcine reproductive and respiratory syndrome virus (PRRSV). Vet Immunol Immunopathol 61:49-66.
43. Van Reeth K, Labarque G, Nauwynck H, Pensaert M. 1999. Differential production of proinflammatory cytokines in the pig lung during different respiratory virus infections: correlations with pathogenicity. Res Vet Sci 67:47-52.
44. Buddaert W, Van Reeth K, Pensaert M. 1998. In vivo and in vitro interferon (IFN) studies with the porcine reproductive and respiratory syndrome virus (PRRSV). Adv Exp Med Biol 440:461-7.
45. Luo R, Xiao S, Jiang Y, Jin H, Wang D, Liu M, Chen H, Fang L. 2008. Porcine reproductive and respiratory syndrome virus (PRRSV) suppresses interferon-beta production by interfering with the RIG-I signaling pathway. Mol Immunol 45:2839-46.
46. Miller LC, Laegreid WW, Bono JL, Chitko-McKown CG, Fox JM. 2004. Interferon type I response in porcine reproductive and respiratory syndrome virus-infected MARC-145 cells. Arch Virol 149:2453-63.
47. Oudshoorn D, van der Hoeven B, Limpens RW, Beugeling C, Snijder EJ, Barcena M, Kikkert M. 2016. Antiviral Innate Immune Response Interferes with the Formation of Replication-Associated Membrane Structures Induced by a Positive-Strand RNA Virus. MBio 7.
48. Knoops K, Barcena M, Limpens RW, Koster AJ, Mommaas AM, Snijder EJ. 2012. Ultrastructural characterization of arterivirus replication structures: reshaping the endoplasmic reticulum to accommodate viral RNA synthesis. J Virol 86:2474-87.
49. Janeway Jr CA, Travers P, Walport M, Shlomchik MJ. 2001. The major histocompatibility complex and its functions.

50. Bhardwaj N, Bender A, Gonzalez N, Bui LK, Garrett MC, Steinman RM. 1994. Influenza virus-infected dendritic cells stimulate strong proliferative and cytolytic responses from human CD8+ T cells. J Clin Invest 94:797-807.
51. Wang X, Eaton M, Mayer M, Li H, He D, Nelson E, Christopher-Hennings J. 2007. Porcine reproductive and respiratory syndrome virus productively infects monocyte-derived dendritic cells and compromises their antigen-presenting ability. Arch Virol 152:289-303.
52. Park JY, Kim HS, Seo SH. 2008. Characterization of interaction between porcine reproductive and respiratory syndrome virus and porcine dendritic cells. J Microbiol Biotechnol 18:1709-16.
53. Du J, Ge X, Liu Y, Jiang P, Wang Z, Zhang R, Zhou L, Guo X, Han J, Yang H. 2015. Targeting Swine Leukocyte Antigen Class I Molecules for Proteasomal Degradation by the nsp1alpha Replicase Protein of the Chinese Highly Pathogenic Porcine Reproductive and Respiratory Syndrome Virus Strain JXwn06. J Virol 90:682-93.
54. Cao QM, Subramaniam S, Ni YY, Cao D, Meng XJ. 2016. The non-structural protein Nsp2TF of porcine reproductive and respiratory syndrome virus down-regulates the expression of Swine Leukocyte Antigen class I. Virology 491:115-24.

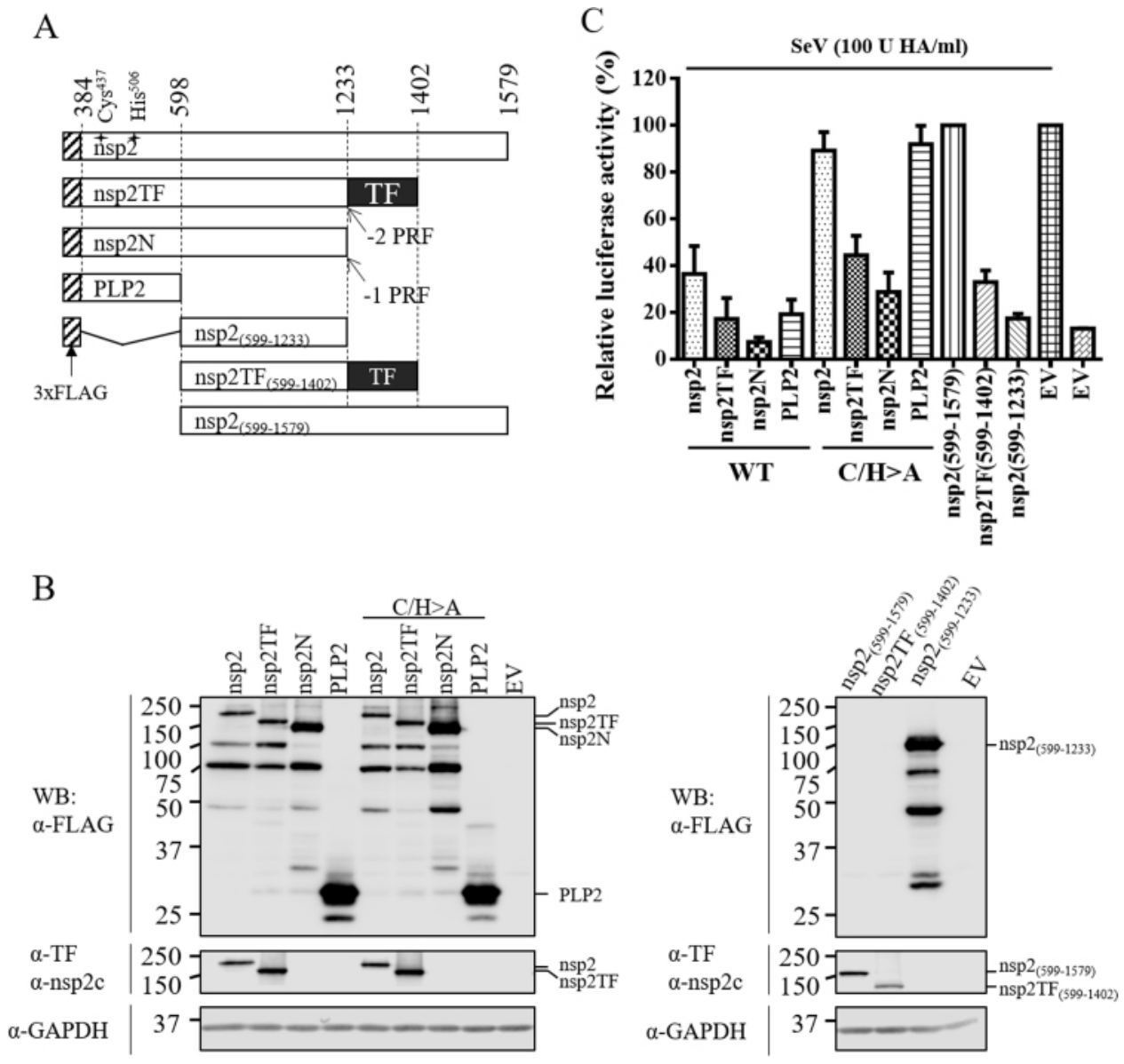
A
384
Cys437
His506
598
1233
1402
1579
nsp2
nsp2TF
TF
nsp2N
-2 PRF
PLP2
-1 PRF
nsp2(599-1233)
3xFLAG
nsp2TF(599-1402)
TF
nsp2(599-1579)
C
SeV (100 U HA/ml)
Relative luciferase activity (%)
120
100
80
60
40
20
0
nsp2
nsp2TF
nsp2N
PLP2
nsp2
nsp2TF
nsp2N
PLP2
WT
C/H>A
nsp2(599-1579)
nsp2TF(599-1402)
nsp2(599-1233)
EV
EV
B
C/H>A
nsp2
nsp2TF
nsp2N
PLP2
nsp2
nsp2TF
nsp2N
PLP2
EV
WB:
α-FLAG
250
150
100
75
50
37
25
nsp2
nsp2TF
nsp2N
PLP2
α-TF
α-nsp2c
250
150
nsp2
nsp2TF
α-GAPDH
37
nsp2(599-1579)
nsp2TF(599-1402)
nsp2(599-1233)
EV
WB:
α-FLAG
250
150
100
75
50
37
25
nsp2(599-1233)
α-TF
α-nsp2c
250
150
nsp2(599-1579)
nsp2TF(599-1402)
α-GAPDH
37

Figure 2.1. PRRSV nsp2 variants suppress type I IFN production.

(A) A schematic diagram of individual PRRSV nsp2 variants (nsp2, nsp2TF and nsp2N) and domains [PLP2, $nsp2_{(599–1233)}$, $nsp2TF_{(599–1402)}$ and $nsp2_{(599–1579)}$]. The numbers show both N- and C-terminal residues on polyprotein 1a for each individual protein. The catalytic residues of the PLP2 domain are labeled as Cys^{437} and His^{506}. (B) Expression of nsp2-related proteins were evaluated by western blot analysis using anti-FLAG M2 mAb. GAPDH was detected as loading control. Rabbit pAb against the unique nsp2 C-terminus was used to confirm the expression of nsp2 and $nsp2_{(599–1579)}$, while rabbit pAb against unique nsp2TF C-terminus was used to confirm the expression of nsp2TF and $nsp2TF_{(599–1402)}$. (C) Effect of nsp2-related proteins on the expression of IFN-β promoter-driven luciferase expression. HEK-293T cells were cotransfected with a plasmid expressing individual nsp2-related proteins or domains, p125-Luc reporter plasmid expressing firefly luciferase under the control of the IFN-β promoter (0.5 μg), and pRL-SV40 reporter plasmid (20 ng). An empty vector (EV) was used as a control. At 24 h posttransfection, cells were stimulated with SeV at 100 HA units/mL or for 16 h. Cell lysates were harvested for measuring luciferase activity. Relative luciferase activities were calculated by normalizing the firefly luciferase to Renilla luciferase activities; the relative luciferase activity in cells with EV-transfection and SeV stimulation was set as 100%. The mean value and SEM of representative experiments are shown. All experiments were repeated at least three times, and duplicates were performed each time.

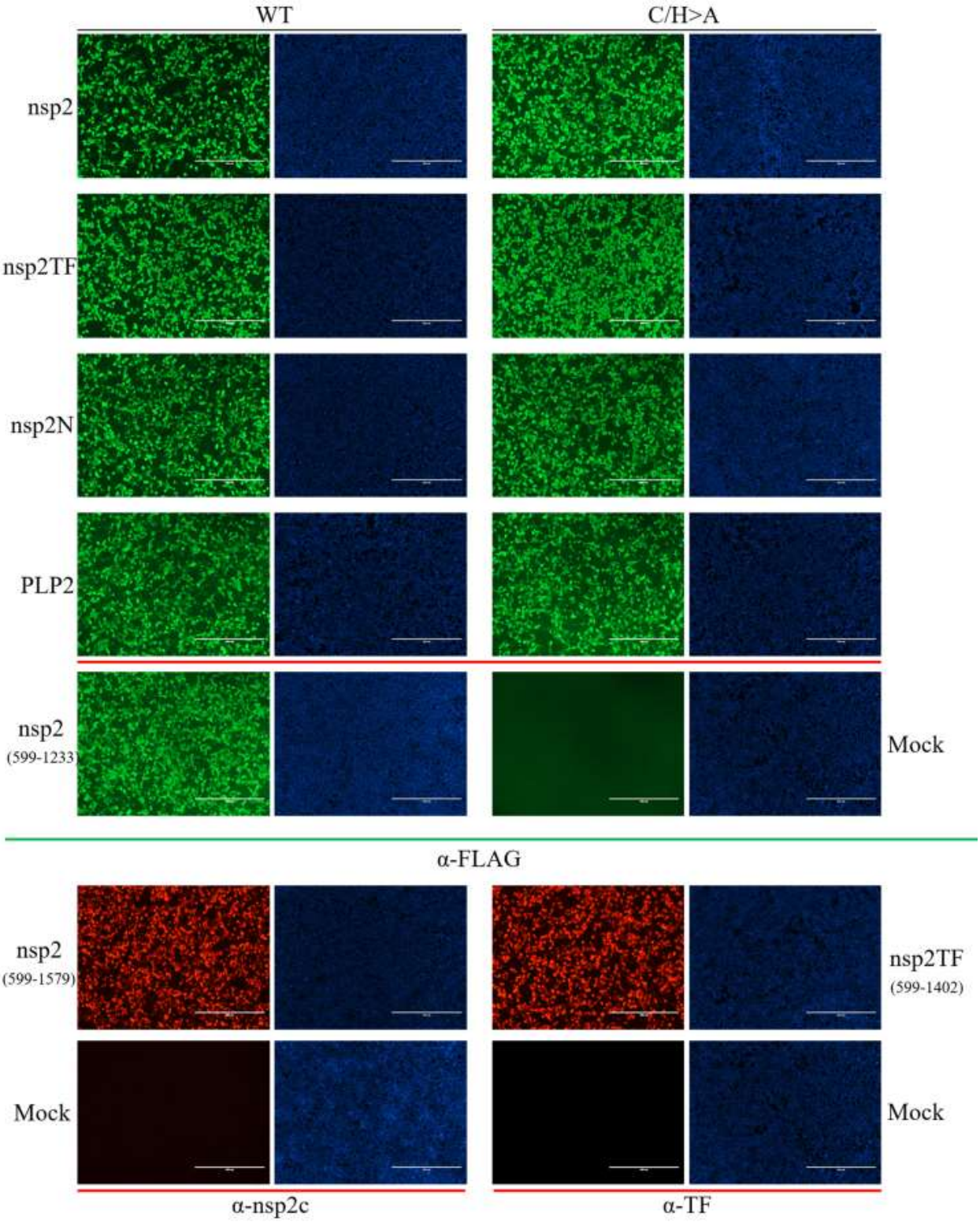
WT
C/H>A
nsp2
nsp2TF
nsp2N
PLP2
nsp2
(599-1233)
Mock
α-FLAG
nsp2
(599-1579)
nsp2TF
(599-1402)
Mock
Mock
α-nsp2c
α-TF

Figure 2.2. Expression of nsp2-related proteins in HEK-293T cell.

HEK-293T cells seeded in a 24-well plate were transfected with a plasmid (0.5 μg) expressing each of nsp2-related protein. At 24 hpi, immunofluorescence assay was performed to evaluate protein expression. The α-FLAG mAb was used to detect the expression of FLAG-tagged proteins. Rabbit pAb (α-TF) specifically recognizing the unique C-terminal domain of nsp2TF was used to detect the expression of full-length nsp2TF (Li et al., 2014), while rabbit pAb (α-nsp2) specifically recognizing the nsp2C-terminus was used to detect the expression of full-length nsp2 (Guo et al., 2016). Cell nucleus was stained with DAPI.

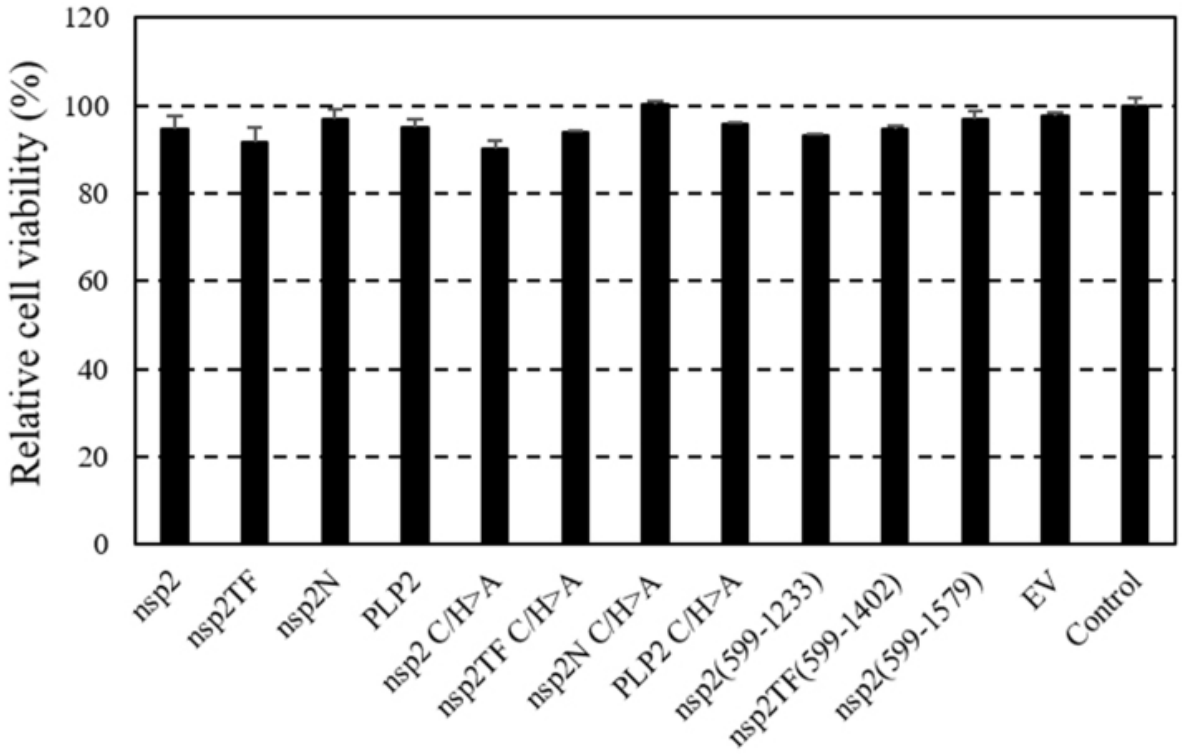

Figure 2.3. Effect of nsp2-related proteins on HEK-293T cell viability.

Cell viability was determined using a CellTiter 96 AQueous cell proliferation assay (Promega). Viability of transfected cells were compared to that of untreated control cells (100%). The average and standard deviation (SD) of a representative experiment are shown. All experiments were repeated twice, and triplicates were performed at each time.

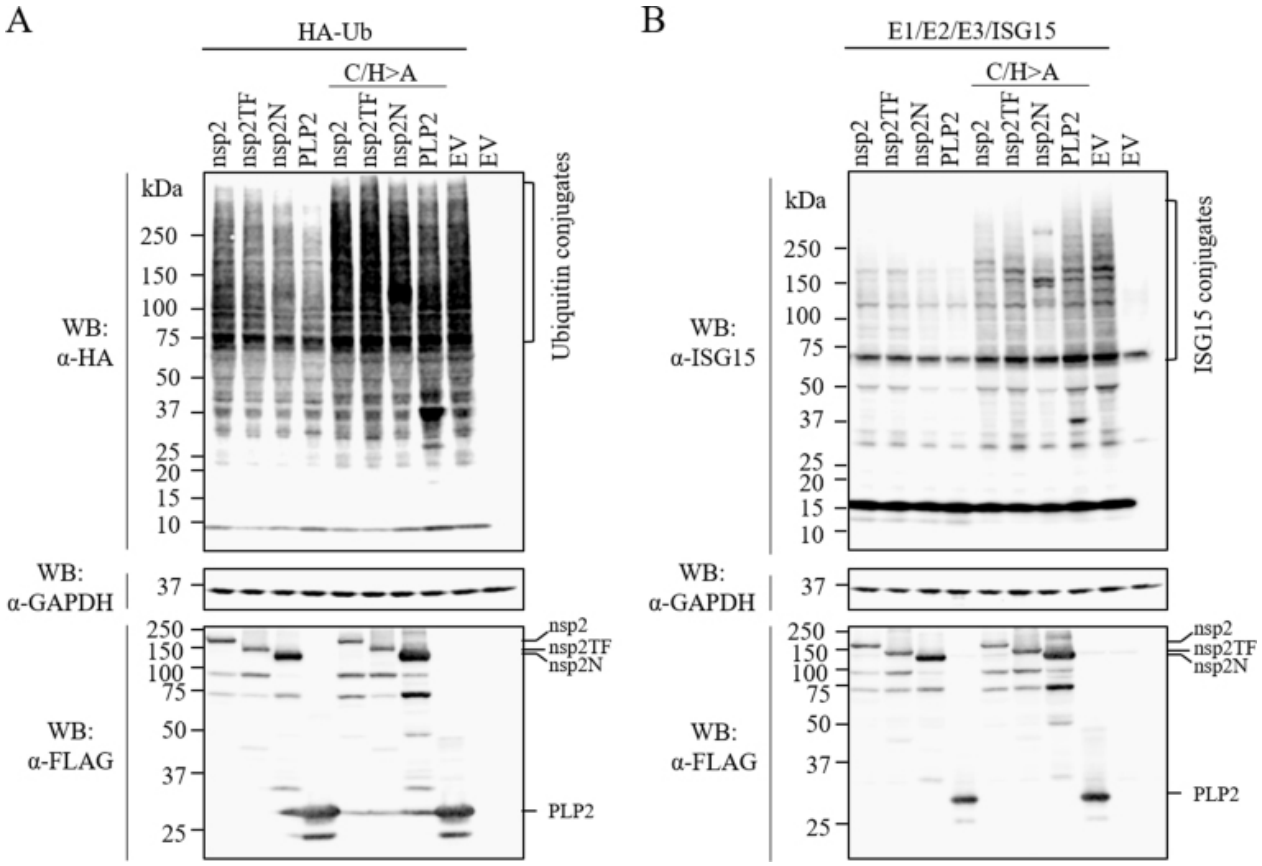

Figure 2.4. The de-ubiquitination and de-ISGylation activities of PRRSV nsp2-related proteins.

(A) Effect of nsp2 related protein expression on ubiquitin conjugation. HEK-293T cells were co-transfected with plasmid DNAs expressing HA-Ub and FLAG-tagged nsp2, nsp2TF, nsp2N, PLP2 or their catalytic site mutants (nsp2-C/H>A, nsp2TF-C/H>A, nsp2N-C/H>A, PLP2-C/H>A). HA-Ub conjugated cellular proteins were visualized by western blot analysis using anti-HA mAb. The expression of FLAG-tagged nsp2 related proteins was detected by anti-FLAG M2 mAb. (B) HEK-293T cells were co-transfected with plasmid DNAs expressing ISG15 and its conjugation enzymes E1/E2/E3, FLAG-tagged nsp2, nsp2TF, nsp2N, PLP2 or their catalytic site mutants (nsp2-C/H>A, nsp2TF-C/H>A, nsp2N-C/H>A, PLP2-C/H>A). ISG15-conjugated cellular proteins were detected by ISG15 specific mAb in western blot analysis. The expression of FLAG-tagged nsp2 related proteins was detected by anti-FLAG M2 mAb. For both assays, the empty p3xFLAG vector plasmid was included as a control, while expression of housekeeping gene GAPDH was detected as a loading control.

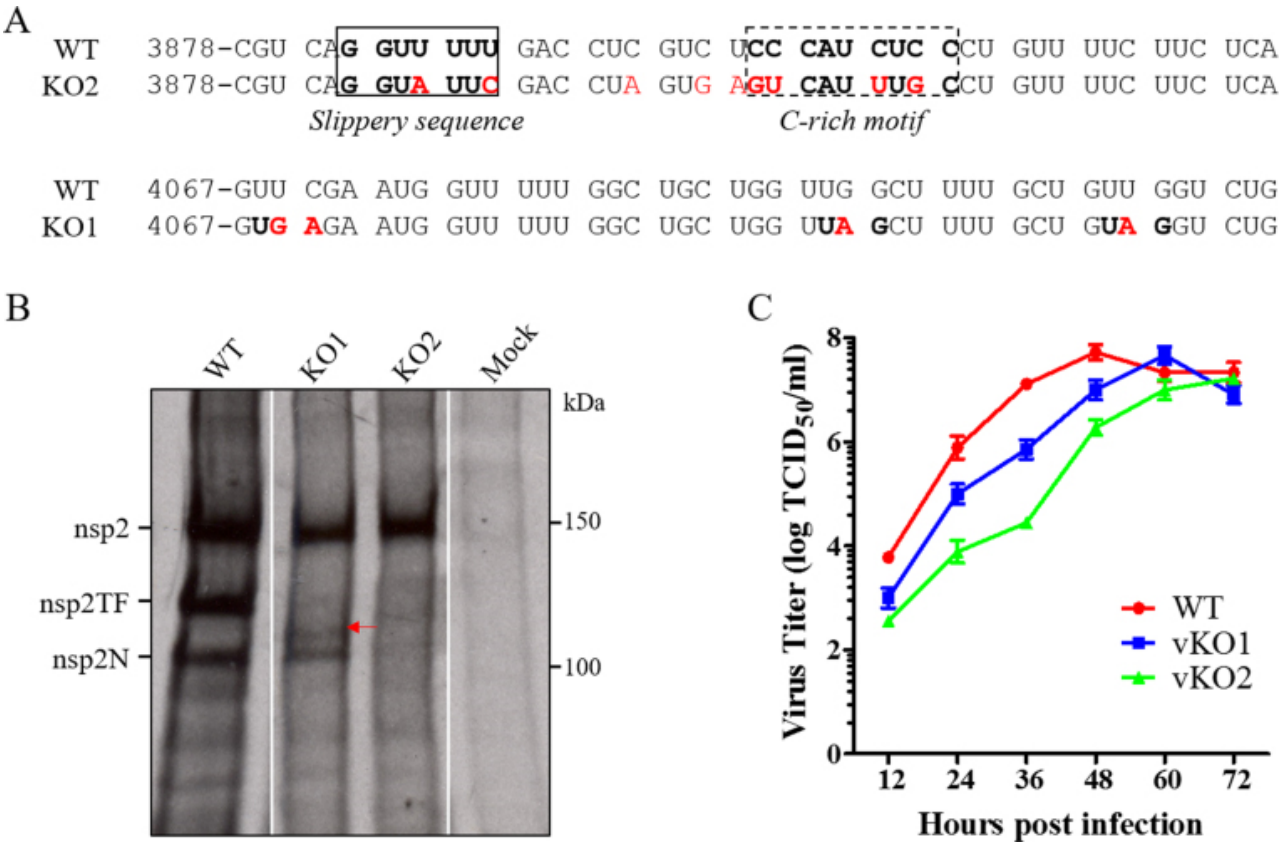

Figure 2.5. Construction and in vitro characterization of nsp2TF/nsp2N-deficient mutants.

(A) Nucleotide sequences in the regions of mutations created in nsp2TF/nsp2N-deficient mutants. KO1, knockout mutant 1 (premature termination codons in TF ORF); KO2, knockout mutant 2 (premature termination codon and disrupted frameshift signal). Mutated nucleotides are shown in red. (B) Radioimmunoprecipitation detection of nsp2-related proteins in virus infected cells. MAb 140-68 was used to recognize the common N-terminal PLP2 domain. The truncated nsp2TF in vKO1-infected cells is indicated with a red arrow. (C) Multiple-step virus growth curve. Each data point shown represents the mean value from duplicates, and error bars show SEM.

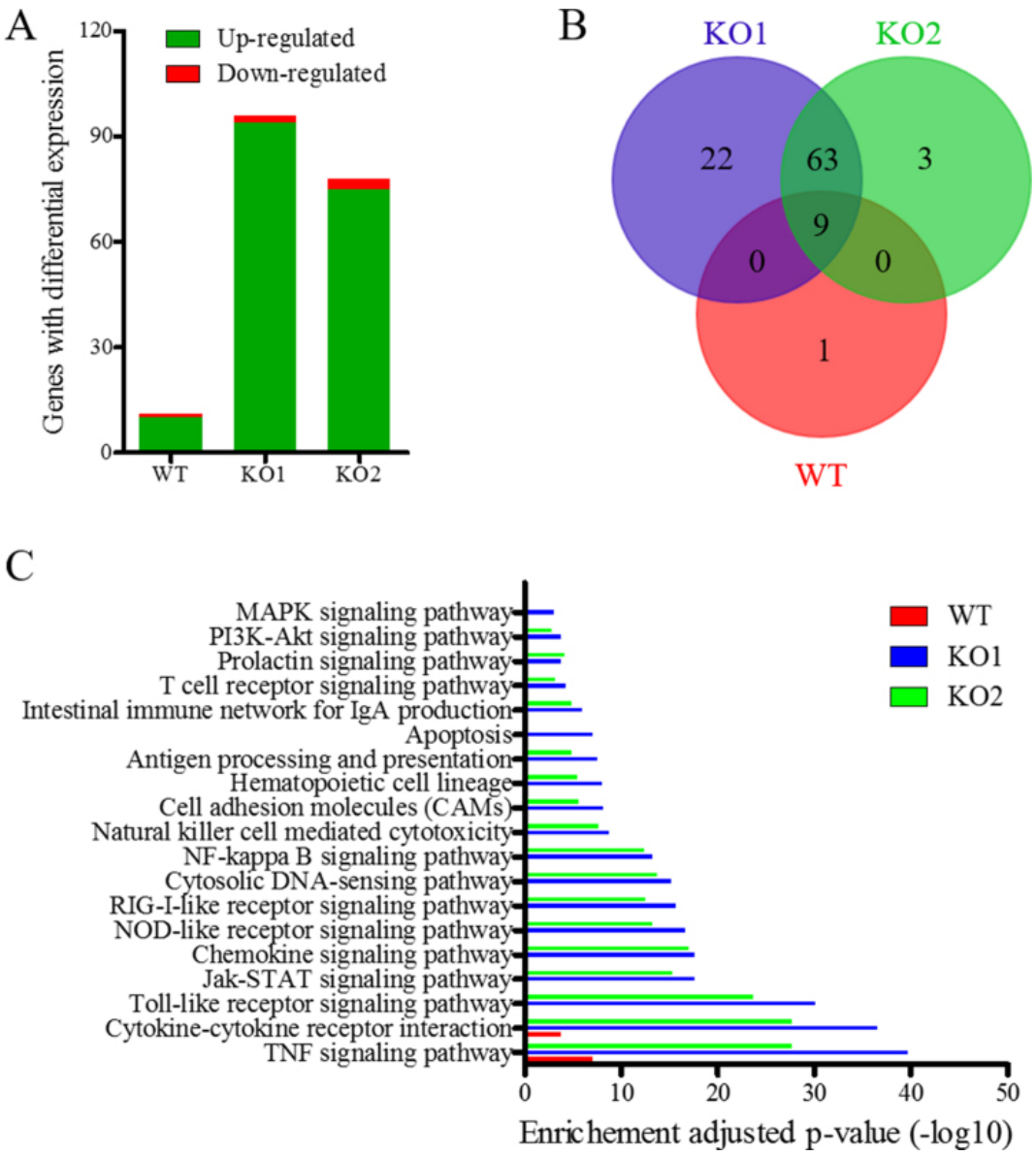

Figure 2.6. nCounter mRNA Profiling of immune gene expression in virus-infected cells.

(A) An overview on the number of differentially expressed genes (DEG) in virus-infected cells at 12 hpi. (B) Common and uniquely upregulated DEGs in virus-infected cells at 12 hpi. (C) Enriched functional categories of DEGs in virus-infected cells at 12 hpi determined by KEGG Pathway Enrichment analysis using DAVID (Huang et al., 2009a, Huang et al., 2009b). P-values adjusted by Benjamini-Hochberg correction less than 0.05 were defined as significant enrichment. The x-axis is the negative log10 of P-value.

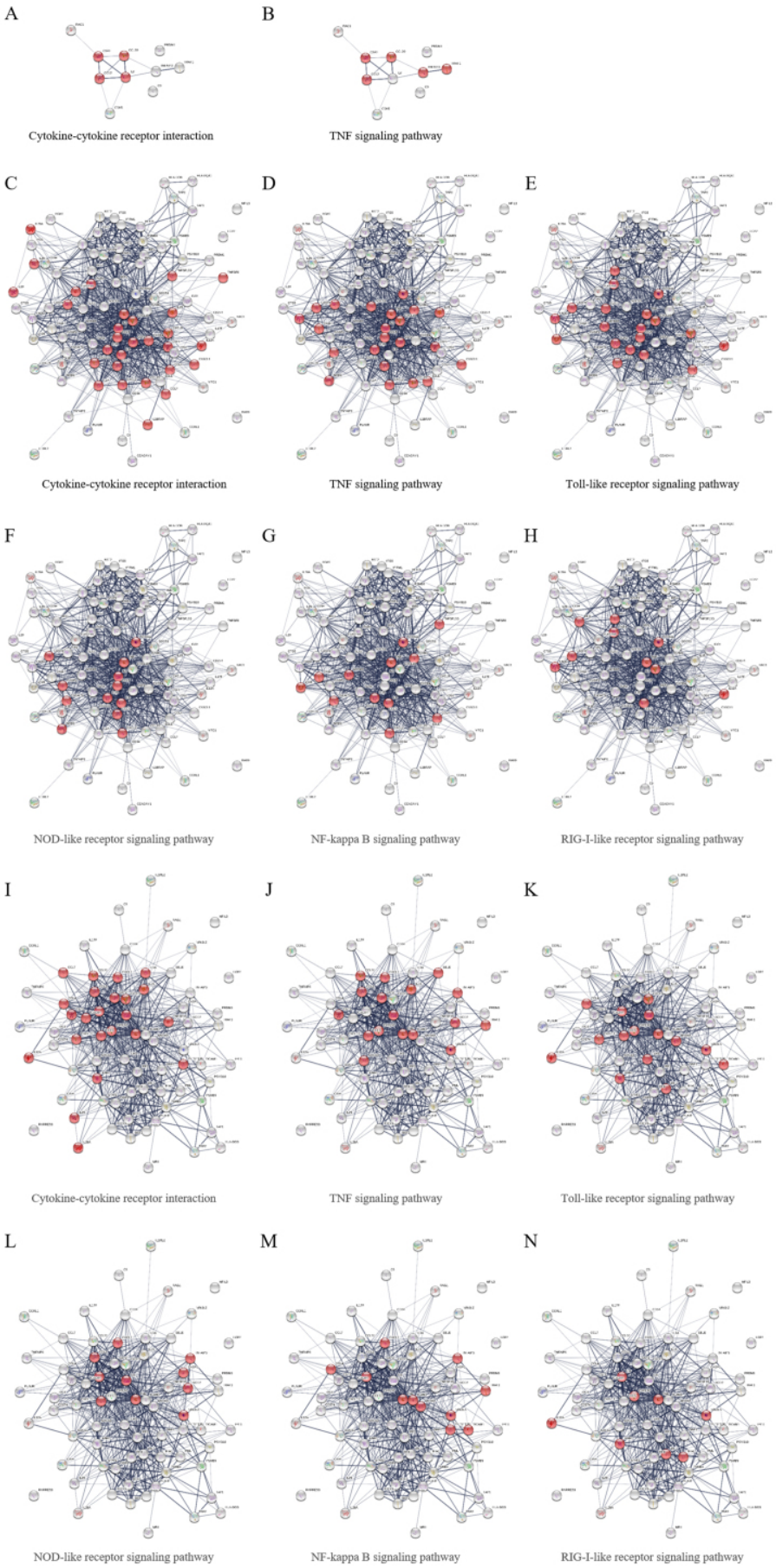
A
Cytokine-cytokine receptor interaction
B
TNF signaling pathway
C
Cytokine-cytokine receptor interaction
D
TNF signaling pathway
E
Toll-like receptor signaling pathway
F
NOD-like receptor signaling pathway
G
NF-kappa B signaling pathway
H
RIG-I-like receptor signaling pathway
I
Cytokine-cytokine receptor interaction
J
TNF signaling pathway
K
Toll-like receptor signaling pathway
L
NOD-like receptor signaling pathway
M
NF-kappa B signaling pathway
N
RIG-I-like receptor signaling pathway

Figure 2.7. Protein-protein interaction networks of DEGs in cells infected with WT virus and nsp2TF/nsp2N-deficient mutants.

Protein-protein interaction networks were constructed for all DEGs in cells infected with WT virus (A-B), vKO1 (C-H), and vKO2 (I-N) using the search tool for the retrieval of interacting genes/proteins (STRING). Confidence view of protein-protein interaction network from DEGs showing the strength of data support is indicated by the thickness of the grey line connecting genes and nodes. The representative pathways enriched in cells infected with WT virus (A-B), vKO1 (C-H), and vKO2 (I-N) were highlighted with red color.

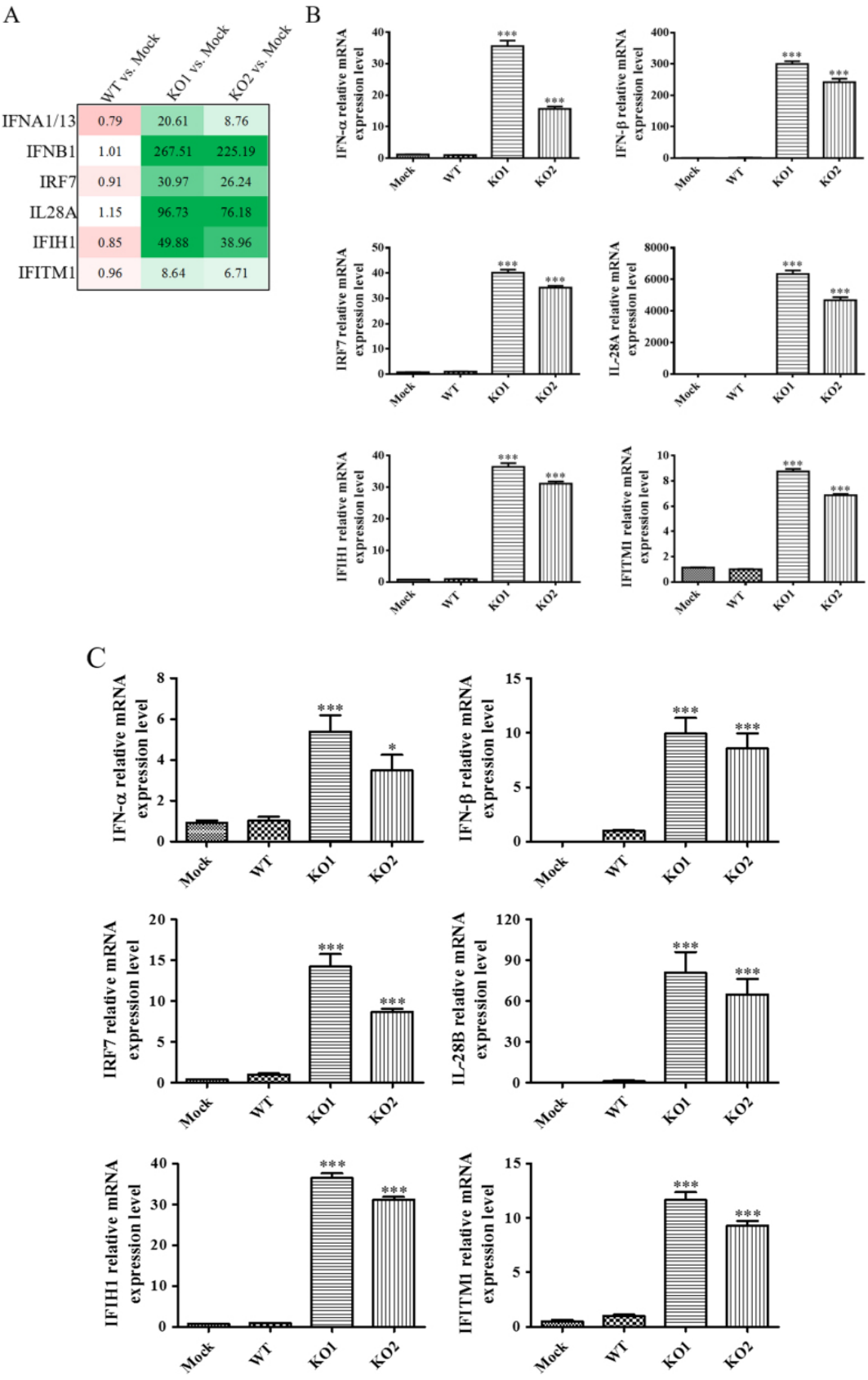
A
WT vs. Mock
KO1 vs. Mock
KO2 vs. Mock
IFNA1/13 0.79 20.61 8.76
IFNB1 1.01 267.51 225.19
IRF7 0.91 30.97 26.24
IL28A 1.15 96.73 76.18
IFIH1 0.85 49.88 38.96
IFITM1 0.96 8.64 6.71
B
IFN-α relative mRNA expression level
IFN-β relative mRNA expression level
IRF7 relative mRNA expression level
IL-28A relative mRNA expression level
IFIH1 relative mRNA expression level
IFITM1 relative mRNA expression level
Mock
WT
KO1
KO2
C
IFN-α relative mRNA expression level
IFN-β relative mRNA expression level
IRF7 relative mRNA expression level
IL-28B relative mRNA expression level
IFIH1 relative mRNA expression level
IFITM1 relative mRNA expression level
Mock
WT
KO1
KO2

Figure 2.8. Quantitative RT-PCR detection on the expression of selected differentially expressed genes in virus-infected cells.

(A) Six selected immune genes with increased expression levels in cells infected by nsp2TF/nsp2N-deficient mutants. Each data point shown represents the mean value from five replicates, and the gene expression levels in mock were treated as 1. (B) The relative expression levels of six immune genes in virus-infected MARC-145 cells at 12 hpi. (C) The relative expression levels of six immune genes in virus-infected PAM at 12 hpi. (B-C) Each data point shown represents the mean value from five replicates, and the gene expression levels in WT infected cells were treated as 1.

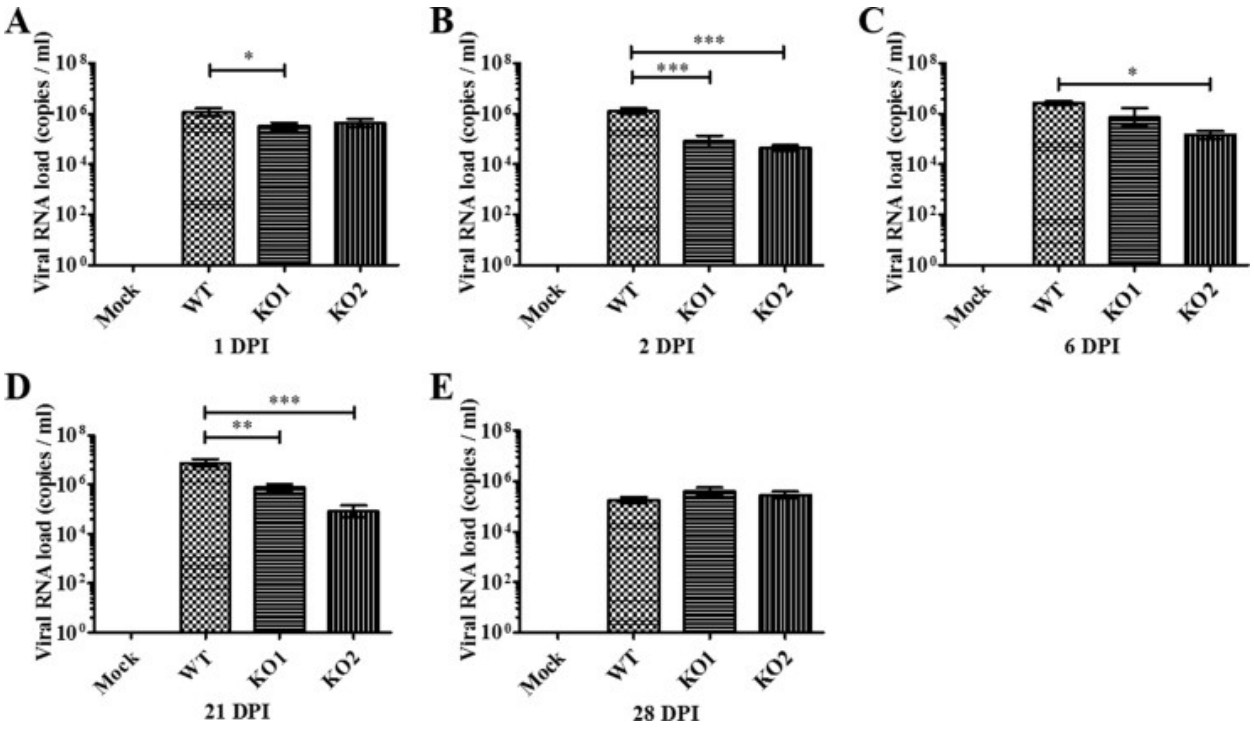

Figure 2.9. Comparison of viral RNA loads in serum samples from pigs inoculated with the WT virus and nsp2TF/nsp2N-deficient mutants.

Pigs were uninfected (mock) or infected with WT PRRSV (WT), vKO1 or vKO2 mutant. Serum samples were collected on the indicated days post-infection. Viral loads in serum samples quantified by quantitative RT-PCR and calculated as viral RNA copies per milliliter. Statistical significance between the WT virus-infected group and mutant virus-infected groups was determined by one-way ANOVA (Tukey's test) and indicated with asterisks (*, $P<0.05$; **, $P<0.01$; ***, $P<0.001$).

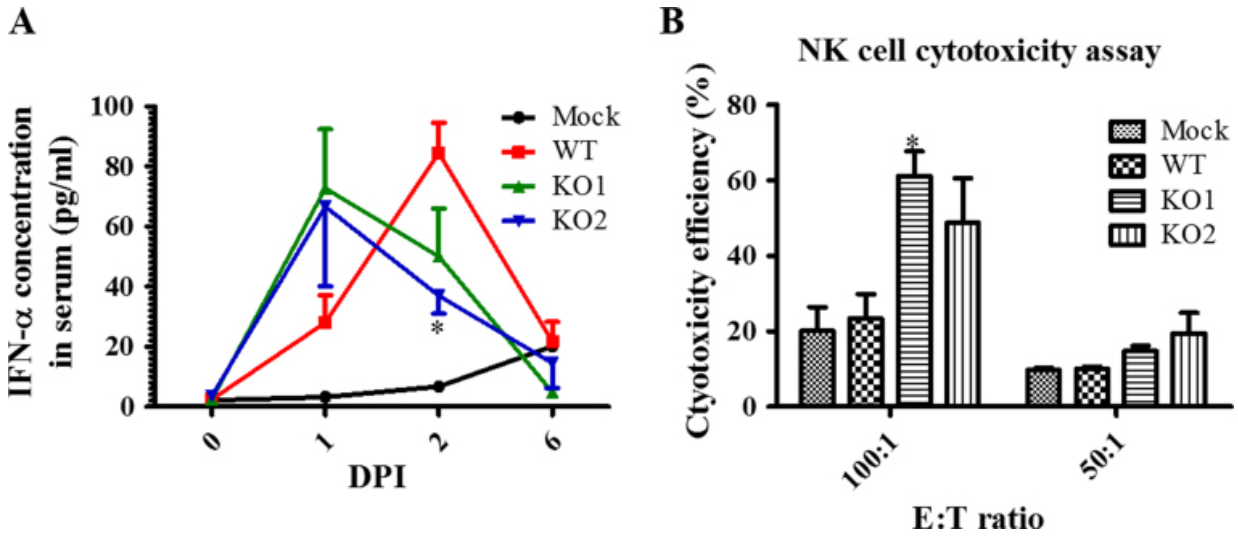

Figure 2.10. Comparison of IFN-α production levels and NK cell cytotoxicity in pigs inoculated with WT virus and nsp2TF/nsp2N-deficient mutants.

Pigs were uninfected (mock) or infected with WT PRRSV (WT), vKO1 or vKO2 mutant. (A) IFN-α levels in serum samples collected at 0, 1, 2 and 6 DPI were analyzed with a ProcartaPlex Porcine IFN alpha Simplex kit. (B) PBMCs (NK effectors) harvested on the day of necropsy (6 DPI) were co-cultured with target cells (K562) at an E:T ratio of 100:1 or 50:1. After overnight incubation, flow cytometry was performed to evaluate the NK cell-specific cytotoxic activity. Each data point represents the mean value and SEM of data from 3 pigs. Statistical significance between the wild-type virus infected group and mutant virus-infected groups was determined by one-way ANOVA (Tukey's test) and indicated with asterisks (*, $P<0.05$; **, $P<0.01$; ***, $P<0.001$).

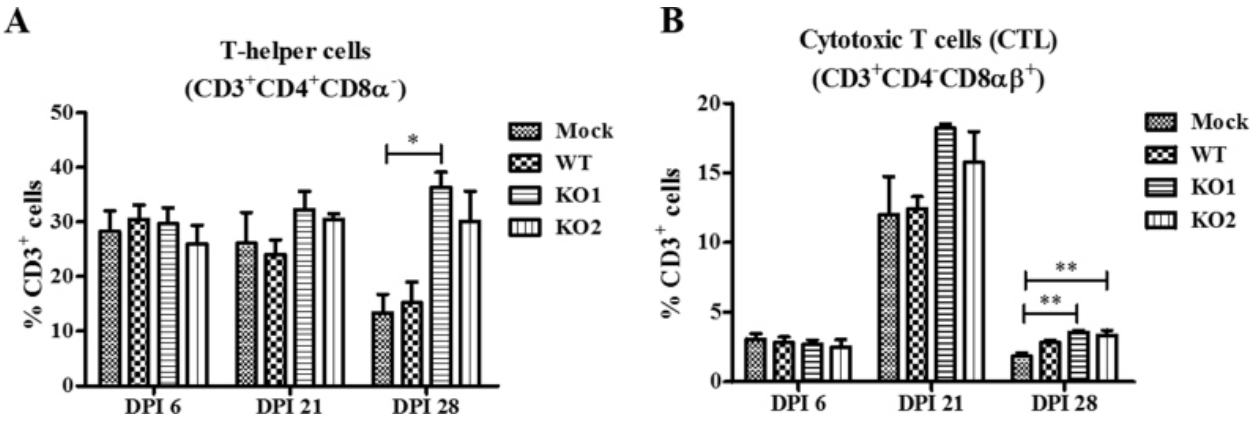

Figure 2.11. T-helper and cytotoxic T cells responses in pigs infected with WT virus and nsp2TF/nsp2N-deficient mutants.

PBMCs isolated at 6, 21 and 28 DPI were unstimulated or restimulated with the WT virus. Cells were immunostained for pig specific markers CD3, CD4, CD8α and CD8β, and the frequency of each lymphocyte subset was grouped based on the combination of markers: (A) $CD3^+CD4^+CD8\alpha^-$ (T-helper cells) and (B) $CD3^+CD4^-CD8\alpha\beta^+$ (cytotoxic T cells) after analysis by flow cytometry. Statistical significance between the groups was determined by one-way analysis of variance (ANOVA) followed by Tukey's post hoc test. (*P<0.05; **P<0.01).

Table 2.1. DEGs identified in Marc-145 cell infected with wild type and mutant viruses

WT virus versus Mock			**vKO1 versus Mock**		
Gene Name	Accession #	Fold change	Gene Name	Accession #	Fold change
C9	NM_001737.3	3.12	BST2	NM_004335.2	10.77
CCL2	NM_002982.3	3.81	C4A/B	NM_007293.2	3.03
CCL20	NM_004591.1	2.05	C9	NM_001737.3	6.72
CDH5	NM_001795.3	2.01	CASP1	NM_001223.3	5.56
CSF2	NM_000758.2	2.52	CASP8	NM_001228.4	2.52
IL8	NM_000584.2	2.25	CCL2	NM_002982.3	13.33
PRDM1	NM_001198.3	2.67	CCL20	NM_004591.1	4.85
RAG1	NM_000448.2	2.55	CCL4	NM_002984.2	5.05
TNFAIP3	NM_006290.2	2.22	CCL5	NM_002985.2	181.39
TRAF1	NM_005658.3	2.61	CCL7	NM_006273.2	2.86
LILRA1	NM_006863.1	-2.24	CCRL1	NM_016557.2	11.74
vKO2 versus Mock			CD1D	NM_001766.3	2.16
Gene Name	Accession #	Fold change	CD274	NM_014143.3	49.82
BST2	NM_004335.2	9.02	CD34	NM_001025109.1	2.38
C4A/B	NM_007293.2	2.45	CD45R0	NM_080921.3	2.19
C9	NM_001737.3	10.91	CEACAM1	NM_001712.3	3.09
CASP1	NM_001223.3	3.43	CISH	NM_145071.2	2.14
CCL2	NM_002982.3	12.62	CLEC7A	NM_197954.2	3.02
CCL20	NM_004591.1	7.02	CSF1	NM_000757.4	2.84
CCL4	NM_002984.2	4.6	CSF2	NM_000758.2	2.11
CCL5	NM_002985.2	107.7	CTSS	NM_004079.3	2.44
CCL7	NM_006273.2	2.03	CX3CL1	NM_002996.3	2.16
CCRL1	NM_016557.2	7.35	CXCL10	NM_001565.1	208.13
CD274	NM_014143.3	34.99	CXCL11	NM_005409.4	2463.04
CD34	NM_001025109.1	2.4	CXCL2	NM_002089.3	4.03
CISH	NM_145071.2	2.99	CXCL9	NM_002416.1	96.18
CSF1	NM_000757.4	2.68	CXCR4	NM_003467.2	2.65
CSF2	NM_000758.2	3.06	EGR1	NM_001964.2	6.19
CXCL10	NM_001565.1	129.88	EGR2	NM_000399.3	2.01
CXCL11	NM_005409.4	1386.08	FADD	NM_003824.2	3.05
CXCL2	NM_002089.3	5.44	FAS	NM_000043.3	2.07
CXCL9	NM_002416.1	59.82	GBP1	NM_002053.1	119.81

CXCR4	NM_003467.2	2.22	HLA-B	NM_005514.6	2.98
EGR1	NM_001964.2	4.73	HLA-DOB	NM_002120.3	2.73
GBP1	NM_002053.1	71.36	HLA-DQA1	NM_002122.3	2.05
HLA-B	NM_005514.6	2.47	ICAM1	NM_000201.2	2.34
HLA-DOB	NM_002120.3	2.21	IDO1	NM_002164.3	130.51
ICAM1	NM_000201.2	3.16	IFI16	NM_005531.1	6.23
IDO1	NM_002164.3	71.25	IFI35	NM_005533.3	5.9
IFI16	NM_005531.1	4.88	IFIH1	NM_022168.2	49.88
IFI35	NM_005533.3	4.77	IFIT2	NM_001547.4	104.49
IFIH1	NM_022168.2	38.96	IFITM1	NM_003641.3	8.64
IFIT2	NM_001547.4	71.94	IFNA1/13	NM_024013.1	20.61
IFITM1	NM_003641.3	6.71	IFNB1	NM_002176.2	267.51
IFNA1/13	NM_024013.1	8.76	IL12A	NM_000882.2	5.04
IFNB1	NM_002176.2	225.19	IL15	NM_172174.1	2.45
IL12A	NM_000882.2	3.84	IL17F	NM_052872.3	2.37
IL15	NM_172174.1	2.61	IL18RAP	NM_003853.2	2.09
IL17F	NM_052872.3	3.17	IL19	NM_013371.3	3
IL1A	NM_000575.3	5.76	IL1A	NM_000575.3	6.57
IL1RL2	NM_003854.2	2.59	IL1B	NM_000576.2	2.73
IL28A	NM_172138.1	76.18	IL1RL2	NM_003854.2	2.6
IL28A/B	NM_172139.2	29.07	IL28A	NM_172138.1	96.73
IL29	NM_172140.1	146.44	IL28A/B	NM_172139.2	35.66
IL6	NM_000600.1	4.57	IL29	NM_172140.1	201.87
IL8	NM_000584.2	4.56	IL6	NM_000600.1	3.97
IRF1	NM_002198.1	17.11	IL8	NM_000584.2	3.64
IRF7	NM_001572.3	26.24	IRF1	NM_002198.1	19.58
IRF8	NM_002163.2	17.38	IRF4	NM_002460.1	2.01
LCP2	NM_005565.3	2.24	IRF7	NM_001572.3	30.97
MR1	NM_001531.2	2.95	IRF8	NM_002163.2	28.54
MYD88	NM_002468.3	4.86	LCP2	NM_005565.3	3.5
NFIL3	NM_005384.2	2.02	LIF	NM_002309.3	2.04
NFKBIA	NM_020529.1	3.1	LY96	NM_015364.2	2.32
NFKBIZ	NM_001005474.1	2.28	MRC1	NM_002438.2	2.89
NOD2	NM_022162.1	3.03	MX1	NM_002462.2	3.2
PLAUR	NM_001005376.1	4.53	MYD88	NM_002468.3	6.33
PML	NM_002675.3	5.15	NFIL3	NM_005384.2	2.24

PRDM1	NM_001198.3	5.82	NFKBIA	NM_020529.1	3.04
PSMB10	NM_002801.2	5.04	NOD2	NM_022162.1	3.27
PSMB8	NM_004159.4	14.68	NOS2	NM_000625.4	2.16
PSMB9	NM_002800.4	21.04	PLAUR	NM_001005376.1	5.95
RAG1	NM_000448.2	5.88	PML	NM_002675.3	5.05
RARRES3	NM_004585.3	2.72	PRDM1	NM_001198.3	4.96
SELE	NM_000450.2	6.12	PSMB10	NM_002801.2	7.43
SOCS1	NM_003745.1	11.36	PSMB8	NM_004159.4	23.21
SOCS3	NM_003955.3	2.38	PSMB9	NM_002800.4	31.43
STAT2	NM_005419.2	6.26	RAG1	NM_000448.2	3.49
TAP1	NM_000593.5	13.57	RARRES3	NM_004585.3	4.24
TAP2	NM_000544.3	4.32	SELE	NM_000450.2	3.35
TICAM1	NM_014261.1	2.19	SOCS1	NM_003745.1	15.46
TLR3	NM_003265.2	3.56	SOCS3	NM_003955.3	2.05
TNF	NM_000594.2	2.73	STAT2	NM_005419.2	7.75
TNFAIP3	NM_006290.2	6.21	TAP1	NM_000593.5	17.78
TNFAIP6	NM_007115.2	2.02	TAP2	NM_000544.3	5.66
TNFSF10	NM_003810.2	5.75	TLR2	NM_003264.3	2.06
TNFSF13B	NM_006573.4	4.3	TLR3	NM_003265.2	5.26
TRAF1	NM_005658.3	7.22	TNF	NM_000594.2	2.78
CTLA4_all	NM_005214.3	-2.1	TNFAIP3	NM_006290.2	4.93
ITLN1	NM_017625.2	-2.52	TNFAIP6	NM_007115.2	2.36
ZAP70	NM_001079.3	-2.08	TNFSF10	NM_003810.2	8.8
			TNFSF13B	NM_006573.4	8.54
			TNFSF8	NM_001244.3	2.2
			TRAF1	NM_005658.3	8.67
			IL23A	NM_016584.2	-2.01
			TGFBR1	NM_004612.2	-2.12

Table 2.2. KEGG pathway enrichment from differentially expressed genes induced by viral infection

WT virus					
Term	Genes	Count	%	P-Value	Benjamini
hsa04668:TNF signaling pathway	TRAF1, CSF2, CCL2, CCL20, TNFAIP3	5	50	2.03E-09	8.34E-08
hsa04060:Cytokine-cytokine receptor interaction	CSF2, CCL2, CCL20, CXCL8	4	40	1.37E-05	1.87E-04
vKO1					
Term	Genes	Count	%	P-Value	Benjamini
hsa04668:TNF signaling pathway	TRAF1, ICAM1, CSF2, IL6, TNF, CCL2, SOCS3, CSF1, CXCL2, NFKBIA, FADD, CX3CL1, IL15, CCL5, CXCL10, LIF, NOD2, CCL20, CASP8, IL1B, FAS, TNFAIP3, SELE	23	25	5.55E-42	1.92E-40
hsa04060:Cytokine-cytokine receptor interaction	CSF2, TNF, CCL2, CSF1, CXCL9, CXCL8, CX3CL1, IL15, CXCL11, CCL5, CCL4, CCL7, CXCL10, LIF, IFNA1, CCL20, CXCR4, IL1B, FAS, IL1A, IL6, IL18RAP, TNFSF8, TNFSF10, TNFSF13B, IFNB1, IL12A	27	29.34783	9.82E-39	2.55E-37
hsa04620:Toll-like receptor signaling pathway	IL6, TNF, LY96, CXCL9, TLR2, CXCL8, TLR3, NFKBIA, FADD, CXCL11, CCL5, CCL4, CXCL10, IFNA1, MYD88, IFNB1, IRF7, CASP8, IL12A, IL1B	20	21.73913	3.31E-32	6.89E-31
hsa04630:Jak-STAT signaling pathway	CSF2, IL6, SOCS3, IL19, SOCS1, IL15, CISH, STAT2, LIF, IFNA1, IFNL2, IFNB1, IL12A, IFNL3	14	15.21739	2.39E-19	2.26E-18

hsa04062:Chemokine signaling pathway	CCL2, CXCL2, CXCL9, CXCL8, NFKBIA, CX3CL1, CXCL11, CCL5, CCL4, CCL7, STAT2, CXCL10, CCL20, CXCR4	14	15.21739	3.02E-19	2.62E-18
hsa04621:NOD-like receptor signaling pathway	IL6, NOD2, TNF, CCL2, CASP8, CXCL8, NFKBIA, IL1B, CCL5, TNFAIP3, CASP1	11	11.95652	3.42E-18	2.54E-17
hsa04622:RIG-I-like receptor signaling pathway	IFIH1, IFNA1, TNF, IFNB1, IRF7, CASP8, IL12A, CXCL8, NFKBIA, FADD, CXCL10	11	11.95652	3.08E-17	2.00E-16
hsa04623:Cytosolic DNA-sensing pathway	IL6, IFNA1, IFNB1, IRF7, NFKBIA, IL1B, CCL5, CASP1, CCL4, CXCL10	10	10.86957	1.39E-16	6.66E-16
hsa04064:NF-kappa B signaling pathway	TRAF1, ICAM1, TNF, MYD88, TNFSF13B, LY96, CXCL8, NFKBIA, IL1B, TNFAIP3, CCL4	11	11.95652	1.23E-14	6.11E-14
hsa04650:Natural killer cell mediated cytotoxicity	CSF2, ICAM1, IFNA1, TNFSF10, TNF, IFNB1, FAS, LCP2	8	8.695652	5.60E-10	1.76E-09
hsa04514:Cell adhesion molecules (CAMs)	ICAM1, PTPRC, CD34, CD274, HLA-B, SELE, HLA-DOB, HLA-DQA1	8	8.695652	2.25E-09	6.89E-09
hsa04640:Hematopoietic cell lineage	CSF2, IL6, TNF, CD34, CSF1, IL1B, IL1A, CD1D	8	8.695652	3.38E-09	1.01E-08
hsa04612:Antigen processing and presentation	TNF, TAP2, TAP1, HLA-B, CTSS, HLA-DOB, HLA-DQA1	7	7.608696	8.76E-09	2.53E-08
hsa04210:Apoptosis	TNFSF10, TNF, CASP8, NFKBIA, FADD, FAS	6	6.521739	3.10E-08	8.48E-08
hsa04672:Intestinal immune network for IgA production	IL6, TNFSF13B, CXCR4, IL15, HLA-DOB, HLA-DQA1	6	6.521739	4.24E-07	1.07E-06
hsa04660:T cell receptor signaling pathway	CSF2, PTPRC, TNF, NFKBIA, LCP2	5	5.434783	2.50E-05	5.65E-05

hsa04917:Prolactin signaling pathway	SOCS3, SOCS1, IRF1, CISH	4	4.347826	6.91E-05	1.50E-04
hsa04151:PI3K-Akt signaling pathway	IL6, IFNA1, IFNB1, CSF1, TLR2	5	5.434783	7.13E-05	1.51E-04
hsa04010:MAPK signaling pathway	TNF, IL1B, FAS, IL1A	4	4.347826	4.44E-04	8.88E-04
vKO2					
Term	Genes	Count	%	P-Value	Benjamini
hsa04060:Cytokine-cytokine receptor interaction	CSF2, IL6, TNF, CCL2, CSF1, CXCL9, CXCL8, IL15, CXCL11, CCL5, CCL4, CCL7, CXCL10, IFNA1, TNFSF10, TNFSF13B, CCL20, CXCR4, IFNB1, IL12A, IL1A	21	28.76712	6.85E-30	2.12E-28
hsa04668:TNF signaling pathway	TRAF1, ICAM1, CSF2, IL6, TNF, CCL2, SOCS3, CSF1, CXCL2, NFKBIA, IL15, CCL5, CXCL10, NOD2, CCL20, TNFAIP3, SELE	17	23.28767	7.98E-30	1.85E-28
hsa04620:Toll-like receptor signaling pathway	IL6, TNF, CXCL9, CXCL8, NFKBIA, TLR3, CXCL11, CCL5, CCL4, CXCL10, IFNA1, MYD88, IFNB1, IRF7, TICAM1, IL12A	16	21.91781	1.22E-25	2.27E-24
hsa04062:Chemokine signaling pathway	CCL2, CCL20, CXCR4, CXCL2, CXCL9, CXCL8, NFKBIA, CCL5, CXCL11, CCL4, CCL7, STAT2, CXCL10	13	17.80822	7.46E-19	9.91E-18
hsa04630:Jak-STAT signaling pathway	CSF2, IL6, IFNA1, IFNL2, SOCS3, IFNB1, SOCS1, IL12A, IL15, IFNL3, CISH, STAT2	12	16.43836	5.45E-17	5.07E-16
hsa04623:Cytosolic DNA-sensing pathway	IL6, IFNA1, IFNB1, IRF7, NFKBIA, CCL5, CASP1, CCL4, CXCL10	9	12.32877	2.56E-15	1.98E-14

hsa04621:NOD-like receptor signaling pathway	IL6, NOD2, TNF, CCL2, CXCL8, NFKBIA, CCL5, TNFAIP3, CASP1	9	12.32877	8.58E-15	6.12E-14
hsa04622:RIG-I-like receptor signaling pathway	IFIH1, IFNA1, TNF, IFNB1, IRF7, IL12A, CXCL8, NFKBIA, CXCL10	9	12.32877	4.61E-14	2.86E-13
hsa04064:NF-kappa B signaling pathway	TRAF1, ICAM1, TNF, MYD88, TNFSF13B, TICAM1, CXCL8, NFKBIA, TNFAIP3, CCL4	10	13.69863	6.49E-14	3.77E-13
hsa04650:Natural killer cell mediated cytotoxicity	CSF2, ICAM1, IFNA1, TNFSF10, TNF, IFNB1, LCP2	7	9.589041	5.39E-09	2.09E-08
hsa04514:Cell adhesion molecules (CAMs)	ICAM1, CD34, CD274, HLA-B, SELE, HLA-DOB	6	8.219178	7.44E-07	2.16E-06
hsa04640:Hematopoietic cell lineage	CSF2, IL6, TNF, CD34, CSF1, IL1A	6	8.219178	9.89E-07	2.79E-06
hsa04672:Intestinal immune network for IgA production	IL6, TNFSF13B, CXCR4, IL15, HLA-DOB	5	6.849315	5.72E-06	1.40E-05
hsa04612:Antigen processing and presentation	TNF, TAP2, TAP1, HLA-B, HLA-DOB	5	6.849315	5.72E-06	1.40E-05
hsa04917:Prolactin signaling pathway	SOCS3, SOCS1, IRF1, CISH	4	5.479452	3.14E-05	7.31E-05
hsa04660:T cell receptor signaling pathway	CSF2, TNF, NFKBIA, LCP2	4	5.479452	3.05E-04	6.60E-04
hsa04151:PI3K-Akt signaling pathway	IL6, IFNA1, IFNB1, CSF1	4	5.479452	6.64E-04	0.0013715

Table 2.3. Common and unique DEGs in cells infected with wild type and mutant viruses

vKO1/vKO2	vKO1/vKO2	WT virus/vKO1/vKO2	WT virus	vKO1	vKO2
BST2	IL1A	C9	CDH5	CASP8	MR1
C4A/B	IL1RL2	CCL2	LILRA1	CD1D	NFKBIZ
CASP1	IL28A	CCL20		CD45R0	TICAM1
CCL4	IL28A/B	CSF2		CEACAM1	IL23A
CCL5	IL29	IL8		CLEC7A	TGFBR1
CCL7	IL6	PRDM1		CTSS	
CCRL1	IRF1	RAG1		CX3CL1	
CD274	IRF7	TNFAIP3		EGR2	
CD34	IRF8	TRAF1		FADD	
CISH	LCP2			FAS	
CSF1	MYD88			HLA-DQA1	
CXCL10	NFIL3			IL18RAP	
CXCL11	NFKBIA			IL19	
CXCL2	NOD2			IL1B	
CXCL9	PLAUR			IRF4	
CXCR4	PML			LIF	
EGR1	PSMB10			LY96	
GBP1	PSMB8			MRC1	
HLA-B	PSMB9			MX1	
HLA-DOB	RARRES3			NOS2	
ICAM1	SELE			TLR2	
IDO1	SOCS1			TNFSF8	
IFI16	SOCS3			CTLA4_all	
IFI35	STAT2			ITLN1	
IFIH1	TAP1			ZAP70	
IFIT2	TAP2				
IFITM1	TLR3				
IFNA1/13	TNF				
IFNB1	TNFAIP6				
IL12A	TNFSF10				
IL15	TNFSF13B				
IL17F					

Chapter 3 - Hyper-phosphorylation on nsp2-related proteins of porcine arterivirus regulates the accumulation of viral RNA

Abstract: Host phosphorylation mechanism is exploited by viruses in order to establish reproductive replication cycle. So far, the nucleocapsid (N) proteins are the only member in the phospho-proteome of nidodviruses. Only the coronaviral N proteins have been characterized functionally. However, whether phosphorylation status of other nidoviral proteins still remain unknown. In this study, we firstly expand the nidoviral phospho-proteome by demonstrating the hyper-phosphorylation status of porcine arterivirus-porcine reproductive and respiratory syndrome virus (PRRSV) replicase nsp2 and two nsp2-related proteins-nsp2TF/nsp2N, which are newly identified -2/-1 programmed ribosomal frameshifting products. Most of phosphorylation sites identified by mass spectrometry are found in the uncharacterized long region between papain-like protease (PLP) 2 domain and -2/-1 frameshifting site. We further subdivided this regions into three structurally distinct domains: two large hypervariable regions with putative intrinsically disordered structures, spaced by a conserved and potentially structured interval domain-IHCD (Inter-HVR Conserved Domain). The extensive phospho-abolishing mutation screening revealed that the phosphorylated status of residue serine^{918} is important for recombinant virus production. The inter-species conserved serine^{918} is located in IHCD. Viral RNA quantification further showed that abolishing phosphorylation of serine^{918} strongly and selectively reduced the accumulation of subgenomic mRNAs, not genomic RNAs. In summary, our research demonstrates the hyper-phosphorylation of nsp2-related proteins, reveals its biological significance, and further highlights the multi-functional roles of nsp2-related proteins in PRRSV life cycle and potential contributions to pathogenesis.

3.1. Introduction

As the most common post-translational modification (PTM) form, protein phosphorylation is actively involved in every celluar processes (1-5). Viruses have evolved to be able to manipulate host signaling pathways regulated by phosphorylation, and acquired abilities to exploit phosphorylation to control the involvement of viral proteins in virus life cycle (6, 7). Phosphorylation on viral proteins regulates protein functionality, virus replication, and control of host cellular responses (6, 7). For instance, the NS5 (or NS5A) proteins of viruses in *Flaviviridae* family including West Nile virus, Yellow fever virus, Dengue virus, Tick-borne encephalitis virus, Japanese encephalitis virus, and Hepatitis C virus have been demonstrated to be phosphorylated. Phosphorylation exerts broad regulatory effects on NS5 (NS5A) functionality, including innate immune suppression, nuclear translocation, viral RNA replication, and viral particle assembly (6, 7).

As a member of family *Arteriviridae* and order *Nidovirales*, porcine reproductive and respiratory syndrome virus (PRRSV) contains an enveloped positive-sense (+) single-stranded (ss) RNA genome (8, 9). PRRSV is partitioned into two genetically highly divergent species-PRRSV-1 and PRRSV-2 (10). Nonstructural proteins-replicases are encoded by 5' proximal ORF1a, ORF1ab, and ORF1aTF/N (8, 9). PRRSV is the most prominent swine pathogen with recurrent large scale outbreaks (8, 9). Ever since its discovery about three decades ago, great efforts have been committed to investigate pathogenesis mechanism and seek for the so-called "virulence factors" (11, 12). In every outbreak, newly emerged pathogenic variants showed up with unique and typical hyper-variation in the long region between papain-like protease (PLP) 2 domain and -2/-1 programmed ribosome frameshifting (PRF) site of nsp2-related proteins. Even though researchers have dedicated to understand the biological significance of molecular

determinants in nsp2-related proteins including papain-like protease (PLP) 2 domain and hypervariability, the full range understanding of the largest proteins in viral proteome in viral life cycle, pathogenicity, and evolution still remains incomplete (11, 12).

Here, we firstly demonstrate that the PRRSV replicase nsp2 and -2/-1 PRF products-nsp2TF and nsp2N are hyper-phosphorylated and further identified a series of phosphorylation sites. Among all these sites, the importance of phosphorylation status of one residue-serine^{918} was later proved in the accumulation of subgenomic mRNA (sgmRNA) and viral production. The less characterized region between PLP2 domain and -2/-1 PRF site was found to be enriched with phosphorylation sites. This long region could be further divided into three domains with distinct structural features: two large hypervariable regions with highly likely intrinsically disordered structures, separated by a conserved and potentially structured interval domain-IHCD (Inter-HVR Conserved Domain). The inter-species conserved serine^{918} is located in the IHCD. In conclusion, our study expands the nidovirus phospho-proteome, and underlines the critical role(s) of phosphorylation in nsp2-related proteins for PRRSV life cycle and potential links with viral pathogenicity.

3.2. Materials and methods

Cells, viruses, and antibodies: BHK-21 cells and MARC-145 cells were cultured in minimum essential medium (MEM) (Gibco, Carlsbad, CA) supplemented with 10% fetal bovine serum (FBS) (Sigma-Aldrich, St. Louis, MO) at the environment of 37°C and 5% CO2 atmosphere. For the maintenance of infected MARC-145 cells, 10% FBS was replaced by 2% horse serum (HyClone, Logan, UT).

The PRRSV-1 strain (SD01-08) used in current study was previously isolated at 2001 in the United States and further used to establish the reverse genetic systems (15).

All the PRRSV-1 specific antibodies used in current research were targeted to SD01-08 strain. Anti-nsp2-related proteins monoclonal antibodies (mAbs)- #36-19 and #58-46 were generated against PLP2 and ES4-5, respectively (14, 16). Anti-nsp1β mAb #22-28 was also described in previous publications (14, 16). Polyclonal antibodies (pAbs) of anti-nsp2-related proteins and anti-nsp2TF were commercially prepared by GenScript Biotech Corporation (Piscataway, NJ). Anti-GAPDH mAb was purchased from Sigma-Aldrich (St. Louis, MO). Six specific anti-phosphorylated serine (pSer) mAbs panel was included in the phosphoserine detection set (Enzo Life Sciences, Ann Arbor, MI). Secondary antibodies-IRDye 800CW goat anti-mouse IgG(H+L) and or IRDye 680RD goat anti-rabbit IgG(H+L) were purchased from Li-Cor Biosciences (Lincoln, NE).

Mass spectrometric analysis of phosphorylation sites: PRRSV nsp2-related proteins were pulled down from virus (SD01-08 strain)-infected MARC-145 cells by immunoprecipitation (IP) as previously described (14). Virus-infected or mock-infected cells were lysed by RIPA buffer (150mM Nacl, 10mM Tris-Hcl, 1mM EDTA, 1% NP-40, 0.5% sodium deoxycholate, 0.1% SDS) supplemented with Alfa Aesar™ Protease Inhibitor Cocktail I (Thermo Fisher Scientific, Carlsbad, CA) and Alfa Aesar™ Phosphatase Inhibitor Cocktail I (Thermo Fisher Scientific, Carlsbad, CA). Cell lysates were pre-cleared with affinity beads-Protein A Sepharose CL-4B (GE Healthcare Bio-Sciences, Pittsburgh, PA), which were bound by normal mouse serum (Santa Cruz Biotechnology, Dallas, TX), at room temperature (RT) for 1 hour to remove non-specifically bound proteins. Then centrifuge briefly, transfer supernatant to a new tube which contains mAb (#36-19) and fresh Sepharose beads, incubated with constant rotation at 4℃ overnight. Wash beads 4 times with RIP buffer (150mM Nacl, 10mM Tris-Hcl, 1mM EDTA, 1% NP-40, 0.5% sodium deoxycholate), then twice with MiliQ water. Bound proteins were then

eluted and denatured by 2x Laemmli sample buffer (Bio-Rad, Hercules, CA) at 95°C for 10 min. PRRSV nsp2-related proteins were separated and analyzed by SDS-PAGE gel, then fixed and stained Coomassie brilliant blue G-250 (Bio-Rad Laboratories, Hercules, CA). The band of PRRSV nsp2 and nsp2TF were excised from gel, and rendered for mass spectrometric analysis. Phosphorylation analysis was performed at the Harvard Microchemistry and Proteomics Analysis Facility by microcapillary reverse-phase HPLC nano-electrospray tandem mass spectrometry (μLC/MS/MS) on a Thermo LTQ-Orbitrap mass spectrometer (54).

Immuno-detection of phosphorylated nsp2-related proteins and gel shifting assay: IP-pulled down proteins were separated by SDS-PAGE gel and transferred onto nitrocellulose (NC) membrane (GE Healthcare Bio-Sciences, Pittsburgh, PA). For phosphorylation immuno-detection by specific anti-pSer mAbs, a manufacturer recommended protocol was applied. 2x phosphate-buffered saline (PBS) with 1% BSA (MP Biochemical, Solon, OH), 1% PVP-10 (polyvinyl-pyrrolidone) (Sigma-Aldrich, St. Louis, MO), 1% PEG 3500 (Sigma-Aldrich, St. Louis, MO), and 0.2% Tween 20 (Sigma-Aldrich, St. Louis, MO) was used as blocking buffer and antibodies diluent. NC membrane was blocked for 2 hour at RT, then incubated with diluted primary antibody for 1 hour at RT. After three times wash with 1x PBST (0.05% Tween-20), proteins on membranes were then reacted with secondary antibody for 45 min at RT. After another three times of wash with 1x PBST (0.05% Tween-20), protein bands were visualized by Odyssey Fc imaging system (Li-Cor Biosciences, Lincoln, NE). Same incubation and wash procedure were still applied to membranes with second time incubation by anti-nsp2-related proteins antibodies.

For gel shifting assay, proteins-bound on Sepharose beads in the IP process were dephosphorylated by Lambda Protein Phosphatase (λPP) [New England BioLabs (NEB),

Ipswich, MA] at 30°C for 2 hour. In control samples, λPP was replaced by equal volume of water. The migration speed changes of nsp2-related proteins after treatment was compared in SDS-PAGE gel and visualized by WB. If only anti-nsp2-related proteins antibodies were used, WB was performed according to previously described routine protocol (55). Pixel intensity of proteins bands in western blot was calculated by Image Studio 5.2 (Li-Cor Biosciences).

Genetic manipulation in PRRSV reverse genetics: T7 promoter and CMV promoter-driven PRRSV-1 (strain SD01-08) cDNA infectious clone systems were constructed in previous studies (15, 56). Site mutagenesis within nsp2-related proteins coding region was performed based on previous description (55). The full-length infectious clone was digested by single restriction enzymes- PmlI/SgrAI, or SgrAI/NotI. Only infectious clone backbone was harvested after double enzyme digestion. Genomic region between PmlI/SgrAI, or SgrAI/NotI were amplified by two PCR reactions (PCR-1/-2). 3' end of PCR1 product and 5' end of PCR2 product were overlapped by ~20-base pair (bp) region with mutation site(s). Primers containing mutations were synthesized from Integrated DNA Technologies (Coralville, IA). To assemble the PCR products with infectious clone backbone with NEBuilder HiFi DNA Assembly cloning kit (New England BioLabs, Ipswich, MA), 5' end of PCR1 product and 3' end of PCR2 product were designed to be overlapped with infectious clone backbone by ~20-bp.

Steady level of genomic and subgenomic RNA quantification : The system of quantitative comparison on the relative accumulation of genomic/subgenomic RNA in transfected cells between WT and mutant viruses was established in current study. *In vitro* RNA transcription was performed at first. Full-length infectious clone pT7-SD01-08 was linearized by XbaI, immediate downstream of HDV ribozyme. Digested DNA used as next step template was extracted using phenol extraction and ethanol precipitation method. 2 μg linearized DNA was used as template

for *in vitro* RNA transcription. After *in vitro* transcription at 37 ℃ for 2 hour, DNA templates were removed by 2 µl TURBO™ DNase (Thermo Fisher Scientific) for 30 min, 37 ℃. *In vitro* transcribed RNAs were purified by NucAway™ Spin Columns (Thermo Fisher Scientific) based on manufacturer's instruction. 1.5 µg *in vitro* transcribed PRRSV genomic RNAs were transfected into BHK-21 cells by using Lipofectamine™ MessengerMAX™ Transfection Reagent (Thermo Fisher Scientific) with a ratio of genomic RNA to MessengerMAX=1:4. Celluar total RNAs were extracted at 18 hour post transfection (hpt) by SV Total RNA Isolation System (Promega, Madison, WI) according to users' manual. Cells at 18hpt were also lysed by Pierce™ IP Lysis Buffer (Thermo Fisher Scientific) for protein expression detection. Cell supernatants were also collected at 18 and 36 hour post transfection (hpt), and subjected to infectious virus titration.

Equal amount (1.5 µg) of total RNAs were reverse transcribed by Maxima H Minus Reverse Transcriptase (Thermo Fisher Scientific). (+) gRNA and (+) sgmRNA were reverse transcribed using two different primers; all (-) viral RNAs were reverse transcribed by using a common primer (Table 3). 20 µl qPCR reaction: 10 µl TaqMan™ Fast Advanced Master Mix (Applied Biosystems, Carlsbad, CA), 0.4 µl Taqman probe (10 µM), 0.25 µl F primer (40 µM), 0.25 µl R primer (40 µM), 2 µl cDNA, and 7.1 µl water. PCR reactions were conducted in CFX96 Touch™ Real-Time PCR Detection System (Bio-Rad, Hercules, CA) with condition: 50 ℃ 2 minutes, 95 ℃ 2 minutes, then 40 cycles for 95 ℃ 3 seconds, 60 ℃ 30 seconds. In addition to viral RNA quantification, host housekeeping gene TBP (TATA-box binding protein) were included in the qPCR assay for gRNA normarlization. TBP cDNA were generated by Maxima™ H Minus cDNA Synthesis Master Mix (Thermo Fisher Scientific). qPCR were performed with commercial primers/probe set (Cg04504571_m1, Thermo Fisher Scientific) using the same

condition abovementioned. The relative accumulation ratio of sgRNAs was quantified with threshold cycle ($_{\Delta\Delta}$CT) method (55). To precisely quantify RNA accumulation and to rule out possible background interference from initial transfected RNA, a transcription-defective mutant was constructed, in which the nucleotide sequence from 495 nt to 515 nt was replaced with 7 consecutive stop codons to terminate the translation of nonstructural polyproteins. The (+) gRNA detected from the defective mutant (+) gRNA transfected BHK-21 cells was considered as background. In the quantification involved in (+) gRNA, the background derived from transfection was deducted at first. For gRNA accumulation comparison among different viruses, gRNA accumulation level were at first normalized by the RNA level of housekeeping TBP.

Infectious particle titration and *in vitro* growth property measurement

Virus titers were measured by micro-titration assay on MARC-145 cells in 96-well plates and calculated as $TCID_{50}$/mL using the Reed and Muench method (57). *In vitro* growth kinetics of recombinant viruses including WT and mutant viruses were quantified by infecting MARC-145 cells at multiplicity of infection (moi) = 0.01. Supernatants of infected cells were collected at 0, 12, 24, 36, 48, 60, 72, 84, and 96 hour post-infection (hpi), then titrated by $TCID_{50}$. Plaque assay were performed as previously described (15).

Intrinsic disorder analysis and structural homology modeling : Multiple sequence alignments were performed by the built-in ClustalW program of CLC Main Workbench 8.1 (CLC bio, Aarhus, Denmark). Intrinsic disorder analysis were conducted by multiple online programs including Pondr-FIT (17), Pondr VL-XT (18), DISOPRED3 (19), MobiDB 3.0 (20), metaPrDOS (21). Homology modeling was conducted by I-TASSER (58), without any explicit specification of templates.

Statistical significance analysis: All data in current study were shown as mean values with standard deviations. Statistical significance were evaluated by one-way analysis of variance (ANOVA) followed by Tukey's post hoc test by using GraphPad Prism 6 (GraphPad, La Jolla, CA). P-values were indicated by asterisks in figures. *: $P<0.05$, **:$P<0.01$, ***:$P<0.001$, ****: $P<0.0001$.

3.3. Results

PRRSV nsp2-related proteins are hyper-phosphorylated

Three nsp2-related proteins-nsp2, nsp2TF, and nsp2N of PRRSV-1 (strain SD01-08) have a predicted molecular weight of 114KDa, 96KDa, and 76KDa, respectively. Molecular weight of PRRSV-2 (strain SD95-21) nsp2-related proteins are 129KDa, 110KDa, and 92KDa, respectively. Interestingly, we are curious about the much larger apparent sizes of nsp2-related proteins in sodium dodecyl sulfate-polyacrylamide gel electrophoresis (SDS-PAGE) (13, 14).

Therefore, we investigated whether there are any possible PTMs which slow down the migration of nsp2-related proteins in SDS-PAGE. In particular, we focus on the most common PTM form. Gel-shift assays were performed initially to determine the potential phosphorylation status of nsp2-related proteins (Fig. 1). Nsp2-related proteins were pulled down by immunoprecipitation (IP) from virus-infected cells using the mAb recognizes the shared N-terminal PLP2 domain region (15, 16). Precipitated nsp2-related proteins were then treated ("on-bead") with λ phosphatase (λPP) and compared with their untreated counterparts by electrophoresis and western blot. Result showed that dephosphorylation increased the apparent mobilities of all three nsp2-related proteins (Fig. 1A), suggesting that they are phosphorylated and phosphorylation affects migration of nsp2-related proteins in electrophoresis. To further confirm the phosphorylation states of nsp2-related proteins, a panel of anti-phosphoserine

monoclonal antibodies (mAbs) was tested for specific reactivity with immunoprecipitated nsp2-related protein in western blot assay. Among the panel of mAbs, anti-pSer mAbs- #4A9 and #7F12 could specifically recognize nsp2 protein (data not shown), confirming that serine residues of nsp2 were phosphorylated. We then used anti-pSer mAbs- #4A9 and #7F12 in the gel shift assay to further compare the pre- and post-treated proteins. After λPP treatment, nsp2 bands with increased mobility could still be recognized by anti-pSer mAb- #4A9 and #7F12 (Fig. 1B). However, the corresponding band pixel intensities of higher-mobility species nsp2 in western blot were reduced by ~63% and ~49%, respectively (Fig. 1B), suggesting that the partial phosphate complement of nsp2 were partly removed after λPP treatment, yielding hypo-phosphorylated nsp2 proteins.

To identify specific phosphorylation sites, immunoprecipitated nsp2 and nsp2TF proteins were subjected for mass spectrometric analysis. Result showed that PRRSV nsp2 and nsp2TF are hyper-phosphorylated with at least eighteen modified sites, including ambiguous ones (Table. 1). Eleven phosphorylation sites were found in nsp2, while twelve sites were identified in nsp2TF. However, threonine^{896} and serine^{897} in nsp2, or serine^{1027} and threonine^{1029} in nsp2TF could be unambiguously distinguished in mass spectrometric peptide analysis. Among these identified sites, up to fifteen phosphorylated residues were located between the N-terminal PLP2 domain and the -2/-1 programmed frameshifting site. This region is shared by all three nsp2-related proteins. Unambiguously identified residues-serine^{687}, serine^{838}, serine^{859}, serine^{863}, serine^{902} and serine^{1010} are found both in nsp2 and nsp2TF. Tyrosine^{1253}, threonine^{1373} and serine^{1440} are located in nsp2-specific regions that include the predicted transmembrane (TM) domain and C-terminal cysteine-rich domain. We also assessed the conservation of these identified phosphorylation sites by quantifying the substitution rates in thirty-seven representative variants

(viral genomes published in Genbank before 2014) (Table 1). Among all these sites, serine^{579}, serine^{827}, serine^{838}, serine^{859}, serine^{863}, serine^{897}, serine^{902}, serine^{918}, tyrosine^{1253} and serine^{1440} showed high conservation with substitution rates of less than 3/37 (conservative transition between serine and threonine not included) (Table 1). Notably, one residue-serine^{918} shows unexpected inter-species conservation (Fig. 3).

Mapping phosphorylation sites to functional domains of nsp2-related proteins

To obtain functional insights into nsp2-related protein phosphorylation, we analyzed the impact of nsp2-related proteins phosphorylation abolishment in virus life cycle and particularly searched for potential functional structures containing key phosphorylated sites. Nsp2-related proteins share a relatively conserved PLP2 domain, a small hypervariable region upstream of PLP2 (HVR-1), and two large hypervariable regions (HVR-2 and HVR-3) located between the PLP2 and -2/-1 PRF site. By definition, HVRs exhibit extremely low inter-species similarity (11, 12). HVR-2 and HVR-3 can be defined as distinct domains due to being separated by a highly conserved domain (11). Sequence analysis and structural modeling on HVR-2 and HVR-3 show that these regions have low sequence complexity and have a lower probability to form stable secondary structures. Furthermore, HVR-2 and HVR-3 were consistently predicted to be intrinsically disordered by a number of disorder prediction algorithms, including Pondr-FIT (17), Pondr VL-XT (18), DISOPRED3 (19), MobiDB 3.0 (20), metaPrDOS (21) (Table 2) (Fig. 2). In contrast, the conserved region spacing HVR-2 and HVR-3 exhibits distinct structural features (Fig. 2). At c-terminal portion of this region, an even more highly conserved structured core could be found, consisting of 4 to 5 putative helics (α1-α4 or α4'), which is most likely to form a helical bundle structure (Fig. 3 and Fig. 4). Moreover, three short peptides with uncharacteristically higher inter-species conservation could be further identified within the

structured core (Fig. 3). The N-terminal portion of the conserved region exhibits potential disordered propensity with few putative secondary structures (Fig. 3). Therefore, based on the structural and sequence variation analysis, we defined this region as an independent structured domain-IHCD (inter-HVR-conserved domain). Phosphorylated residues are mapped to specific regions on nsp2-related proteins. Serine^{667}, threonine^{685}, and serine^{687} are localized in HVR-2; serine^{1010}, serine^{1027}, and threonine^{1029} are located in HVR-3; the less structured N-terminal portion of IHCD are enriched with phosphorylation sites-serine^{827}, serine^{838}, serine^{859}, serine^{863}, serine^{897}, and serine^{902}; serine^{918} is located in the C-terminal structural core (Fig. 2). Serine^{918} is included in the first inter-species conserved short peptide in c-terminal portion of IHCD.

The phospohrylation of serine^{918} regulates infectious particle production and accumulation of subgenomic mRNAs

To determine potential role(s) of phosphorylation on nsp2-related proteins in replication, a panel of phospho-ablatant mutations (serine or threonine replaced by alanine, tyrosine replaced by phenylalanine) were introduced into full-length cDNA infectious clone of PRRSV-1 (22). Each residue was changed individually, while adjacent mutations were also combined in analysis (Fig. 5). Tyr^{1253} is located in nsp2 specific region with is overlapped with -2 ORF coding nsp2TF. To avoid non-target mutation in nsp2TF, the phospho-ablatant mutation Y1253F was introduced into a previously constructed nsp2TF/nsp2N-knockout mutant KO2 (13, 14).

Using this panel of phospho-abalatant mutants, we first determined the impact of nsp2-related protein phosphorylation on recombinant virus production. Full-length cDNA infectious clone of each mutant was transfected into the BHK-21 cells and cell culture supernatant was harvested at 48 hours post transfection. Compare with the wild type virus, the mutant S918A showed significantly lower viral yield with one log decreased titer (Fig. 5). We further confirmed

this result by determining the impact of serine^{918} mutation on viral genomic RNA (gRNA) and sgmRNA accumulation. Viral RNA was transcribed from the T7 promoter-driven full-length cDNA infectious clone of S918A mutation, and then transfected into BHK-21 cells. The expression of both plus (+) and minus (-) strand gRNA and subgenomic RNA (sgRNA) was measured by qRT-PCR. In comparison to the WT virus, mutant S918A showed no significant changes in levels of (+) and (-) gRNA (Fig. 6A-B). However, the relative accumulations of three representative sgRNAs, sgRNA 2, 6 and 7 were significantly reduced in mutant S918A transfected cells (Fig. 6A). The ratio of (+) sgRNA2/6/7 to (+) gRNA was reduced by ~48%, ~44%, and ~57%, respectively (Fig. 6A). Consistently, the relative ratios of (-) sgRNA2/6/7 were reduced by ~26%, ~65%, and ~77%, respectively (Fig. 6B). Reduced levels of sgRNAs would result in the decreased expression of structural proteins. As expected, the steady level of structural protein-N protein were significantly decreased by about 56% in S918A mutant RNA transfected BHK-21 cells, compared with WT (Fig. 6C). In contrast, the accumulated level of nonstructural protein-nsp1β was not significantly changed by the S918A phospho-ablatant mutation (Fig. 6C). Decreased structural proteins expression will inevitably inhibit virus packaging. Consistently, infectious virus production of mutant S918A was reduced by 0.78 and 0.77 $\log_{10}$ ($TCID_{50}$/ml) at 18 and 36 hpt, respectively (Fig. 6D), which is also consistent with the first round screening result (Fig. 5). Besides, a phospho-mimetic mutation S918D was also included in this assay (Fig. 6). However, it failed to restore the phenotype loss of phospho-ablatant mutation, only partially recover the decrease of (-) sgRNA 6 and 7 (Fig. 6).

Moreover, the *in vitro* growth kinetic phospho-ablatant mutant S918A was also compared with that of WT virus (Fig. 7). Infected PRRSV-permissive MARC-145 cell supernatants were harvested at 0, 12, 24, 36, 48, 60, 72, 84, and 96 hpi, and titrated with $TCID_{50}$ method. Result

showed that the mutant S918A has a significantly attenuated replication ability in MARC-145 cells (Fig. 7A). WT virus reached the infectious virus titer peak of 6.32 $\log_{10}$ ($TCID_{50}$/ml) at 60 hpi. In contrast, the virus production peak of mutant S918A showed up between 60hpi and 84hpi and was decreased by 1 $\log_{10}$ ($TCID_{50}$/ml) (Fig. 7A). Consistently, the cytolytic ability of mutant S918A was severely attenuated with barely no detectable ability to form plaques in MARC-145 in 4 day post infection (Fig. 7B).

3.4. Discussion

As the most ubiquitous PTM form, protein phosphorylation is indispensable in the modulation of all fundamental biological activities (1-5). Viruses also exploit host phosphorylation mechanism to benefit viral life cycle including replication processes and immune evasion (6, 7). Critical effects of phosphorylation of viral protein factors on replication are broadly reported and characterized in both RNA and DNA viruses (6, 7). Previous characterization of nidoviral protein phosphorylation focused exclusively on N proteins (23, 24), including murine hepatitis virus (MHV), infectious bronchitis virus (IBV), transmissible gastroenteritis coronavirus (TGEV), severe acute respiratory syndrome coronavirus (SARS-CoV), equine arteritis virus (EAV), and PRRSV (24-35). Biological consequences of these phosphorylation events in viral replication were extensively investigated only in coronaviruses (23, 24). For example, the phosphorylation state of IBV N protein regulates its affinity to the viral leader sequence, suggesting that phosphorylation plays critical roles in RNA transcription (29, 32). Phosphorylation by the host GSK3 kinase appears to affect conformational transitions of the MHV N protein and regulates its interaction with the DDX1 helicase to fine-tune the discontinuous transcription of sgmRNAs (36). The N protein of PRRSV has also been reported

as a phosphorylated protein (12, 37, 38). However, exact roles of phosphorylated N proteins for PRRSV life cycle still remain unclear (12, 37, 38).

Our current study is the first to demonstrate the importance of phosphorylation of nidoviral (PRRSV) proteins other than N proteins in viral replication. It reveals regulatory role of PRRSV nsp2-related protein phosphorylation involving in sgmRNA accumulation, possibly in the discontinuous transcription. The primary role of nsp2 in viral replication is to function as a protease (PLP2) in the proteolytic processing of viral replicase polyproteins (39). Arteriviral nsp2 was also reported to play important roles in mediating the formation of viral replication organelle-double membrane vesicles (DMVs) and anchor the replication and transcription complex (RTC) (12, 40, 41). The discovery of novel -2/-1 frameshifting mechanism and identification two frameshifting products-nsp2TF and nsp2N (12-14, 42) in nsp2 region increase the versatility and functional complexity of this set of proteins. We observed that all three nsp2-related proteins (nsp2, nsp2TF, and nsp2N) are phosphorylated. Mutations introduced into the phosphorylation sites serine^{918} attenuated the *in vitro* viral replication; especially, disrupting the phosphorylation state of serine^{918} in the virus downregulates the steady-state levels of sgmRNAs without affecting gRNA accumulation. Whether nsp2-related proteins, as trans-acting factor(s), directly regulate arterivirus discontinuous transcription warrants further investigation. In PRRSV-infected cells, nsp2TF was found to have a different subcellular localization pattern than that of nsp2 (Fang et al., 2012), suggesting that phosphorylation state of these proteins may regulate the viral replication by different mechanism or only one of the proteins is involved in sgmRNA synthesis.

Compared with other conserved domains in nsp2-related proteins, the functionally obscure region between PLP2 domain and PRF site stands out the most. We subdivided this large

region into two HVRs separated by relatively conserved inter-HVR region, which contains a highly conserved domain-IHCD in both PRRSV-1 and PRRSV-2. In previous studies, serial deletions were introduced into HVR and IHCD. In PRRSV-1 (strain SD01-08), HVR-2 contains two known epitopes-ES3 (691aa-722aa of pp1a) and ES4 (736aa-790aa of pp1a); ES7 (1015aa-1040aa of pp1a) is located in HVR-3; ES5 (822aa-832aa of pp1a) could be found in the N-terminal portion of IHCD; ES6 (895aa-922aa of pp1a) is located in the junction of two portions of IHCD (43) (Fig. 2). ES3 deletion caused enhanced cytolyticty and more vigorous *in vitro* growth kinetics; ES4 and ES7 deletion mutants exhibited opposite *in vitro* growth properties (43). In contrast, deletion of IHCD epitopes-ES5 and ES6 is proved to be lethal for viable virus rescue (43). *In vivo* characterization of ES3, ES4, and ES7 deletion mutants displayed viremic phenotypes consistent with that of *in vitro* (43). In addition, the mRNA and protein expression level of IL-1β and TNF-α were downregulated in ES3 deletion mutant-infected macrophages (43). In PRRSV-2 (strain VR-2332), specific regions in nsp2 that are dispensable for replication were also identified (44). Deletions of residues 324-523 and 543-632 (covering HVR-2), 633-726 (overlapping with IHCD), and 727-813 (partially overlapping HVR-3) could rescue viable recombinant viruses, but incurred severe fitness loss (44). These results indicate that HVR-2/HVR-3 and IHCD are associated with viral fitness and basic replication. In the current study, mass-spectrometric analysis of PRRSV-1 identified that most of the phosphorylation sites are located in these HVRs and inter-HVR regions, in which nsp2 contains 6 phosphorylated sites and nsp2TF contains 7 sites. Besides the in-depth analysis S918 involved in regulation of sgmRNA accumulation, the functional importance of other phosphorylated residues needs to be elucidated in the future. Previous studies showed that PRRSV nsp2-related proteins are enriched with immune-dominant B-cell epitopes (12, 43, 45, 46), as well as predicted T-cell epitopes.

Interestingly, serine^{827} is located in epitope ES5; threonine^{896} (or serine^{897}), serine^{902} and serine^{918} are found in epitope ES6; serine^{1027} or threonine^{1029} is located in epitope ES7 (Table 1). Our previous study demonstrated the necessity of intact IHCD epitopes-ES5, ES6, and ES7 for viral viability or fitness (43). Current study further revealed the critical role of phosphorylated serine^{918} in ES6 for viral sgmRNA accumulation, possibly for the discontinuous transcription process.

Our sequence analysis showed that the region between PLP2 and -2/-1 PRF site contains IDRs, which has limited homology with any other known proteins/domains. In general, IDRs/IDPs lack hydrophobic residues to support formation of well-defined and folded hydrophobic cores and do not adopt stable tertiary structures in the absence of binding partners (47-51). Conformations of IDPs/IDRs are more typically represented as dynamic ensembles (47-51). The functional advantages and features of structural disorder have been well documented (47-51). One advantage is that disordered region can present highly diversified binding sites for other macromolecular partners (47-51). As intracellular parasites, the life cycle of viruses depends critically upon interactions between viral proteins and host components. The absence of strong structural constraints correlates with less restriction on selection of structured sequences and higher tolerance to sequence substitution (48-50, 52, 53). Furthermore, loose constraints in conformation permits dynamic display of PTM sites, such as phosphorylation, in order to facilitate transient interactions with modifying enzymes; and allow the easy access and recognition of modified sites for downstream interactions (48-50). These properties would allow viruses to respond to rapidly changing host environments. In the case of PRRSV nsp2-related proteins, the two large putative IDRs associated with the HVRs and hyper-phosphorylation sites support the functional connection between sequence variability and mechanistic roles (Fig. 2).

Given the fact that nsp2-related proteins contain the most apparent disordered regions in the viral proteome (Fig. 8-9), the hyper-phosphorylated IDRs in nsp2-related proteins may function as evolutionary “hot-spots” for fast adaptation to the constantly changing host environment-including immunological and physiological conditions, and greatly diversified host genetic background.

3.5. Reference

1. Humphrey SJ, James DE, Mann M. 2015. Protein phosphorylation: a major switch mechanism for metabolic regulation. Trends in Endocrinology & Metabolism 26:676-687.
2. Hunter T. 1995. Protein kinases and phosphatases: the yin and yang of protein phosphorylation and signaling. Cell 80:225-236.
3. Johnson LN. 2009. The regulation of protein phosphorylation. Biochemical Society Transactions 37:627-641.
4. Tarrant MK, Cole PA. 2009. The chemical biology of protein phosphorylation. Annual review of biochemistry 78:797-825.
5. Ubersax JA, Ferrell Jr JE. 2007. Mechanisms of specificity in protein phosphorylation. Nature reviews Molecular cell biology 8:530.
6. Keating JA, Striker R. 2012. Phosphorylation events during viral infections provide potential therapeutic targets. Reviews in medical virology 22:166-181.
7. Keck F, Ataey P, Amaya M, Bailey C, Narayanan A. 2015. Phosphorylation of single stranded RNA virus proteins and potential for novel therapeutic strategies. Viruses 7:5257-5273.
8. Ying Fang, Snijder EJ. 2010. The PRRSV replicase: Exploring the multifunctionality of an intriguing set of nonstructural proteins. Virus Research 154 61-76.
9. Eric J. Snijder, Marjolein Kikkert, Fang Y. 2013. Arterivirus molecular biology and pathogenesis. Journal of General Virology 94:2141–2163.
10. Kuhn JH, Lauck M, Bailey AL, Shchetinin AM, Vishnevskaya TV, Bào Y, Ng TFF, LeBreton M, Schneider BS, Gillis A. 2016. Reorganization and expansion of the nidoviral family Arteriviridae. Archives of virology 161:755-768.
11. Fang Y, Snijder EJ. 2010. The PRRSV replicase: exploring the multifunctionality of an intriguing set of nonstructural proteins. Virus research 154:61-76.
12. Snijder EJ, Kikkert M, Fang Y. 2013. Arterivirus molecular biology and pathogenesis. Journal of General Virology 94:2141-2163.
13. Li Y, Shang P, Shyu D, Carrillo C, Naraghi-Arani P, Jaing CJ, Renukaradhya G, Firth A, Snijder E, Fang Y. 2018. Nonstructural proteins nsp2TF and nsp2N of porcine

reproductive and respiratory syndrome virus (PRRSV) play important roles in suppressing host innate immune responses. Virology.

14. Fang Y, Treffers EE, Li Y, Tas A, Sun Z, Van Der Meer Y, De Ru AH, Van Veelen PA, Atkins JF, Snijder EJ. 2012. Efficient− 2 frameshifting by mammalian ribosomes to synthesize an additional arterivirus protein. proceedings of the National Academy of Sciences 109:E2920-E2928.
15. Fang Y, Rowland RR, Roof M, Lunney JK, Christopher-Hennings J, Nelson EA. 2006. A full-length cDNA infectious clone of North American type 1 porcine reproductive and respiratory syndrome virus: expression of green fluorescent protein in the Nsp2 region. Journal of virology 80:11447-11455.
16. Li Y, Tas A, Snijder EJ, Fang Y. 2012. Identification of porcine reproductive and respiratory syndrome virus ORF1a-encoded non-structural proteins in virus-infected cells. Journal of general virology 93:829-839.
17. Xue B, Dunbrack RL, Williams RW, Dunker AK, Uversky VN. 2010. PONDR-FIT: a meta-predictor of intrinsically disordered amino acids. Biochimica et Biophysica Acta (BBA)-Proteins and Proteomics 1804:996-1010.
18. Bomma R, Venkatesh P, Dlvnsssr A, Babu A, Rao S. 2012. PONDR (predicators of natural disorder regions). Int J Comput Technol Electron Eng IJCTEE 2:1-10.
19. Jones DT, Cozzetto D. 2014. DISOPRED3: precise disordered region predictions with annotated protein-binding activity. Bioinformatics 31:857-863.
20. Piovesan D, Tabaro F, Paladin L, Necci M, Mičetić I, Camilloni C, Davey N, Dosztányi Z, Mészáros B, Monzon AM. 2017. MobiDB 3.0: more annotations for intrinsic disorder, conformational diversity and interactions in proteins. Nucleic acids research 46:D471-D476.
21. Ishida T, Kinoshita K. 2008. Prediction of disordered regions in proteins based on the meta approach. Bioinformatics 24:1344-1348.
22. Dephoure N, Gould KL, Gygi SP, Kellogg DR. 2013. Mapping and analysis of phosphorylation sites: a quick guide for cell biologists. Molecular biology of the cell 24:535-542.
23. Dokland T. 2010. The structural biology of PRRSV. Virus research 154:86-97.

24. McBride R, van Zyl M, Fielding BC. 2014. The coronavirus nucleocapsid is a multifunctional protein. Viruses 6:2991-3018.
25. Wu C-H, Yeh S-H, Tsay Y-G, Shieh Y-H, Kao C-L, Chen Y-S, Wang S-H, Kuo T-J, Chen D-S, Chen P-J. 2009. Glycogen synthase kinase-3 regulates the phosphorylation of severe acute respiratory syndrome coronavirus nucleocapsid protein and viral replication. Journal of Biological Chemistry 284:5229-5239.
26. White TC, Yi Z, Hogue BG. 2007. Identification of mouse hepatitis coronavirus A59 nucleocapsid protein phosphorylation sites. Virus research 126:139-148.
27. Surjit M, Kumar R, Mishra RN, Reddy MK, Chow VT, Lal SK. 2005. The severe acute respiratory syndrome coronavirus nucleocapsid protein is phosphorylated and localizes in the cytoplasm by 14-3-3-mediated translocation. Journal of virology 79:11476-11486.
28. Stohlman S, Lai M. 1979. Phosphoproteins of murine hepatitis viruses. Journal of virology 32:672-675.
29. Spencer K-A, Dee M, Britton P, Hiscox JA. 2008. Role of phosphorylation clusters in the biology of the coronavirus infectious bronchitis virus nucleocapsid protein. Virology 370:373-381.
30. Peng TY, Lee KR, Tarn WY. 2008. Phosphorylation of the arginine/serine dipeptide‐rich motif of the severe acute respiratory syndrome coronavirus nucleocapsid protein modulates its multimerization, translation inhibitory activity and cellular localization. The FEBS journal 275:4152-4163.
31. Mohandas DV, Dales S. 1991. Endosomal association of a protein phosphatase with high dephosphorylating activity against a coronavirus nucleocapsid protein. FEBS letters 282:419-424.
32. Chen H, Gill A, Dove BK, Emmett SR, Kemp CF, Ritchie MA, Dee M, Hiscox JA. 2005. Mass spectroscopic characterization of the coronavirus infectious bronchitis virus nucleoprotein and elucidation of the role of phosphorylation in RNA binding by using surface plasmon resonance. Journal of virology 79:1164-1179.
33. Chang C-K, Hsu Y-L, Chang Y-H, Chao F-A, Wu M-C, Huang Y-S, Hu C-K, Huang T-H. 2009. Multiple nucleic acid binding sites and intrinsic disorder of severe acute respiratory syndrome coronavirus nucleocapsid protein: implications for ribonucleocapsid protein packaging. Journal of virology 83:2255-2264.

34. Calvo E, Escors D, Lopez J, Gonzalez J, Alvarez A, Arza E, Enjuanes L. 2005. Phosphorylation and subcellular localization of transmissible gastroenteritis virus nucleocapsid protein in infected cells. Journal of general virology 86:2255-2267.
35. Zeegers J, Van der Zeijst B, Horzinek M. 1976. The structural proteins of equine arteritis virus. Virology 73:200-205.
36. Wu C-H, Chen P-J, Yeh S-H. 2014. Nucleocapsid phosphorylation and RNA helicase DDX1 recruitment enables coronavirus transition from discontinuous to continuous transcription. Cell host & microbe 16:462-472.
37. Wootton SK, Rowland RR, Yoo D. 2002. Phosphorylation of the porcine reproductive and respiratory syndrome virus nucleocapsid protein. Journal of virology 76:10569-10576.
38. Yoo D, Wootton SK, Li G, Song C, Rowland RR. 2003. Colocalization and interaction of the porcine arterivirus nucleocapsid protein with the small nucleolar RNA-associated protein fibrillarin. Journal of virology 77:12173-12183.
39. Wassenaar A, Spaan W, Gorbalenya AE, Snijder EJ. 1997. Alternative proteolytic processing of the arterivirus replicase ORF1a polyprotein: evidence that NSP2 acts as a cofactor for the NSP4 serine protease. Journal of virology 71:9313-9322.
40. Snijder EJ, van Tol H, Roos N, Pedersen KW. 2001. Non-structural proteins 2 and 3 interact to modify host cell membranes during the formation of the arterivirus replication complex. Journal of General Virology 82:985-994.
41. Posthuma CC, Pedersen KW, Lu Z, Joosten RG, Roos N, Zevenhoven-Dobbe JC, Snijder EJ. 2008. Formation of the arterivirus replication/transcription complex: a key role for nonstructural protein 3 in the remodeling of intracellular membranes. Journal of virology 82:4480-4491.
42. Li Y, Treffers EE, Napthine S, Tas A, Zhu L, Sun Z, Bell S, Mark BL, van Veelen PA, van Hemert MJ. 2014. Transactivation of programmed ribosomal frameshifting by a viral protein. Proceedings of the National Academy of Sciences 111:E2172-E2181.
43. Chen Z, Zhou X, Lunney JK, Lawson S, Sun Z, Brown E, Christopher-Hennings J, Knudsen D, Nelson E, Fang Y. 2010. Immunodominant epitopes in nsp2 of porcine reproductive and respiratory syndrome virus are dispensable for replication, but play an

important role in modulation of the host immune response. Journal of general virology 91:1047-1057.

44. Han J, Liu G, Wang Y, Faaberg KS. 2007. Identification of nonessential regions of the nsp2 replicase protein of porcine reproductive and respiratory syndrome virus strain VR-2332 for replication in cell culture. Journal of virology 81:9878-9890.
45. de Lima M, Pattnaik A, Flores E, Osorio F. 2006. Mapping of B-cell linear epitopes on Nsp2 and structural proteins of a North American strain of porcine reproductive and respiratory syndrome virus. Virology 353:410-421.
46. Oleksiewicz M, Bøtner A, Toft P, Normann P, Storgaard T. 2001. Epitope mapping porcine reproductive and respiratory syndrome virus by phage display: the nsp2 fragment of the replicase polyprotein contains a cluster of B-cell epitopes. Journal of virology 75:3277-3290.
47. Wright PE, Dyson HJ. 2015. Intrinsically disordered proteins in cellular signalling and regulation. Nature reviews Molecular cell biology 16:18.
48. Van Der Lee R, Buljan M, Lang B, Weatheritt RJ, Daughdrill GW, Dunker AK, Fuxreiter M, Gough J, Gsponer J, Jones DT. 2014. Classification of intrinsically disordered regions and proteins. Chemical reviews 114:6589-6631.
49. Oldfield CJ, Dunker AK. 2014. Intrinsically disordered proteins and intrinsically disordered protein regions. Annual review of biochemistry 83:553-584.
50. Uversky VN. 2013. A decade and a half of protein intrinsic disorder: biology still waits for physics. Protein Science 22:693-724.
51. Dyson HJ, Wright PE. 2005. Intrinsically unstructured proteins and their functions. Nature reviews Molecular cell biology 6:197.
52. Xue B, Blocquel D, Habchi J, Uversky AV, Kurgan L, Uversky VN, Longhi S. 2014. Structural disorder in viral proteins. Chemical reviews 114:6880-6911.
53. Gitlin L, Hagai T, LaBarbera A, Solovey M, Andino R. 2014. Rapid evolution of virus sequences in intrinsically disordered protein regions. PLoS pathogens 10:e1004529.
54. Taniguchi T, Garcia-Higuera I, Xu B, Andreassen PR, Gregory RC, Kim S-T, Lane WS, Kastan MB, D'Andrea AD. 2002. Convergence of the fanconi anemia and ataxia telangiectasia signaling pathways. Cell 109:459-472.

55. Shang P, Misra S, Hause B, Fang Y. 2017. A naturally occurring recombinant enterovirus expresses a torovirus deubiquitinase. Journal of virology 91:e00450-17.
56. Li Y, Zhu L, Lawson SR, Fang Y. 2013. Targeted mutations in a highly conserved motif of the nsp1β protein impair the interferon antagonizing activity of porcine reproductive and respiratory syndrome virus. Journal of General Virology 94:1972-1983.
57. Reed LJ, Muench H. 1938. A simple method of estimating fifty per cent endpoints. American journal of epidemiology 27:493-497.
58. Yang J, Yan R, Roy A, Xu D, Poisson J, Zhang Y. 2015. The I-TASSER Suite: protein structure and function prediction. Nature methods 12:7.

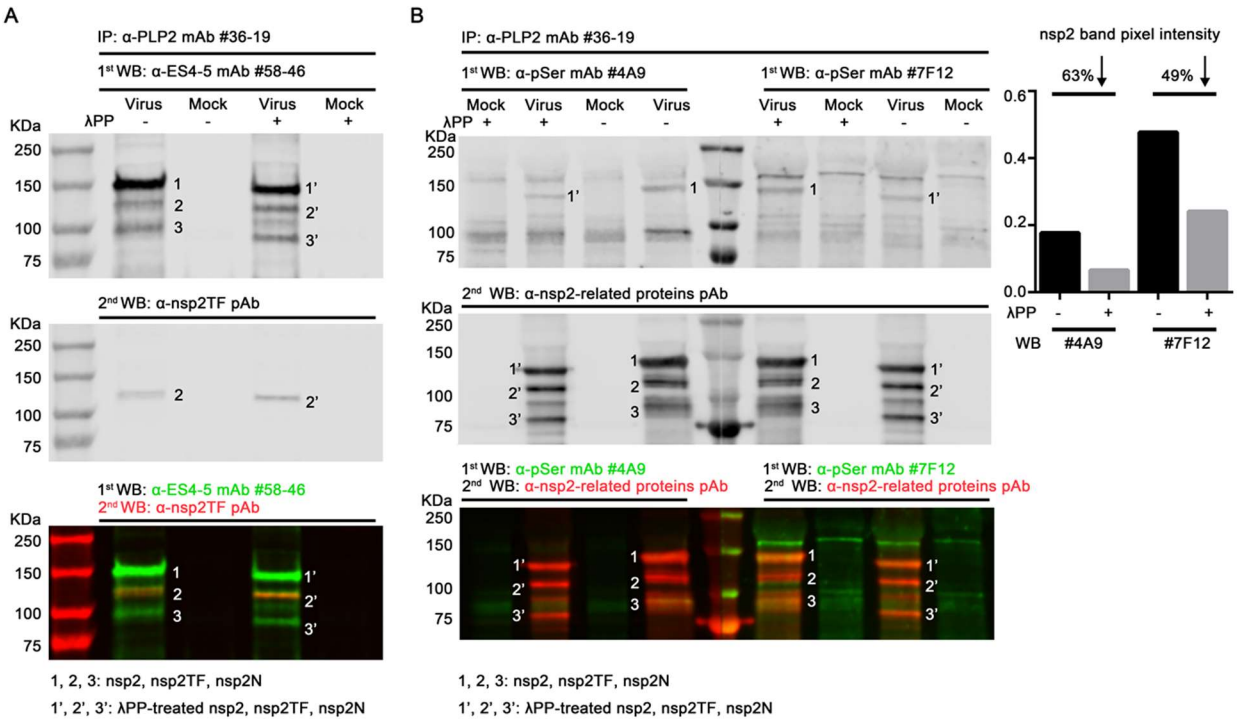

Figure 3.1. Immuno-detection of PRRSV-1 nsp2-related proteins phosphorylation

(A) Gel shifting assay. Nsp2-related proteins bound on Sepharose beads were treated with λPP, then separated by SDS-PAGE. α-PLP2 mAb #36-19 was used in IP. α-ES4-5 mAb #58-46 and α-nsp2TF pAb were used in WB to visualize apparent size changes before and after treatment. (B) WB detection of nsp2-related proteins phosphorylation state post λPP treatment. α-pSer mAbs-#4A9 and #7F12 capable to detect the phosphorylation state of nsp2 was used in WB. Pixel intensity of nsp2 bands was calculated by Image Studio 5.2 (Li-Cor Biosciences). Confirmation of the specific reactivity of α-pSer mAbs, α-nsp2-related proteins pAb was used to detect nsp2-related proteins in WB.

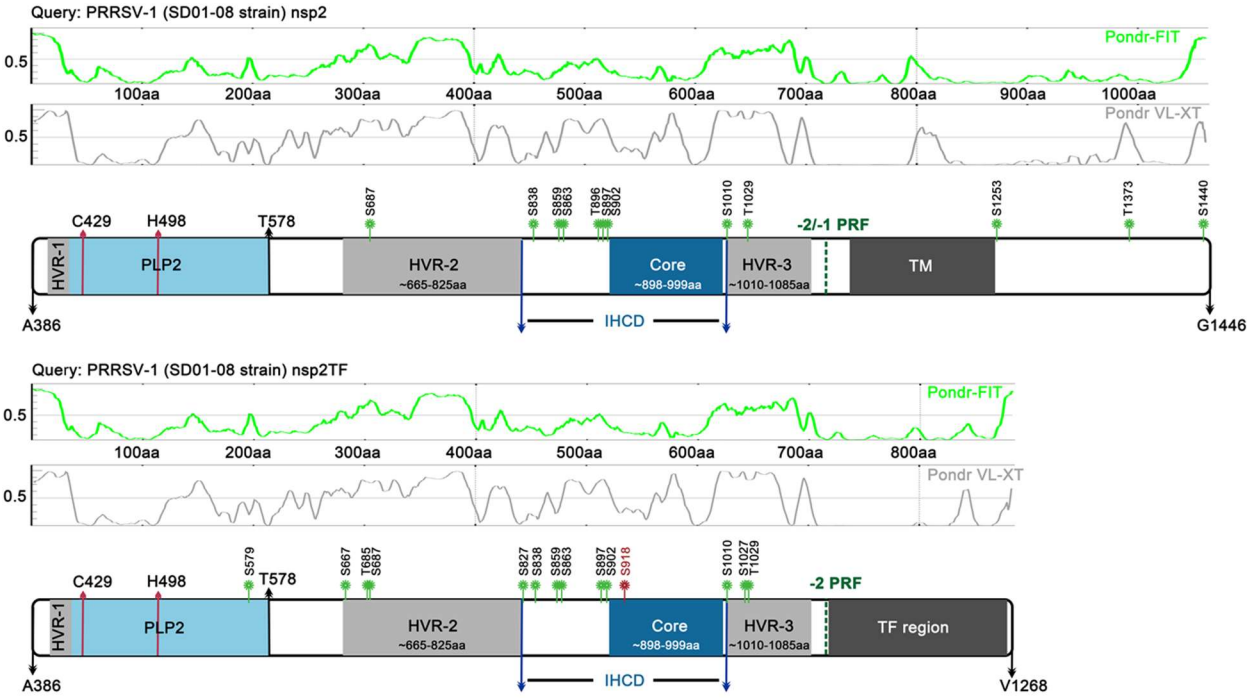

Figure 3.2. Mapping phosphorylation sites to domains of PRRSV-1 nsp2-related proteins

Phosphorylation sites were mapped to corresponding domains of nsp2 and nsp2TF, indicated by green or red flower-like symbol. Red symbols represent the critical phosphorylation site-serine^{918}. Light blue, grey, dark blue, and black shadows indicate PLP2, HVRs, IHCD structure core, and TM domains, respectively. Corresponding approximate borders were shown beneath these domains. Green dashed line indicates 2/-1 PRF site. Possible structural features about intrinsic disorder of nsp2 and nsp2TF were analyzed by online programs-Pondr-FIT and Pondr VL-XT.

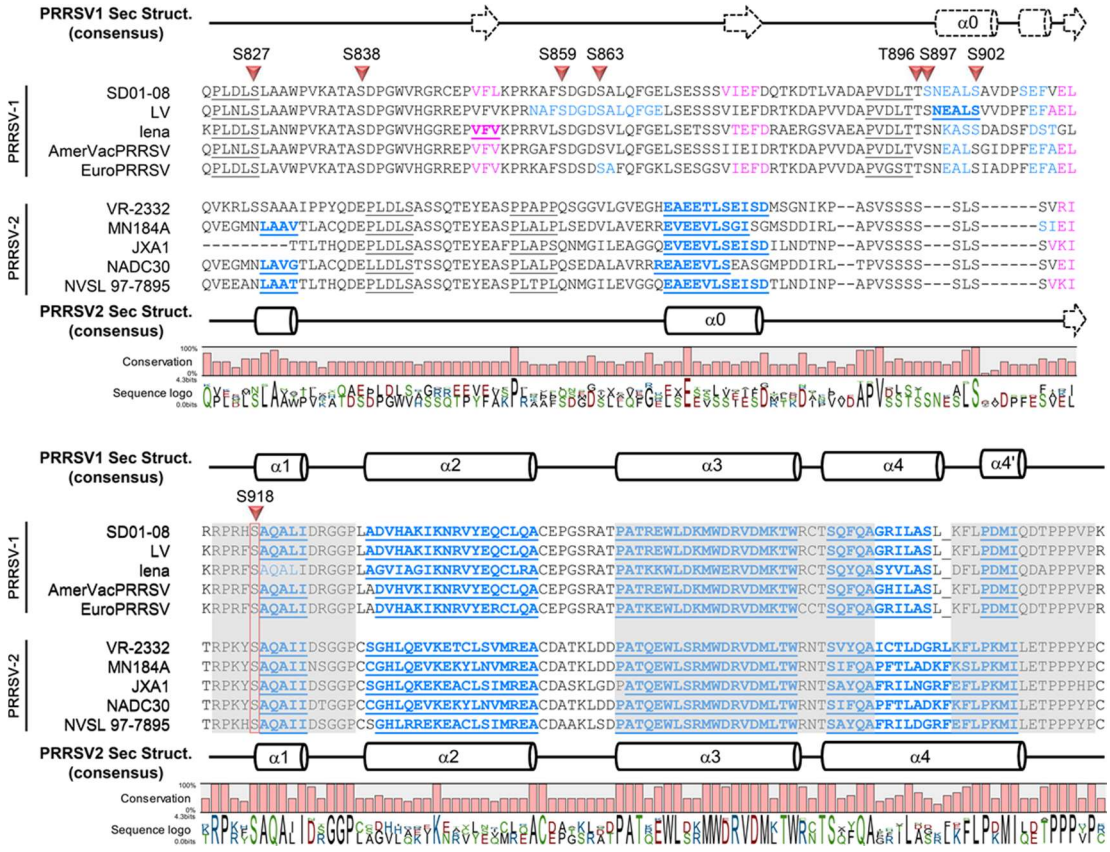

Figure 3.3. The inter-HVR conserved domain (IHCD) of PRRSV nsp2-related proteins

The region of nsp2-related proteins containing three phosphorylated residues-serine^{838}, serine^{859}, and serine^{918} were aligned by CLC Main Workbench 8.1 (CLC bio). PRRSV-1 strains-SD01-08 (Genbank DQ489311.1), Lelystad virus (LV) (Genbank M96262.2), lena (Genbank JF802085.1), Amervac PRRS (Genbank GU067771.1), EuroPRRSV (Genbank AY366525.1) and PRRSV-2 strains-VR-2332 (Genbank AY150564.1), MN184A (Genbank DQ176019.1), JXA1 (Genbank EF112445.1), NADC30 (Genbank JN654459.1), and NVSL 97-7895 (Genbank AY545985.1) were selected for alignment. Peptide sequences with great inter-species conservation were highlighted by grey shadows. Secondary structures predicted by I-TASSER based on PRRSV-1/-2 IHCD sequences were presented above or beneath corresponding amino acids. Cylinder indicates α helix; arrow head indicates β sheet. Sequences forming putative α-helix and β-sheet structures were shown in blue and magenta color. Predicted structures with high confidence were highlighted in underlined bold font. Sequence conservation and logo analyzed by CLC Main Workbench 8.1 (CLC bio) were shown underneath. Phosphorylated sites were labelled by red triangle. The critical residue-serine^{918} is indicated by red frame.

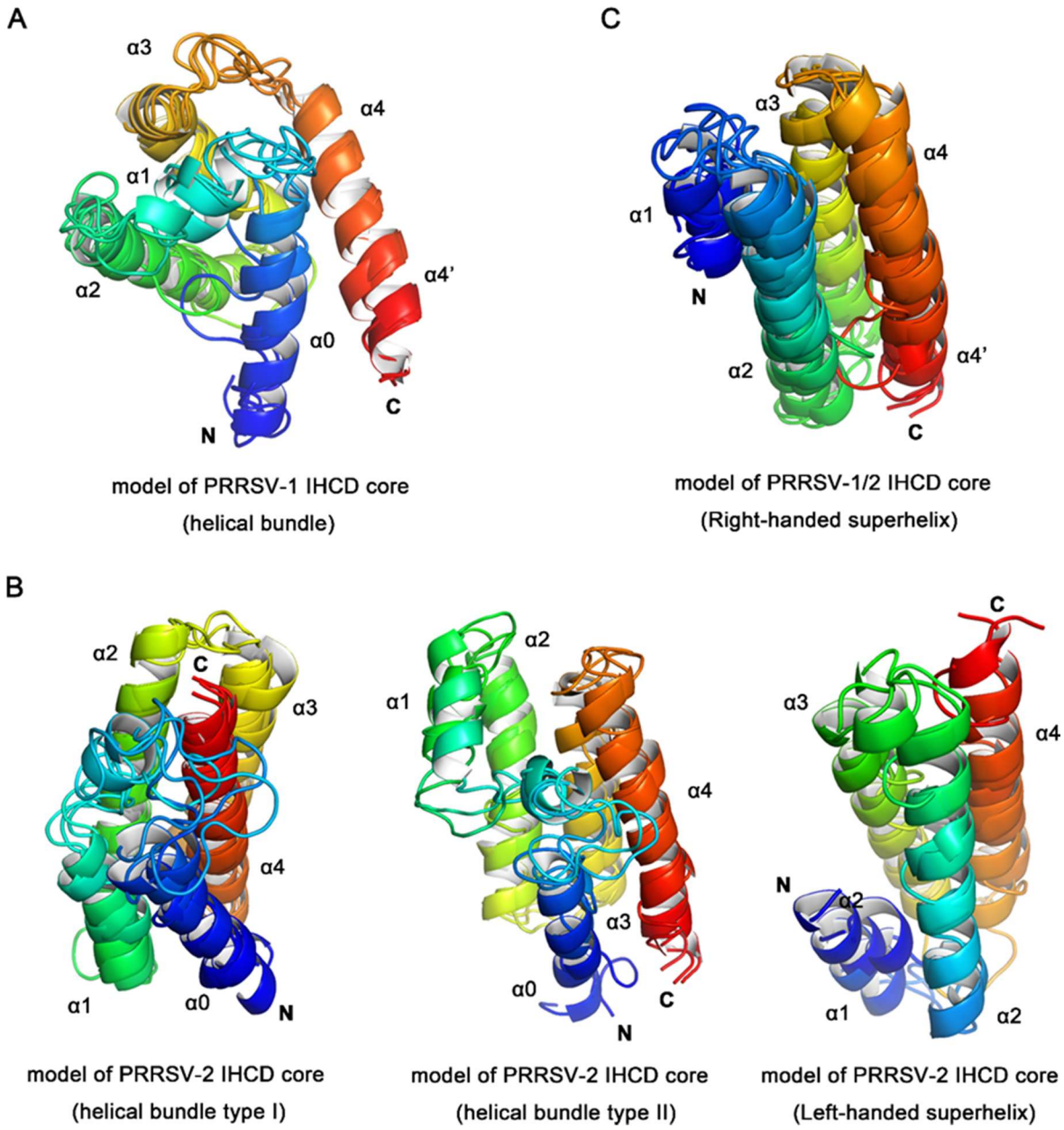

Figure 3.4. Predicted helical bundle models of IHCD structured core

(A) Predicted helical bundle structure of PRRSV-1 IHCD core. (B) Predicted helical bundle structures of PRRSV-2 IHCD core. (C) Predicted right-handed superhelix structure of PRRSV-1/-2 IHCD core.

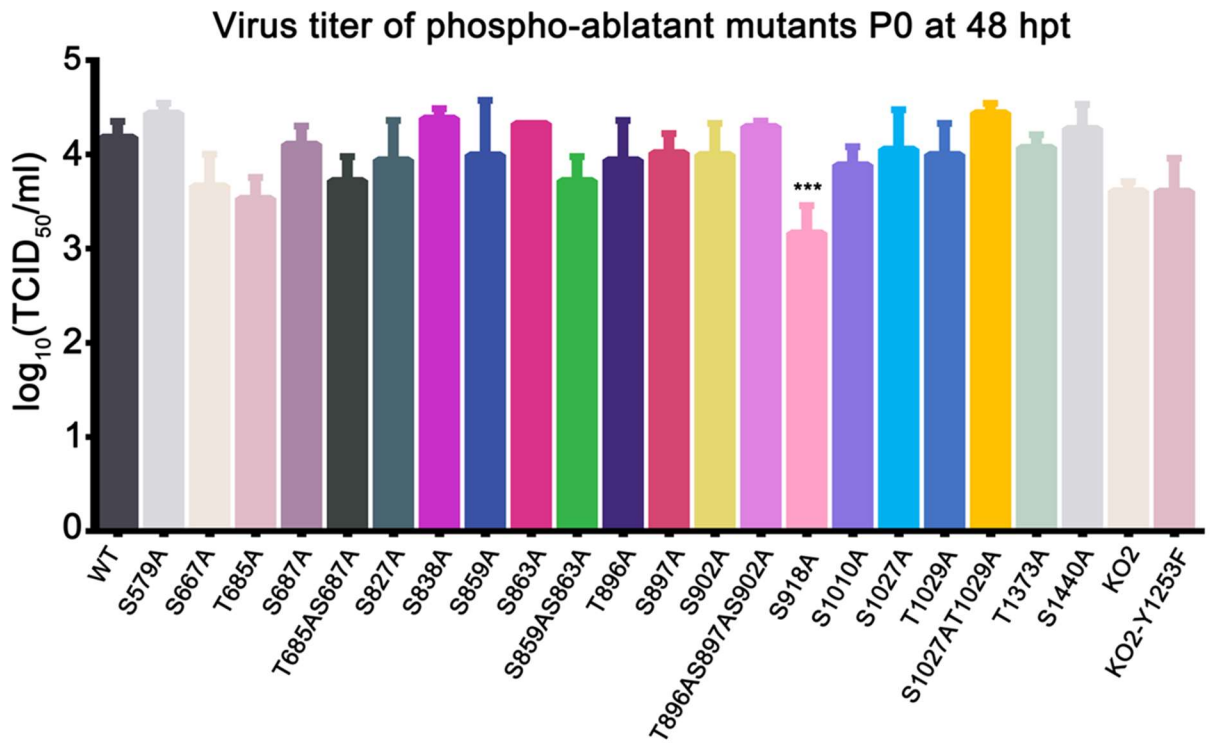

Figure 3.5. Rescue efficiency of phospho-ablatant mutants in transfected cells.

A panel of PRRSV cDNA infectious clones with phospho-ablatant mutations was transfected into BHK-21 cells. Cell culture supernatants were harvested 48 hour post transfection (hpt), and titrated for rescued recombinant virus production on MARC-145 cells with $TCID_{50}$ method. Experiment was performed in biological triplicates. ***:P<0.001.

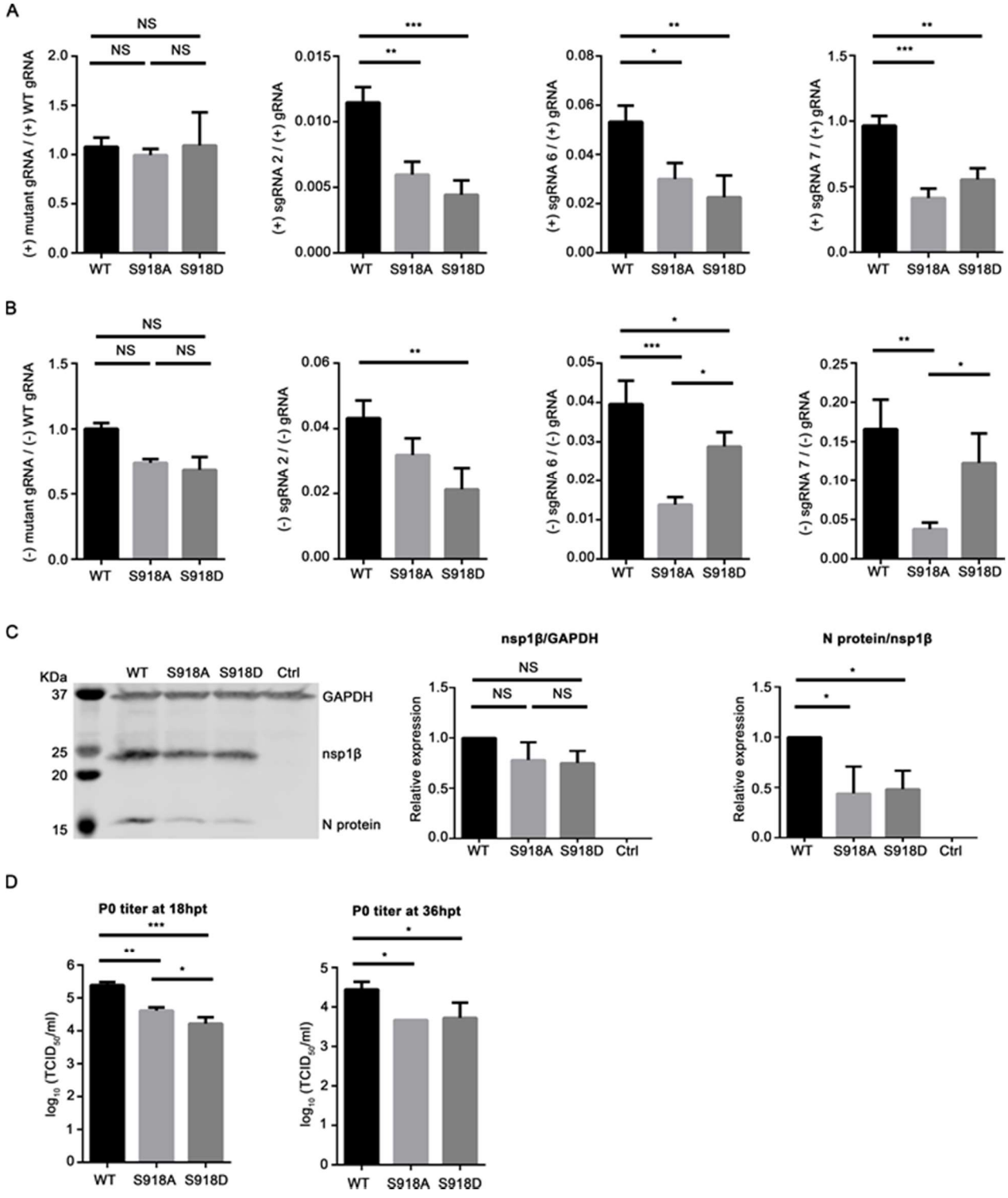
A
(+) mutant gRNA / (+) WT gRNA
(+) sgRNA 2 / (+) gRNA
(+) sgRNA 6 / (+) gRNA
(+) sgRNA 7 / (+) gRNA
B
(-) mutant gRNA / (-) WT gRNA
(-) sgRNA 2 / (-) gRNA
(-) sgRNA 6 / (-) gRNA
(-) sgRNA 7 / (-) gRNA
NS
WT
S918A
S918D
C
KDa
Ctrl
GAPDH
nsp1β
N protein
nsp1β/GAPDH
N protein/nsp1β
Relative expression
D
P0 titer at 18hpt
P0 titer at 36hpt
log10 (TCID50/ml)

Figure 3.6. Phosphorylation at serine^{918} of nsp2-related proteins influences relative accumulation of subgenomic RNAs

(A) and (B) ratios of plus-and minus-strand RNA. *In vitro* transcribed genomic RNA of WT virus, mutant S918A, and phospho-mimetic mutant S918D were transfected into BHK-21 cells. At 18 hpt, BHK-21 cells were lysed for plus and minus genomic/subgenomic RNA qRT-PCR quantification. (C) Structural and nonstructural proteins expression in BHK-21 cells. The expression of viral N proteins and nsp1β in BHK-21 cells at 18 hpt was visualized by western blot by using α-N mAb #14-126 and α-nsp1β #22-28. Pixel intensity was quantified Image Studio 5.2 (Li-Cor Biosciences). Host housekeeping protein-GAPDH was recognized by specific mAb. The expression of nsp1β was normalized with GAPDH; N protein expression was compared with corresponding expression of nsp1β. The pixel intensity of WT sample was taken as 1 for the convenience of comparison. (D) Rescued virus yield comparison. BHK-21 cell supernatants were harvested at 18 hpt and 36 hpt to titrate infectious virus production by $TCID_{50}$ method. All experiments were performed in biological triplicates. *: $P<0.05$, **:$P<0.01$, ***:$P<0.001$, NS: $P>0.05$.

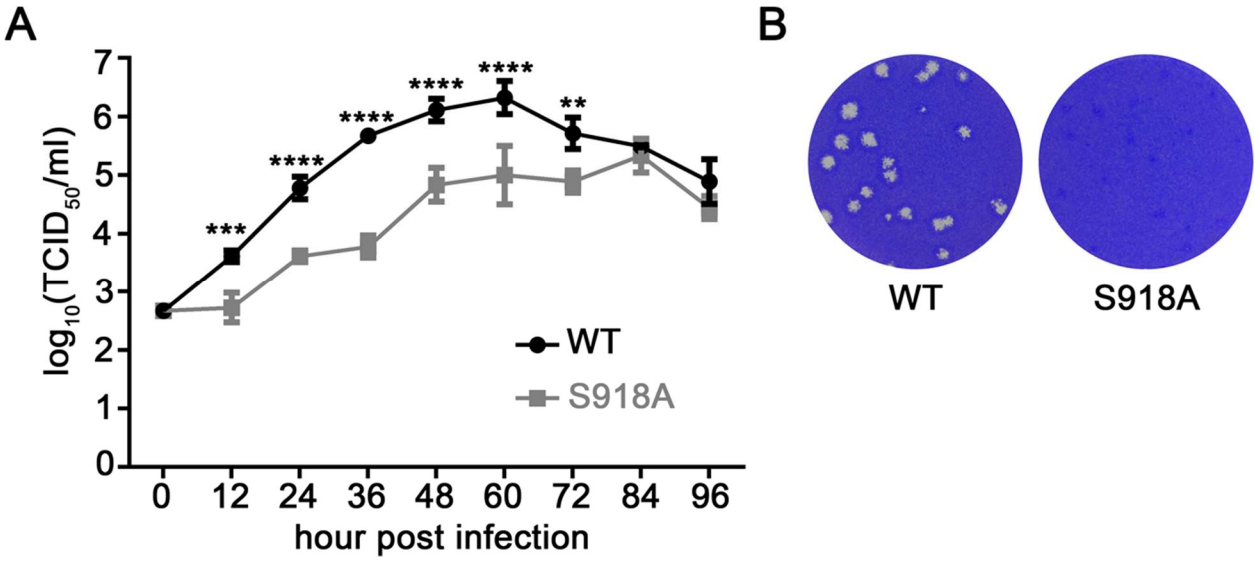

Figure 3.7. Attenuated replication ability of phospho-ablatant mutant S918A in MARC-145 cells

(A) *In vitro* growth curve. MARC-145 cells were infected at moi=0.01 by WT and S918A mutant virus, respectively. Cell supernatants were harvested and titrated every 12 hpi. (B) Plaque assay. Infected MARC-145 cells were stained by crystal violet solution at 4 dpi.

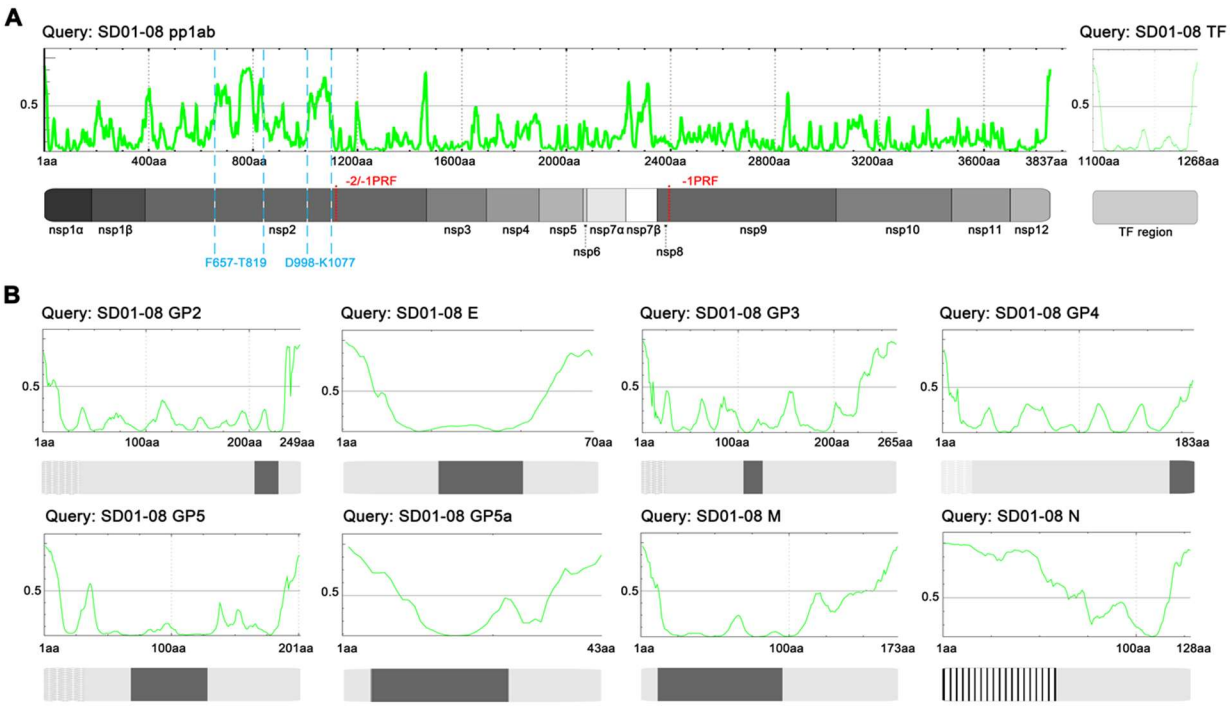

Figure 3.8. Intrinsic disorder *in silico* analysis of PRRSV-1 proteome

Intrinsically disordered tendency of known proteome of PRRSV-1 (SD01-08 strain, Genbank DQ489311.1) including pp1ab, nsp2TF -2 ORF, GP2, E, GP3, GP4, GP5, GP5a, M, and N were analyzed by program Pondr-FIT (A and B). (A) Most outstanding IDRs in pp1ab were marked by blue dashed lines. (B) Putative signal peptides and TM regions were shown as grey mesh and grey shadow, respectively (23). Vertical bar region in the N-terminal of N protein indicates the RNA-binding domain (23).

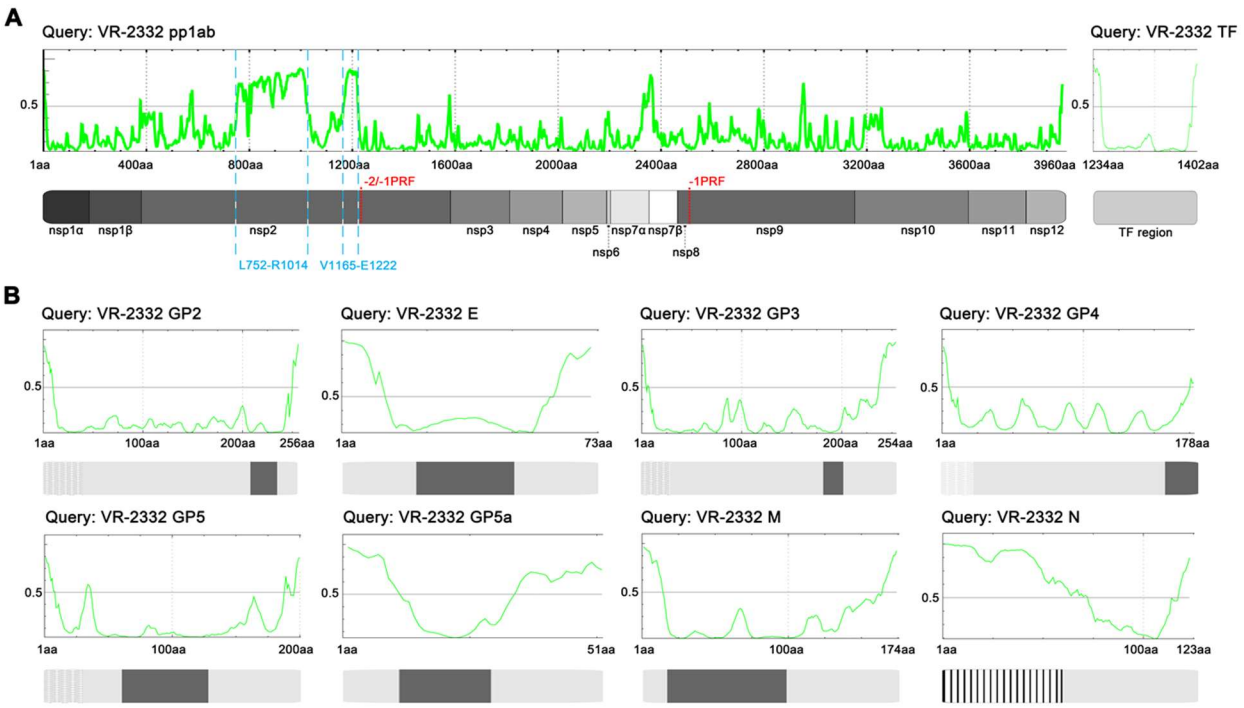

Figure 3.9. Intrinsic disorder *in silico* analysis of PRRSV-2 proteome

Intrinsically disordered tendency of known proteome of PRRSV-1 (VR-2332 strain, Genbank AY150564.1) including pp1ab, nsp2TF -2 ORF, GP2, E, GP3, GP4, GP5, GP5a, M, and N were analyzed by program Pondr-FIT (A and B). (A) Most outstanding IDRs in pp1ab were marked by blue dashed lines. (B) Putative signal peptides and TM regions were shown as grey mesh and grey shadow, respectively (23). Vertical bar region in the N-terminal of N protein indicates the RNA-binding domain (23).

Table 3.1. Identification PRRSV-1 nsp2 and nsp2TF phosphorylation sites by mass spectrometry

Nsp2 residues (position in pp1a /nsp2)	Mass spec identified peptide	Nsp2TF residue (position in pp1a/nsp2TF)	Mass spec identified peptide	Substitution rate	Localization in B-cell epitopes
		S579 / S194	TLDKMLTSPSPERSGF	2/37	
		S667 / S282	SPGAAVALCSPDAK	17/37	
		T685 / T300	SPDAKGFEGTASEEAQESGHKA	31/37	
S687 / S302	GFEGTASEEAQESGHK	S687 / S302	GFEGTASEEAQESGHK	36/37	
		S827 / S442	LDLSLAAW	0/37	ES5
S838 / S453	TASDPGWVRG KATASDPGWVRG TASDPGWVR	S838 / S453	AAWPVKATASDPGW ATASDPGWVR KATASDPGWVRG	0/37	
S859 / S474	FSDGDSA FSDGDSALQFGEL	S859 / S474	FSDGDSALQ FSDGDSALQFGEL	0/37	
S863 / S478	FSDGDSALQFGELSES	S863 / S478	FLKPRKAFSDGDSA	0/37	
T896* / T511*	DAPVDLTTSNEALSA			11/37	ES6
S897* / S512*	DAPVDLTTSNEALSAVDPS DAPVDLTTSNEALS DAPVDLTTSNEAL	S897 / S512	DAPVDLTTSNEALSAVDPS DAPVDLTTSNEALS	1/37	ES6
S902 / S517	DAPVDLTTSNEALSAVDPS	S902 / S517	DAPVDLTTSNEALSAVDPS	2/37	ES6
		S918 / S533	HSAQALIDR	0/37	ES6
S1010 / S625	RASDSAGLKQLVA RASDSAGLKQLV	S1010 / S625	RASDSAGLKQLVA RASDSAGLKQL	7/37	
		S1027* / S642*	DKKLSVTPPPKSAGL KLSVTPPPK	4/37	ES7
T1029 / T644	RWDKKLSVTPPPKSA DKKLSVTPPPKSAGL SVTPPPKSAGL SVTPPPKSA KLSVTPPPK LSVTPPPK	T1029* / T644*	RWDKKLSVTPPPKSAGL DKKLSVTPPPKSAGL SVTPPPKSAGL KKLSVTPPPK KLSVTPPPK SVTPPPKSA	11/37	ES7
Y1253# / Y868#	ALSLVYVVSQGR			0/37	
T1373# / T988#	VLQAGGAIVDQPTPEVVR			6/37	
S1440# / S1055#	NQTPLRDSASTKTTGG LNQTPLRDSASTKTTGGTK			0/37	

Red highlight: identified phosphorylation sites in peptide analysis;
*: ambiguously identified phosphorylation sites;
#: phosphorylation sites which only exist in ORF1a reading frame.

Table 3.2. Comparative analysis on intrinsically disordered regions between PLP2 domain and -2/-1 PRF site

	HVR approximate positions (positions in pp1a)	Positions of putative IDRs between PLP2 and -2/-1 PRF (positions in pp1a)				
		Pondr-FIT	**Pondr VL-XT**	**DISOPRED3**	**MobiDB 3.0**	**metaPrDOS**
PRRSV-1 nsp2 (SD01-08 strain)	HVR-2: 665aa-825aa	657aa-819aa	661aa-781aa	680aa-913aa	728-758aa	655aa-710aa 727aa-780aa 799aa-814aa 863aa-900aa
	HVR-3: 1010aa-1085aa	998aa-1077aa	998aa-1075aa	1005aa-1079aa	1031-1064aa	1003aa-1066aa
PRRSV-2 nsp2 (VR-2332 strain)	HVR-2: 843aa-993aa	752aa-1014aa	628aa-661aa 732aa-782aa 807aa-852aa 865aa-1028aa 1040aa-1052aa	683aa-739aa 815aa-1017aa	809aa-856aa 899aa-936aa 948aa-979aa	751aa-770aa 813aa-1013aa
	HVR-3: 1143aa-1213aa	1185aa-1222aa	1108aa-1227aa	1115aa-1205aa	1156aa-1221aa	1149aa-1213aa

Table 3.3. Primer and probe sequences for qRT-PCR detection of PRRSV genomic/subgenomic RNA

ID	Primer/probe sequence	Genomic locations	Application
Leader-F	5' TGTGTACTTTGGAGGCGTGG 3'	47nt-66nt	gRNA detection; reverse transcription (RT) primer for all minus-strand RNAs detection
gRNA-R	5' CATGCACCGGGAGAACGT 3'	231nt-248nt	gRNA detection; gRNA cDNA RT primer
5UTR-probe 1	5' CCTCCCGAGTATTTCCGGAGAGCACC 3'	168nt-193nt	gRNA detection
sgRNA2-F	5' GGAAGGACCTCCCGAGTATT 3'	161nt-180nt	sgRNA 2 detection
sgRNA2-R	5' CACTCCAAGTTTACGGCTCTC 3'	11724nt-11744nt	sgRNA 2 detection
sgRNA2-probe*	5' CTCCACCCKTAAACCCCGGCTGC 3'		sgRNA 2 detection
sgRNA6-F	5' GGAAGGACCTCCCGAGTATTT 3'	161nt-181nt	sgRNA 6 detection
sgRNA6-R	5' TTATCTAGGCCTCCCATTGCT 3'	14032nt-14052nt	sgRNA 6 detection
sgRNA6-probe*	5' TCCACCCYTCAACCCTTGACGAGAA 3'		sgRNA 6 detection
sgRNA7-F	5' AGTATTTCCGGAGAGCACCT 3'	175nt-194nt	sgRNA 7 detection
sgRNA7-R	5' GCACAGTTGATTGACTGGCT 3'	14608nt-14627nt	sgRNA 7 detection
sgRNA7-probe*#	5' CTTGACGAGGTTAAMGGGTGGAGATCC 3'		sgRNA 7 detection
END-R	5' AATTTCGGTCACATGGTTCC 3'	15028nt-15047nt	sgRNA2/6/7 cDNA RT primer

Chapter 4 - A naturally occurring recombinant enterovirus expresses a torovirus deubiquitinase

Abstract: Enteroviruses (EVs) are implicated in a wide range of diseases in humans and animals. In this study, a novel enterovirus (enterovirus species G [EVG]) (EVG 08/NC_USA/2015) was isolated from a diagnostic sample from a neonatal pig diarrhea case and identified by using metagenomics and complete genome sequencing. The viral genome shares 75.4% nucleotide identity with a prototypic EVG strain (PEV9 UKG/410/73). Remarkably, a 582-nucleotide insertion, flanked by $3C^{pro}$ cleavage sites at the 5′ and 3′ ends, was found in the 2C/3A junction region of the viral genome. This insertion encodes a predicted protease with 54 to 68% amino acid identity to torovirus (ToV) papain-like protease (PLP) (ToV-PLP). Structural homology modeling predicts that this protease adopts a fold and a catalytic site characteristic of minimal PLP catalytic domains. This structure is similar to those of core catalytic domains of the foot-and-mouth disease virus leader protease and coronavirus PLPs, which act as deubiquitinating and deISGylating (interferon [IFN]-stimulated gene 15 [ISG15]-removing) enzymes on host cell substrates. Importantly, the recombinant ToV-PLP protein derived from this novel enterovirus also showed strong deubiquitination and deISGylation activities and demonstrated the ability to suppress IFN-β expression. Using reverse genetics, we generated a ToV-PLP knockout recombinant virus. Compared to the wild-type virus, the ToV-PLP knockout mutant virus showed impaired growth and induced higher expression levels of innate immune genes in infected cells. These results suggest that ToV-PLP functions as an innate immune antagonist; enterovirus G may therefore gain fitness through the acquisition of ToV-PLP from a recombination event.

4.1. Introduction

Enteroviruses belong to order *Picornavirales*, family *Picornaviridae* (1). The EV genus includes viruses that infect humans (species A to D), bovines (species E and F), swine (species G), and nonhuman primates (species A, B, D, H, and J). Currently, EV species G (EVG) is divided into 11 types, EV-G1 to EV-G11 (2-4). Enteroviruses are small nonenveloped viruses that contain positive-strand RNA genomes of approximately 7,400 to 7,500 nucleotides (nt). Enteroviral genomes contain a single open reading frame (ORF), flanked by 5′ and 3′ untranslated regions (UTR) and a 3′ poly(A) tail. The relatively long 5′ UTR extends about 700 to 825 nt and contains secondary structural elements essential for RNA replication as well as an internal ribosomal entry site (IRES) for the initiation of translation. The 3′ UTR is considerably shorter, at 75 to 100 nt long, and contains complex cis-acting elements that are important for RNA replication (5). Genome translation generates a large polyprotein that is proteolytically processed into four structural proteins (VP1, VP2, VP3, and VP4) and seven nonstructural viral proteins ($2A^{pro}$, 2B, 2C, 3A, 3B, $3C^{pro}$ and $3D^{pol}$) (6-8).

Enteroviruses comprise a highly diverse group of viruses characterized by high mutation and recombination rates (9-13). Recombination is considered to be a major factor that drives viral evolution (14, 15). The majority of reported recombination events involve members of the same species. Recombination usually occurs in the nonstructural genome region, most frequently in the 2A-2C portion of the enterovirus genome (16, 17). Intratypic recombinants are produced about 100 times more often than intertypic recombinants (18). Genetic recombination between viruses from two different families/orders seems to occur much less frequently. However, in this study, we discovered a novel example of a cross-order recombinant in which an exogenous papain-like protease (PLP) gene of torovirus (order Nidovirales) naturally recombined into the

2C/3A junction of the genome of enterovirus G (order Picornavirales), generating a chimeric virus designated EVG 08/NC_USA/2015.

Torovirus belongs to the family Coronaviridae in the order Nidovirales. In previous studies, PLPs derived from nidoviruses have been reported to possess deubiquitination (DUB) activity, a mechanism to disrupt innate immune signaling and suppress host immune responses (19-29). Many key signaling proteins that regulate the expression of host cellular immune genes are dynamically modulated by protein posttranslational modifications. In particular, the covalent conjugation of ubiquitin (Ub) or Ub-like proteins, such as interferon (IFN)-stimulated gene 15 (ISG15), is a critical mechanism for the orchestration of appropriate innate immune responses (30-33). Ub conjugation (ubiquitination) and ISG15 conjugation (ISGylation) to cellular substrate proteins occur through similar mechanisms (33-35). Together with other posttranslational modifications, they fine-tune the activation, strength, and duration of the antiviral immune responses (30, 32, 33, 35-37). PLPs from several viral species of the *Nidovirales* function as deubiquitinases that cleave and remove Ub and Ub-like modifiers from host cell substrates (21, 24, 26, 27, 38, 39). Such PLPs possess general DUB activity toward cellular ubiquitin conjugates and also cleave the IFN-induced Ub homologue ISG15 (deISGylation) from cellular proteins.

In this study, we characterized the novel recombinant virus EVG 08/NC_USA/2015. We elucidated the DUB function of the EVG ToV-PLP protein and investigated its effect on host cell innate immune responses. Using reverse genetics, we generated a ToV-PLP knockout recombinant virus and analyzed its ability to induce innate immune responses in infected cells. Our study reveals a novel cross-order recombination event and provides new insights into enterovirus genome plasticity and its influence on viral pathogenesis.

4.2. Materials and Methods

Cells and viruses: ST, BHK-21, and HEK-293T cells were cultured in minimum essential medium (MEM) (Gibco, Carlsbad, CA) supplemented with 10% fetal bovine serum (Sigma-Aldrich, St. Louis, MO), antibiotics (100 U/ml of penicillin [Gibco, Carlsbad, CA] and 100 μg/ml of streptomycin [Gibco, Carlsbad, CA]), and 0.25 μg/ml amphotericin B (Fungizone; Gibco, Carlsbad, CA) at 37°C with 5% CO2. Infected ST or HEK-293T cells were maintained in 2% horse serum (HyClone, Logan, UT) at 37°C with 5% CO2.

The EVG-positive fecal sample was obtained from a piglet diarrhea case submitted to KSVDL in 2015. EVG was initially identified by metagenomics, and the virus was subsequently isolated after inoculation into ST cells. The isolated virus was plaque purified and designated EVG 08/NC_USA/2015. The recombinant viruses vEVG (cloned virus) and vPLP-KO (PLP knockout virus) were rescued from BHK-21 cells transfected with plasmid DNA of EVG full-length cDNA infectious clones. Rescued recombinant viruses were passaged on ST cells. For both parental and recombinant viruses, passage 2 viruses on ST cells were used for subsequent experiments. The SeV Cantell strain, cultured in embryonated chicken eggs, was used to stimulate type I IFN responses. As a control, PRRSV strain SD95-21 was used for the expression of the PRRSV-PLP2 domain (26, 27).

Sequence analysis: Fecal samples submitted to KSVDL were subjected to metagenomic sequencing as previously described (40). Sequence reads were mapped to the host Sus scrofa genome, and unmapped reads were assembled de novo by using CLC Genomics. Contigs were identified by BLASTN. A majority of the reads mapped to a 7,492-bp contig that contained a 6,561-bp open reading frame, which was incomplete at the 3′ end. The genome sequence was completed with GeneRacer (Invitrogen) and Sanger sequencing. The complete genome sequence

of EVG 08/NC_USA/2015 was aligned to those of representative members of the genus Enterovirus by using the ClustalW algorithm in MEGA 7.0. Phylogeny was inferred by using the maximum likelihood algorithm, using the best-fitting model with a gamma distribution. Tree topology was assessed by using 500 bootstrap replicates.

PLP structural analysis: Disorder prediction of the ToV-PLP sequence using GlobPlot (41) suggested that PLP is comprised primarily of a single core domain with less-ordered flanking regions. Homology modeling of EVG ToV-PLP was carried out by using I-TASSER (42) without explicit specification of any template models. Structural predictions of ToV-PLP input sequences were conducted with different boundaries in order to reduce the impact of disordered sequences at the N and C termini and to help define the core domain of the protease. The removal of ~10 N-terminal and ~20 C-terminal residues resulted in consistent predictions, with I-TASSER C scores of −0.8 to −0.9 and high structural homology to the leader protease of foot-and-mouth disease virus, with 23 to 24% sequence identity over ~87 to 89% coverage of the input sequences (43, 44). The majority of other structurally homologous templates identified by I-TASSER were eukaryotic ubiquitin-specific proteases/deubiquitinating enzymes (18 to 25% sequence identity over 78 to 94% coverage). The final structural model was further optimized, and its geometry was corrected by using ModRefiner (45). Structural figures were generated by using PyMOL (PyMOL Molecular Graphics System, version 1.7, Schrödinger, LLC).

Plasmids: The plasmid expressing ToV-PLP was constructed by RT-PCR amplification of the region spanning nt 5061 to 5642 of the EVG 08/NC_USA/2015 genome, while the plasmid expressing PRRSV-PLP2 was constructed by RT-PCR amplification of the region spanning nt 1340 to 2218 of the PRRSV SD95-21 genome (GenBank accession no. KC469618.1). For protein expression in mammalian cells, the PCR products were cloned into a eukaryotic

expression vector, pFLAG-CMV-24 (Sigma-Aldrich, St. Louis, MO), and designated pFLAG-ToV-PLP and pFLAG-PRRSV-PLP2, respectively. For protein expression in E. coli, the PCR products were cloned into the prokaryotic expression vector pDB-His-GST-TEV (46) to yield the plasmid pDB-His-GST-PLP. Specific mutations in the catalytic sites of the protease (C_{1449}/ H_{1557}/ D_{1572} to A_{1449}/ A_{1557}/ A_{1572}) were introduced by overlapping extension PCR as described previously (47), and the resulting plasmid is designated pDB-His-GST-PLP-C/H/D>A. Plasmid p3xFLAG-ISG15 for the expression of FLAG-tagged ISG15 was constructed as described previously (27), while plasmid pcDNA3.1(+)-HA-Ub for the expression of HA-tagged ubiquitin was provided by Domenico Tortorella (Mount Sinai School of Medicine, NY) (26).

Antibodies: MAb 115-5 (anti-VP1) and MAb 129-28 (anti-PLP) were generated by immunizing BALB/c mice with VP1 and PLP recombinant proteins, respectively. Detailed experimental procedures for MAb production were described previously (48, 49). The mAb #140-68 against PRRSV-PLP2 was produced in our previous study (50). The anti-FLAG M2 MAb (Sigma-Aldrich, St. Louis, MO) was used for the detection of Flag-tagged proteins. ISGylated cellular proteins were detected by anti-Flag M2 MAb (Sigma-Aldrich, St. Louis, MO) or anti-ISG15 MAb F-9 (Santa Cruz, Dallas, TX), while HA-Ub-conjugated cellular proteins were detected by anti-HA MAb 16B12 (Abcam, Cambridge, MA). Additionally, an anti-glyceraldehyde-3-phosphate dehydrogenase (GAPDH) polyclonal antibody (PAb) (Santa Cruz, Dallas, TX) was used to detect the expression of the GAPDH housekeeping gene.

Recombinant ToV-PLP expression and purification: His–glutathione S-transferase (GST)-tagged EVG ToV-PLP and its catalytic-site mutant were expressed in E. coli as previously described (51). Plasmid pDB-His-GST-PLP or pDB-His-GST-PLP-C/H/D>A was transformed into E. coli BL21(DE3) cells and cultured in 2× YT medium (Fisher Scientific, Pittsburgh, PA)

at 37°C. Recombinant protein expression was induced overnight at 25°C with 0.1 mM isopropyl-β-d-thiogalactopyranoside (IPTG). Recombinant proteins were purified with Ni-nitrilotriacetic acid (NTA) agarose (Qiagen, Valencia, CA) under native conditions according to the manufacturer's instructions. The protein concentration was determined by the absorbance at 280 nm.

Western blot: Western blotting was performed using the modified method described previously (47). Briefly, cells were lysed by using Pierce IP lysis buffer (Thermo Fisher Scientific, Carlsbad, CA) and then centrifuged at 12,000 rpm for 10 min to clean up cell debris. Cell lysates were mixed with 4× Laemmli sample buffer (Bio-Rad, Hercules, CA), denatured at 95°C for 10 min, and then separated by sodium dodecyl sulfate-polyacrylamide gel electrophoresis (SDS-PAGE). Proteins were then transferred onto a nitrocellulose membrane (GE Healthcare Bio-Sciences, Pittsburgh, PA). The membrane was blocked with 5% nonfat milk in PBST (phosphate-buffered saline [PBS] supplemented with 0.05% Tween 20) at room temperature (RT) for 1 h, followed by incubation with the appropriate primary antibody at RT for 1 h. After three washes with PBST, the membrane was incubated with IRDye 800CW goat anti-mouse IgG(H+L) and/or IRDye 680RD goat anti-rabbit IgG(H+L) (Li-Cor Biosciences, Lincoln, NE) for another 45 min at RT. Specific protein bands were visualized by using an Odyssey Fc imaging system (Li-Cor Biosciences, Lincoln, NE).

Deubiquitination assays: To determine the DUB activity of ToV-PLP in an in vitro expression system, HEK-293T cells were cotransfected with 0.5 μg plasmid DNA of pcDNA3.1(+)-HA-Ub with 0.5 μg pFLAG-ToV-PLP, pFLAG-PRRSV-PLP2, or its catalytic-site mutant. Cells cotransfected with plasmid DNA of pcDNA3.1(+)-HA-Ub and the empty vector were used as positive controls, while cells transfected with 1 μg plasmid DNA of the empty vector only were

used as negative controls. At 36 h posttransfection, cell lysates were harvested and subjected to Western blot analysis. The Ub-conjugated host cellular proteins were detected by using anti-HA MAb. The expression of ToV-PLP and PRRSV-PLP2 was detected by using an anti-FLAG M2 MAb. The expression of the housekeeping gene GAPDH was detected by a PAb as a loading control.

To determine the DUB activity of ToV-PLP in the context of viral infection, HEK-293T cells were initially transfected with 0.5 μg plasmid DNA of pcDNA3.1-HA-Ub or the empty plasmid vector as the control. After 24 h posttransfection, cells were infected with wild-type EVG 08/NC_USA/2015, the cloned virus vEVG, or the ToV-PLP knockout recombinant virus at a multiplicity of infection (MOI) of 3 (see below for the construction of recombinant EVG mutants). After 10 hpi, host protein ubiquitination was detected by Western blotting as described above, while the expression of ToV-PLP was detected by anti-PLP MAb 129-28.

Poly-ubiquitin chain cleavage activity of the ToV-PLP was determined in cell free condition as described previously (28, 52, 53). Briefly, 2.5 μg of K48-, K63-, or M1-linked polyubiquitin chains (Boston Biochem, Cambridge, MA) was incubated with serial dilutions (1 μg, 0.5 μg, and 0.25 μg) of purified recombinant GST-PLP or its catalytic-site mutant (GST-PLP C/H/D>A) in a final volume of 10 μl assay buffer (50 mM Tris, 5 mM $MgCl_2$, 2 mM dithiothreitol [DTT] [pH 7.5]) for 2 h at 37°C. The reaction was terminated with 4× loading buffer (Bio-Rad, Hercules, CA) at 37°C for 20 min. Cleavage products were separated by SDS-PAGE and visualized by Coomassie brilliant blue staining.

DeISGylation assays: To investigate the deISGylation activity of ToV-PLP in an in vitro expression system, HEK-293T cells cultured in 24-well plates were transfected with 0.5 μg of plasmid DNA expressing ToV-PLP or PRRSV-PLP2, together with 0.15 μg of pCAGGS-HA-

UbE1L (E1), 0.1 μg of p3xFLAG-UbcH8 (E2), 0.25 μg of pcDNA-TAP-HA-HERC5 (E3), and 0.25 μg of p3xFLAG-ISG15 plasmid DNAs. Cells transfected with plasmid DNA of the empty vector were used as a control. At 36 h posttransfection, cell lysates were harvested and subjected to Western blot analysis. The ISG15-conjugated host cellular proteins were detected by using anti-ISG15 MAb F-9. The expression of ToV-PLP and PRRSV-PLP2 was detected by MAb 129-28 and MAb 140-68, respectively. The expression of GAPDH was detected by a specific PAb as a loading control.

To determine the deISGylation activity of ToV-PLP in the context of viral infection, HEK-293T cells were initially transfected with plasmid DNAs of ISGylation machinery (0.15 μg of pCAGGS-HA-UbE1L [E1], 0.1 μg of p3xFLAG-UbcH8 [E2], 0.25 μg of pcDNA-TAP-HA-HERC5 [E3], and 0.25 μg of p3xFLAG-ISG15). Cells transfected with plasmid DNA of the empty vector were used as a control. After 24 h posttransfection, cells were infected with wild-type EVG 08/NC_USA/2015, the cloned virus vEVG, or the vPLP-KO mutant at an MOI of 3 (see below for the construction of recombinant EVG mutants). At 48 hpi, cell lysates were harvested and subjected to Western blot analysis. Anti-Flag M2 MAb was used to visualize ISGylated host proteins, while the expression of ToV-PLP was detected by MAb 129-28.

ToV-PLP cleavage activity toward ISG15 precursor (proISG15) substrate was determined using a cell free assay as described previously (22, 52). Briefly, 2.5 μg of the proISG15 (Boston Biochem, Cambridge, MA) substrate was mixed with 40 nM purified recombinant GST-PLP or GST-PLP C/H/D>A in a final volume of 10 μl assay buffer and incubated at 37°C. The catalytic reaction was stopped at different time points (1 min, 2 min, 5 min, and 10 min) by the addition of 3.5 μl of 4× Laemmli sample buffer (Bio-Rad, Hercules, CA), and the mixture was incubated at 37°C for 20 min. Proteins were separated in an SDS-

polyacrylamide gradient gel (Thermo Fisher Scientific, Carlsbad, CA) and stained with Coomassie brilliant blue.

Luciferase assay: HEK-293T cells (0.5×10^5 cells/ml) seeded into 24-well plates were cotransfected with 1 μg plasmid DNA expressing a PLP (ToV-PLP, PRRSV-PLP2, or their corresponding mutants), 0.5 μg firefly luciferase reporter plasmid p125-Luc, and 30 ng Renilla luciferase expression plasmid pRL-SV40. Cells transfected with the empty plasmid vector and p125-Luc/pRL-SV40 were used as the control. Transfection was performed by using Lipofectamine 3000 reagent (Invitrogen, Carlsbad, CA) according to the manufacturer's instructions. At 24 h posttransfection, cells were mock treated or stimulated with SeV at 100 hemagglutination (HA) units/ml for 16 h. Subsequently, cells were lysed and analyzed for reporter gene expression by using a dual-luciferase reporter system (Promega, Madison, WI) according to the manufacturer's instructions. Firefly and Renilla luciferase activities were measured by using a FLUOstar Omega microplate reader (BMG Labtech, Cary, NC). The relative luciferase activity value for each sample was defined as the ratio of firefly luciferase activity to Renilla luciferase activity.

Real-time RT-PCR for detection of innate immune gene expression: Cell lysates collected from virus-infected cells or plasmid DNA-transfected cells were used for analysis of immune gene expression. Cellular total RNA was extracted by using an SV Total RNA isolation kit (Promega, Madison, WI) according to the manufacturer's instructions. First-strand cDNA was generated with a SuperScript VILO cDNA synthesis kit (Thermo Fisher Scientific, Carlsbad, CA). PCR was prepared with TaqMan Fast Advanced master mix (Thermo Fisher Scientific, Carlsbad, CA) and specific primer and probe sets for IFNA1, IFNB1, IL28B, IL29, IRF7, and ISG15 (Thermo Fisher Scientific, Carlsbad, CA). The housekeeping gene GAPDH was used as

an internal control for PCR in ST cells, while the TBP (TATA box-binding protein) housekeeping gene was used as an internal control for PCR in HEK-293T cells. Reactions were performed on a CFX96 real-time PCR system (Bio-Rad, Hercules, CA). Relative quantification of target gene expression was performed by using cycle threshold (CT) values (54), and the results for each treatment were compared with the value for the control culture. Mean values were obtained from three repeated experiments.

Construction of full-length cDNA clones of EVG 08/NC_USA/2015: The full-length genome sequence of purified virus was obtained by next-generation sequencing. The 3′-terminal genomic sequences were determined by using a GeneRacer core kit (Invitrogen, Carlsbad, CA). The strategy for the construction of the full-length cDNA clone is illustrated in Fig. 6. The pACYC177 vector containing a CMV promoter was generated by inserting the CMV sequence into the SphI and XbaI restriction enzyme sites, two viral genomic fragments were amplified with Phusion High-Fidelity DNA polymerase (New England BioLabs, Ipswich, MA), and the hepatitis delta virus (HDV) ribozyme element was synthesized by Integrated DNA Technologies (Coralville, IA) (47). The assembly of these DNA fragments was performed by using a NEBuilder HiFi DNA Assembly cloning kit (New England BioLabs, Ipswich, MA). To construct the PLP knockout mutant, the upstream and downstream regions of PLP were amplified and assembled by using a NEBuilder HiFi DNA Assembly cloning kit.

Recovery of recombinant viruses from full-length cDNA infectious clones: BHK-21 cells seeded into 6-well plate were transfected with the full-length cDNA infectious clone of the wild-type virus or its mutant. Transfection was conducted by using Lipofectamine 3000 reagent (Invitrogen, Carlsbad, CA) according to the manufacturer's instructions. At 48 h posttransfection, the cell culture supernatant was transferred to ST cells. After another 48 h of incubation, the cell

culture supernatant was harvested from ST cells, and cells were fixed with 4% paraformaldehyde (pH 7.2) for 15 min. Fixed cells were permeabilized with 0.5% Triton X-100 in PBS for 10 min and then blocked with 1% bovine serum albumin (BSA) in PBS for 30 min. Cells were then incubated with the primary anti-VP1 MAb or anti-PLP MAb for 1 h at 37°C. Alexa Fluor 488 AffiniPure donkey anti-mouse IgG(H+L) (Jackson Immuno Research, West Grove, PA) was used as the secondary antibody. The cell nucleus was stained with 4′,6-diamidino-2-phenylindole (DAPI) (Thermo Fisher Scientific, Carlsbad, CA). Immunofluorescent signals were visualized with the Evos FL cell imaging system (Thermo Fisher Scientific, Carlsbad, CA).

***In vitro* growth characterization of recombinant viruses:** Passage 2 of recombinant viruses in ST cells was used to characterize in vitro growth properties. Confluent ST cells were inoculated with the recombinant virus at an MOI of 0.01. The cell culture supernatant was serially harvested at 0, 2, 4, 6, 8, 10, and 12 hpi. The virus titer was measured by a microtitration assay using ST cells in 96-well plates and calculated as FFU per milliliter by using a method described previously (26).

Statistical analysis: All the data are shown as mean values with standard deviations and were evaluated by one-way analysis of variance (ANOVA) followed by Tukey's post hoc test using programs in GraphPad Prism 6 (GraphPad, La Jolla, CA). Significant differences are indicated by asterisks in the figure legends.

Accession number: The genome sequence of EVG 08/NC_USA/2015 determined in this study was submitted to GenBank under accession no. KY761948.

4.3. Results

Identification of a naturally occurring recombinant virus EVG 08/NC_USA/2015

In 2015, fecal samples from neonatal pigs with diarrhea symptoms were submitted to the Kansas State Veterinary Diagnostic Laboratory (KSVDL) for diagnostic testing. Inoculation of a 0.2-μm filtered fecal slurry onto a monolayer of swine testicular (ST) cells yielded cytopathic effects in ~48 h. By using metagenomic sequencing, a novel enterovirus G genome was assembled, which contained an ~600-nt foreign gene insertion within the 2C/3A region. We observed a mixed population of foreign gene insertions by next-generation sequencing (NGS) analysis, in which two different lengths, 582 nt and 648 nt, were observed. In comparison to the 582-nt foreign gene sequence, the 648-nt insertion contains an additional 66 nt at the C terminus (data not shown). BLAST search results showed that this 66-nt sequence has little or no homology to any other sequences in GenBank. This virus was subsequently purified by using a plaque assay. Nine large plaques were selected for sequencing analysis of the foreign gene insertion region. The recombinant viruses obtained from these 9 plaques contained only the 582-nt insertion, which was determined to be stable in 10 passages in ST cells. We also directly passaged the original sample (without plaque purification) on ST cells for 10 passages and sequenced the foreign gene insertion region. Quantitative reverse transcription-PCR (RT-PCR) and sequencing results showed that about 60% of the population contained the 648-nt insertion and that about 40% of the population contained the 582-nt insertion at passage 2. However, only about 20% of the population contained the 648-nt insertion at passage 3, while no 648-nt insertion was detected at passage 4 (data not shown). These results indicate that the C-terminal 66 nt of the 648-nt insertion is not stable and may be lost through adaptation of the recombinant virus in the host cells.

One of the largest plaques, EVG 08/NC_USA/2015, was isolated for complete genome characterization. The full-length genome of EVG 08/NC_USA/2015 is 7,981 nt long, excluding

the poly(A) tail. A long ORF of 7,098 nt, encoding a 2,365-amino-acid (aa) polyprotein precursor, is flanked by an 812-nt 5′ UTR and a 71-nt 3′ UTR. The P1, P2, and P3 regions of EVG 08/NC_USA/2015 contain 2,514 nt (838 aa), 1,734 nt (538 aa), and 2,265 nt (755 aa), respectively (Fig. 1). The full-length genome sequences of EVG 08/NC_USA/2015 show 75.4% nucleotide identity to the sequence of prototypic EVG strain PEV9 UKG/410/73 (GenBank accession no. Y14459.1) (Table 1). Phylogenetic analysis shows that the novel recombinant virus EVG 08/NC_USA/2015 is most closely related to a group of EVGs detected in 2012 in pigs in the ThanhBinh and CaoLanh areas of Vietnam (Fig. 2).

Full-length genome sequencing of EVG 08/NC_USA/2015 identified a 582-nt-long foreign gene insertion at the 2C/3A junction of the enterovirus genome (Fig. 1). BLAST search results showed that this foreign gene is most homologous to the PLP gene located in the nsp3-like region of the torovirus genome (54 to 68% amino acid identity). Phylogenetic analysis further showed that this foreign PLP forms a well-supported clade with PLPs of other toroviruses, including bovine, porcine, and equine toroviruses (Fig. 3) (55, 56). We designated this foreign gene ToV-PLP. In the genome of EVG 08/NC_USA/2015, the recombinant ToV-PLP gene is flanked by two predicted $3C^{pro}$ cleavage sites, ALFQ|GPPVFR and AEFQ|GPPTFK, at its 5′ and 3′ ends, respectively (Fig. 1). This suggests that ToV-PLP may be cleaved at both ends, minimizing its potential influence on proteolytic processing and maturation of enteroviral 2C and 3A proteins.

Recombinant EVG ToV-PLP functions as a deubiquitinase and deISGylase to suppress host cell innate immune responses

To obtain insights into potential functions of ToV-PLP within the context of EVG 08/NC_USA/2015, we explored the structural homology between this PLP and other viral

proteases. Iterative modeling using I-TASSER (42) pinpointed sequence and structural similarities between EVG ToV-PLP and the leader protease of foot-and-mouth disease virus (FMDV-L^{pro}) (Fig. 4 and 5), although EVG ToV-PLP and FMDV-L^{pro} have limited homology at the sequence level (24.3% amino acid identity) (Fig. 3). A previous study pointed out sequence similarities between FMDV-L^{pro} and another toroviral PLP, that of Breda-1 bovine torovirus (57). Like the FMDV-L^{pro}, EVG ToV-PLP appears to adopt a minimal papain-like fold with a characteristic arrangement of its Cys-His-Asp catalytic triad (43, 44). The Cys residue is located near the N-terminal cap of the first helix of the primarily helical N-terminal subdomain of the core domain, while the His and Asp residues are located near each other within the beta-stranded subdomain in the C-terminal half of the core domain (Fig. 5). EVG ToV-PLP also exhibits structural homology to portions of the catalytic domains of several eukaryotic deubiquitinating enzymes and ubiquitin proteases, including USP2, USP4, USP14, USP18, and USP46. Furthermore, ToV-PLP exhibits various levels of sequence and structural homology to the N- and C-terminal subdomains of severe acute respiratory syndrome coronavirus (SARS-CoV) and Middle East respiratory syndrome CoV (MERS-CoV) PLPs, which are similar to those of mammalian deubiquitinating enzymes (Fig. 4 and 5). A major distinction is that the minimal protease domains of ToV-PLP (and FMDV-L^{pro}) lack the primarily β-stranded "finger domains" that bridge the N- and C-terminal subdomains, e.g., "thumb and palm domains," in the catalytic folds of coronaviral proteases and eukaryotic deubiquitinases (58). Moreover, the EVG ToV-PLP and FMDV-L^{pro} are structurally distinct from the PLPs/Otubain-like deubiquitinases of selected nidoviruses and arteriviruses. The latter deubiquitinases also utilize Cys-His-Asp/Asn catalytic triads but have different catalytic residue arrangements and overall topologies (38). Intriguingly, FMDV-L^{pro} possesses de-ubiquitinating activity against innate immune signaling

components, including RIG-I, TRAF6 and TBK1 (59). PLPs from the SARS and MERS coronaviruses also possess DUB as well as deISGylating (ISG15-removing) activities (21, 25, 60, 61).

To determine whether the torovirus-derived PLP domain of EVG 08/NC_USA/2015 also possesses DUB and/or deISGylation activities, we carried out cell-based DUB and deISGylation assays. HEK-293T cells were transfected with a plasmid expressing hemagglutinin (HA)-tagged ubiquitin (HA-Ub) and a plasmid expressing wild-type ToV-PLP or a catalytic-site mutant of ToV-PLP (mutations introduced into the putative catalytic triad, - C_{1449}/ H_{1557}/ D_{1572} to A_{1449}/ A_{1557}/ A_{1572}). An empty plasmid vector and a plasmid expressing the PLP2 domain of porcine reproductive and respiratory syndrome virus (PRRSV) were used as controls (26, 27). The expression of each PLP and HA-Ub in transfected cells was confirmed by Western blotting (Fig. 6A, bottom). In comparison to cells transfected with the empty plasmid, the expression of wild-type PLP from either ToV or PRRSV reduced the levels of ubiquitin-conjugated proteins (Fig. 6A, top, compare lanes 2 and 4 with lane 6), indicating that EVG ToV-PLP antagonizes the ubiquitination process of host cellular proteins. As we expected, the DUB activities of both ToV-PLP and PRRSV-PLP2 were abolished by mutations of the putative catalytic-triad residues. Next, we investigated the effect of ToV-PLP expression on host protein ISGylation. ISG15 conjugates were generated by transfecting HEK-293T cells with plasmids that express Flag-tagged ISG15 and ISG15-specific E1, E2, and E3 enzymes. Cells were cotransfected with the ToV-PLP expression vector. Once more, we used PRRSV-PLP2, which also possesses deISGylating activity, as a positive control (27). Co-expression of wild-type PLPs resulted in a clear decrease in the levels of ISGylated proteins (Fig. 6B; compare lanes 2 and 4 with lane 6).

The deISGylation activities of the PLPs were abolished by mutations of the putative catalytic residues. This result confirmed that the ToV-PLP domain possesses deISGylation activity.

To further verify that the ToV-PLP domain directly targets the conjugation of the polyubiquitin chain, we carried out *in vitro* ubiquitin deconjugation assays using recombinant ToV-PLP purified from *Escherichia coli.* K48-, K63-, or M1 (linear)-linked polyubiquitin chains were incubated with serial dilutions of recombinant PLPs (Fig. 6C to E). Both K48- and K63-linked polyubiquitin substrates are efficiently cleaved to monomeric ubiquitin by recombinant ToV-PLP. Interestingly, ToV-PLP also cleaves linear polyubiquitin (M1), a modification involved in NF-κB activation, among other innate immune pathways (31). In contrast, the polyubiquitin cleavage activity was totally abolished by mutations of the putative catalytic triad (Fig. 6C, D and E).

To confirm the deISGylation activity of this recombinant PLP, we carried out an in vitro proteolytic assay using an ISG15 precursor (proISG15) as a cleavage substrate (22, 52). Reactions were terminated at specific time points through the time course of the assay. Wild-type ToV-PLP cleaves the majority of proISG15 into mature forms in 10 min (Fig. 6F). In contrast, a ToV-PLP mutant that contains mutations in the putative catalytic triad exhibits no deISGylation activity (Fig. 6F).

Since ubiquitination affects innate immune gene signaling pathways (35-37), we investigated whether ToV-PLP also influences innate immune gene expression in a host cell context. We first carried out luciferase reporter assays using a luciferase reporter plasmid (p125-Luc) that expresses firefly luciferase under the control of the IFN-β promoter. HEK-293T cells were cotransfected with plasmids that express wild-type or mutant ToV-PLP, p125-Luc, and Renilla luciferase (pRL-SV40) to normalize the expression levels of the samples. As a positive

control, we cotransfected cells with the reporter plasmid along with a plasmid containing the nidoviral Otubain-like deubiquitinase PRRSV-PLP2. At 24 h posttransfection, cells were infected with Sendai virus (SeV) to induce luciferase production. As we expected, the expression of PRRSV-PLP2 significantly inhibited luciferase gene expression. In contrast, a strong reporter signal was observed in cells transfected with the empty plasmid after SeV infection. Cells expressing ToV-PLP exhibited a 12-fold reduction of the IFN-β promoter-driven luciferase reporter signal (Fig. 7A). Quantitative RT-PCR results also showed that the IFN-β mRNA expression level was significantly decreased by 3-fold in ToV-PLP-transfected cells (Fig. 7B), while mutations introduced into catalytic sites of the protease increased reporter gene and IFN-β mRNA expression levels (Fig. 7A and B). These data indicate that the ToV-PLP protein may function as an innate immune antagonist through its DUB/deISGylation activities.

Growth of ToV-PLP knockout recombinant enterovirus is attenuated in cell culture

To explore the potential contribution of torovirus PLP recombination to the growth and fitness of enterovirus, we generated a full-length cDNA infectious clone of EVG 08/NC_USA/2015 (pEVG) (Fig. 8A). The pEVG construct contains a cytomegalovirus (CMV) promoter at the 5′ terminus of the viral genome, the 7,981-nucleotide full-length genome of EVG 08/NC_USA/2015, and a 20-nt poly(A) tail incorporated at the 3′ end of the genome (Fig. 8A). Compared to the genome sequence of the parental virus, the DNA sequence of pEVG contained 3-nt differences at the following genome positions: T_{14}, G_{2029}, and A_{7724}. The T_{14} to C mutation is located within the 5'-UTR region, the A_{7724} to G mutation is a synonymous mutation, and the G_{2029} to T mutation changed the amino acid sequence from glycine to valine. To rescue the cloned virus, plasmid DNA of pEVG was transfected into BHK-21 cells, and the cell culture supernatant from the transfected cells was passaged onto ST cells at 48 h posttransfection. At 18

h postinfection (hpi), infected ST cells were stained by using PLP and VP1 protein-specific monoclonal antibodies (MAbs) (Fig. 8C). These results indicate that viable cloned virus (vEVG) was recovered from the full-length cDNA infectious clone pEVG. Sequence analysis confirmed that vEVG genome contains C_{14}, T_{2029}, and G_{7724} mutations, which differentiate vEVG from wild type virus EVG 16-08.

By using the pEVG infectious clone, a PLP gene knockout mutant (vPLP-KO) was generated (Fig. 8B). Growth kinetics of the parental virus EVG 08/NC_USA/2015, the cloned virus (vEVG), and the PLP knockout mutant (vPLP-KO) were compared. Cells were infected with each of the viruses and harvested at 0, 2, 4, 6, 8, 10, and 12 hpi. These results showed that vEVG exhibits growth kinetics similar to those of the parental virus EVG 08/NC_USA/2015 (Fig. 9). Both the parental virus and the cloned virus reached titers of $10^{3.2}$ FFU/ml and $10^{3.4}$ FFU/ml at 12 hpi, respectively. In contrast, vPLP-KO was impaired in growth in ST cells, with an ~1-log-lower virus titer at 12 hpi (Fig. 9).

The ToV-PLP knock out recombinant enterovirus showed a reduced ability to inhibit innate immune gene expression in infected cells

To determine whether the knockout of ToV-PLP affects the innate immune suppression ability of the virus, we analyzed DUB and deISGylation activities of wild-type and mutant ToV-PLP knockout viruses. Compared to uninfected cells (Fig. 10A, lane 3), the amount of Ub-conjugated proteins was decreased by about 95% in both EVG 08/NC_USA/2015- and vEVG-infected cells (Fig. 10A, lanes 4 and 5). In contrast, levels of Ub-conjugated proteins were elevated 8.7-fold in vPLP-KO-infected cells, compared to cells infected with the cloned virus vEVG (Fig. 10A, lanes 5 and 6). In addition, the amount of ISG15-conjugated proteins in cells infected with vPLP-KO was elevated 47-fold compared to that in cells infected with EVG

08/NC_USA/2015 or vEVG (Fig. 10B, lanes 4 to 6). We observed no significant difference in the DUB/deISGylation abilities of parental and cloned viruses; similar levels of Ub/ISG15-conjugated host proteins were detected in cells infected with EVG 08/NC_USA/2015 and vEVG (Fig. 10).

To extend these observations, we investigated the effect of the PLP knockout on innate immune gene expression in infected cells. ST cells were infected with EVG 08/NC_USA/2015, vEVG, or vPLP-KO, and innate immune gene expression was analyzed at 10 hpi. As expected, similar levels of IFN-β, interleukin-28B (IL-28B), and ISG15 expression were observed in cells infected with EVG 08/NC_USA/2015 and vEVG. In comparison to those in vEVG-infected cells, there were 6.6-, 5.3-, and 4.1-fold increased expression levels of type I IFN (IFN-β), type III IFN (IL-28B), and ISG15 in vPLP-KO-infected cells, respectively (Fig. 11A to C). To confirm this result, we further tested innate immune gene expression levels in infected cells stimulated by SeV. EVG 08/NC_USA/2015-, vEVG-, or vPLP-KO-infected cells were stimulated with SeV at 6 hpi. An extended panel of innate immune gene expression was analyzed at 4 h poststimulation. The results consistently showed that EVG 08/NC_USA/2015 and vEVG largely suppressed the expression of both type I interferons (Fig. 11D and E) and type III interferons (Fig. 11F and G) as well as the expression of the selected ISGs IFN regulatory factor 7 (IRF7) (Fig. 11H) and ISG15 (Fig. 11I) to similar levels. In contrast, vPLP-KO exhibited a reduced ability to antagonize the expression of SeV-induced innate immune genes. mRNA expression levels of the type I interferons IFN-α1 and IFN-β were increased by 4-fold and 13-fold, respectively (Fig. 11D and E), in vPLP-KO-infected cells compared to vEVG-infected cells. Similarly, IL-29 and IL-28B expression levels were increased by 8.3- and 12.7-fold, respectively (Fig. 11F and G) in vPLP-KO-infected cells compared to vEVG-infected cells. In

addition, we also observed increased expression levels of ISGs, including IRF7 (7.4-fold increase) and ISG15 (17.9-fold increase), in vPLP-KO-infected cells (Fig. 11H and I).

4.4. Discussion

Recombination events potentially exert a major influence on multiple aspects of viral evolution and pathogenesis, including the emergence of new virus variants, changes of host ranges and tissue tropism, increases in virulence, evasion of host immunity, and resistance to antivirals (14, 15, 62). Enteroviruses are known for their high recombination rates, and recombination has been reported to contribute significantly to enteroviral genetic diversity (9-12). This is well illustrated by the example of a prototypic human enterovirus, poliovirus (PV). The discovery of PV recombination may date as far back as the 1960s (63). The widely used oral poliovirus vaccine (OPV) contains a cocktail of three attenuated serotypes, which facilitates intratypic recombination (64, 65). Recombinant PV can be easily detected in both healthy vaccinees and vaccine-associated paralytic poliomyelitis patients (64-68). The intertypic recombination of PV with human enterovirus C (HEV-C) species also appears to occur under natural conditions (16, 17, 64, 69). Furthermore, the highly recombinogenic nature of PV was associated with the emergence of pathogenic vaccine-derived viruses during the global polio eradication campaign (10-12). Recombination within animal species of simian, swine, and bovine enteroviruses has also been documented (70-72). A typical example is the emergence of swine vesicular disease virus (SVDV), which is genetically closely linked to coxsackievirus B5 (CV-B5). Their close phylogenetic relationship suggests that SVDV may have arisen from CV-B5 by recombination (73, 74). To our knowledge, all enterovirus recombinants that have been reported so far arose through recombination events within a species or genus. Our present study identified a unique cross-order recombination event between viruses of the orders *Nidovirale*

(torovirus) and *Picornavirales* (enterovirus). Considering the strikingly different genome organizations and protein expression and processing mechanisms of viruses of these two orders, it is intriguing to understand how this rare recombination event occurred. Moreover, it is also important to understand how the enteroviral genome backbone was modified to overcome potential nucleotide- and protein-level incompatibilities in order to allow the insertion of the heterologous gene. Proposed factors that control the occurrence of recombination include local sequence homology, RNA secondary structural elements, coinfection, subcellular colocalization, and/or coreplication of the parental viruses in the same host (15, 62). At the PLP gene insertion site, the 2C/3A cleavage junction, the original 3C protease cleavage site was duplicated and flanks both the 5′ and 3′ ends of the PLP-coding sequence. This suggests that the "foreign" PLP may be cleaved off from the enterovirus polyprotein, thereby avoiding a disruption of the proteolytic processing of the polyprotein and preserving the functions of other enterovirus proteins. Such a recombination event may have occurred within a host animal that was simultaneously infected with enterovirus and torovirus. Notably, enterovirus and torovirus are frequently detected in swine hosts, and more importantly, both viruses are associated with enteric infection (2, 4, 72, 75-85). Our metagenomic sequencing uncovered no ToV-derived genetic material other than the ToV-PLP sequence in the sample from which we isolated EVG 08/NC_USA/2015. This suggests that the recombination event occurred prior to infection of the particular piglet from which the sample was obtained. Phylogenetic analysis shows that this novel virus is most closely related to EVGs detected in pigs from the ThanhBinh and CaoLanh areas of Vietnam in 2012. However, the viruses isolated from these Vietnamese pigs were not reported to contain the ToV-PLP gene insertion. The origin of this novel recombinant virus therefore needs to be explored further in the future.

We determined that the 582-nt ToV-PLP gene segment inserted into the enterovirus genome encodes an enzyme with deubiquitinase activity. Structural homology modeling and sequence analysis suggest that ToV-PLP may be grouped along with the leader proteases of FMDV and, potentially, ERAV (equine rhinitis A virus) into a novel class of structurally minimal PLPs with deubiquitinating and deISGylating activities (57, 59). The catalytic domains of these PLPs assume folds similar to the core papain fold, with few or no substantial added domains and relatively short loops connecting the main structural elements (86). This is intriguing given that toroviruses belong to the *Coronaviridae*, while FMDV and ERAV are members of the *Picornaviridae*. Notably, PLPs from coronaviruses other than toroviruses are substantially larger. Moreover, ToV-PLP and FMDV-L^{pro} do not contain the finger subdomain characteristic of other coronaviral PLPs/deubiquitinating enzymes.

The minimal nature of the ToV-PLP and FMDV-L^{pro} folds suggests that they may have descended from an ancestral papain-like fold that gained deubiquitination function. It is unclear whether this gain of function occurred separately in the *Coronaviridae* and *Picornaviridae* or represents a holdover from a more ancestral virus. It is noteworthy that the FMDV-L^{pro}, in its capacity as a protease, recognizes basic motifs that also contain glycines/serines. In particular, FMDV-L^{pro} cleaves between a basic residue and glycine, with a strong preference for Leucine at the P2 position (86). Such motifs are present not only in the FMDV viral polyprotein that is cleaved by the protease (87), but also in several host cell targets, including eukaryotic initiation factor 4G (eIF4G) and the IRES-binding protein Gemin5. Cleavage of these targets suppresses host cell protein synthesis and promotes the translation of viral gene products (88-90). In contrast, larger coronaviral PLPs, such as SARS-CoV PLP, recognize LXGG motifs specifically (91, 92); thus, the targets of their classical protease activity and deubiquitinating/deISGylating

activity are equivalent, as ubiquitin and ISG15 terminate in RLRGG sequences. It is unclear whether ToV-PLP possesses protease sequence specificity similar to that of FMDV-Lpro. However, ToV-PLP may also potentiate viral replication and pathogenesis by acting on host translation factors or on antiviral pathways other than innate immunity.

Interestingly, ToV-PLP and FMDV-L^{pro}, but not PLpro of SARS-CoV and related CoVs, contain additional acidic residues located immediately C terminal to the catalytic Asp residues. These acidic motifs form a loop proximal to the catalytic triad and may help to establish proteolytic sequence specificity in these minimal PLPs. However, proteolytic target sequences may bind to the ToV-PLP and FMDV-L^{pro} active sites in a different manner than the extended, flexible C-terminal sequences of ubiquitin/ISG15 that are also cleaved by these enzymes.

In SARS-CoV PLpro and related coronaviral PLPs, the principal binding sites for the globular portions of ubiquitin and ISG15 are located at an interface between the finger and C-terminal (palm) subdomains (93). A second, distal site is formed primarily by residues on the N-terminal thumb subdomain, which are also not present in FMDV-L^{pro} and ToV-PLP. From the principal binding site, the flexible C-terminal tail of ubiquitin extends into the catalytic site, stabilized by an extensive hydrogen-bonding network with residues near the catalytic triad (93). The ubiquitin/ISG15 C termini may follow a path to the active site of ToV-PLP and FMDV-L^{pro} similar to that of SARS-CoV PLpro. However, it is not yet clear exactly where the principal and/or secondary binding surfaces for the globular domains of polyubiquitin and ISG15 are located on the minimal catalytic domains of ToV-PLP and FMDV-L^{pro}. Structural elucidation of complexes of these enzymes with ubiquitin and ISG15 is required to answer this question and to clarify the nature of polyubiquitin chain specificity and substrate preferences for these viral proteases.

Ubiquitination and ISGylation play important roles in regulation of host antiviral immune responses (30-35). In previous studies, PLPs of nidoviruses were shown to disrupt innate immune signaling pathways through their deubiquitination/deISGylation activities, which have been proposed to be associated with viral pathogenicity (24, 44, 77, 80-82). In our study, the novel ToV-PLP robustly disassembles both K48- and K63-linked polyubiquitins as well as linear polyubiquitin. These polyubiquitins are the primary ubiquitin species that regulate specific innate immune signaling pathways. ToV-PLP overexpression in cell culture also reduced the levels of ISG15-conjugated cellular proteins, and we further confirmed its deISGylation activity using *in vitro* assays. The biological significance of these DUB and deISGylation activities was further supported by the fact that ToV-PLP is able to inhibit the mRNA expression of IFN-β. When we introduced a targeted deletion to knock out ToV-PLP expression, a recombinant mutant virus was rescued in cell culture, suggesting that ToV-PLP is not absolutely essential for viral replication. However, these mutants exhibited reduced DUB/deISGylation activity and enhanced the expression levels of representative innate immune genes in infected swine cells.

Like most enteroviral infections, EVG infection is generally considered to be asymptomatic, with limited evidence to support its association with clinical diseases (72, 83, 84, 94). However, in the present study, this unique enterovirus strain (EVG 08/NC_USA/2015) was isolated from a fecal sample of a piglet experiencing diarrhea. The acquisition of a foreign innate immune antagonist, ToV-PLP, may explain the pathogenicity in the natural host. Further in vivo characterization of this emerging chimeric virus is needed to fulfill Koch's postulates and evaluate the contribution of exogenous ToV-PLP in the pathogenesis of EVG in animals.

4.5. Reference

1. Knowles NJ HT, Hyypiä T, King AMQ, Lindberg AM, Pallansch MA, Palmenberg AC, Simmonds P, Skern T, Stanway G, Yamashita T, Zell R. 2012. Virus taxonomy : classification and nomenclature of viruses : ninth report of the International Committee on Taxonomy of Viruses. Elsevier, San Diego.
2. Boros Á, Nemes C, Pankovics P, Bíró H, Kapusinszky B, Delwart E, Reuter G. 2012. Characterization of a novel porcine enterovirus in wild boars in Hungary. Archives of virology 157:981-986.
3. Boros Á, Pankovics P, Knowles NJ, Reuter G. 2012. Natural interspecies recombinant bovine/porcine enterovirus in sheep. Journal of General Virology 93:1941-1951.
4. Moon H-J, Song D, Seon BH, Kim H-K, Park S-J, An D-J, Kim J-M, Kang B-K, Park B-K. 2012. Complete genome analysis of porcine enterovirus B isolated in Korea. Journal of virology 86:10250-10250.
5. Zoll J, Heus HA, van Kuppeveld FJ, Melchers WJ. 2009. The structure‐function relationship of the enterovirus 3′-UTR. Virus research 139:209-216.
6. Dewalt PG, Semler BL. 1989. Molecular biology and genetics of poliovirus protein processing. Molecular aspects of picornavirus infection and detection American Society for Microbiology, Washington, DC:73-93.
7. Semler BL, Wimmer E. 2002. Molecular biology of picornaviruses. ASM press.
8. Wimmer E, Hellen CU, Cao X. 1993. Genetics of poliovirus. Annual review of genetics 27:353-436.
9. Agol VI. 2006. Molecular mechanisms of poliovirus variation and evolution. Curr Top Microbiol Immunol 299:211-59.
10. Lukashev AN. 2005. Role of recombination in evolution of enteroviruses. Rev Med Virol 15:157-67.
11. Lukashev AN. 2010. Recombination among picornaviruses. Rev Med Virol 20:327-37.
12. Savolainen-Kopra C, Blomqvist S. 2010. Mechanisms of genetic variation in polioviruses. Rev Med Virol 20:358-71.
13. Simmonds P, Welch J. 2006. Frequency and dynamics of recombination within different species of human enteroviruses. J Virol 80:483-93.

14. Perez-Losada M, Arenas M, Galan JC, Palero F, Gonzalez-Candelas F. 2015. Recombination in viruses: mechanisms, methods of study, and evolutionary consequences. Infect Genet Evol 30:296-307.
15. Simon-Loriere E, Holmes EC. 2011. Why do RNA viruses recombine? Nat Rev Microbiol 9:617-26.
16. Holmblat B, Jegouic S, Muslin C, Blondel B, Joffret ML, Delpeyroux F. 2014. Nonhomologous recombination between defective poliovirus and coxsackievirus genomes suggests a new model of genetic plasticity for picornaviruses. MBio 5:e01119-14.
17. Muslin C, Joffret M-L, Pelletier I, Blondel B, Delpeyroux F. 2015. Evolution and Emergence of Enteroviruses through Intra-and Inter-species Recombination: Plasticity and Phenotypic Impact of Modular Genetic Exchanges in the 5'Untranslated Region. PLoS Pathog 11:e1005266.
18. Kirkegaard K, Baltimore D. 1986. The mechanism of RNA recombination in poliovirus. Cell 47:433-443.
19. Baez-Santos YM, Mielech AM, Deng X, Baker S, Mesecar AD. 2014. Catalytic function and substrate specificity of the papain-like protease domain of nsp3 from the Middle East respiratory syndrome coronavirus. J Virol 88:12511-27.
20. Bailey-Elkin BA, Knaap RC, Johnson GG, Dalebout TJ, Ninaber DK, van Kasteren PB, Bredenbeek PJ, Snijder EJ, Kikkert M, Mark BL. 2014. Crystal structure of the Middle East respiratory syndrome coronavirus (MERS-CoV) papain-like protease bound to ubiquitin facilitates targeted disruption of deubiquitinating activity to demonstrate its role in innate immune suppression. J Biol Chem 289:34667-82.
21. Barretto N, Jukneliene D, Ratia K, Chen Z, Mesecar AD, Baker SC. 2005. The papain-like protease of severe acute respiratory syndrome coronavirus has deubiquitinating activity. J Virol 79:15189-98.
22. Deaton MK, Dzimianski JV, Daczkowski CM, Whitney GK, Mank NJ, Parham MM, Bergeron E, Pegan SD. 2016. Biochemical and Structural Insights into the Preference of Nairoviral DeISGylases for Interferon-Stimulated Gene Product 15 Originating from Certain Species. J Virol 90:8314-27.

23. Lindner HA, Fotouhi-Ardakani N, Lytvyn V, Lachance P, Sulea T, Menard R. 2005. The papain-like protease from the severe acute respiratory syndrome coronavirus is a deubiquitinating enzyme. J Virol 79:15199-208.
24. Mielech AM, Chen Y, Mesecar AD, Baker SC. 2014. Nidovirus papain-like proteases: multifunctional enzymes with protease, deubiquitinating and deISGylating activities. Virus Res 194:184-90.
25. Mielech AM, Kilianski A, Baez-Santos YM, Mesecar AD, Baker SC. 2014. MERS-CoV papain-like protease has deISGylating and deubiquitinating activities. Virology 450-451:64-70.
26. Sun Z, Chen Z, Lawson SR, Fang Y. 2010. The cysteine protease domain of porcine reproductive and respiratory syndrome virus nonstructural protein 2 possesses deubiquitinating and interferon antagonism functions. J Virol 84:7832-46.
27. Sun Z, Li Y, Ransburgh R, Snijder EJ, Fang Y. 2012. Nonstructural protein 2 of porcine reproductive and respiratory syndrome virus inhibits the antiviral function of interferon-stimulated gene 15. J Virol 86:3839-50.
28. van Kasteren PB, Beugeling C, Ninaber DK, Frias-Staheli N, van Boheemen S, Garcia-Sastre A, Snijder EJ, Kikkert M. 2012. Arterivirus and nairovirus ovarian tumor domain-containing Deubiquitinases target activated RIG-I to control innate immune signaling. J Virol 86:773-85.
29. van Kasteren PBB-E, B. A; James, T. W.; Ninaber, D. K; Beugeling, C; Khajehpour, M; Snijder, E. J; Mark, B.L; Kikkert, M. 2013. Deubiquitinase function of arterivirus papain-like protease 2 suppresses the innate immune response in infected host cells. Proc Natl Acad Sci U S A 110:E838-47.
30. Davis ME, Gack MU. 2015. Ubiquitination in the antiviral immune response. Virology 479-480:52-65.
31. Shimizu Y, Taraborrelli L, Walczak H. 2015. Linear ubiquitination in immunity. Immunological reviews 266:190-207.
32. Skaug B, Chen ZJ. 2010. Emerging role of ISG15 in antiviral immunity. Cell 143:187-90.
33. Zhao C, Collins MN, Hsiang TY, Krug RM. 2013. Interferon-induced ISG15 pathway: an ongoing virus-host battle. Trends Microbiol 21:181-6.
34. Komander D, Rape M. 2012. The ubiquitin code. Annu Rev Biochem 81:203-29.

35. Zhang D, Zhang DE. 2011. Interferon-stimulated gene 15 and the protein ISGylation system. J Interferon Cytokine Res 31:119-30.
36. Maelfait J, Beyaert R. 2012. Emerging role of ubiquitination in antiviral RIG-I signaling. Microbiol Mol Biol Rev 76:33-45.
37. Sun SC. 2008. Deubiquitylation and regulation of the immune response. Nat Rev Immunol 8:501-11.
38. Bailey-Elkin BA, van Kasteren PB, Snijder EJ, Kikkert M, Mark BL. 2014. Viral OTU deubiquitinases: a structural and functional comparison. PLoS Pathog 10:e1003894.
39. Yang X, Chen X, Bian G, Tu J, Xing Y, Wang Y, Chen Z. 2014. Proteolytic processing, deubiquitinase and interferon antagonist activities of Middle East respiratory syndrome coronavirus papain-like protease. J Gen Virol 95:614-26.
40. Hause BM, Collin EA, Anderson J, Hesse RA, Anderson G. 2015. Bovine rhinitis viruses are common in US cattle with bovine respiratory disease. PloS one 10:e0121998.
41. Linding R, Russell RB, Neduva V, Gibson TJ. 2003. GlobPlot: Exploring protein sequences for globularity and disorder. Nucleic acids research 31:3701-3708.
42. Yang J, Yan R, Roy A, Xu D, Poisson J, Zhang Y. 2015. The I-TASSER Suite: protein structure and function prediction. Nature methods 12:7-8.
43. Guarné A, Hampoelz B, Glaser W, Carpena X, Tormo J, Fita I, Skern T. 2000. Structural and biochemical features distinguish the foot-and-mouth disease virus leader proteinase from other papain-like enzymes. Journal of molecular biology 302:1227-1240.
44. Guarné A, Tormo J, Kirchweger R, Pfistermueller D, Fita I, Skern T. 1998. Structure of the foot‐and‐mouth disease virus leader protease: a papain‐like fold adapted for self‐processing and eIF4G recognition. The EMBO journal 17:7469-7479.
45. Xu D, Zhang Y. 2011. Improving the physical realism and structural accuracy of protein models by a two-step atomic-level energy minimization. Biophysical journal 101:2525-2534.
46. Seiler CY, Park JG, Sharma A, Hunter P, Surapaneni P, Sedillo C, Field J, Algar R, Price A, Steel J. 2013. DNASU plasmid and PSI: Biology-Materials repositories: resources to accelerate biological research. Nucleic acids research:gkt1060.
47. Li Y, Shyu DL, Shang P, Bai J, Ouyang K, Dhakal S, Hiremath J, Binjawadagi B, Renukaradhya GJ, Fang Y. 2016. Mutations in a Highly Conserved Motif of nsp1beta

Protein Attenuate the Innate Immune Suppression Function of Porcine Reproductive and Respiratory Syndrome Virus. J Virol 90:3584-99.

48. Li YH, Tas A, Snijder EJ, Fang Y. 2012. Identification of porcine reproductive and respiratory syndrome virus ORF1a-encoded non-structural proteins in virus-infected cells. Journal of General Virology 93:829-839.
49. Rowland RRR, Chauhan V, Fang Y, Pekosz A, Kerrigan M, Burton MD. 2005. Intracellular localization of the severe acute respiratory syndrome coronavirus nucleocapsid protein: Absence of nucleolar accumulation during infection and after expression as a recombinant protein in Vero cells. Journal of Virology 79:11507-11512.
50. Li Y, Tas A, Snijder EJ, Fang Y. 2012. Identification of porcine reproductive and respiratory syndrome virus ORF1a-encoded non-structural proteins in virus-infected cells. Journal of general virology 93:829-839.
51. Li Y, Zhu L, Lawson SR, Fang Y. 2013. Targeted mutations in a highly conserved motif of the nsp1beta protein impair the interferon antagonizing activity of porcine reproductive and respiratory syndrome virus. J Gen Virol 94:1972-83.
52. Capodagli GC, Deaton MK, Baker EA, Lumpkin RJ, Pegan SD. 2013. Diversity of ubiquitin and ISG15 specificity among nairoviruses' viral ovarian tumor domain proteases. J Virol 87:3815-27.
53. Deaton MK, Spear A, Faaberg KS, Pegan SD. 2014. The vOTU domain of highly-pathogenic porcine reproductive and respiratory syndrome virus displays a differential substrate preference. Virology 454-455:247-53.
54. Tian B, Zhao Y, Kalita M, Edeh CB, Paessler S, Casola A, Teng MN, Garofalo RP, Brasier AR. 2013. CDK9-dependent transcriptional elongation in the innate interferon-stimulated gene response to respiratory syncytial virus infection in airway epithelial cells. Journal of virology 87:7075-7092.
55. Angelini MM, Neuman BW, Buchmeier MJ. 2014. Untangling membrane rearrangement in the nidovirales. DNA and cell biology 33:122-127.
56. Smits SL, Snijder EJ, de Groot RJ. 2006. Characterization of a torovirus main proteinase. J Virol 80:4157-67.
57. Draker R, Roper RL, Petric M, Tellier R. 2006. The complete sequence of the bovine torovirus genome. Virus research 115:56-68.

58. Hu M, Li P, Li M, Li W, Yao T, Wu J-W, Gu W, Cohen RE, Shi Y. 2002. Crystal structure of a UBP-family deubiquitinating enzyme in isolation and in complex with ubiquitin aldehyde. Cell 111:1041-1054.
59. Wang D, Fang L, Li P, Sun L, Fan J, Zhang Q, Luo R, Liu X, Li K, Chen H, Chen Z, Xiao S. 2011. The leader proteinase of foot-and-mouth disease virus negatively regulates the type I interferon pathway by acting as a viral deubiquitinase. J Virol 85:3758-66.
60. Lindner HA, Fotouhi-Ardakani N, Lytvyn V, Lachance P, Sulea T, Ménard R. 2005. The papain-like protease from the severe acute respiratory syndrome coronavirus is a deubiquitinating enzyme. Journal of virology 79:15199-15208.
61. Lindner HA, Lytvyn V, Qi H, Lachance P, Ziomek E, Ménard R. 2007. Selectivity in ISG15 and ubiquitin recognition by the SARS coronavirus papain-like protease. Archives of biochemistry and biophysics 466:8-14.
62. Worobey MH, E.C. 1999. Evolutionary aspects of recombination in RNA viruses. J Gen Virol 80:2535–2543.
63. Ledinko N. 1963. Genetic recombination with poliovirus type 1: studies of crosses between a normal horseserum resistant mutant and several guanidine-resistant mutants of the same strain. . Virology 20:107–119.
64. Cammack NP, A; Dunn, G; Patel, V; Minor, P. D. 1988. Intertypic genomic rearrangements of poliovirus strains in vaccinees. . Virology 167:507–514.
65. Minor PDJ, A; Ferguson, M; Icenogle, J. P. 1986. Antigenic and molecular evolution of the vaccine strain of type 3 poliovirus during the period of excretion by primary vaccinee. J Gen Virol 67:693–706.
66. Cuervo NS, Guillot S, Romanenkova N, Combiescu M, Aubert-Combiescu A, Seghier M, Caro V, Crainic R, Delpeyroux F. 2001. Genomic features of intertypic recombinant sabin poliovirus strains excreted by primary vaccinees. J Virol 75:5740-51.
67. Lipskaya GYM, A. R; Kutitova, O, K; Maslova, S. V; Equestre, M; Drozdov, S. G; Bercoff, R. P; Agol, V. I. 1991. Frequent isolation of intertypic poliovirus recombinants with serotype 2 specificity from vaccine-associated polio cases. Journal of Medical Virology 35:290–296.
68. Georgopoulou AM, P. 2001. Sabin type 2 polioviruses with intertypic vaccine/vaccine recombinant genomes. Eur J Clin Microbiol Infect Dis 20:792-9.

69. Agol VIG, V. P; Drozdov, S. G; Kolesnikova, M. S; Kozlov, V.G; Ralph, N. M; Romanova, L. I; Tolskaya, E. A; Tyufanov, A. V; Viktorova, E. G. 1985. Construction and properties of intertypic poliovirus recombinants: first approximation mapping of the major determinants of neurovirulence. Virology 136:41-55.
70. Oberste MS, Maher K, Pallansch MA. 2007. Complete genome sequences for nine simian enteroviruses. Journal of General Virology 88:3360-3372.
71. Hoey E. 2006. Molecular-based reclassification of the bovine enteroviruses.
72. Van Dung N, Anh PH, Van Cuong N, Hoa NT, Carrique-Mas J, Hien VB, Campbell J, Baker S, Farrar J, Woolhouse ME, Bryant JE, Simmonds P. 2014. Prevalence, genetic diversity and recombination of species G enteroviruses infecting pigs in Vietnam. J Gen Virol 95:549-56.
73. Zhang G, Haydon DT, Knowles NJ, McCauley JW. 1999. Molecular evolution of swine vesicular disease virus. Journal of General virology 80:639-651.
74. Zhang G, Wilsden G, Knowles NJ, McCauley JW. 1993. Complete nucleotide sequence of a coxsackie B5 virus and its relationship to swine vesicular disease virus. Journal of General Virology 74:845-853.
75. Durham PJ, Hassard LE, Norman GB, Yemen RL. 1989. Viruses and virus-like particles detected during examination of feces from calves and piglets with diarrhea. The Canadian Veterinary Journal 30:876.
76. Liu X, Zhou Y, Yang F, Liu P, Cai Y, Huang J, Zhu L, Xu Z. 2016. Rapid and sensitive detection of porcine torovirus by a reverse transcription loop-mediated isothermal amplification assay (RT-LAMP). Journal of virological methods 228:103-107.
77. Penrith M, Gerdes G. 1992. Breda virus-like particles in pigs in South Africa. Journal of the South African Veterinary Association 63.
78. Pignatelli J, Grau-Roma L, Jimenez M, Segales J, Rodriguez D. 2010. Longitudinal serological and virological study on porcine torovirus (PToV) in piglets from Spanish farms. Veterinary microbiology 146:260-268.
79. Zhou L, Wei H, Zhou Y, Xu Z, Zhu L, Horne J. 2014. Molecular epidemiology of Porcine torovirus (PToV) in Sichuan Province, China: 2011–2013. Virology journal 11:106.

80. Zhou Y, Chen L, Zhu L, Xu Z. 2013. Molecular Detection of Porcine Torovirus in Piglets with Diarrhea in Southwest China. The Scientific World Journal 2013.
81. Anbalagan S, Hesse RA, Hause BM. 2014. First identification and characterization of porcine enterovirus G in the United States. PLoS One 9:e97517.
82. Kroneman A, Cornelissen L, Horzinek M, De Groot R, Egberink H. 1998. Identification and characterization of a porcine torovirus. Journal of virology 72:3507-3511.
83. Prodelalova J. 2012. The survey of porcine teschoviruses, sapeloviruses and enteroviruses B infecting domestic pigs and wild boars in the Czech Republic between 2005 and 2011. Infect Genet Evol 12:1447-51.
84. Yang S, Wang Y, Shen Q, Zhang W, Hua X. 2013. Prevalence of porcine enterovirus 9 in pigs in middle and eastern China. Virol J 10:99.
85. Zhang W, Yang S, Shen Q, Ren L, Shan T, Wei J, Cui L, Hua X. 2012. Complete genome sequence of a novel porcine enterovirus strain in China. J Virol 86:7008-9.
86. Steinberger J, Skern T. 2014. The leader proteinase of foot-and-mouth disease virus: structure-function relationships in a proteolytic virulence factor. Biological chemistry 395:1179-1185.
87. Strebel K, Beck E. 1986. A second protease of foot-and-mouth disease virus. Journal of virology 58:893-899.
88. Kirchweger R, Ziegler E, Lamphear B, Waters D, Liebig H, Sommergruber W, Sobrino F, Hohenadl C, Blaas D, Rhoads R. 1994. Foot-and-mouth disease virus leader proteinase: purification of the Lb form and determination of its cleavage site on eIF-4 gamma. Journal of Virology 68:5677-5684.
89. Piñeiro D, Ramajo J, Bradrick SS, Martínez-Salas E. 2012. Gemin5 proteolysis reveals a novel motif to identify L protease targets. Nucleic acids research:gks172.
90. Gradi A, Foeger N, Strong R, Svitkin YV, Sonenberg N, Skern T, Belsham GJ. 2004. Cleavage of eukaryotic translation initiation factor 4GII within foot-and-mouth disease virus-infected cells: identification of the L-protease cleavage site in vitro. Journal of virology 78:3271-3278.
91. Harcourt BH, Jukneliene D, Kanjanahaluethai A, Bechill J, Severson KM, Smith CM, Rota PA, Baker SC. 2004. Identification of severe acute respiratory syndrome

coronavirus replicase products and characterization of papain-like protease activity. Journal of virology 78:13600-13612.

92. Kilianski A, Mielech AM, Deng X, Baker SC. 2013. Assessing activity and inhibition of Middle East respiratory syndrome coronavirus papain-like and 3C-like proteases using luciferase-based biosensors. Journal of virology 87:11955-11962.
93. Ratia K, Kilianski A, Baez-Santos YM, Baker SC, Mesecar A. 2014. Structural basis for the ubiquitin-linkage specificity and deISGylating activity of SARS-CoV papain-like protease. PLoS Pathog 10:e1004113.
94. Knowles NJ. 2006. Porcine enteric picornaviruses, 9 ed. Wiley-Blackwell, Oxford, UK.
95. Agol VI, Gmyl AP. 2010. Viral security proteins: counteracting host defences. Nat Rev Microbiol 8:867-78.
96. Basters A, Geurink PP, Röcker A, Witting KF, Tadayon R, Hess S, Semrau MS, Storici P, Ovaa H, Knobeloch K-P. 2017. Structural basis of the specificity of USP18 toward ISG15. Nature Structural & Molecular Biology.

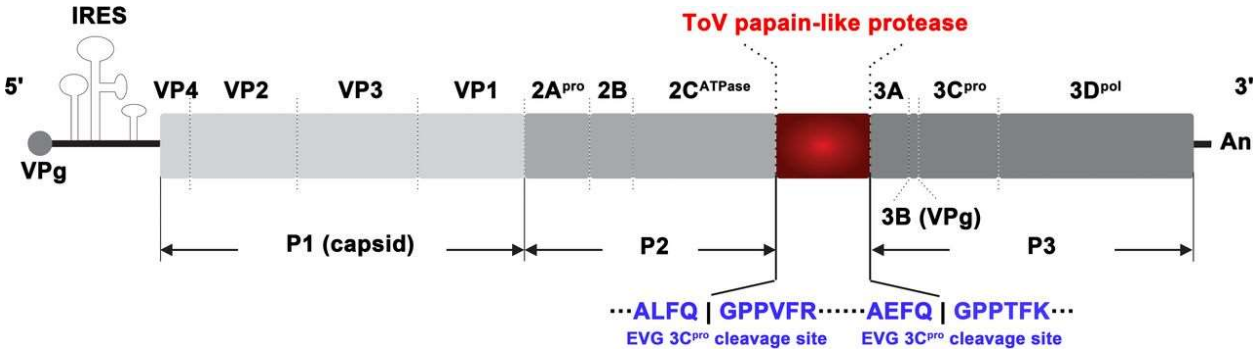

Figure 4.1. Schematic diagram of EVG 08/NC_USA/2015 genome organization.

Schematic diagram of the genome organization of EVG 08/NC_USA/2015. The single ORF is flanked by a long 5′ UTR (812 nucleotides) and a short 3′ UTR (72 nucleotides), followed by a poly(A) tail. Secondary structural elements in the 5′ UTR were adapted as previously described (Agol and Gmyl, 2010). The ToV-PLP gene is presented as a red box that is inserted at the 2C/3A cleavage junction. The 5′- and 3′-flanking sequences of 3C protease cleavage sites are shown in blue. Vertical lines indicate the polyprotein processing site by the 3C protease. IRES, internal ribosome entry site. An, poly(A) tail.

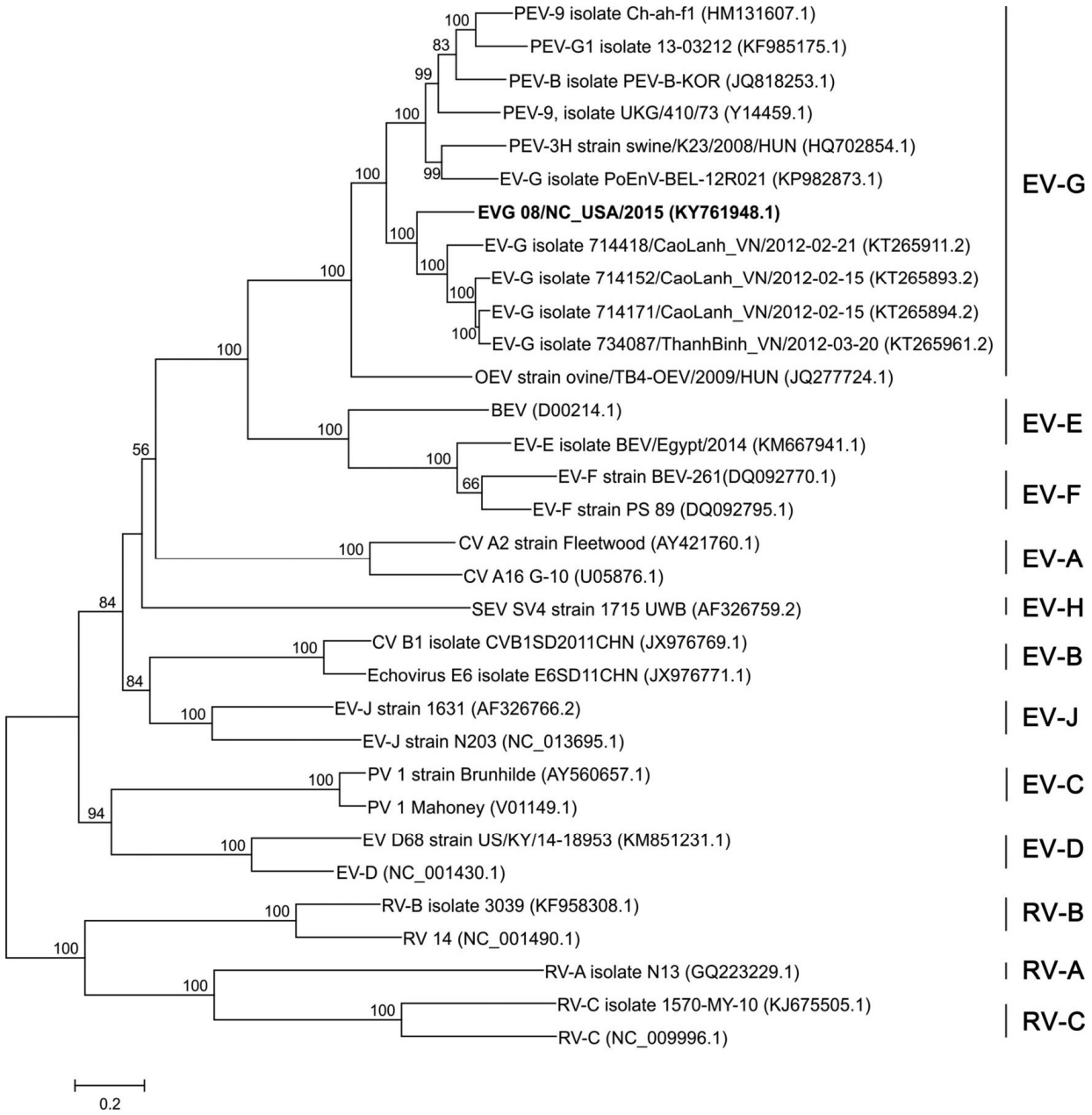

Figure 4.2. Phylogenetic analysis of enterovirus full-length genome nucleotide sequences.

Phylogenetic analysis of enterovirus full-length genome nucleotide sequences. The phylogenetic tree was constructed by the maximum likelihood method using the best-fitting general time-reversible model with a gamma distribution. The numbers on branches are bootstrap values (percent) from 500 replicates. Bootstrap values of <50% are not shown. GenBank accession numbers are given in parentheses after the name of each isolate. Enterovirus, rhinovirus, porcine enterovirus, ovine enterovirus, simian enterovirus, coxsackievirus, and poliovirus are denoted EV, RV, PEV, OEV, SEV, CV, and PV, respectively.

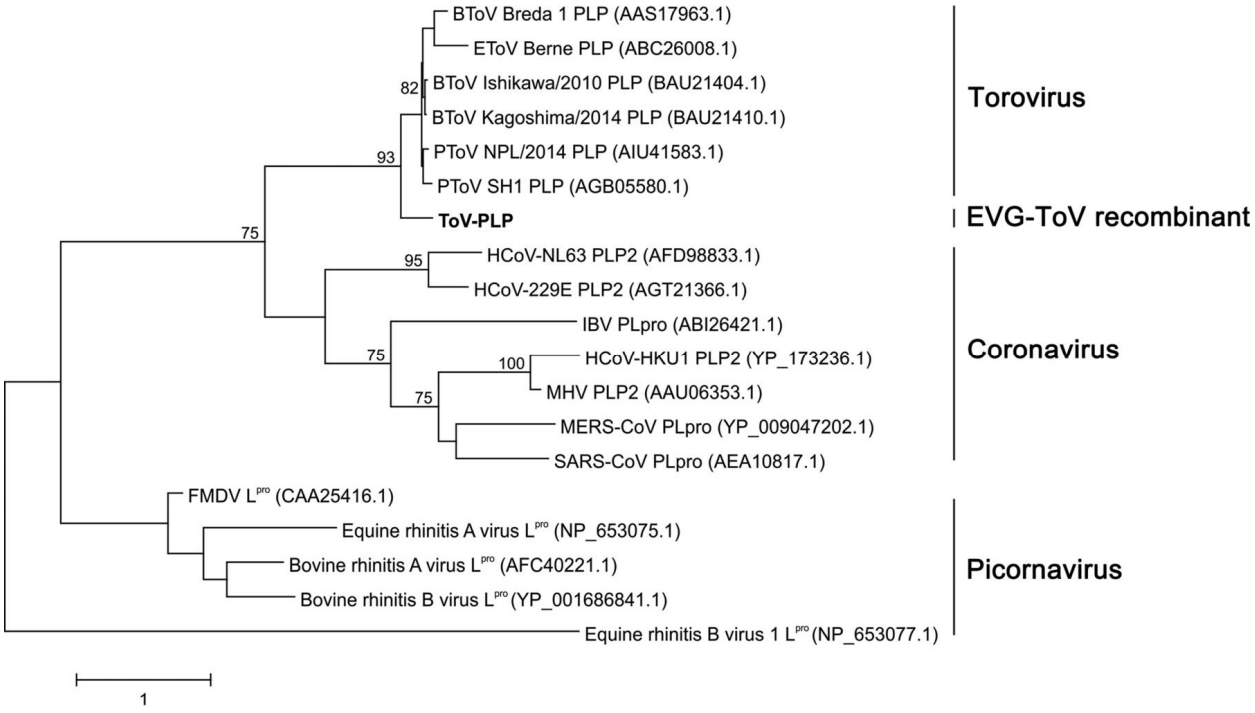

Figure 4.3. Phylogenetic analysis of coronaviral and picornaviral papain-like proteases.

The phylogenetic tree was constructed by the maximum likelihood method using the best-fitting algorithm Whelan-and-Goldman model. The numbers on branches are bootstrap values (percent) from 500 replicates. Bootstrap values of <50% are not shown. Amino acid sequences of PLPs are acquired from coronaviral, toroviral, and picornaviral polyproteins, with GenBank accession numbers shown in parentheses after the name of each protein entry.

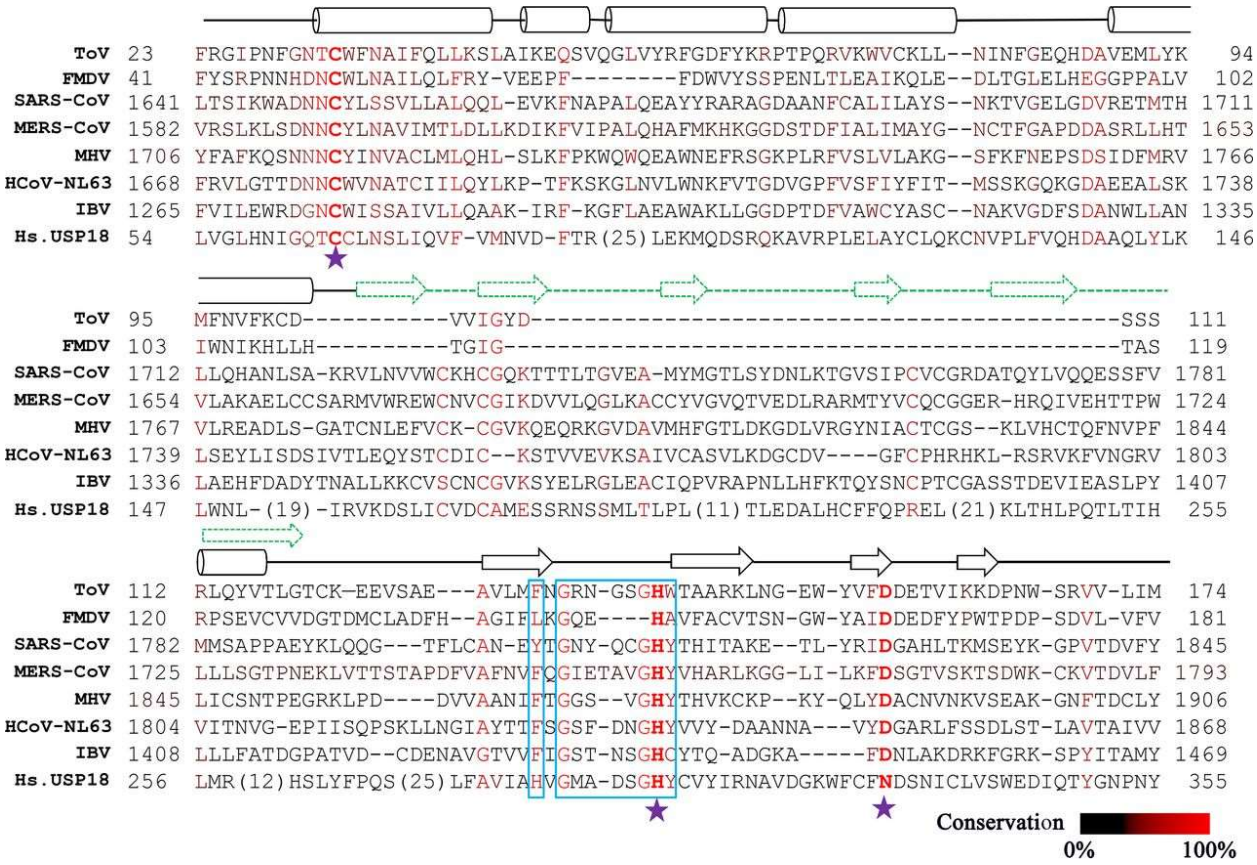

Figure 4.4. Amino acid sequence alignment of the EVG ToV-PLP protein with other known papain-like proteases.

Shown is structure- and sequence-guided alignment of EVG ToV-PLP with the corresponding catalytic domains of the FMDV leader protease, coronaviral PLPs, and the human deubiquitinating/deISGylating enzyme USP18. Sequences and numbering correspond to the following GenBank protein accession numbers: CAA25416.1 for the FMDV leader protease, AEA10817.1 for SARS coronavirus PLP, YP_009047202.1 for MERS coronavirus PLP, AAU06353.1 for murine hepatitis virus (MHV) PLP2, AFD98833.1 for human coronavirus NL63 PLP2, ABI26421.1 for infectious bronchitis virus (IBV) PLP, and AAD49967.1 for human USP18. The secondary structures of ToV-PLP and FMDV-L^{pro} are shown in black above the sequences. The secondary structure of an inserted β-sheet domain that is not present in the core fold of FMDV-L^{pro} but found in the other sequences is shown above the alignment in green. The catalytic-triad residues are marked with purple stars, and a DUB-specific "signature" motif in the protease catalytic sites is indicated with a light blue box (75). Hs., *Homo sapiens.*

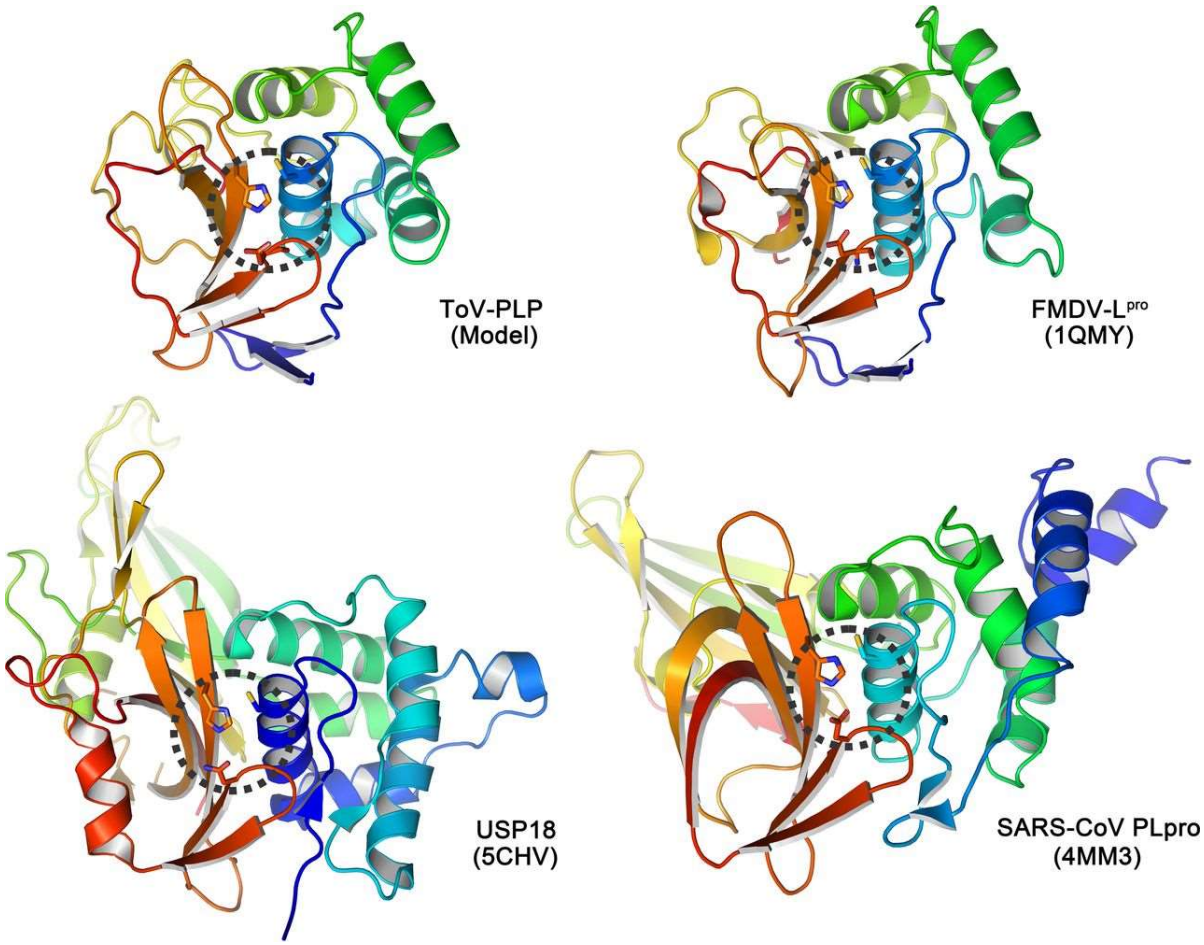

Figure 4.5. Structural modeling and comparison of EVG ToV-PLP protein with other known papain-like proteases.

Structures of the homology model of the core ToV-PLP catalytic domain were compared with those of the catalytic domains of representative viral proteases from FMDV (94), SARS-CoV (141) and the eukaryotic USP18 deubiquitinating enzyme (143). Each representation is colored by sequence progression from N to C termini (blue to red) and is shown in an approximately equivalent orientation. The side chains of the catalytic Cys, His, and Asp residues from each enzyme are circled and shown in a stick representation. PDB accession numbers are shown in parentheses.

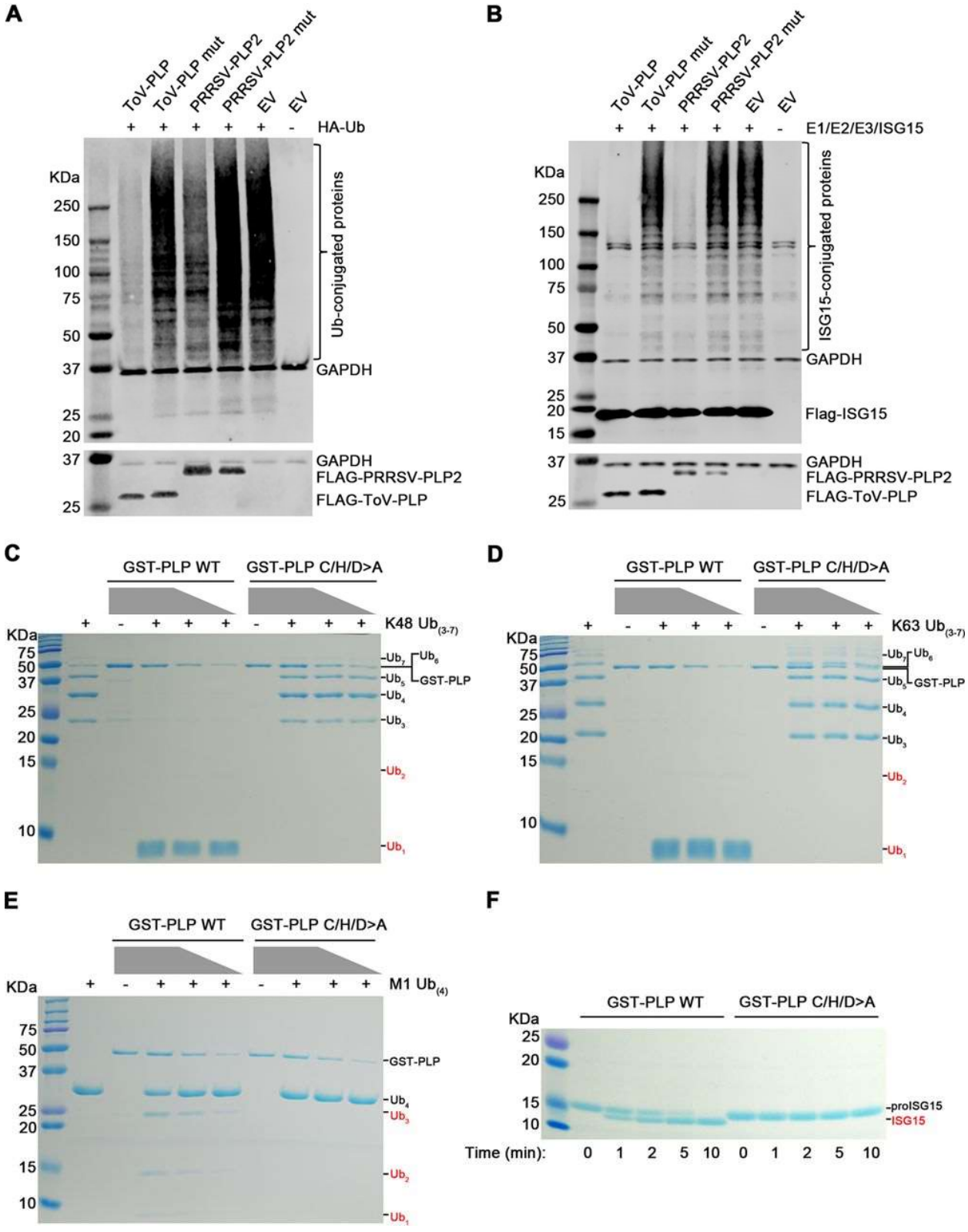
A
ToV-PLP
ToV-PLP mut
PRRSV-PLP2
PRRSV-PLP2 mut
EV
EV
HA-Ub
KDa
250
150
100
75
50
37
25
20
Ub-conjugated proteins
GAPDH
37
25
GAPDH
FLAG-PRRSV-PLP2
FLAG-ToV-PLP
B
E1/E2/E3/ISG15
ISG15-conjugated proteins
Flag-ISG15
C
GST-PLP WT
GST-PLP C/H/D>A
K48 Ub(3-7)
Ub7
Ub6
Ub5
GST-PLP
Ub4
Ub3
Ub2
Ub1
D
K63 Ub(3-7)
E
M1 Ub(4)
F
proISG15
ISG15
Time (min):
0 1 2 5 10 0 1 2 5 10

Figure 4.6. Deubiquitination and deISGylation activities of the recombinant ToV-PLP protease.

(A and B) Effect of PLP expression on Ub or ISG15 conjugation. (A) HEK-293T cells were cotransfected with plasmid DNAs expressing HA-Ub and FLAG-tagged ToV-PLP or PRRSV-PLP2 or their catalytic-site mutants (ToV-PLP mut and PRRSV-PLP2 mut, respectively). HA-Ub-conjugated cellular proteins were visualized by Western blotting using anti-HA MAb. The expression of FLAG-tagged PLPs was detected by anti-FLAG MAb M2. (B). HEK-293T cells were cotransfected with plasmid DNAs expressing ISG15 and its conjugation enzyme E1/E2/E3, ToV-PLP, or PRRSV-PLP2 or their catalytic-site mutants. ISG15-conjugated cellular proteins were detected with an ISG15-specific MAb by Western blot analysis. For both panels A and B, the empty pCAGGS vector plasmid was included as a control, while the expression of the GAPDH housekeeping gene was detected as a loading control. (C to E) Ubiquitin cleavage activity of recombinant ToV-PLP on K48/K63/M1-linked polyubiquitin chains. Cell-free deubiquitination activity was analyzed by using K48-linked polyubiquitin chains (Ub_{3-7}) (C), K63-linked polyubiquitin chains (D), or M1-linked polyubiquitin chains (E) as the substrates and incubation with serially diluted GST-PLP (1 μg, 0.5 μg, and 0.25 μg) or equal amounts of the catalytic-site mutant (GST-PLP C/H/D>A) at 37°C for 2 h. Cleaved ubiquitin products were visualized by SDS-PAGE and are labeled in red. Note that the molecular mass of Ub6 (51 kDa) is close to that of GST-PLP (50.4 kDa). WT, wild type. (F) DeISGylation activities of GST-tagged recombinant ToV-PLP (left) and its catalytic-site mutant (right). The ISG15 precursor (proISG15) was incubated with 40 nM GST-PLP or equal amounts of the catalytic-site mutant (GST-PLP C/H/D>A) at 37°C for a series of time points (1 min, 2 min, 5 min, and 10 min). The mature form of ISG15 was visualized by SDS-PAGE and is labeled in red.

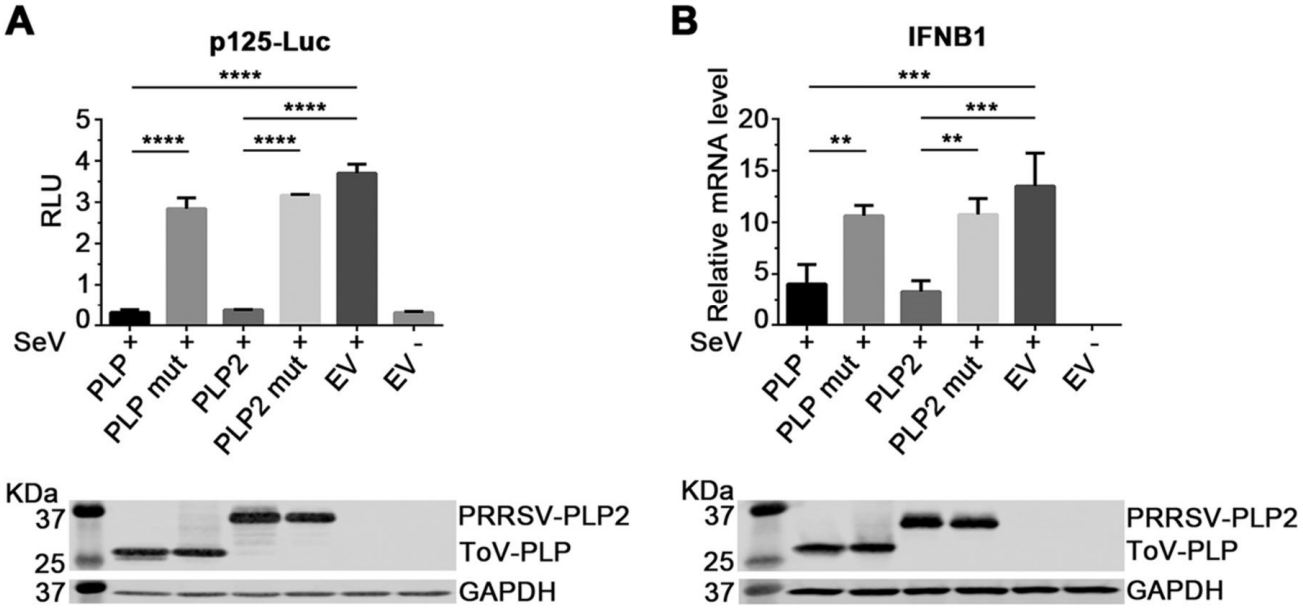

Figure 4.7. Effect of ToV-PLP expression on IFN-β expression.

(A) ToV-PLP affects reporter gene expression derived by the IFN-β promoter. HEK-293T cells were transfected with a plasmid expressing ToV-PLP, the PRRSV-PLP2 domain, or the catalytic-site mutant (PLP mut and PLP2 mut, respectively), along with the firefly luciferase reporter plasmid (p125-Luc) and Renilla luciferase expression plasmid pRL-SV40. Cells were stimulated by SeV at 24 h posttransfection. Luciferase activity was measured at 16 h poststimulation. Relative luciferase activity is defined as the ratio of firefly luciferase reporter activity to Renilla luciferase activity. Each data point represents the mean value from three experiments. Error bars show standard deviations of the normalized data. The expression of PLPs was detected by Western blotting using anti-FLAG MAb M2. The expression of the GAPDH housekeeping gene was detected as a loading control. RLU, relative light units. (B) ToV-PLP affects IFN-β mRNA expression. HEK-293T cells were transfected with a plasmid expressing ToV-PLP or PRRSV-PLP2 (wild type or mutant). At 24 h posttransfection, cells were stimulated with SeV. At 16 h poststimulation, quantitative RT-PCR was performed to evaluate the innate immune response. The relative mRNA expression level of IFN-β was acquired by normalization to the value for the TBP housekeeping gene. Mean values with standard deviations are shown. P values of <0.01 (**), <0.001 (***), and <0.0001 (****) are indicated.

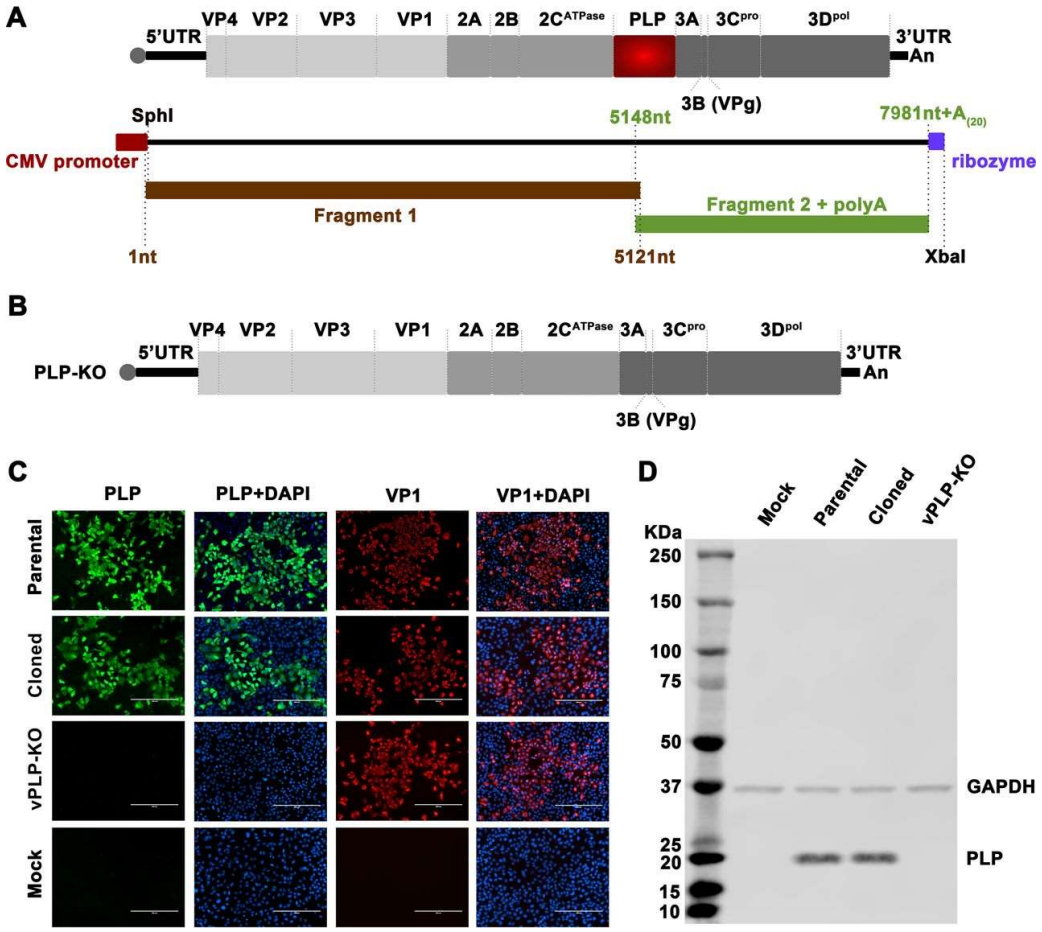

Figure 4.8. Construction of EVG 08/NC_USA/2015 infectious clone and rescuing recombinant viruses.

(A) Strategy for assembling the full-length cDNA infectious clone of EVG 08/NC_USA/2015. Two RT-PCR-amplified genomic fragments and a synthesized HDV ribozyme gene were assembled into the pACYC177 vector by using the NEBuilder HiFi DNA assembly method. The CMV promoter sequence was inserted at the 5′ end of the genome. (B) Schematic diagram of the PLP knockout mutant (vPLP-KO). (C) Immunofluorescence detection of recombinant viruses rescued from full-length cDNA clones. BHK-21C cells were initially transfected with plasmid DNA of the full-length cDNA clone pEVG or its mutant. ST cells were subsequently infected with the cloned viruses rescued from BHK cells. The expression of ToV-PLP and the structural protein VP1 was detected by specific MAb 128-28 and MAb 115-5, respectively. The cell nucleus is stained with DAPI. (D) Western blot detection of PLP expression in recombinant virus-infected ST cells. The membrane was probed with ToV-PLP-specific MAb 128-28. The expression of the GAPDH housekeeping gene was detected as a loading control.

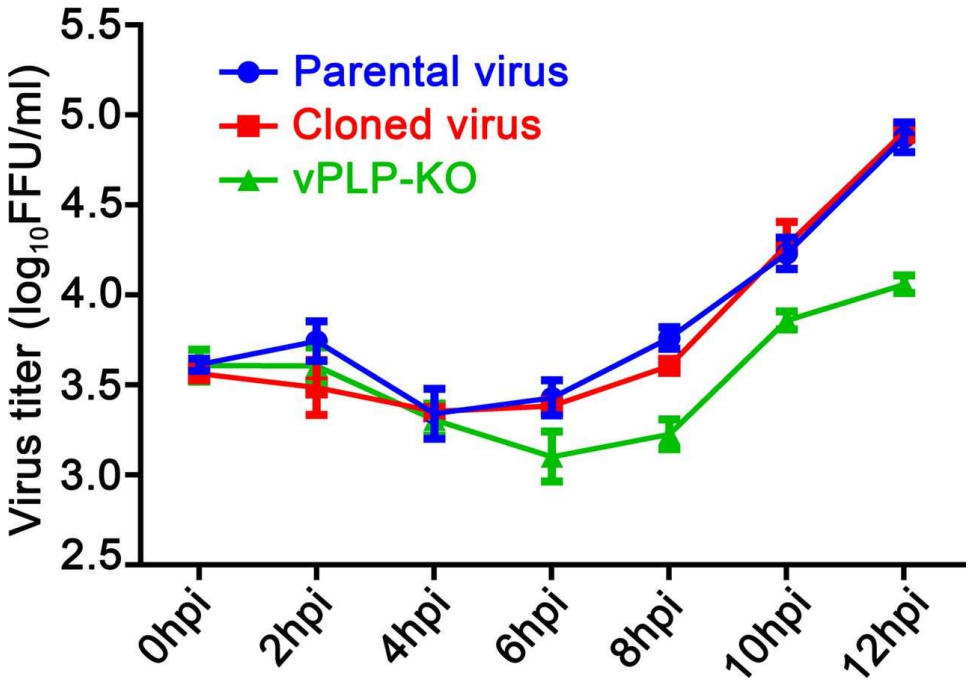

Figure 4.9. Characterization of *in vitro* growth properties of EVG recombinant viruses rescued from full-length cDNA infectious clones.

Confluent ST cells were initially inoculated with the recombinant virus at an MOI of 0.01, and the cell culture supernatant was serially harvested at 0, 2, 4, 6, 8, 10, and 12 hpi. The virus titer was measured by a microtitration assay. The results shown are mean values from three replicates, with error bars showing standard deviations. Virus titers are expressed as numbers of FFU per milliliter.

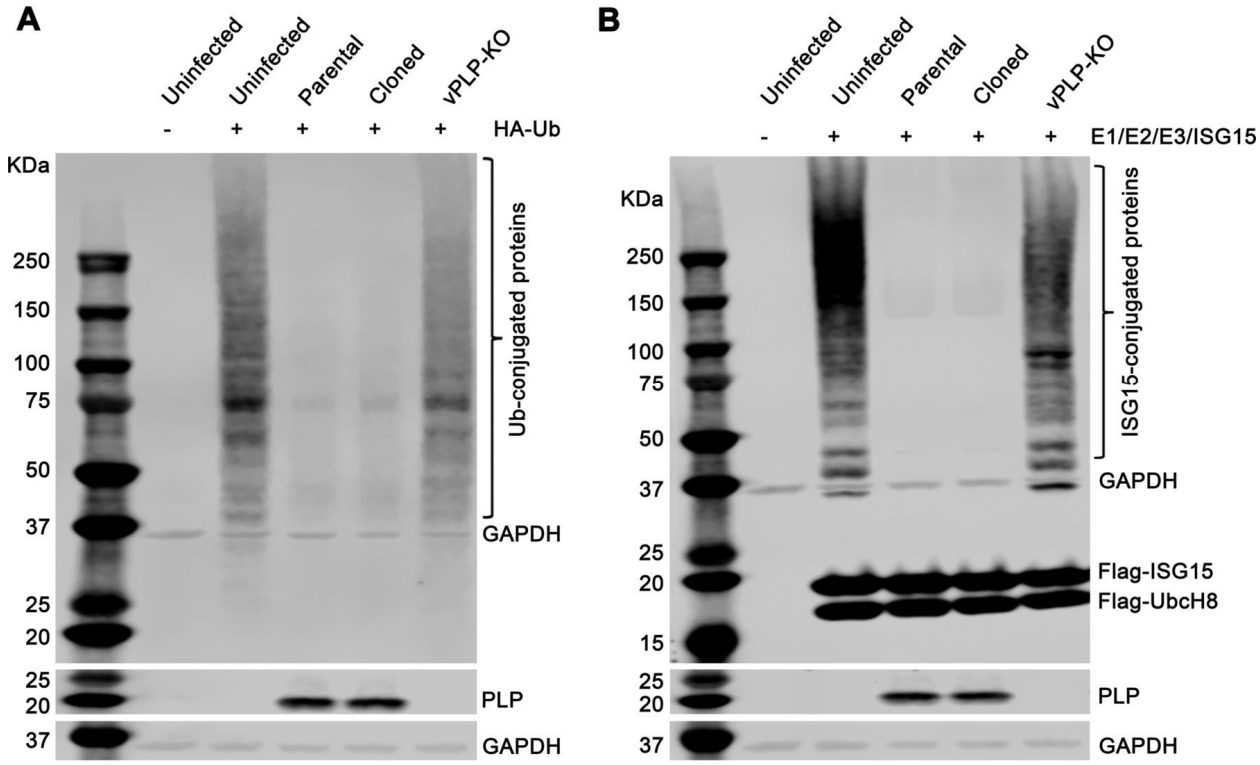

Figure 4.10. Effect of ToV-PLP deletion on the deubiquitination and deISGylation abilities of enterovirus.

(A) HEK-293T cells were transfected with plasmid DNAs expressing HA-Ub and then infected with the parental virus EVG 08/NC_USA/2015, the cloned virus vEVG, or vPLP-KO. Ubiquitin-conjugated cellular proteins were detected by Western blotting using an anti-HA MAb. (B) HEK-293T cells were cotransfected with plasmid DNAs expressing FLAG-tagged ISG15 and its conjugation enzyme E1/E2/E3 and then infected with the parental virus EVG 08/NC_USA/2015, the cloned virus vEVG, or vPLP-KO. ISGylated host proteins were visualized by Western blotting using anti-FLAG MAb. ToV-PLP-specific MAb 128-28 was used to detect the expression of PLP in infected cells. The expression of the GAPDH housekeeping gene was detected as a loading control.

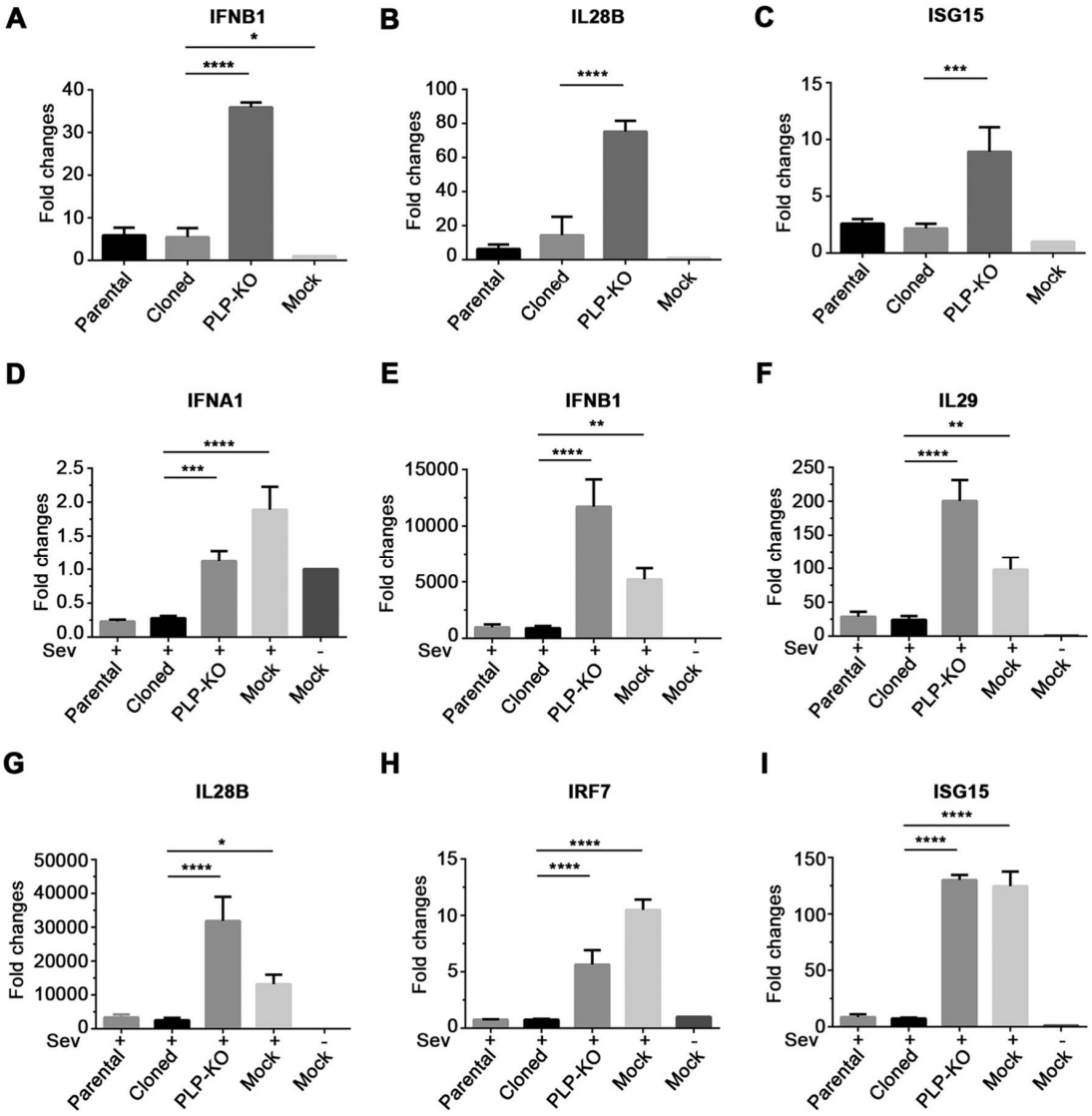

Figure 4.11. Effect of ToV-PLP deletion on innate immune gene expression levels.

ST cells were infected with the parental virus EVG 08/NC_USA/2015, the cloned virus vEVG, or the PLP knockout mutant vPLP-KO at an MOI of 3. Mock-infected cells were used as a control. Total RNAs were then extracted from cell lysates to perform real-time RT-PCR. (A to C) Innate immune gene expression levels were measured at 10 hpi. (D to I) At 6 hpi, cells were stimulated with SeV (200 HA units/ml) for 4 h. Total RNAs were then extracted to perform real-time RT-PCR. Relative expression levels of innate immune genes were assessed by comparison with the values for the mock control. The experiment was repeated three times. Results are shown as mean values for each group. P values of <0.05 (*), <0.01 (**), <0.001 (***), and <0.0001 (****) are indicated.

Table 4.1. Genome comparison of EVG 08/NC_USA/2015 with prototype EVG (PEV9 UKG/410/73)

Nucleotide or Amino acid		Length (EVG 08/NC_USA/2015)	Length (PEV9 UKG/410/73)	% Identity
Nucleotides				
5′-UTR		812	756[a]	87.5
Polyprotein		7098	6507	73.5
P1		2514	2505	68.1
P2		1734	1734	77.9
P3		2265	2265	77.0
3′-UTR		71	72	88.4
Complete		7981	7335	75.4
Amino acids				
P1	VP4	69	69	91.3
	VP2	246	246	82.9
	VP3	280	277	71.8
	VP1	243	243	60.1
P2	$2A^{pro}$	150	150	80.0
	2B	99	99	80.8
	$2C^{ATPase}$	329	329	85.4
PLP		194	N/A[b]	N/A
P3	3A	89	89	87.6
	3B (VPg)	22	22	95.5
	$3C^{pro}$	183	183	83.6
	$3D^{pol}$	461	461	88.5

[a] 5′ terminus of PEV9 not being determined.

[b] No PLP gene in PEV9.

[c] NA, not applicable.

Chapter 5 - Conclusion and Future prospects

Papain-like proteases (PLPs)-related proteins encoded by viruses have been demonstrated to play critical roles in host immune evasion and virus replication. In this dissertation, we investigated and elucidated the important impacts of swine nidoviral PLPs-related proteins on virus life cycle including both innate immune suppression and viral RNA transcription.

As the most prominent swine disease worldwide, understanding the PRRSV pathogenesis and development efficient vaccines are of importance for disease control and prevention. PRRSV nonstructural protein 2 (nsp2)-related proteins including nsp2 and two newly identified programmed ribosomal frameshifting (PRF) products-nsp2TF/nsp2N share the same N-terminal PLP2 domain. Studies in Chapter 2 have demonstrated the critical inhibitory impacts of nsp2TF and nsp2N on host anti-viral innate immunity. PLP2 domain-mediated deubiquitination (DUB) and deISGylation effects were determined to contribute to the immune modulation functions of nsp2TF and nsp2N. Interestingly, the long uncharacterized region between PLP2 domain and PRF site, shared by nsp2-related proteins, was also found to be involved in innate immunity suppression. Infection of mutant viruses with PRF products knockout significantly upregulated host innate immune responses both *in vitro* and *in vivo*. Moreover, *in vivo* characterization further showed that manipulating the expression of PRF products could enhance adaptive immunity responses, shedding lights on the development of genetically modified live vaccines. Based on the current knowledge we acquired on nsp2-related proteins, next steps could be to investigate the exact DUB/deISGylation target of PLP2 domain in innate immunity pathways and the interaction of PLP2 downstream region with innate immunity pathways.

In addition to the PLP2 domain, we also examined and characterized the biochemical nature and functional roles of the long uncharacterized PLP2 downstream region in Chapter 3.

We initially demonstrated the hyper-phosphorylation state of nsp2-related proteins, which expands the phospho-proteome of nidoviruses. The PLP2 downstream region containsmost of phosphorylation sites. By mapping the hyper-phosphorylation sites on the functional domains of nsp2-related proteins, we further subdivided this uncharacterized region into three domains with distinct biophysical features: two hypervariable regions (HVRs) with putative intrinsically disordered structures separated by a potentially structured interval domain-IHCD (Inter-HVR Conserved Domain) with rare inter-species conservation. Extensive phospho-abolishing mutagenesis revealed that the phosphorylated status of residue serine^{918} is important for rescued recombinant virus production. Further investigations showed abolishing the phosphorylation of serine^{918} selectively decreased the accumulation of viral subgenomic mRNAs. The inter-species conserved serine918 is located in IHCD, suggesting a potential regulatory role(s) of IHCD for PRRSV discontinuous transcription. Results in chapter 3 open several prospective gates for future investigations. Potential directions include: 1) identify the phosphorylation sites and functional significance of hyper-phosphorylation in nsp2-related proteins of clinically more important PRRSV-2; 2) to examine whether and how hyper-phosphorylation will affect the innate immunity suppression activities of PRRSV nsp2-related proteins; 3) to resolve the structure of IHCD and confirm the disordered properties of HVRs; 4) to search functional interaction of nsp2-related proteins with host/viral partners, since HVRs are enrich with potential interaction motifs like SH3-domain interaction motif and CtBP interaction motf; 5) to explore contributions of structural disorder in nsp2-related proteins for protein-protein interactions and hyper-phosphorylation; 6) to investigate whether the hypervariability of nsp2-related proteins contributes to the regulation of host-virus interplay and corresponding significance in pathogenesis and virus evolution.

Investigations PLP-related proteins help elucidate their functional roles in PRRSV life cycle, and, more importantly, provide promising targeted methods to fast attenuate pathogenic viruses and generate genetically modified live vaccines. Therefore, we then tested whether this strategy to manipulate the expression or biochemical nature of viral PLP-related proteins could be expanded to other viruses for solving more clinical problems. In 2015, Kansas State Veterinary Diagnostic Laboratory detected a unique pathogen from fecal samples of neonatal piglet experiencing with diarrhea symptoms. In the studies of Chapter 4, by using the knowledge acquired before on viral PLP-related proteins, we tried to explain the potential causes of piglet diarrhea by functionally characterizing this potential etiological agent. This pathogen was identified as a unique naturally occurred cross-order recombinant enterovirus G encoding a torovirus (ToV) PLP, which was discovered for the first time. In our studies, the exogenous ToV-PLP was consistently determined to be a robust deubiquinase/deISGylase and strong innate immune antagonist. The cross-order recombination event offers enterovirus G with an additional enzyme with unprecedented DUB and deISGylation activities. Chimeric virus showed enhanced performances in innate immunity suppression and *in vitro* growth ability than ToV-PLP knockout mutant. Studies on the rare cross-order recombination event highlight the contributions of PLP-related proteins for viral fitness and possibly pathogenicity, and further provide an ideal example about how recombination shapes virus evolution. Since enterovirus G is commonly found in pigs and could only cause subclinical infection under most circumstances, future studies should focus on whether the exogenous PLP could possibly elevate viral pathogenicity in pigs (i.e. to fulfil Koch's postulate), as indicated by *in vitro* characterization.

In conclusion, research in this dissertation demonstrate the critical roles of swine nidoviral PLPs-related proteins for innate immunity evasion and virus replication, more

importantly, for viral pathogenicity, and provide basic knowledge for implication in development of vaccines and other control strategies.

Publishers' permission to reproducing published materials

Chapter 1 related:

Figure 1.1-1.2:

Order Details

The Journal of general virology

Billing Status: **N/A**

Order detail ID:	71622398
ISSN:	0022-1317
Publication Type:	Journal
Volume:	
Issue:	
Start page:	
Publisher:	Microbiology Society
Author/Editor:	FEDERATION OF EUROPEAN MICROBIOLOGICAL SOCIETIES ; SOCIETY FOR GENERAL MICROBIOLOGY

Permission Status: Granted

Permission type: Republish or display content
Type of use: Republish in a thesis/dissertation
Order License Id: 4454460197279

Hide details

Requestor type	Academic institution
Format	Electronic
Portion	image/photo
Number of images/photos requested	2
The requesting person/organization	Pengcheng Shang
Title or numeric reference of the portion(s)	Chapter 1, Figure 1.1 Genome architecture of porcine reproductive and respiratory syndrome virus; Chapter 1, Figure 1.2 Subgenome transcription strategy of arteriviruses and coronaviruses.
Title of the article or chapter the portion is from	N/A
Editor of portion(s)	N/A
Author of portion(s)	N/A
Volume of serial or monograph	N/A
Page range of portion	About page 66
Publication date of portion	Dec. 15, 2018
Rights for	Main product
Duration of use	Current edition and up to 5 years
Creation of copies for the disabled	yes
With minor editing privileges	no
For distribution to	United States
In the following language(s)	Original language of publication
With incidental promotional use	no
Lifetime unit quantity of new product	Up to 499
Title	The roles of papain-like protease-related proteins in viral replication and host immunity
Institution name	Kansas State University
Expected presentation date	Oct 2018

Note: This item was invoiced separately through our **RightsLink service.** More info **$ 0.00**

Total order items: 1 **Order Total: $0.00**

Figure 1.3:

The journal of experimental medicine

Order detail ID:	71622403
Order License Id:	4454460896451
ISSN:	1540-9538
Publication Type:	e-Journal
Volume:	
Issue:	
Start page:	
Publisher:	ROCKEFELLER UNIVERSITY PRESS

Permission Status: Granted

Permission type: Republish or display content
Type of use: Thesis/Dissertation

Requestor type	Academic institution
Format	Electronic
Portion	image/photo
Number of images/photos requested	1
The requesting person/organization	Pengcheng Shang
Title or numeric reference of the portion(s)	Chapter 1, Figure 1.3 Host ubiquitination mechanism and strategies of viral manipulation.
Title of the article or chapter the portion is from	NA
Editor of portion(s)	NA
Author of portion(s)	NA
Volume of serial or monograph	NA
Issue, if republishing an article from a serial	NA
Page range of portion	About page 67
Publication date of portion	Dec. 15, 2018
Rights for	Main product
Duration of use	Current edition and up to 5 years
Creation of copies for the disabled	yes
With minor editing privileges	no
For distribution to	United States
In the following language(s)	Original language of publication
With incidental promotional use	no
Lifetime unit quantity of new product	Up to 499
Title	The roles of papain-like protease-related proteins in viral replication and host immunity
Institution name	Kansas State University
Expected presentation date	Oct 2018

Figure 1.4-1.5:

This Agreement between Pengcheng Shang ("You") and Elsevier ("Elsevier") consists of your license details and the terms and conditions provided by Elsevier and Copyright Clearance Center.

License Number	4454461365921
License date	Oct 22, 2018
Licensed Content Publisher	Elsevier
Licensed Content Publication	Virology
Licensed Content Title	Ubiquitination in the antiviral immune response
Licensed Content Author	Meredith E. Davis,Michaela U. Gack
Licensed Content Date	May 1, 2015
Licensed Content Volume	479
Licensed Content Issue	n/a
Licensed Content Pages	14
Start Page	52
End Page	65
Type of Use	reuse in a thesis/dissertation
Portion	figures/tables/illustrations
Number of figures/tables/illustrations	3
Format	electronic
Are you the author of this Elsevier article?	No
Will you be translating?	No
Original figure numbers	Fig. 2, 3, 5
Title of your thesis/dissertation	The roles of papain-like protease-related proteins in viral replication and host immunity
Publisher of new work	Kansas State University
Expected completion date	Oct 2018
Estimated size (number of pages)	1
Requestor Location	Pengcheng Shang 1800 Denision Ave Mosier Hall Manhattan, KS 66502 United States Attn:
Publisher Tax ID	98-0397604
Total	0.00 USD
Terms and Conditions	

Figure 1.6:

This Agreement between Pengcheng Shang ("You") and Springer Nature ("Springer Nature") consists of your license details and the terms and conditions provided by Springer Nature and Copyright Clearance Center.

License Number	4454470159495
License date	Oct 22, 2018
Licensed Content Publisher	Springer Nature
Licensed Content Publication	Nature Reviews Microbiology
Licensed Content Title	ISG15 in antiviral immunity and beyond
Licensed Content Author	Yi-Chieh Perng et al
Licensed Content Date	May 16, 2018
Type of Use	Thesis/Dissertation
Requestor type	academic/university or research institute
Format	electronic
Portion	figures/tables/illustrations
Number of figures/tables/illustrations	1
High-res required	no
Will you be translating?	no
Circulation/distribution	<501
Author of this Springer Nature content	no
Title	The roles of papain-like protease-related proteins in viral replication and host immunity
Institution name	Kansas State University
Expected presentation date	Oct 2018
Portions	Figure. 1
Requestor Location	Pengcheng Shang 1800 Denision Ave Mosier Hall Manhattan, KS 66502 United States Attn:
Billing Type	Invoice
Billing Address	Pengcheng Shang 1800 Denision Ave Mosier Hall Manhattan, KS 66502 United States Attn: Pengcheng Shang
Total	0.00 USD

Figure 1.7:

This Agreement between Pengcheng Shang ("You") and Elsevier ("Elsevier") consists of your license details and the terms and conditions provided by Elsevier and Copyright Clearance Center.

License Number	4454470326391
License date	Oct 22, 2018
Licensed Content Publisher	Elsevier
Licensed Content Publication	Journal of Molecular Biology
Licensed Content Title	Structure and Function of Viral Deubiquitinating Enzymes
Licensed Content Author	Ben A. Bailey-Elkin,Robert C.M. Knaap,Marjolein Kikkert,Brian L. Mark
Licensed Content Date	Nov 10, 2017
Licensed Content Volume	429
Licensed Content Issue	22
Licensed Content Pages	30
Start Page	3441
End Page	3470
Type of Use	reuse in a thesis/dissertation
Intended publisher of new work	other
Portion	figures/tables/illustrations
Number of figures/tables/illustrations	1
Format	electronic
Are you the author of this Elsevier article?	No
Will you be translating?	No
Original figure numbers	Figure 2
Title of your thesis/dissertation	The roles of papain-like protease-related proteins in viral replication and host immunity
Publisher of new work	Kansas State University
Expected completion date	Oct 2018
Estimated size (number of pages)	1
Requestor Location	Pengcheng Shang 1800 Denision Ave Mosier Hall Manhattan, KS 66502 United States Attn:
Publisher Tax ID	98-0397604

Chapter 2 related:

https://www.sciencedirect.com/science/article/pii/S0042682217304221?via%3Dihub

Elsevier does not view the following uses of a work as prior publication: publication in the form of an abstract; publication as an academic thesis; publication as an electronic preprint. Information on prior publication is included within each Elsevier journal's Guide for Authors. Note: Cell Press, The Lancet, and some society-owned titles have different policies on prior publication. Information on these is available on the journal homepage. (https://www.elsevier.com/authors/journal-authors/policies-and-ethics)

Chapter 4 related: https://jvi.asm.org/content/91/14/e00450-17

Authors in ASM journals retain the right to republish discrete portions of his/her article in any other publication (including print, CD-ROM, and other electronic formats) of which he or she is author or editor, provided that proper credit is given to the original ASM publication. ASM authors also retain the right to reuse the full article in his/her dissertation or thesis. For a full list of author rights, please see: http://journals.asm.org/site/misc/ASM_Author_Statement.xhtml